A New Kind of Microplasma for Nitrogen-Fixation Multifunctional Nanoparticle Synthesis Towards Selected Applications

by

Hue Quoc Pho

M. Sc. (Biomedical Engineering),
Chung Yuan Christian University - Taiwan, 2017

Dissertation submitted in fulfilment of the requirements for

Jointly Awarded Doctor of Philosophy

in

School of Chemical Engineering and Advanced Materials
The University of Adelaide

&

School of Engineering
The University of Warwick

09 February 2023

Supervisors from home institution, The University of Adelaide:

Professor Volker Hessel,
School of Chemical Engineering and Advanced Materials,
The University of Adelaide

Professor Dusan Losic,
School of Chemical Engineering and Advanced Materials,
The University of Adelaide

Supervisors from host institution, The University of Warwick:

Professor Evgeny V. Rebrov,
School of Engineering,
The University of Warwick

Associate Professor Petr Denissenko,
School of Engineering,
The University of Warwick

Table of Contents

Table of Contents iii

Summary v

State of Originality viii

Acknowledgements x

Preface xii

Chapter 1. Introduction 1

1.1. Abstract 2

1.2. Introduction 3

1.3. Research Background 6

1.3.1. Nitrogen-fixation plasma 6

1.3.2. N-doped carbon quantum dots as an emerging advanced nanomaterial 8

1.3.3. Properties of N-doped carbon quantum dots 12

1.3.3.1. Adsorption 13

1.3.3.2. Fluorescence property 13

1.3.3.3. Phosphorescence 15

1.3.3.4. Chemiluminescence 15

1.3.3.5. Photoluminescence 16

1.3.3.6. Optoelectronic properties 16

1.3.3.7. Quantum Yield 17

1.3.4. Various synthesis methodologies of N-doped carbon dots 17

1.3.4.1. Top-down approaches 20

1.3.4.2. Bottom-up approaches 21

1.3.5. Characterisation methods of N-doped carbon quantum dots 23

1.3.6. Microplasma-assisted synthesis of N-doped carbon quantum dots 24

1.3.7. kINPen®IND microplasma jet 27

1.3.8. Potential applications of N-doped carbon quantum dots 28

1.3.8.1. N-doped carbon quantum dots as potential nanopesticides 28

1.3.8.2. N-doped carbon quantum dots as photocatalysts for wastewater treatment 30

1.3.8.3. N-doped carbon quantum dots as theranostic agents in biomedical applications . 31

1.4. Research aims and objectives 33

1.5. Thesis outline 36

1.6. Budget and Research Funding 39
1.7. Thesis Editing & Format 39
1.8. References 40

Chapter 2. Literature review 39

Chapter 3. Sustainability assessment of various large-scale synthesis processes of NCQDs 39

Chapter 4. Process intensification for gram scale synthesis of NCQDs 59

Chapter 5. Rationally designed microplasma synthesis of NCQDs for targeted applications 73

Chapter 6. Insight into plasma-catalysis in triphasic microplasma synthesis for NCQDs 89

Chapter 7. Stagnant Liquid Layer as "Microreaction System" in Submerged Plasma Micro-Jet . 125

Chapter 8. Conclusions & Perspectives 158

Summary

N-doped carbon quantum dot (NCQDs) is an emerging material in the carbon family, which possess many advantageous qualities such as low toxicity, good compatibility with living cells, stability in chemical reactions, strong photoluminescence, photocatalysis, and efficient transfer of electrons when exposed to light. These properties make CDs a highly promising material to mitigate the current challenges in pest control, environmental treatment and theranostic medicine. This thesis study carried out a comprehensive literature review on the potential applications of these materials in pest control. Although a tremendous benefit from NCQDs has been revealed, generating these materials in large-scale production in a green and sustainable manner is still challenging. Therefore, a comprehensive assessment of all available large-scale production of NCQDs in terms of sustainability is significant. It has been revealed that non-thermal nitrogen fixation microplasma is a potential large-scale synthesis method in terms of sustainability while lacking mass efficiency. Therefore, it is crucial to overcome the improvement of mass efficiency of the non-thermal nitrogen fixation microplasma method. In addition, most of these CD synthesis strategies are classified as the trial-and-error approach. It is a time-consuming journey with cost- and process inefficiency to create CDs with a suitable structure and properties available for a specific application.

For this reason, it is also urgent to develop a rational design strategy for synthesising NCQDs towards selected applications (pest control, environmental treatment and theranostic medicine), which are emerging issues mentioned above. It has been revealed that the photoluminescence of the as-prepared NCQD increases by 18.4% in the presence of metal flakes as catalysts. However, the role of plasma-liquid-catalyst interaction in the production of NCQDs is still unclear. Therefore, it is also significant to have a deep understanding of the plasma-liquid-catalyst mechanism in the reaction to control the large-scale production of NCQDs better. Finally, it has also been important to have an insight into the reaction rate in the production of NCQDs and to determine factors (viscosity and liquid surface area) that affect the reaction rate.

The primary aim of this thesis is to develop a new kind of microplasma to address the challenges associated with the large-scale production of N-fixation multifunctional N-doped carbon quantum dots (NCQD) for selected applications. The objectives of this thesis are

organised into 8 chapters that will be presented in the form of a collection of published and submitted papers, which are the research outcomes. In addition, a literature review has been provided to establish the background of microplasma-assisted synthesis of NCQDs and highlight the potential applications of this material in agriculture. Overall, this thesis's main contributions to developing a new kind of microplasma-assisted synthesis process are discovering, investigating, understanding, designing, fabricating, and improving the concept of using the non-thermal nitrogen fixation microplasma process to generate high-quality NCQDs for selected applications. The main contributions are summarised in the following chapters:

- **Chapter 2.** Literature review: Perspectives on the plasma-assisted synthesis of N-doped nanoparticles as nanopesticides for crop pest control (Published paper 1).
- **Chapter 3.** Sustainability assessment of large-scale synthesis processes of NCQDs (Published paper 2).
- **Chapter 4.** Process intensification for gram-scale synthesis of NCQDs (Published Paper 3).
- **Chapter 5.** Rationally designed microplasma synthesis of NCQDs for targeted applications (Published paper 4).
- **Chapter 6.** Insight into plasma-catalysis in triphasic microplasma synthesis for NCQDs (Ready manuscript 5).
- **Chapter 7.** Stagnant Liquid Layer as “Microreaction System” in Submerged Plasma Micro-Jet for Formation of Carbon Quantum Dots (Submitted).

BLANK PAGE

State of Originality

I certify that this work contains no materials which have been accepted for the award of any other degree or diploma in my name, in any university or tertiary institution and, to the best of my knowledge and belief, contains no material previously published or written by another person, except where due reference has been made in the text. In addition, I certify that no part of this work will, in the future, be used in a submission in my name for any other degree or diploma in any university or other tertiary institution without the prior approval of the University of Adelaide and where applicable, any partner institution responsible for the joint-award of this degree.

I acknowledge that the copyright of published works contained within the thesis besides with the copyright holder(s) of those works.

I also give permission for the digital version of my thesis to be made available on the web via the University's digital research repository, the Library Search and also through web search engines unless permission has been granted by the University to restrict access for a period of time.

Hue Quoc Pho Adelaide, 09 February 2023.

BLANK PAGE

Acknowledgements

First of all, I would like to express "thank you" to **Dr Triet Friedhoff** – a friend and talented mentor. Your precious advice and experience in preparing for the graduate school applications you shared with me have always been helpful until now.

I am honoured to thank everyone who accompanied me during this incredible journey to "make my own history" at the University of Adelaide. Especially from the bottom of my heart, I would like to express my sincerest appreciation to my principal supervisor, **Prof Volker Hessel,** for offering me "unique" opportunities to conduct interdisciplinary research with international collaborations in "SCOPE project" funded by European Commission. Without his enthusiasm, tremendous guidance, and inspiration to supervise me, I could not go this far in accomplishing this journey. I also would like to thank **Prof Evgeny V. Rebrov** and **Associate Prof Petr Denissenko** for their full support and supervision in the joint PhD program between Adelaide-Warwick University.

I would like to thank my co-supervisor at the Adelaide University, **Prof Dusan Losic,** who gave me full access to laboratory equipment and materials necessary for my study. I also would like to extend my gratitude to **Dr Nam Nghiep Tran and Dr Tung Tran** two big brothers in my academia and life, for sharing their priceless advice, scientific insights, and knowledge in this journey.

My study in this beautiful city of Adelaide would not be exciting without my research colleagues' companionship, assistance, and encouragement. **Dr Mohsen Sarafraz, Dr Van Long Nguyen, Don Tran, Svenja Schmidt, Chang Ping Zhuang, Tu Le,** and other friends in Adelaide are very supportive. In addition, I would like to thank all of the awesome administrative, academic, and workshop staff at The School of Chemical Engineering for their very kind support related to my PhD study.

Last but not least, my journey would have never been completed without my loved family and friends in Vietnam. My special thanks go to my dear parents - **Tua Chau and Ngoan Pho,** to my brother – **Vinh Pho** and my sister – **Yen Pho**, for their love and support.

*"All challenges in life are catalysts to make you more mature. Be calm and confident towards challenges! You will seek light at the end of your journey" – **Hue Pho (Bill Fu)**.*

BLANK PAGE

Preface

This thesis is submitted as a "thesis by publication" in accordance with the "Specifications for Thesis 2023" of The University of Adelaide. This thesis contains the following list of publications over a span of three and a half years of my PhD candidature. The outcomes generated during my PhD candidature include **14 published-or-under-reviewed journal articles and book chapters** (7 first-authored, 7 co-authored), **7 conference presentations**, and **8 awards & achievements**, as well as involving **various administration and leadership positions** at school and university levels.

First-authored Journal Articles & Book Chapter

[7]. **Pho, Q.H.,** Lin, L., Rebrov, E.V., Sarafraz, M.M., Tran, T.T., Tran, N.N., Losic, D. and Hessel, V., 2023. Process intensification for gram-scale synthesis of N-doped carbon quantum dots immersing a microplasma jet in a gas-liquid reactor. Chemical Engineering Journal, 452, p.139164. **(Q1, IF = 16.744)** **<Link>**

[6]. **Pho, Q.H.,** Lin, L., Tran, N.N., Tran, T.T., Nguyen, A.H., Losic, D., Rebrov, E.V. and Hessel, V., 2022. Rational design for the microplasma synthesis from vitamin B9 to N-doped carbon quantum dots towards selected applications. Carbon, 198, pp.22-33**. (Q1, IF = 11.307)** **<Link>**

[5]. **Pho, Q.H.,** Escriba-Gelonch, M., Losic, D., Rebrov, E.V., Tran, N.N. and Hessel, V., 2021. Survey of synthesis processes for N-doped carbon dots assessed by green chemistry and circular and EcoScale metrics. ACS Sustainable Chemistry & Engineering, 9(13), pp.4755-4770. **(Q1, IF = 9.224)** **<Link>**

[4]. **Pho, Q.H.,** Losic, D., Ostrikov, K.K., Tran, N.N. and Hessel, V., 2020. Perspectives on plasma-assisted synthesis of N-doped nanoparticles as nanopesticides for pest control in crops. Reaction Chemistry & Engineering, 5(8), pp.1374-1396. **(Q1, IF = 5.2)** **<Link>**

[3]. **Pho, Q.H.,** Jiao, Y. R., Jiao Y., Sun, W., Tansu, N., Wojnicki, M., Shabbir, H., Rogoz, K., Tran, N. N., Lewis, D., and Hessel, V., 2023. Quantum Materials, Ullmann's Encyclopedia of Industrial Chemistry, Wiley, Germany. (**Book Chapter, Accepted)**

[2]. **Pho, Q.H.,** Tran, H.Q., Zhuang C.P., Nguyen, V.L., Tran, N.N., Rebrov, E.V., Losic, D., and Hessel, V., 2023. Deciphering Plasma-Catalysis in Triphasic Microplasma for N-doped Carbon Quantum Dots from Vitamin B9 via Optical Emission Spectroscopy. Chemical Engineering Journal. **(Ready manuscript)**

[1]. **Pho, Q.H.,** Hessel, V., Rebrov, E.V., Lamichhane, P., Tran, N.N., and Losic, D., 2023. Stagnant Liquid Layer as "Microreaction System" in Submerged Plasma Micro-Jet for Formation of Carbon Quantum Dots. Chemical Engineering Journal. **(Submitted)**

Co-authored Journal Articles & Book Chapters

[7]. Tran, T. T., Pereira, A. L. C, Poloni, E., Dang, N. M., Wang, J., Dinh, T. S., Kim, Y., **Pho, Q. H.,** J., Nine, Md J., Hessel, V., and Losic, D., 2023, Irradiation Methods for Graphene-based Materials Production, Applied Physics Review.(**Q1, IF = 19.527, Accepted)**

[6]. Tran, N.N, Escriba-Gelonch, M., Sarafraz, M.M., **Pho, Q.H.,** Sagadevan, S., and Hessel, V., 2023. Process Technology and Sustainability Assessment of Wastewater Treatment. Industrial & Engineering Chemistry Research. **(Q1, IF = 4.326)** <Link>

[5]. Sang, N.X., Na, T.T.L., Anh, L.T.L., Thuy, P.T., Tuan, N.T., Tung, T.T., Tran, A.T.T., **Pho, Q.H.,** Shearer, C.J. and Losic, D., 2022. Engineering of ZnO/graphene nanocomposite for enhancing visible photocatalytic ability. Physica status solidi (a), p.2200172. **(IF = 3.277)** <Link>

[4]. Tran, N.N., Le, T.N.Q., **Pho, Q.H.,** Tran, T.T. and Hessel, V., 2022. Nanofertilizers and Nanopesticides for Crop Growth. In Plant and Nanoparticles (pp. 367-394). Springer, Singapore. (**Book Chapter)** <Link>

[3]. Lin, L., **Pho, Q.H.,** Zong, L., Li, S., Pourali, N., Rebrov, E., Tran, N.N., Ostrikov, K.K. and Hessel, V., 2021. Microfluidic plasmas: Novel technique for chemistry and chemical engineering. Chemical Engineering Journal, 417, p.129355. **(Q1, IF = 16.744)** <Link>

[2]. Warne, G.R., Williams, P.M., **Pho, Q. H.,** Tran, N.N., Hessel, V. and Fisk, I.D., 2021. Impact of cold plasma on the biomolecules and organoleptic properties of foods: A review. Journal of Food Science, 86(9), pp.3762-3777. **(IF = 3.693)** <Link>

[1]. Anh, N.T.H., Phuc, T.T., An, T.N.M., **Pho, Q.H.** and Van Cuong, N., 2020. Microwave-assisted preparation of magnetic citric acid-sugarcane bagasse for removal of textile dyes. Indonesian Journal of Chemistry, 20(5), pp.1101-1109. <Link>

Conferences

[7]. **Pho, Q.H.,** Lin, L., Tran, N.N., Tran, T.T., Nguyen, A.H., Losic, D., Rebrov, E.V. and Hessel, V., 2022. Rational design for the microplasma synthesis from vitamin B9 to N-doped carbon quantum dots towards selected applications, the first 2022 CEAM HDR Conference, The University of Adelaide, Australia, 7 December, 2022. **(Oral Presentation)**

[6]. **Pho, Q.H.,** Lin, L., Rebrov, E.V., Sarafraz, M.M., Tran, T.T., Tran, N.N., Losic, D. and Hessel, V., 2022. Process intensification for gram-scale synthesis of N-doped carbon quantum dots immersing a microplasma jet in a gas-liquid reactor. Second International Conference on Unconventional Catalysis, Reactors and Applications, Warwickshire, United Kingdom, 21-23 Septemper, 2022. **(Oral Presentation)**

[5]. **Pho, Q.H.,** Lin, L., Tran, N.N., Tran, T.T., Nguyen, A.H., Losic, D., Rebrov, E.V. and Hessel, V., 2022. Rational design for the microplasma synthesis from vitamin B9 to N-doped carbon quantum dots towards selected applications, Seventh International Conference on Multifunctional, Hybrid and Nanomaterials, Genova, Italy, 19 – 22 October 2022. **(Oral presentation)**

[4]. **Pho, Q.H.,** Tran, N. N., Losic, D., Hessel, V., Gram-scale process of n-doped of carbon dots using microplasma: Recycling and purification, Chemeca 2021: Advance, Disrupt and Sustain: Advance, Disrupt and Sustain, Engineers Australia Barton, ACT2021, pp. 311-312. **(Oral Presentation)**

[3]. Fisk, I., Tran, N.N., Hessel, V., Warne, G., Williams, P., Schmidt, S. **Pho, Q.H.,** Development of a novel processing system for food personalisation during space travel, 43rd COSPAR Scientific Assembly. Held 28 January-4 February 43 (2021) 2058. **(Poster presentation)**

[2]. **Pho, Q.H.,** Tran, N. N., Losic, D., Rebrov, E, Hessel, V., Gram-scale process of n-doped of carbon dots using microplasma: Recycling and purification, The Warwick Engineering PGR Symposium, The University of Warwick, Conventry, United Kingdom, 12-17 July 2021. **(Poster presentation)**

[1]. **Pho, Q.H.,** Lin, L., Tran, N.N., Tran, T.T., Nguyen, A.H., Losic, D., Rebrov, E.V. and Hessel, V.,. Rational design for the microplasma synthesis from vitamin B9 to N-doped carbon quantum dots towards selected applications, Advanced Materials Workshop and Networking Event 2022: Research and Applications of Nanomaterials of Chemical Engineering Processes, National Wine Center, Adelaide, Australia, 2022. **(Poster Prensentation)**

Awards & Acheivements

[8]. **CEAM HDR Travel Grant**, School of Chemical Engineering and Advanced Materials, The Univerisity of Adelaide, 2022.

[7]. **DAAD Scholarship** for Research Exchange in Germany, 2022.

[6]. **Adelaide -Warwick University joint PhD award**, 2019-2023.

[5]. **"SCOPE" project travel grant** from European Comission, 2022.

[4]. **Excellence in Research Award (Poster Presentation),** Advanced Materials Workshop and Networking Event 2022: Research and Applications of Nanomaterials of Chemical Engineering Processes, National Wine Center, Adelaide, SA, Australia, 2022.

[3]. **The ECMS Faculty People's Choice Prize in 3-Minute-Thesis Competition**, Faculty of Engineering, Computer, and Maths Science, The University of Adelaide, SA, Australia, 2021.

[2]. Faculty of Engineering, Computer & Mathematical Sciences **(ECMS) Divisional Scholarship**, The University of Adelaide, SA, Australia, 2019.

[1]. **Full fee Scholarship**, The University of Adelaide, SA, Australia, 2019.

Administration and leadership

[1]. **Chair of CEAM HDR Comittitee** at School of Chemical Engineering and Advanced Materials, 2021-2022.
[2]. **Key board member** of Adelaide University Postgraduate Society, 2020-2021.
[3]. **CEAM HDR comittitee leader** of organizing members of the 1st CEAM HDR Conference, 7 December, 2022.

BLANK PAGE

Chapter 1

Introduction

This introductory chapter describes the motivation for considering the problems that this dissertation addresses and discusses the challenging nature of those problems. The chapter also summaries the contributions made in the following chapters and provides an overview of the dissertation's structure.

1.1. Abstract

The increasing world population and its demands for food, agriculture-based products, industrial activities, environmental degradation, and health care system are major challenges that government bodies will have to address in the future. Industrial production of fertilizers has become essential for agricultural crop productivity. Nitrogen-fixation process is key to overcoming the challenges of food demand and can generate new types of nitrogen-containing multifunctional materials for use in environmental treatment and health care. Non-thermal microplasma technology, which utilizes high-energy positively and negatively charged gases, has become an emerging material in nitrogen fixation processes because of its ability to break the triple bonds of dinitrogenous molecules in the air into active free nitrogen, which can react with water or hydrogen to form NH_3 or other related compounds and perform nitrogen doping on the surface of materials. Non-thermal microplasma technology can generate high-quality nitrogen-doped carbon quantum dots (NCQDs). NCQDs have shown promising potential in various applications, particularly in photocatalysis due to their ultrasmall size, water solubility and excellent optical properties, and their ability to strongly decompose pollutants in wastewater under solar irradiation can be enhanced by doping nitrogen on the surface of CDs, making them suitable for multifunctional uses in health care, pest control, and environmental treatment. The outstanding properties of NCQDs make them suitable for various applications, but fabricating these advanced materials using traditional synthesis techniques can be time-consuming and inefficient. Non-thermal microplasma technology is a key solution to overcome these challenges in creating CDs with suitable structures and properties for targeted applications. This study proposes to innovate a new kind of microplasma for synthesising N-doped carbon quantum dots using a microplasma jet-based reactor and aims to benefit from a commercial design with intended industrial use. The research aims to develop a new type of microplasma reactor that can rationally design N-doped carbon quantum dots from folic acid (vitamin B9) for selected applications while also exploring the massive synthesis and process intensification, and gaining deep insights into plasma catalysis in production processes.

1.2. Introduction

With an alarming rate of population escalation, a census has been reached that the world's population has currently passed 7.7 billion in 2019, and is predicted to increase by more than 9.7 billion in 2050, according to "the World Population Prospects 2019: Highlights" from United Nations Organization. Therefore, an increase by 50 – 80 % in crop production is estimated to high demand for food and agriculture-based products by 2050 [1]. This also means an emerging demand for an extremely large number of fertilisers and nanopesticides to facilitate the agricultural sector to adequately provide food for people worldwide. In addition, along with population growth, industrial activities, especially textile and food industries, have also been triggered to improve human life [2]. As a result, this will lead to environmental degradation due to contaminated wastewater leakage into surrounding groundwater from industrial zones [3]. According to a United Nations report on the state of the world's water, more than 5 billion people could suffer inadequate water supplies by 2050 because of several reasons related to global climate warming and contaminated soil, air and water resources [4]. In addition, with an increasing rate of population, it is estimated that the world's burden of health care is put on the government bodies. Therefore, health care, food demand and environmental deterioration are three foreseen challenges that all government bodies need to adequately control in the forthcoming future.

From the aspect of food supplies, agricultural production is still predicted to be a primary source of food demand by 2050. However, agricultural production has always confronted many unforeseen factors, such as global warming, degraded cultivating land, and pesticide-resisted phytopathogen that adversely affect crop productivity leading to approximately 40% of crop loss [5-7]. Consequently, this will result in a remarkable decrease in biodiversity and impairment of ecosystem functions needed for a green agroecosystem. Based on the emerging need for agricultural crop productivity, industrial production of fertilisers has become indispensable. Although nitrogen sources are abundant on earth, nitrogen provision as nutrients for plants is always challenging. It is a motivation to discover an alternative nitrogen fixation that converts nitrogen molecules in the air into nitrogen-containing compounds, that can be efficiently used as pesticides and/or fertilisers.

As far as environmental degradation is concerned, contaminated water with heavy metals [10] and dye wastewater [11] are always classified as one of the most problematic pollution groups due to their severe toxicity to human well-beings and natural habitats. With a remarkable growth in industrial activities due to the escalation of the world's population, a

tremendous amount of wastewater must be under the pre-treatment process before releasing into the natural environment. This is predicted to be challenging in the next few decades. Therefore, seeking an optimal solution to this environmental issue is essential for protecting our way of life. Among several wastewater treatment methods, photocatalysis degradation, also known as an advanced oxidation process, is one of the most effective and practical approaches in terms of energy-efficiency [12] and eco-friendliness [13, 14] due to their capacity to lessen undesirable effects on the environment. In advanced oxidation processes, highly reactive oxygen species, such as hydroxyl radicals (●OH), can decompose complex organic compounds into carbon dioxide, inorganic ions, and more simple structured compounds [15]. It has been recently noticed that introducing nitrogen into the surface of photocatalysts can enhance photocatalysis degradation in wastewater treatment [16]. Therefore, it is also a driving force to look for a nitrogen fixation process that can convert nitrogen from the air into nitrogen-containing compounds, that can be efficiently used as strong photocatalysts.

Regarding health care, breast cancer is a disease caused by the uncontrolled growth of cells that develop and form a tumour [17]. This tumour becomes oncogenic if cancer cells invade nor metastasize the blood or the network of lymphatic vessels. The limitations of current clinical imaging systems for diagnosis and conventional chemotherapy strategies for breast cancer treatment, such as the undesirable side effects to patients and the high-cost of treatment, bring about this phenomenon. Hence, a great effort has been made recently to develop new theranostic or multifunctional nanoparticles (NPs) to combat cancer disease more effectively. It also has been noticed that introducing nitrogen can enhance the intensity of photoluminescence of multifunctional nanoparticles [18], thus improving theranostic applications in cancer treatment. For this reason, nitrogen fixation also plays an important role in generating nitrogen-containing multifunctional nanoparticles for theranostic applications.

Mitigating issues in food demand, environmental degradation, and health care have become more and more challenging in the next decades. As discussed above, an alternative nitrogen-fixation is the key to overcoming these challenges. In other words, this nitrogen fixation process can generate a new type of nitrogen-containing multifunctional materials that can be used as fertilisers and/or nanopesticides, photocatalysts, and theranostic medicine.

In spite of being newly discovered in the last decade, carbon dots (CDs) have shown their more prominent potential in comparison with semiconductor quantum dots in many

applications, especially in photocatalysis due to their high-quality ultrasmall size [19-21], water solubility [22, 23] and excellent optical properties [24, 25]. CDs are able to strongly decompose pollutants in wastewater under solar irradiation [26-28]. In addition, it has been recently reported that the photocatalytic properties of CDs can be enhanced by doping nitrogen on the surface of CDs [29]. It is because the nitrogen atoms in CDs can provide excess electrons and inject them into CDs, thus increasing significant optical properties, especially fluorescence quantum yields. Therefore, it is strongly believed that this type of material can meet the requirement of new multifunctional materials as theranostic medicine in health care as fertilisers and/or nanopesticides in pest control and photocatalysts in environmental treatment.

Because of the outstanding properties of CDs for various applications, fabricating these advanced materials has become urgent. Various synthesis techniques have been used to fabricate CDs, such as laser ablation, arc discharge, hydrothermal, pyrolysis, solvothermal, ultrasonic, etc. Most of these CD synthesis strategies can be classified as the trial-and-error approach in searching for suitable applications. It is a time-consuming journey with cost- and process inefficiency to create CDs with suitable structures and properties available for a targeted application. Among these synthesis technologies, non-thermal microplasma technology is the key to overcoming these synthesis challenges.

Non-thermal microplasma technology with major components of high-energy positively and negatively charged gases has become emerging in nitrogen fixation processes because of several atmospheric pressure operations, non-equilibrium chemistry, important specific power densities, microscale geometries, and self-assembly phenomena. These properties make them particularly suitable for the cost-effective and highly efficient production of high-quality nanomaterials [30]. Firstly, it has been assumed that these charged gases and free radicals can break the triple bonds of dinitrogenous molecules in the air into active free nitrogen, which is ready to react with water or hydrogen to form NH_3 or other related compounds [31]. In addition, it is also proven that non-thermal microplasma can cause a chemistry reaction, which performs nitrogen doping on the surface of materials [32]. Secondly, non-thermal microplasma technology, previously much to energy-intensive, is slowly closing its energy- efficiency gap to industrial needs. It can be operated with high safety control because it is operated under atmospheric pressure and low temperature [33]. Therefore, it becomes more attractive for ammonia synthesis and, as a more disruptive industrial scenario, for nanofabrication [34-40]. There have been increasing findings

showing that confining plasma to a smaller size will result in new physical properties that conventional plasma could not possess. The electric field distributions are changed [41]. Plasma, which is confined to a millimetre size, is called microplasma. It is explained because of the increased ratio of surface to volume and the significantly decreased size and space; these are the winning points of microreactors, which are applied on an industrial scale these days. For this reason, in order to maintain the plasma at non-equilibrium state at atmospheric pressure and temperature, the operation parameters such as pressure, gas composition, input power and electrodes distance must be controlled.

As for such beneficial reasons of microplasma, in this study, it is proposed to innovate a new kind of microplasma for synthesising N-doped carbon quantum dots. This innovative idea is based on a microplasma jet-based reactor. We aim to profit from a commercial design with intended industrial use, developed by our plasma technology collaboration partner Ronny Brandenburg (Uni Greifswald, Germany) [42]. Microplasma jet (kINPen®IND) provides microplasma over the surface of the liquid. This research work generally attempted to develop a microplasma jet (kINPen®IND)-based reactor that could rationally design N-doped carbon quantum dots from folic acid (vitamin B9) for selected applications (nanopesticides and nanofertilizers). Mass synthesis of NCQDs has also been explored by means of process intensification. Also affected were the deep insights into plasma catalysis in production processes. It is characterized by emission spectroscopy.

1.3. Research Background

1.3.1. Nitrogen-fixation plasma

Nitrogen fixation process is defined as a nitrogen transformation in the atmospheric air into ammonia, nitrates, and other valuable nitrogen-containing substances (Figure 1) [43-45]. However, it is believed that most biological processes in nature cannot undergo the metabolization of these di-nitrogenous molecules because it is not easy to break their triple bonds and very stable electronic configuration [45]. In the 21st century, nitrogen fixation has become one of the most essential processes in the chemical industry due to outstanding applications of their nitrogen- fixed products, e.g. ammonia NH_3, in many industrial sectors. In terms of the history of nitrogen fixation, Joseph Priestley dating back in 1774, first discovered ammonia [46]. Over a decade later, William Austin attempted to synthesize ammonia for the first time, which is known as a chemical nitrogen fixation. Until 1880, Herman Hellriegel and Hermann Wilfarth first confirmed that living organisms could

biologically transform nitrogen in the air into nitrogenous compounds known as biological nitrogen fixation. In 1903, Kristian Birkeland and Samuel Eyde introduced a new nitrogen fixation process by passing air through an electric arc to produce nitrogen oxides. In 1909, Fritz Haber first tried synthesising ammonia from nitrogen and hydrogen gas. This process was scaled up to massive production by Carl Bosch, known as Haber-Bosch process, making it one of the most important processes in the 20th century. In 2014, the power consumption in the ammonia synthesis process was estimated from 33 to 36 GJ/ton N [44]. The Haber-Bosch process consumes 1-2% of all energy in this planet.

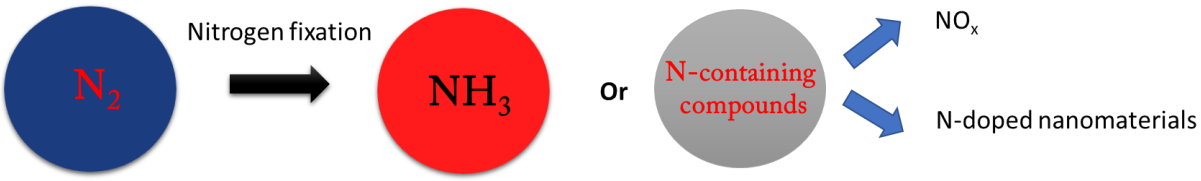

Figure 1. Nitrogen fixation process to convert nitrogen gas into other nitrogen-containing compounds

Recently, various types of plasma have received immense attention in the nitrogen fixation process, including thermal and non-thermal plasma nitrogen fixation [47]. Concerning the former, an illustrative example is the Birkland-Eyde process for nitrogen oxide synthesis, which utilizes an electrical arc discharge to form a high-temperature thermal plasma. However, the low energy efficiency of this process is challenging, leading to less progression in recent years. The key to any industrial application is to bring the energy efficiency of non-thermal plasma nitrogen fixation down to an industrially acceptable range, and the non-thermal plasma foreseen is on its way, allowing to keep reaction temperature and energy consumption relatively low [48]. Microplasma refers to a type of plasma that is smaller in scale than traditional plasmas, often on the order of micrometres or millimetres. In the context of nonthermal nitrogen fixation, microplasma may be used to create the high-energy conditions necessary to convert N_2 to a usable form without the need for high temperatures (Figure 2). Research in this area is still in its early stages, but it has the potential to be a sustainable and energy-efficient method for producing fertilizer.

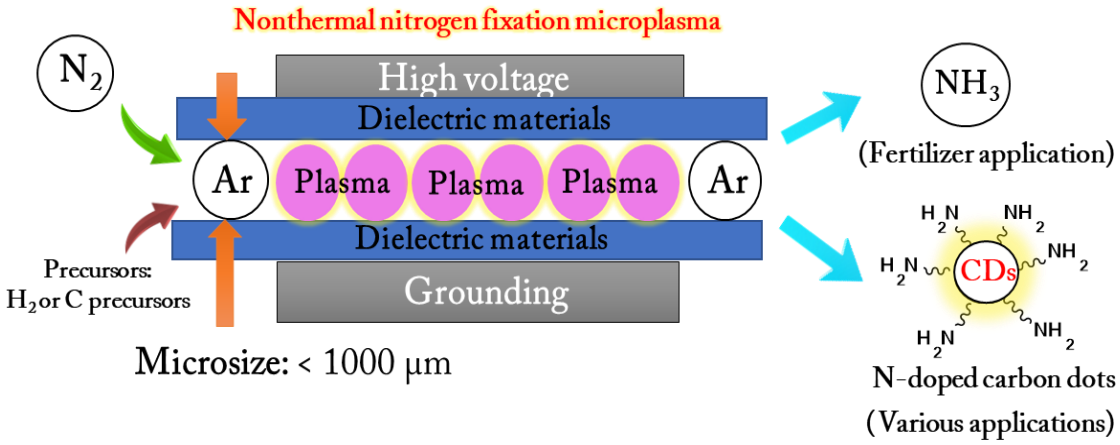

Figure 2. Nonthermal nitrogen fixation microplasma process

Nonthermal nitrogen fixation microplasma is a promising new approach to producing nitrogen-containing compounds. The process utilizes a microplasma to ionize the atmospheric nitrogen (N_2) to form reactive nitrogen species (RNS), which can then react with other molecules. The high energy conditions created by the microplasma can facilitate these reactions without the need for high temperatures traditionally required for nitrogen fixation.

One of the advantages of this approach is that it does not require the use of high-pressure vessels or catalysts, which can make the process more cost-effective and sustainable. Additionally, since it uses atmospheric nitrogen as the starting material, it does not rely on finite resources such as natural gas or coal. Currently, research on nonthermal nitrogen fixation using microplasma mainly focuses on laboratory-scale experiments, but there are ongoing efforts to develop a commercial-scale technology. It should be noted that this technology is still in the early stages of development and is not yet commercially available. In practice, nitrogen fixation and oxidation should both occur. This means that the surface of NCQDs is functionalised with NH_2 (nitrogen fixation) and -OH (oxidation). However, in order to improve the quantum yield and fluorescence intensity, nitrogen doping on the surface by nitrogen fixation plays a key role. Therefore, the author emphasises nitrogen fixation's importance in this study, as described in the thesis's title.

1.3.2. N-doped carbon quantum dots as an emerging advanced nanomaterial

Carbon-based materials are important in the field of materials science and have a wide range of applications. From traditional industrial carbon materials like activated carbon

and carbon black, to newer industrial carbon materials like carbon fibres and graphite, to newer carbon nanomaterials like graphene and carbon nanotubes (CNTs), research and applications of carbon-based materials have been popular due to their environmentally friendly properties. However, macroscopic carbon materials typically lack an appropriate band gap, making them poor candidates for use as fluorescent materials.

Carbon dots, or CDs, are an emerging material in the carbon family, which is zero-dimension carbon-based nanomaterials that measure less than 10 nanometres in size. They are a newly developed carbon nanomaterial made up of small, spherical particles. CDs were first found in 2004 during the purification process of single-walled carbon nanotubes [49] and were later named "carbon quantum dots" by Sun et al. in 2006 [50]. They are being considered for various applications [51-58] due to their unique structure and properties, such as simple synthesis methods and enhancement of fluorescence emission through surface passivation and chemical modification [59]. After their discovery, CDs gained a lot of interest due to their unique structure and properties. As a new form of carbon, they possess many advantageous qualities such as low toxicity [60], good compatibility with living cells [61], stability in chemical reactions [62], ability to efficiently absorb light [62], and efficient transfer of electrons when exposed to light [63]. These properties make CDs a highly promising material for a wide range of applications, including biosensors [64], bioimaging [65], optoelectronic devices [66], and solar cells [67].

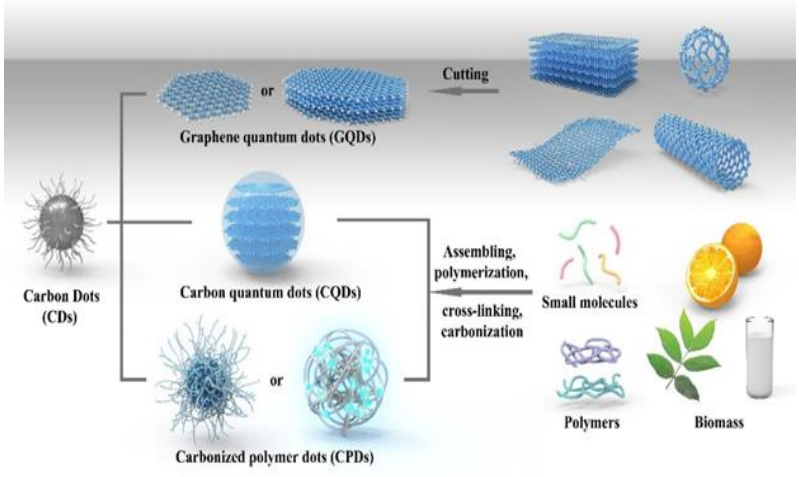

Figure 3. Classification of carbon dots based on their formation mechanism, micro-and nanostructures, and properties (This figure is adapted from [71], Copyright 2020, American Chemical Society)

Carbon dots, also known as small carbon nanoparticles that can be found in aqueous or other suspensions, are typically divided into three categories (Figure 3): graphene quantum dots (GQDs), carbon nanodots (CNDs), and carbonized polymeric dots (CPDs). The classification is not fixed; one type can be transformed into another by adjusting the graphene layers and carbonization degree. They are often composed of a hybridized sp^2/sp^3 carbon core with surface functional groups. For example, GQDs are composed of single or multiple layers of nanosized graphite, with functional groups or defects on the surface or at the edges. They have an anisotropic shape with larger lateral dimensions than height [68, 69]. The optical properties of GQDs mainly depend on the size of the π-conjugated domains and surface/edge structures [70].

In contrast to GQDs, CQDs and CPDs typically have a spherical core connected to surface groups. The spherical core of CQDs is composed of multiple layers of graphite. Their ability to emit light (photoluminescence) is primarily determined by the intrinsic state of luminescence and the quantum confinement effect of size [72]. CPDs combine aggregated/cross-linked carbon cores and polymer chain shells. The optical properties of CPDs are mainly influenced by the molecular state and cross-link structure [73].

The various structures of CDs are influenced by different synthesis methods, which can be broadly categorized into "bottom-up" and "top-down" strategies [71, 74-79]. CQDs and CPDs are often produced from small molecules, polymers, or biomass by assembling, polymerization, crosslinking, and carbonization via “bottom-up” methods (e.g., combustion, thermal treatment) [52, 80-82], while GQDs are typically obtained through "top-down" methods, such as cutting larger graphitized carbon materials into small pieces [83]. The surface functional groups of CDs can be altered by using different synthesis methods, allowing for tunable light emission. Additionally, the modified surface moieties of CDs allow for expansion of the light utilization range from different states of emissive trap due to their efficient up-converted photoluminescence behaviour [84], meaning that efficient visible-light-responsive CDs can be designed to utilize the full spectrum of sunlight. Furthermore, the ability of CDs-based composites to absorb light improves photocatalytic efficiency through photoexcited electron transfer [85].

Non-doped or pristine carbon dots (CDs) and N-doped CDs have some key differences in their properties due to the presence of nitrogen atoms in the latter. Here are some comparative differences between non-doped and N-doped CDs:

- Optical Properties: N-doped CDs have red-shifted absorption and emission spectra compared to non-doped CDs. This is due to the incorporation of nitrogen atoms into the carbon matrix, which creates new energy levels in the electronic band structure of the CDs. The presence of nitrogen also enhances the quantum yield and stability of the CDs.
- Chemical Properties: The introduction of nitrogen atoms in CDs changes their chemical properties, such as surface charge, hydrophilicity, and chemical reactivity. N-doped CDs tend to have a more hydrophilic surface due to the presence of polar nitrogen atoms, making them more biocompatible and suitable for biological applications.
- Electronic Properties: N-doped CDs have a higher electron density and electrical conductivity than non-doped CDs due to the doping of nitrogen atoms. Nitrogen also enhances the CDs' electron transfer properties, making them useful for applications in electrochemistry and energy storage.
- Morphology: N-doped CDs tend to have larger particle sizes and a more spherical morphology than non-doped CDs. This can be attributed to the introduction of nitrogen atoms, which can influence the growth and morphology of the CDs during synthesis.

Defects in the carbon dot (CD) structure (i.e. N-doped carbon dots) can have an impact on their optical, electronic, and chemical properties. However, the synthesis of CDs is a relatively new field, and there is still ongoing research into the factors that influence the formation of defects in CDs. Here are some strategies that have been proposed to reduce or control crystal defects in CDs:

- Precursor and Synthesis Conditions: The choice of precursor and synthesis conditions can have a significant impact on the formation of defects in CDs. Careful selection of the carbon source and the reaction conditions, such as temperature, time, and pH, can reduce the formation of defects. For example, using a carbon source with a high degree of purity and controlling the reaction temperature can help minimize the formation of defects.
- Post-Synthesis Purification: Purification of CDs after synthesis can help eliminate or reduce the number of defects. Purification methods such as dialysis or centrifugation can help remove impurities and stabilize the CDs, improving crystal quality.

- Doping: Doping of CDs with heteroatoms, such as nitrogen, can modify the electronic properties of the CDs and reduce the formation of defects. Nitrogen-doped CDs have been shown to have improved optical and electronic properties compared to non-doped CDs, which can be attributed to the reduced number of defects.
- Surface Passivation: Surface passivation can be used to reduce the formation of surface defects in CDs. Coating the surface of CDs with a layer of a passivating material, such as silica or polymers, can protect the CDs from oxidation and reduce the formation of surface defects.

1.3.3. Properties of N-doped carbon quantum dots

CQDs are commonly classified into three types: GQDs, CQDs, and CPDs. These types are defined in terms of their "core-shell" nanostructure, which consists of a nanoscale carbon core and surface functional groups. The optical properties, electronic properties, and catalytic properties of CQDs are determined by their different structures. GQDs have high quantum yield and strong fluorescence, CQDs have good biocompatibility and stability, and CPDs have high surface area and catalytic activity (Figure 4).

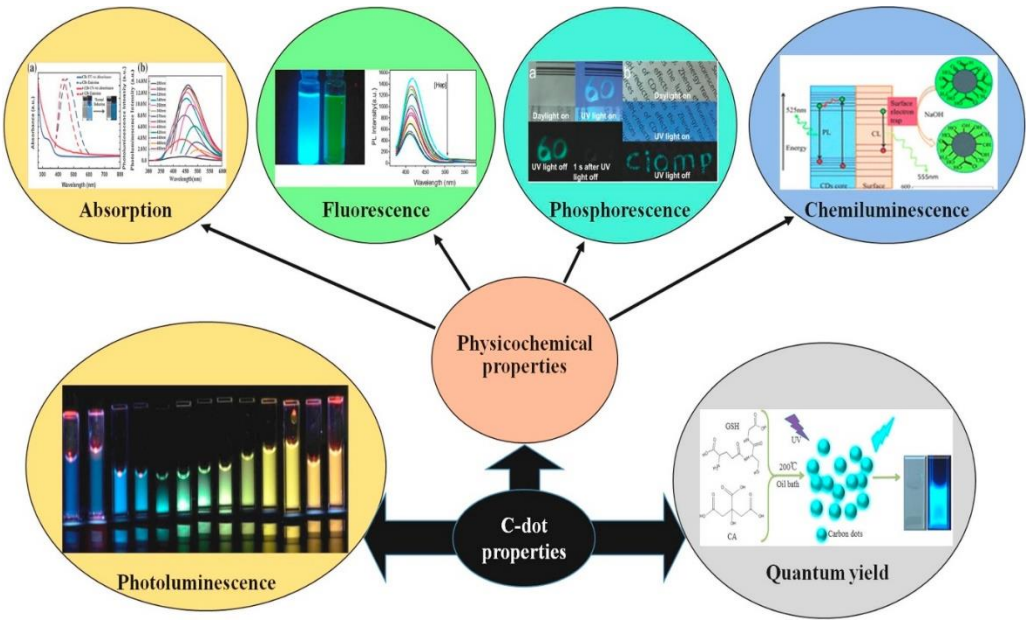

Figure 4. Outstanding properties of carbon dots based on their surface and core structure (this figure is adapted from the original work [86], copyright 2018, Elsevier)

1.3.3.1. Adsorption

CDs have strong optical absorption in the ultraviolet (UV) region (mainly 280–360 nm). Surface modifications can regulate the absorption band of CDs, and the emission properties of CDs generally depend on the level of excitation [87]. Surface functional moieties play an important role in determining the absorption ranges of CDs. Passivating CDs with polyethyleneimine (PEI) can produce red (330–355 nm), blue (460–495 nm) or green (530–550 nm) luminescence. However, the nonuniformity of PEI passivation on CDs can disrupt the photoluminescence and cause excitation at longer wavelengths [88]. CDs show optical absorption in the UV region and some traces of absorption in the visible region. Top-down fabricated CDs show size-dependent absorption from 200 to 252 nm (6.20–4.92 eV) with an increase in diameter from 12 to 22 nm. However, CDs fabricated from the same material but using different fabrication techniques, such as microwave, ultrasonic, and hydrothermal approaches, show different absorption bands within the 250–300 nm range [89].

1.3.3.2. Fluorescence property

The fluorescence emission of CQDs is one of their most attractive features and has been used in various fields. CQDs have properties such as excitation wavelength-dependent PL emission, tunable PL emission, extraordinary up-converted PL, good fluorescence stability and efficient photobleaching resistance. The PL emissions of CQDs are dependent on their structural characteristics. They can be divided into two categories: one is due to electron transitions corresponding to internal factors dominated emission, which includes the conjugation effect, the surface state and the synergistic effect [90]. This model is suitable for explaining the PL of GQDs with lattice structures or a high degree of graphitization. GQDs have a certain degree of crystallinity and an average lattice parameter of 0.24 nm. The PL emission of CQDs can be tuned by adjusting the size of the conjugated π-domains rather than the actual particle size, as their sizes are smaller than their exciton Bohr radius [91]. The quantum confinement effect of GQDs was supported by theoretical calculations method, as reported by Sk et al., who studied the PL emission of pristine zigzag-edged GQDs with different diameters using Gaussian and time-dependent density-function theory (DFT) [91]. The wavelength of photoluminescence (PL) emissions of graphene quantum dots (GQDs) can vary depending on their diameter. The smallest GQDs with a diameter of 0.5 nm have a wavelength of 235.2 nm, while GQDs with a diameter of 2.31

nm has a wavelength of 999.5 nm. The PL emission of GQDs is observed in the entire visible region (400-770 nm), with the different diameters of GQDs increasing from 0.89 to 1.80 nm, which is attributed to the quantum confinement effect. This particle size dependence is consistent with the quantum confinement effect. The intrinsic state of GQDs also determines their PL emission behaviour due to the quantum confinement effect. The conjugated π-domains are regarded as intrinsic PL centre. The band gaps of GQDs decrease as aromatic rings increase, indicating that PL emissions of GQDs can be adjusted by tuning the size of the conjugated π-domains. By changing the size or shape of GQDs, the electronic transitions can be tuned in nanometer-sized GQDs [92, 93].

In addition to the quantum confinement effect, the surface configurations or surface/edge state of GQDs can also play a key role in the photoluminescence (PL) emission of GQDs [94]. Surface defects, triple carbene at the zigzag edges, and oxygen-containing/other functional groups can induce PL emission with different characteristics. Heteroatom doping is also used to alter the electronic structures of GQDs and is also attributed to the surface state effect [95]. The PL emission of GQDs can also be pH dependent. It can be affected under a strongly acidic atmosphere due to protonation or deprotonation of functional moieties on the surface of the carbon core-edge state. Different types of organic solvents can also lead to different surface passivation, resulting in different PL emission characteristics [96]. Ding and co-workers proposed a hydrothermal method to prepare a series of GQDs with similar size distributions [61]. These GQDs show surface oxidation-dependent PL emission in the 440-625 nm wavelength range and have potential applications in different fields. The independent PL emission of GQDs is attributed to the presence of a self-passivated layer. Lin et al. discovered that GQDs with zigzag edges have smaller energy gaps than those with armchair edges. PL emission likely originated from triple carbene states instead of quantum confinement effects, which can be quenched and recovered under acidic or alkaline conditions [97].

In addition to the previously mentioned properties of GQDs, it has also been discovered that the hybridization of amine moieties and the carbon core can tune the PL emission [98]. This is due to the modified electronic structure of GQDs through the effective orbital resonance effect. Density functional theory calculations have shown that this method can also decrease the band gap of GQDs. Jin et al. also found that GQDs have two independent molecule-like states attributed to the surface moieties' structure, further emphasizing the impact of the surface state on PL emission. It is important to note that an

individual effect cannot fully explain PL emission in GQDs and that synergistic effect models have been proposed to interpret the PL emission mechanism of CDs.

The PL emission mechanisms of CQDs (carbon quantum dots) have been found to include various factors, such as the carbon core and surface state, the conjugation effect and surface functional groups, and the conjugation effect and defects. These mechanisms are thought to originate from the surface/edge state and conjugated π-domains. However, Wang et al. proposed that the PL behaviours of GQDs are likely associated with oxygen-containing functional moieties on the surface of the carbon core, as determined by single-particle spectroscopic measurements [99]. The photoexcited electrons relax from π* orbit to sp^2 intrinsic and defect states, resulting in blue and green PL emissions, respectively.

1.3.3.3. Phosphorescence

CDs have been shown to have phosphorescence properties when used as a water-soluble material. When mixed with a matrix of polyvinyl alcohol (PVA), CDs exhibit clear phosphorescence under UV light. The phosphorescence is believed to be caused by the presence of aromatic carbonyl groups on the surface of the CDs, which provide a triplet excited state [79]. In other words, the phosphorescence observed in CDs is primarily caused by the radiation transition of the triplet excited state (Tn). As shown in Fig. 1, initially, electrons in the ground state (S_0) are excited and transferred to the singlet excited state (Sn). Then, the electrons relax to the lowest singlet excited state (S1), where they reach Tn through an intersystem crossing (ISC) process. Finally, the electrons fly back from T_1 to S_0 and generate phosphorescence. Deng et al. also reported on the phosphorescence properties of a CD-based water-soluble phosphorescent material, and found that clear phosphorescence is detected at room temperature.

1.3.3.4. Chemiluminescence

The chemiluminescence of CDs is used for the determination of radioactive substances. The intensity of the chemiluminescence depends solely on the concentration of CDs within a certain absorption range. For example, Lin et al. mixed CDs with oxidants, including cerium and potassium permanganate ($KMNO_4$), resulting in the chemiluminescence of the CDs [100]. Reversely, Zhao et al. reported that CDs have excellent electron-donating properties towards dissolved oxygen to generate reactive oxygen

species (O_2^-) in strong alkali solutions, such as NaOH or KOH, which results in chemiluminescence.

1.3.3.5. Photoluminescence

Photoluminescence (PL) is one of the most outstanding features of CDs. While there is an ongoing debate about the source of PL in CDs, it is known that a key aspect is a diameter of less than 10 nm and a zero-dimensional structure. CDs' morphology, composition, size, and crystalline nature also affect their PL properties, which are determined by the initial precursors and fabrication techniques used to form the CDs [101]. Researchers have reported enhanced PL properties in CDs through surface modulation. New fabrication strategies, such as exposure to a single UV light, have been developed to produce CDs that emit blue, green, and red light. Nitrogen-doped CDs have been fabricated using a one-step hydrothermal treatment with m-aminobenzoic acid as a precursor for the detection of iron ions. They have been found to have a charge density that changes according to their electron richness, leading to higher QY (quantum yield) and a stronger peak of PL at 415 nm [102].

1.3.3.6. Optoelectronic properties

The optoelectronic properties of carbon dots are highly dependent on their surface chemistry. The surface chemistry of CDs can be modified by various chemical functionalization strategies such as surface oxidation, surface passivation, and surface doping. These modifications can alter CDs' chemical composition, surface charge, and surface energy, leading to changes in their optoelectronic properties. One of the key optoelectronic properties of CDs that is affected by surface chemistry is their fluorescence emission. The fluorescence emission of CDs is highly dependent on the surface functional groups present on their surface. For example, CDs functionalized with carboxylic acid groups exhibit a blue-shifted emission spectrum compared to CDs functionalized with amine groups, which exhibit a red-shifted emission spectrum. This difference in emission wavelength can be attributed to the variation in the surface energy of CDs with different surface functional groups.

Another optoelectronic property that can be affected by surface chemistry is the absorption spectrum of CDs. CDs with different surface chemistries exhibit different absorption spectra due to the variation in the electronic band structure of the CDs. For example, CDs

functionalized with nitrogen-doped groups exhibit a red-shifted absorption spectrum compared to undoped CDs, which can be attributed to the introduction of new energy levels in the electronic band structure of the CDs.

1.3.3.7. Quantum Yield

Carbon dots (CDs) have been found to exhibit high fluorescence quantum yields (QYs) in the range of 50-90%, depending on the synthesis method and surface chemistry of the CDs. These high QYs are due to the presence of quantum dots (QDs) within the CDs, which act as efficient light-emitting centres. Several factors can affect the quantum yield of CDs, including the size and shape of the QDs, the surface chemistry of the CDs, and the environment in which they are used. For example, the surface modification of CDs can greatly enhance the fluorescence quantum yield by reducing the nonradiative relaxation pathways. Moreover, it was reported that the QY of CDs could be increased by controlling the size and shape of the CDs and by functionalizing their surfaces with molecules that can improve their stability and biocompatibility. Overall, carbon dots (CDs) have been found to exhibit high fluorescence quantum yields (QYs), which make them useful for a wide range of applications in fields such as imaging, sensing, and biotechnology. However, it's important to note that the QY of CDs may vary depending on the synthesis method, surface chemistry, and the environment in which they are used.

1.3.4. Various synthesis methodologies of N-doped carbon dots

Various methods have been proposed in recent years to create CDs with specific properties for different applications. These methods can be broadly categorized into two types: "top-down" and "bottom-up" (Figure 5).

Top-down methods involve techniques such as ultrasonic synthesis, chemical exfoliation, electrochemical oxidation, arc-discharge, and laser ablation, to exfoliate and cut macroscopic carbon structures, like graphite powder, carbon black, activated carbon, carbon nanotubes, carbon soot, and carbon fibres, to produce GQDs, which are 2D nanoparticles [103]. In contrast to top-down methods, bottom-up methods typically involve the polymerization of molecular precursors, such as glucose, sucrose, and citric acid, through techniques like microwave pyrolysis, solvothermal reactions, plasma treatment, and chemical vapour deposition to produce CQDs and CPDs, which are 3D nanoparticles with spherical

cores [103]. These methods are generally faster, more controllable, and less expensive than top-down methods.

Additionally, bottom-up methods often produce fewer defects and have high controllability. Here, we will delve into the primary methods for synthesizing CDs, controlling their size, and modifying their surface properties through confined pyrolysis and modification techniques. The surface properties of CDs can also be optimized during preparation or through further treatment for specific applications.

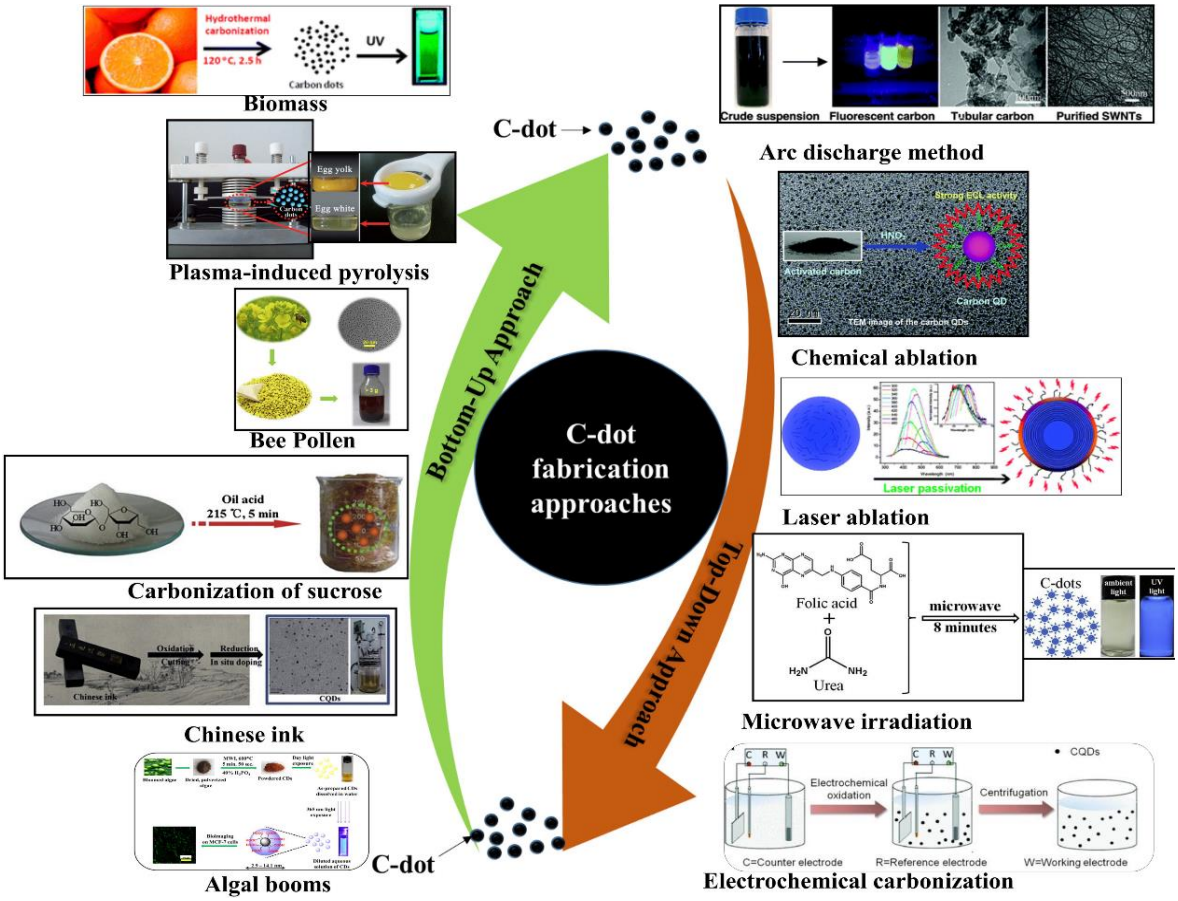

Figure 5. Various synthesis approaches of carbon dots (This figure is adapted from the original work [86], copyright 2018, Elsevier)

Based on the literature review, all of the reported large-scale microplasma syntheses of NCQDs are batch-type reactor configurations. Therefore, the flow-type reactor was not discussed and assessed in this study. However, the authors also found that a flow-type reactor or microplasma microfluidic device is an advanced and scalable technology. Therefore, the

authors also discussed this novel technology in another topic "Microfluidic plasmas: Novel technique for chemistry and chemical engineering" by Lin et al. 2021.

Controlling the reaction time, heat, and mass transport in a static batch-type reactor require careful monitoring and management of the operating conditions, mixing system, and heating or cooling system. By optimizing these factors, you can improve the efficiency and effectiveness of the reaction. The following steps are suggested to control reaction time and heat and mass transport in a static batch-type reactor:

- Set the operating conditions: Before starting the reaction, set the desired temperature, pressure, and concentration of reactants. These operating conditions will play a critical role in determining the reaction time, heat, and mass transport.
- Monitor the temperature: Use a thermometer to monitor the temperature inside the reactor. If the temperature deviates from the desired set point, adjust the heating or cooling system accordingly to maintain the temperature.
- Control the reaction time: The reaction time can be controlled by monitoring the progress of the reaction. You can use techniques such as sampling, pH monitoring, or turbidity to determine the completion of the reaction. Adjust the reaction time by extending or reducing the time allowed for the reaction to take place.
- Manage mass transport: The mixing system plays a critical role in managing mass transport. Ensure that the reactor is properly mixed to prevent concentration gradients from forming. If concentration gradients do form, adjust the mixing speed or add baffles to the reactor to help promote mixing.
- Manage heat transport: The reactor's design and heating or cooling system will affect heat transport. Ensure that the reactor is designed to promote efficient heat transfer. If heat is not being transferred effectively, adjust the reactor's design or heating/cooling system accordingly.
- Optimize the reaction conditions: Adjust the operating conditions to optimize the reaction. This may include changing the concentration of reactants, adjusting the temperature or pressure, or modifying the mixing system.
- Control byproduct formation: Monitor the reaction for the formation of byproducts. Byproducts can affect the reaction time, heat, and mass transport. Adjust the reaction conditions or use a catalyst to prevent byproduct formation

1.3.4.1. Top-down approaches

Chemical exfoliation. It is a simple and efficient method for the mass production of high-quality CDs without complex equipment. This method clears precursor carbon materials such as carbon fibres, graphene oxide, and carbon nanotubes by strong acids or oxidizing agents. Mao and co-workers were the first to create fluorescent GQDs with different sizes from candle soot using HNO_3 at a relatively high temperature in 2007 [104]. Later, Peng et al. used H_2SO_4 and HNO_3 to prepare GQDs through the chemical exfoliation of carbon fibres [105]. The resulting GQDs with different size ranges showed yellow, green, and blue PL emissions under different stirring temperatures, indicating that chemically cleaving carbon fibres can successfully prepare GQDs. Researchers have also used low-cost materials as precursors to prepare GQDs under strong acid conditions. For example, Ye and his team used coal to prepare hexagonal GQDs with a size range of 3-6 nm. Zhao et al. also used asphaltene to fabricate GQDs with excitation-dependent PL emission. However, it is tedious to further purify the product by removing excess H_2SO_4, which increases the overall synthesis cost [106].

Laser ablation. It is a unique and promising synthesis method for CDs due to its short period and simple operation. Sun et al. were the first to use laser ablation to synthesize GQDs from graphite [59]. Li et al. used rapid laser passivation of carbon particles to prepare GQDs with visible, stable, and tunable PL performance [107]. They also showed that passivation by laser irradiation significantly impacts the origin of PL. Similarly, Hu et al. proposed a simple method to synthesize fluorescent carbon nanoparticles by laser ablation of carbon powder suspensions in organic solvents [108]. The surface of the resulting GQDs can be modified by choosing appropriate solvents, which allows for tuning the PL emission of the GQDs by changing their surface functional groups. Kang proposed a rapid method to synthesize GQDs from multi-wall carbon nanotubes with excellent optoelectronic properties [109]. The synthesized GQDs show stable blue PL emission and a PL quantum yield of 12%, making them suitable for optoelectronic applications. Ren et al. used laser ablation of carbonized Platanus biomass in a formamide solution to prepare NM-CQDs, which showed dual-wavelength PL emission [110]. They also proposed an ultrafast method to fabricate homogeneous CQDs through dual-beam pulsed laser ablation, which improves preparation efficiency. A schematic diagram of the synthesis of CQDs from carbon fibre is also presented.

Ultrasonic-assisted method. It is a low-cost and simple method for preparing CDs. Alternate high-pressure waves and low-pressure are generated in the ultrasound process, which results in the formation and collapse of small bubbles in the liquid. These bubbles produce strong hydrodynamic shear forces that cut macroscopic carbon materials into nanoscale CDs. Researchers can prepare CDs with different properties by adjusting the ultrasonic power, reaction time, and the ratio of carbon sources and solvents. Zhuo et al. first reported the preparation of GQDs through ultrasonic exfoliation of graphene [111]. Since then, many researchers have used ultrasonic-assisted treatment to prepare GQDs from carbon materials such as graphite, MWCNTs, GO, and carbon fibre in either aqueous or organic solvents. Song and his team prepared GQDs from the aqueous dispersion of graphite and potassium sodium tartrate by ultrasonic-assisted treatment, which showed blue luminescent emission [112]. The ultrasonic approach also fabricated heteroatom-doped GQDs. Zhao et al. synthesized chlorine-doped GQDs from chlorinated CF precursors through direct ultrasonic exfoliation [113]. Carbon-containing waste materials, such as food waste, have also been used to prepare CQDs through ultrasonic irradiation treatment. Park et al. synthesized water-soluble CQDs from food waste-derived carbon sources and found that about 120g of CDs with an average diameter of 2-4 nm could be produced from a 100 kg mixture of ethanol and food waste [114]. These CDs have good PL properties, low cytotoxicity and high photostability for in vitro bioimaging.

1.3.4.2. Bottom-up approaches

Microwave-assisted synthesis. It is a cost-effective and efficient method for synthesizing CDs. Using microwaves can provide uniform heat for the formation of CDs. Li et al. were the first to use this method to synthesize green fluorescent GQDs using microwave-assisted chemical cleavage of GO sheets under acidic conditions [115]. The obtained GQDs with a single-layer have an average diameter of 4.5 nm, and can be further designed to have blue fluorescent properties by reducing surface radical moieties. Wang and co-workers reported a simple one-pot microwave-assisted approach to fabricate water-soluble CDs from protein-rich eggshell membranes [116]. The resulting CQDs show excellent fluorescence emission with a quantum yield of about 14% and can simultaneously detect Cu^{2+} and glutathione. Yao et al. proposed a new route to produce novel fluorescent CQDs from transition-metal ions and crab shells using microwave-assisted hydrothermal [117]. The resulting Gd@CQDs display high stability against pH and NaCl concentration,

indicating potential application in drug delivery. CDs were also obtained from Mangifera indica leaves by a simple microwave-assisted hydrothermal, which possess good biocompatibility and high photostability and can be used as an intracellular temperature sensor. Wang et al. proposed a two-step microwave heating process to produce CDs from raw cashew gum, which have good biocompatibility and low cytotoxicity and can be used in live-cell imaging [118].

Hydrothermal synthesis. It is a cost-effective and non-toxic method for preparing CDs. It is a simple approach to synthesize CQDs where a mixture of water solution is enclosed in Teflon and heated at high pressure and high temperature [119]. Pan et al. were the first to use this method to prepare blue fluorescence CQDs [95]. Epoxy moieties on the surface of GO sheets were completely broken down into CQDs during hydrothermal treatment. Subsequently, Zhao's group reported a simple and highly efficient route to prepare CQDs by hydrothermal treatment [120]. Some researchers also utilized oxidants to accelerate the hydrothermal reaction. For example, Halder et al. reported a simple hydrothermal method to prepare GQDs by adding H_2O_2 to accelerate GO sheets' exfoliation, indicating effective scissors of the GO sheets by H_2O_2 during hydrothermal reaction [121]. Mehta et al. used a plant-based hydrothermal route to synthesize water-soluble fluorescent CQDs from Saccharum officinarum juice, which were used to detect Cu^{2+} [122]. Lu et al. proposed a hydrothermal route to produce CQDs from pomelo peel, which was used to detect Hg^{2+} in lake water samples [123].

Solvothermal synthesis. This preparation method of CDs has the advantages of low-cost and simple equipment compared to the hydrothermal method [124]. This method replaces water solution with one or several solvents sealed with Teflon equipped with a steel autoclave. Zhu et al. used this method to prepare green fluorescent GQDs with a PL quantum yield of 11% [125]. Shin and co-workers chemically oxidized natural carbon precursors by using ozone as a non-acid mild oxidant, resulting in GQDs with a high quantum yield and blue PL emission [125]. Tian et al. synthesized blue fluorescent GQDs by solvothermal exfoliation of graphite with the help of mild H_2O_2, which showed a high quantum yield of 15% and good photoluminescence stability in different pH conditions [126]. Liu and his co-workers established a green one-step solvothermal route to fabricate CQDs from L-ascorbic acid and glycol solution in an autoclave at 160 °C for 4 h, which exhibited a strong green fluorescent emission for cell labelling [127].

Pyrolysis. It is a powerful technique for fabricating fluorescent CDs using macroscopic carbon structures as precursors. This method offers the advantages of short reaction time, low cost, easy operation, solvent-free approaches and scalable production. The four main processes, heating, dehydration, degradation and carbonization, are critical for converting organic carbon-containing substances into CQDs under high temperatures. Carbon precursors are cleaved into carbon nanoparticles using high-concentration alkali or acid in the pyrolysis process. Ma et al. fabricated N-GQDs by the direct carbonization of ethylene diaminetetra acetic acid at 260–280 °C and proposed a growth mechanism for GQDs [128]. Various types of CQDs were reported by ion doping; for example, Li and co-workers fabricated Cl-GQDs by introducing HCl through the dehydration and formation of GQD nuclei under hydrothermal treatment [129].

Chemical vapour deposition (CVD) method. It is used to fabricate CQDs, which has recently been widely explored. The size of the ultimate product can be determined by tuning parameters, including the carbon source, growth time, the flow rate of hydrogen (H_2) and temperature of the substrate. Fan et al. proposed the CVD method to prepare CQDs using methane as a carbon source [130]. Specifically, oxidation groups on the surface of a copper foil were cleaned using alcohol and HCl. Then, the substrate was heated to 1000 °C in H_2 and Ar ambient conditions. H_2 supply was turned off, and Ar was continuously supplied to remove H_2 residues. Afterwards, methane gas (CH_4) was pumped in the furnace at a flow rate of 2 mL/min for only 3 s in an Ar environment. The size of the as-synthesized CQDs was distributed in the range of 5–15 nm, and the height profile thereof was 1–3 nm, indicating the successful preparation of few-layer-thick CQDs.

1.3.5. Characterisation methods of N-doped carbon quantum dots

CQDs, or colloidal quantum dots, are semiconductor nanomaterials with different structures depending on the precursor used to produce them. The size of CQDs can also be adjusted by using different nanocomposites. There are several analytical techniques (Figure 6) that can be used to characterize CQDs, including UV-vis spectroscopy, fluorescence spectroscopy, transmission electron microscopy (TEM), x-ray diffraction (XRD), Fourier transform infrared spectroscopy (FTIR), dynamic light scattering (DLS), atomic force microscopy (AFM), and x-ray photoelectron spectroscopy (XPS) [130]. These techniques can be used to study various properties of CQDs, such as size, composition, crystal structure, and surface chemistry.

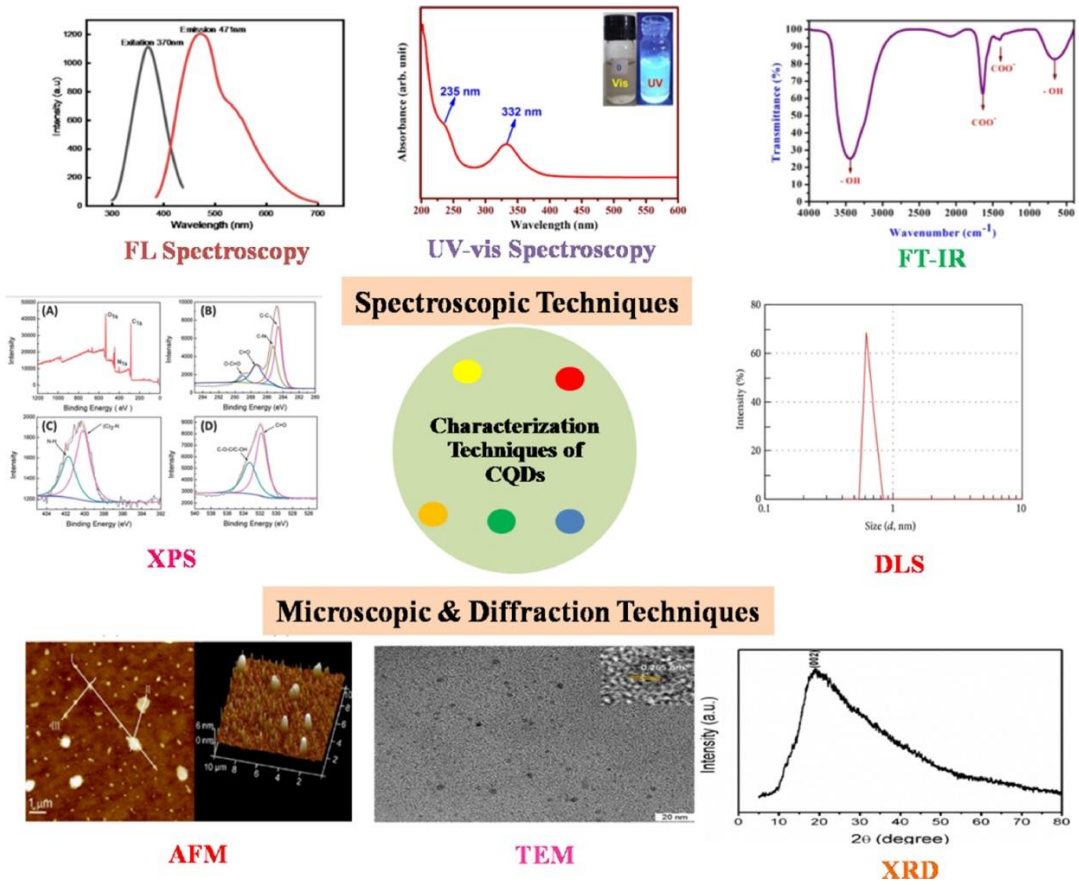

Figure 6. Characterisation technique for analysing the properties of NCQDs (This figure is adapted from the original work [131], Copyright 2022, Elsevier Publishing)

CQDs are typically small particles between 1 and 10 nm in size and are composed of elements such as C, H, O, and N. TEM and AFM are commonly used to analyse the size distribution of CQDs. XPS and EDX are used to confirm the composition of CQDs, while XRD patterns reveal the amorphous or crystalline structure of the particles. FTIR is used to identify the functional groups present in CQDs, such as C-O-C, COOH, C-OH, C-H, and C-C. UV-vis and fluorescence spectroscopy are used to study the optical properties of CQDs, such as absorption, emission, and excitation peak, typically observed at 280–451 nm, 340 nm, and 480 nm.

1.3.6. Microplasma-assisted synthesis of N-doped carbon quantum dots

Despite being discovered in the last decades, NCQDs have become one of the most advanced materials, which can be used for various applications. For this reason, many different fabrication methods have been attempted to produce high-quality N-doped carbon quantum dots. Microplasma synthesis is a method for producing carbon quantum dots

(CQDs) using a low-temperature plasma. Recently, the microplasma system has shown its significant advantages in producing N-doped carbon quantum dots. Microplasma synthesis is a relatively simple and low-cost method for producing CQDs and can be easily scaled up for large-scale production. The method involves using a low-temperature plasma, typically generated by a radio frequency (RF) or microwave discharge, to vaporize a carbon-containing precursor. The resulting carbon atoms then condense to form CQDs. N-doping, or the introduction of nitrogen atoms into the CQDs, can be achieved by using a nitrogen-containing precursor such as urea or melamine in the synthesis process. The amount of nitrogen doping can be controlled by adjusting the ratio of the carbon and nitrogen precursors. The nitrogen atoms can be distributed throughout the CQDs in different forms (pyridinic, pyrrolic or graphitic). N-doped CQDs have been shown to have improved optical and electronic properties compared to non-doped CQDs, making them useful in various applications such as bioimaging and solar cells.

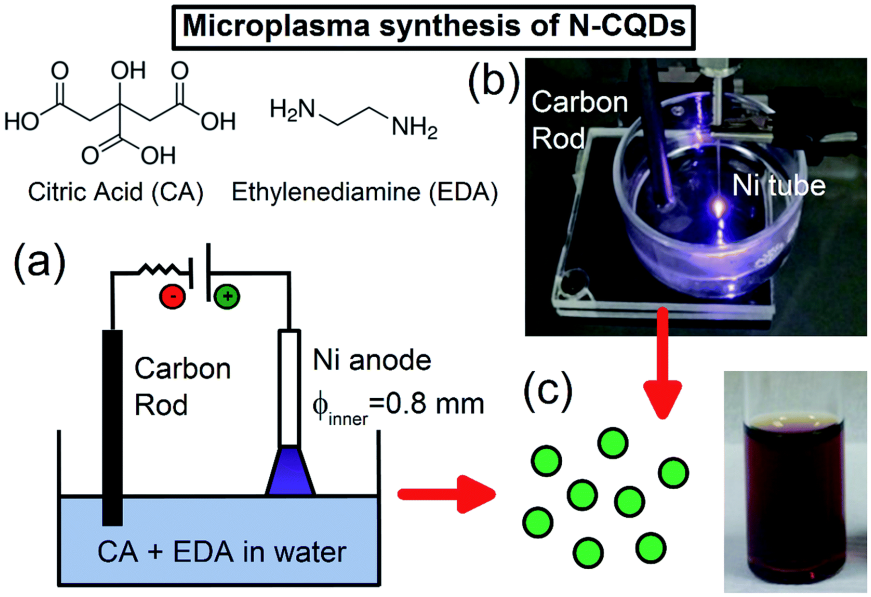

Figure 7. Microplasma synthesis of nitrogen-doped carbon dots (NCQDs) from molecular precursors, (a) schematic of the setup used, (b) digital photograph of the microplasma–liquid interaction and (c) the NCQDs produced from this setup with 1.05 g citric acid and 556 µL ethylenediamine dissolved in 10 mL water. (This figure is adapted from the original work [132], Copyright 2017, RSC Publishing)

Plasma-assisted microplasma synthesis of N-doped carbon quantum dots can either carry out in the form of an indirect or direct plasma-liquid interaction system. Indirect

plasma-liquid interaction indicates a system with a plasma generation above the electrolyte solution's surface. In contrast, direct plasma-liquid interaction is described as a setting where plasma is formed within the liquid. In a study, microplasma under atmospheric pressure generated from indirect plasma-liquid interaction produces N-doped CD (Figure 7) [132]. Citric acid (CA) and ethylenediamine (EDA) as starting materials. Typically, a given amount of citric acid (CA) and ethylenediamine (EDA) is used to dissolve in deionized water. Later, a microplasma produced by a DC power under atmospheric pressure is set above the solution's surface.

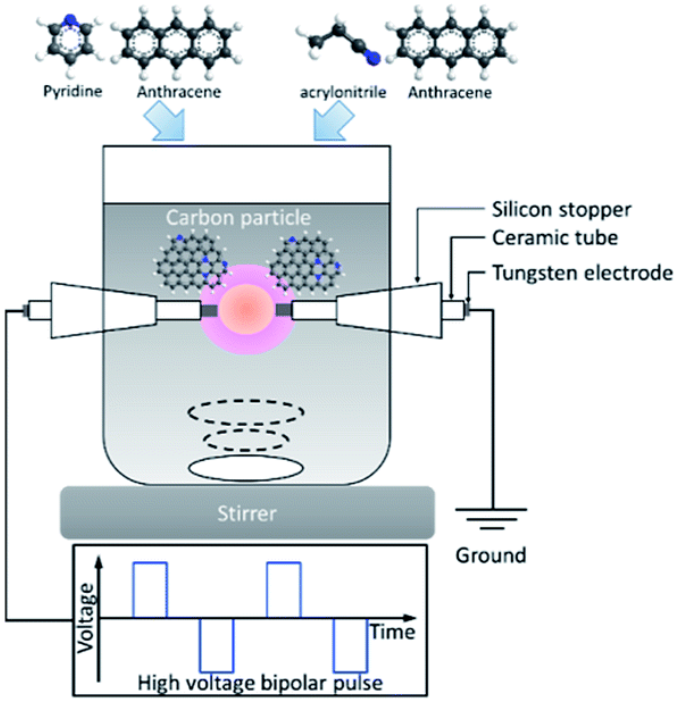

Figure 8. Schematic image of the experimental setup of direct plasma-liquid interaction with various types of precursors. (This figure is adapted from the original work [133], Copyright 2017 RSC Publishing)

Regarding direct plasma-liquid interaction, the use of plasma gas is indispensable. Two types of the most well-known electrodes are pin-to-pin and pin-to-plate geometries. A solution plasma process is introduced to produce N-doped carbon quantum dots using acrylonitrile and pyrazine as precursor sources. Microplasma treatment time is about 20 min under stirring [19]. Similarly, another study has also been conducted to fabricate N-doped carbon quantum dots, but the precursor sources for the synthesis are benzene and pyrazine (Figure 8) [133]. In particular, a tungsten wire with a diameter of 1 mm is designed as

electrodes and shielded by a ceramic tube. The starting materials to synthesize N-doped carbon quantum dots are benzene and pyrazine. Microplasma is introduced into the mixed starting materials under vigorous stirring for 20 min. When the microplasma is produced between the electrodes, N-doped carbon quantum dots are formed. The aforementioned evidence demonstrated that microplasma can be used to synthesize N-doped carbon quantum dots from various starting materials. Therefore, it is hypothesised that the two new designs of microplasma reactors are able to generate high-quality N-doped carbon quantum dots.

1.3.7. kINPen®IND microplasma jet

kINPen®IND is a handheld plasma jet device used for various applications such as wound healing, sterilization, and tissue ablation (Figure 9) [42, 134]. The device uses a low-temperature plasma to generate reactive species such as ions, electrons, and radicals that can interact with biological materials. The plasma jet is generated by passing a gas mixture through a high-voltage electric field, which ionizes the gas and creates the plasma. The device is portable, easy to use, and is said to be effective in promoting wound healing and reducing bacterial load. It is designed for use in various settings, including hospitals, clinics, and remote locations.

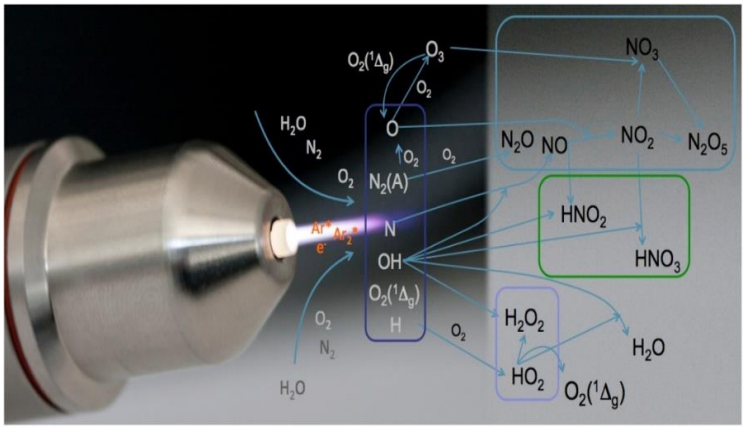

Figure 9. Atmospheric pressure plasma jet kINPen initiates strongly non-equilibrium chemical processes (This figure is adapted from the original work [42], Copyright 2018 OP Publishing)

The kINPen®IND plasma jet device uses a mixture of gases, typically argon and oxygen, to generate the plasma. The device has a nozzle through which the plasma is emitted, and the plasma jet can be directed onto the target area. The plasma jet is said to have a temperature of around 5,000 K, which is relatively low compared to other plasma-based devices. This low temperature is believed to reduce the risk of thermal damage to the surrounding tissue. The device is designed to be used in various settings, including hospitals, clinics, and remote locations. It has been used for various applications, such as wound healing, sterilization, and tissue ablation. In wound healing, the plasma jet promotes the formation of new blood vessels, which can help speed up the healing process. The plasma jet kills bacteria, viruses, and other microorganisms in sterilisation. In tissue ablation, the plasma jet removes unwanted tissue, such as tumours or warts. The device is considered safe and has been cleared by the FDA for use in the United States and CE mark in European Union. It is important to note that the device is still considered as an experimental device, and more research is needed to confirm its effectiveness and safety.

1.3.8. Potential applications of N-doped carbon quantum dots

1.3.8.1. N-doped carbon quantum dots as potential nanopesticides

N-doped carbon quantum dots (NCQDs) have been studied as potential nanopesticides due to their unique properties, such as high biocompatibility, low toxicity, and strong fluorescence. These properties make NCQDs suitable for the targeted delivery of pesticides to pests and for detecting pests in agricultural settings.

Several studies have investigated the use of NCQDs as nanopesticides [135]. For example, NCQDs are effective against various plant pests, such as cotton bollworm and rice stem borer. The NCQDs have also been found to be toxic to various fungal pathogens, such as Fusarium oxysporum and Botrytis cinerea. Additionally, NCQDs have been explored for their ability to enhance the efficacy of traditional pesticides. For example, NCQDs have been found to increase the effectiveness of carbendazim, a fungicide commonly used in agriculture, against Fusarium oxysporum.

Although CDs can express antifungal and bactericidal activity, these properties are not strong enough under visible light, which limits their potential for pest control. Therefore, nanotechnologists thought of a novel solution to enhance this characteristic under visible light. One of the most efficient methods is to modify the surface of CDs by doping with nitrogen atoms to form N-doped carbon quantum dots since the nitrogen atoms in CDs can

provide access electrons and inject into carbon dots, thus changing their photocatalytic and optical properties. As a result, the light absorption of N-doped carbon quantum dots can extend from UV to visible light. Therefore, N-doped carbon quantum dots are more dominant than CDs in antibacterial and antifungal activity under visible light. It is shown that 25 and 75 $\mu L.mL^{-1}$ of N-doped carbon quantum dots could induce 100% antibacterial activity in the case of E. Coli and S. Aureus, respectively [136]. It is concluded that nitrogen-containing groups such as amides and amines are of utmost importance in improving antibacterial activity [137]. It is also believed that the death cause of bacteria is involved electrostatic force between protonated forms in nitrogen-containing groups and lipids in the cellular membrane of bacteria. Another explanation for bacterial and fungal death is that CDs can produce active oxygen species to damage the cellular components of bacteria and fungi. Though there are a few studies of N-doped carbon quantum dots, the evidence above strongly showed that this type of material could be very promising candidate in inhibiting the growth of fungi-and bacteria-caused pathogens throughout photocatalysis under visible light in crops.

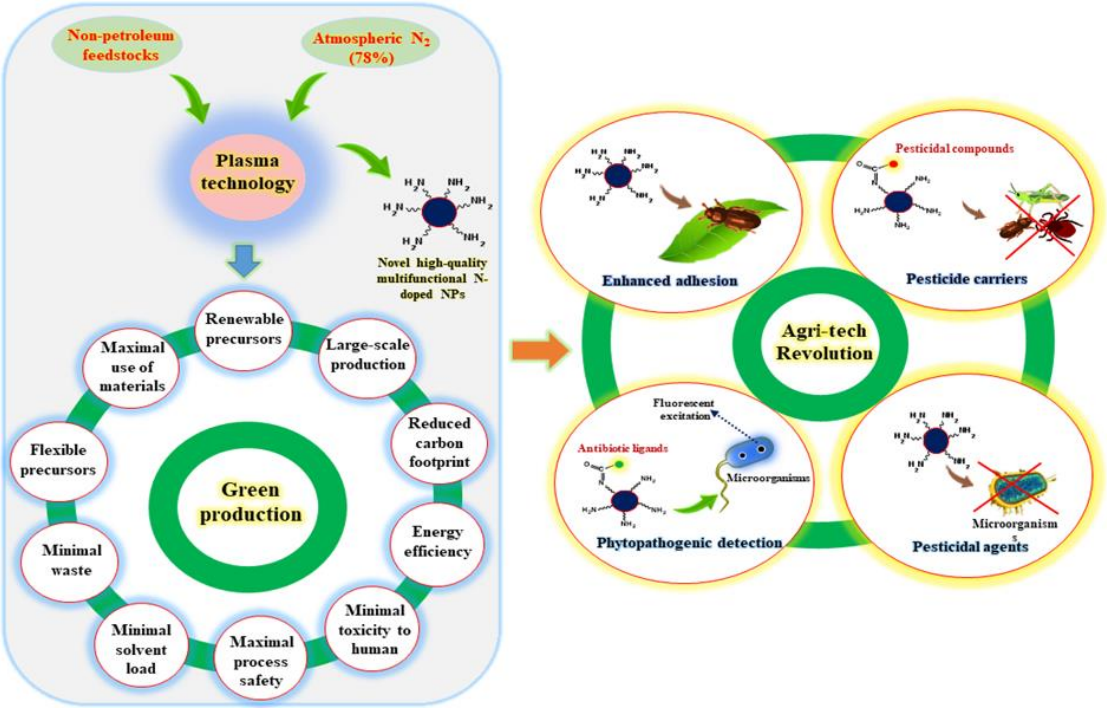

Figure 10. Potential applications of plasma technology-assisted N-doped CDs in the new agritech revolution (This figure is adapted from the original work [135], Copyright 2020RSC Publishing)

Overall, NCQDs have shown great potential as nanopesticides due to their unique properties and potential to enhance the efficacy of traditional pesticides. However, more research is needed to fully understand the mechanism of action of NCQDs as nanopesticides and to optimize their performance in agricultural applications.

1.3.8.2. N-doped carbon quantum dots as photocatalysts for wastewater treatment

N-doped carbon quantum dots (NCQDs) have been studied as photocatalysts in wastewater treatment due to their unique properties, such as high conductivity, high surface area, and strong fluorescence. These properties make NCQDs suitable for photocatalytic reactions to degrade pollutants in wastewater.

Research has shown that NCQDs have high photocatalytic activity under visible light irradiation due to the presence of nitrogen dopants, which can act as electron acceptors, enhancing the separation of photogenerated electron-hole pairs. NCQDs is effective in degrading various pollutants, such as dyes, phenols, and organic pollutants, due to their high surface area, conductivity, and stability. They have also been effective in degrading recalcitrant pollutants such as pharmaceuticals, personal care products and endocrine disruptors. NCQDs have also been effective in removing heavy metals from wastewater. The high surface area of NCQDs provides a large area for the adsorption of heavy metals. Their high conductivity allows for the efficient transfer of electrons to facilitate the reduction of heavy metals. Furthermore, NCQDs have been explored for their ability to enhance the photocatalytic activity of other materials, such as TiO_2, by acting as a co-catalyst. NCQDs have been found to increase the photocatalytic activity of TiO_2 for the degradation of pollutants in wastewater by enhancing the separation of photogenerated electron-hole pairs.

It has been proved that CDs exhibit high photocatalytic activity under UV irradiation with dominant properties such as water solubility, non-toxicity, and high chemical stability compared with conventional photocatalysts. Some recent studies have demonstrated the photocatalysis of CDs for the decomposition of ampicillin antibiotics [138], organic/industrial dyes [26], NO [132], naproxen [139], and tetracycline [140]. In addition, it has been proved that the interaction of plasma with water produces UV light sources and reactive oxygen species (ROS) radicals. These species function as reducing agents, which can decompose complex structures in wastewater, such as dye compounds [141]. Therefore, a combination of N-doped carbon quantum dots and plasma is strongly believed to synergistically affect the decomposition of complex compounds in wastewater.

Overall, N-doped carbon quantum dots have shown great potential as photocatalysts in wastewater treatment due to their unique properties and ability to enhance the photocatalytic activity of other materials. However, research is ongoing to further understand the mechanism of action of NCQDs as photocatalysts and to optimize their performance in wastewater treatment applications.

1.3.8.3. N-doped carbon quantum dots as theranostic agents in biomedical applications

N-doped carbon quantum dots (NCQDs) have been studied as theranostic agents in biomedical applications due to their unique properties, such as high biocompatibility, low toxicity, and strong fluorescence. These properties make NCQDs suitable for use as both diagnostic and therapeutic agents in the biomedical field.

Research has shown that NCQDs have potential applications as imaging agents for in vivo imaging and diagnostic imaging. NCQDs have been found to have high fluorescence intensity and strong near-infrared (NIR) absorption, making them suitable for deep-tissue imaging. They have also been found to be biocompatible and non-toxic, making them suitable for use in vivo. Furthermore, NCQDs have been explored for their potential therapeutic applications. Research has shown that NCQDs have potential applications in cancer therapy due to their ability to generate reactive oxygen species (ROS) and their ability to act as a photosensitiser. NCQDs have been found to have high cytotoxicity against cancer cells and have been found to induce apoptosis in cancer cells.

Additionally, NCQDs have been found to have potential applications in drug delivery systems. NCQDs have been found to have high stability and a large surface area, making them suitable for use in drug delivery systems. They have also been found to protect the drugs from degradation and enhance drug efficacy.

One area of research is in the field of biosensing. NCQDs have been found to have high sensitivity and selectivity in detecting biomolecules, such as DNA and proteins, making them suitable for use in biosensing applications. They also have high stability and a large surface area, making them suitable for biosensing devices.

Another area of research is in the field of regenerative medicine. NCQDs have been found to have potential applications in stem cell labelling and tracking due to their biocompatibility and fluorescence properties. They have also been found to have potential applications in promoting the proliferation and differentiation of stem cells, making them suitable for use in regenerative medicine applications.

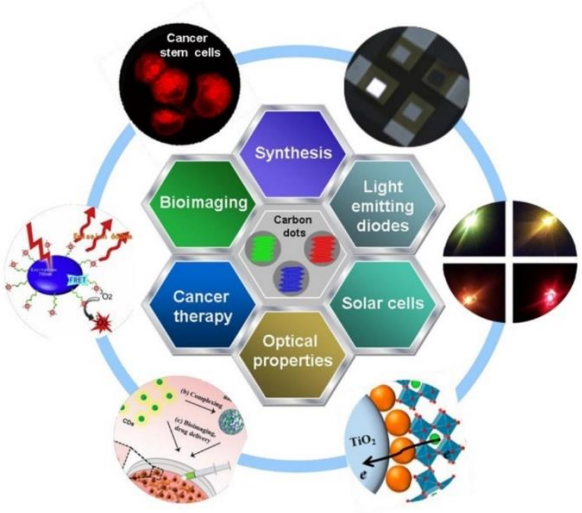

Figure 11. Potential applications of N-doped carbon quantum dots in biomedical applications (This figure is adapted from the original work [150], Copyright 2016 Elsevier Publishing)

It has been investigated that the wavelength range of carbon dots is from 330 nm to 475 nm. Reports have shown that carbon dots (CDs) possess high optical properties compared to other materials, such as quantum dots. In particular, strong fluorescence of carbon dots can be seen in blue and green to yellow (>460 nm). Unlike other traditional fluorescent materials, CDs show single-photon emission with down-conversion fluorescence and two and multi-photon fluorescence emission with up-conversion fluorescence [142]. Based on such outstanding fluorescent properties, many studies indicated that carbon dots are one of the most effective theranostic agents in biomedical applications. Single photon fluorescence emission is used for imaging organs in living systems and cells in vitro [143]. Two-photon fluorescence emission is used for imaging live cells and tissues at different pH values [144]. Apart from their unique optical properties, CDs also possess some important features which make them an exceptional vehicle for fluorescence labelling and imaging: low toxicity [145], fairly good biocompatibility and permeability [146], weak interactions with proteins [147], resistance to swelling and photobleaching [148], low cost [149]. These features make them a solid base for diagnostics. N-doped carbon quantum dots are a new type of CDs in which nitrogen is doped onto the surface to enhance their optical properties [18]. In addition, the existence of -COOH and -NH_2 on the surface enables N-doped carbon quantum dots to conjugate with drugs for various disease treatments [86]. Therefore,

it is strongly believed that N-doped carbon quantum dots are potential for theranostic applications.

Overall, N-doped carbon quantum dots have shown great potential as theranostic agents in biomedical applications (Figure 11) due to their unique properties, such as high biocompatibility, low toxicity, and strong fluorescence. They have many applications in imaging, therapy, and drug delivery systems. However, more research is needed to fully understand the mechanism of action of NCQDs as theranostic agents and to optimize their performance in biomedical applications.

1.4. Research aims and objectives

The primary aim of this thesis is to develop a new kind of microplasma to address the challenges associated with the large-scale production of N-fixation multifunctional N-doped carbon quantum dots (NCQD) for selected applications. A comprehensive literature review of the agricultural applications of NCQD was conducted. A comprehensive assessment of the current large-scale synthesis of NCQD in terms of substantivity was carried out using green chemistry and EcoScale metrics.

This research generally attempted to develop a new kind of microplasma reactor that can rationally design N-doped carbon quantum dots from folic acid (vitamin B9) for selected applications (nanopesticides and nanofertilizers). Large-scale synthesis of NCQD was also considered by the process intensification method. A deep insight into plasma catalysis in the production process characterised by optical emission spectroscopy was also concerned. From the recognized knowledge gaps in the microplasma synthesis of NCQD, the following research aims and objectives were developed:

Aim 1: To understand the potentials of plasma-assisted synthesis of N-doped nanoparticles (NPs) for pesticidal applications in crops (Paper 1) comprehensively

- Objective 1: to provide perspectives of promising applications of N-doped NPs as emerging nanopesticides.
- Objective 2: to review the opportunities plasma-enabled NP technology offers for the scalable production of N-doped NPs based on a green, eco-friendly and sustainable approach.

Aim 2: To assess the overall sustainability of the up-to-date large-scale synthesis processes of nitrogen-doped carbon quantum dots (Paper 2)

- Objective 1: To have an overview of the state-of-the-art synthesis technologies of nitrogen-doped carbon quantum dots
- Objective 2: To assess all large-scale synthesis processes of nitrogen-doped carbon quantum dots using green chemistry, circular and EcoScale metrics.

Aim 3: To develop a rational design concept to synthesise nitrogen-doped carbon quantum dots from Vitamin B9 (Paper 3)

- Objective 1: To develop a rational design strategy for fabricating nitrogen-doped carbon quantum dots from Vitamin B9.
- Objective 2: To fabricate NCQD from the rational design concept using the kINPen®IND microplasma jet.
- Objective 3: To prove the potential of the rationally designed NCQD towards selected applications by physicochemical characterisation.

Aim 4: To prove and achieve the fundamental concept to govern the mass-based intensification by process design (Paper 4)

- Objective 1: To explore the KINPen®IND microplasma jet reactor to synthesise N-doped carbon nanodots from folic acid (Vitamin B9) in an aqueous solution.
- Objective 2: To optimise the plasma jet-liquid distance, metal-plasma interaction, and recycling towards mass-based intensification.
- Objective 3: To explore the mechanism of the microplasma synthesis of N-doped carbon quantum dots.

Aim 5: To decipher plasma-catalysis in triphasic microplasma synthesis for N-doped carbon quantum dots from vitamin B9 via optical emission spectroscopy (Paper 5)

Objective 1: To optimise excited species formation in different plasma-liquid-solid process designs

Objective 2: To optimise metallic catalysts for the triphasic microplasma synthesis of N-doped carbon dots

Objective 3: To explore the mechanism of plasma-liquid-catalysts synthesis of N-doped carbon quantum dots.

Aim 6: intensify reactivity via bespoke transient hydrodynamics in a plasma-activated three-phase catalyst system for formation of N-doped carbon quantum dots (Paper 6)

Objective 1: To understand how the interface between the plasma and the liquid is deformed and how that might be utilised to increase mass transport.
Objective 2: To study the effect of diffusivity of the liquid reactant on the reaction rate by changing the liquid viscosity.
Objective 3: To investigate catalytic activity using metal flakes as bed.

1.5. Thesis outline

This PhD thesis is organized into 8 chapters: an introduction, a literature review (review paper), four other chapters adapted from the original research publications, and finally, a chapter of conclusions and suggested future research works. A summary of each chapter is given below (Figure 12).

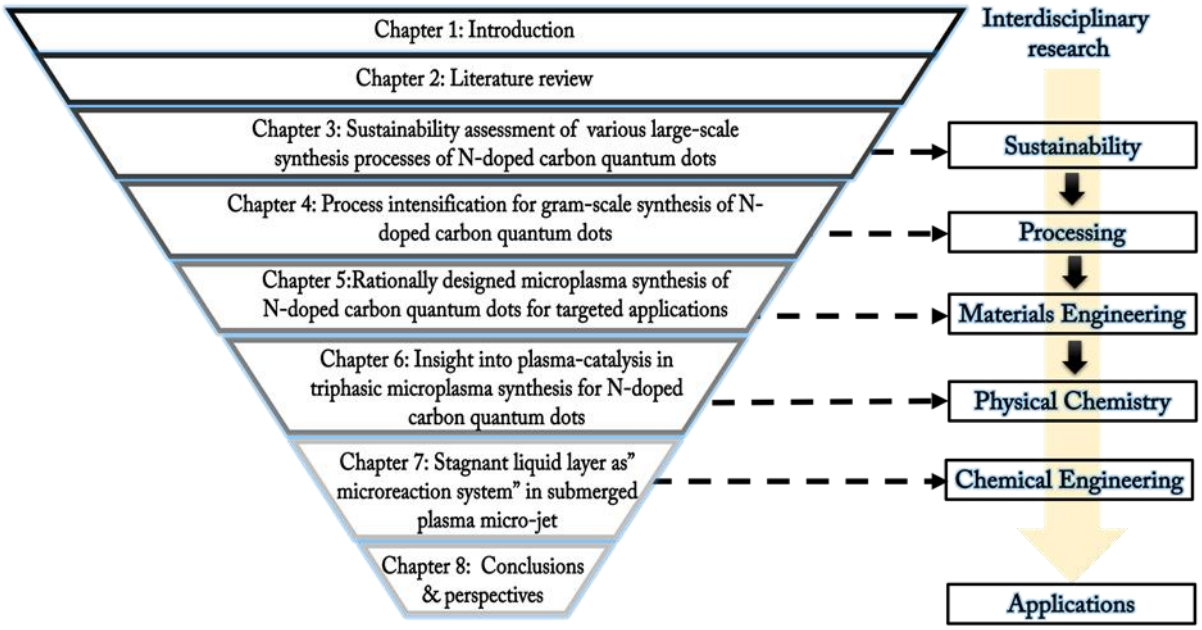

Figure 12. The overall outline of the dissertation with interdisciplinary research topics

Chapter 1. Introduction. This chapter introduces the emerging issue in global food demand due to huge crop loss and unsustainable agriculture production. This chapter highlights the potential and promise of using nitrogen-fixation microplasma technology to produce high-quality multifunctional nanoparticles, which are keys for an agritech revolution to achieve a more sustainable and resilient agriculture. Finally, this chapter discusses the motivation of this research topic, current research gaps, and research aims.

Chapter 2. Literature review. In this chapter, N-doped ZnO and N-doped TiO_2 NPs will be introduced and reviewed as the first examples of these nanomaterials that have been successfully proven as nanopesticides. Following the first demonstration and the application of N-doped carbon dots (N-doped carbon quantum dots), various agricultural applications such as nanopesticides, pesticide nanocarriers, disease detection, and pest targeting will be reviewed, showing their enormous potential to be translated into real applications. The plasma technology comes into play when the focus is on the manufacturing process of these

nanomaterials since, in pest control, producing high-quality nanopesticides is indispensable and challenging. The implementation of this technology and the introduction of N-doped NPs as new powerful pesticidal agents could make a significant impact on improved crop production.

The main contribution of this chapter is to provide perspectives of promising applications of N-doped NPs as emerging nanopesticides and a comprehensive overview on the opportunities that plasma-enabled NP technology offers for the scalable production of N-doped NPs based on a green, eco-friendly and sustainable approach.

Chapter 3. Sustainability assessment of various large-scale synthesis processes of N-doped carbon quantum dots. In this chapter, six of the most promising lab-scale synthesis process methodologies for N-doped carbon dots (NCDs) are selected and compared in terms of green chemistry and circular and EcoScale/Good-Manufacturing Practice metrics. I compared a new innovative route, the low-temperature plasma-enabled synthesis of carbon dots, e.g., from citric acid and monoethanolamine, to more-established literature processes, such as thermochemical processes, from the same or other materials. Along with this study, the advantages and disadvantages of each method are depicted in manifold sustainability facets. It is shown how recycling/reuse of unconverted starting materials and solvents can improve the sustainability profile. In addition, safety constraints, cost analysis, and energy consumption are considered. The analysis showed that the thermal process from citric acid and monoethanolamine gives the best performance concerning the sustainability assessment chosen here.

The main contribution of this chapter is to provide a comprehensive assessment of the most promising lab-scale synthesis process methodologies for N-doped carbon quantum dots to learn more about which of these methods are most promising for scaling-up and industrial manufacturing of N-doped carbon quantum dots.

Chapter 4. Process intensification for gram-scale synthesis of N-doped carbon quantum dots. In this chapter, the distance of the tip of the microplasma jet to the water surface is changed in three steps, named distant, contact, and deflection modes. As a further variation, the liquid volume is either stirred or unstirred and may contain glass beads or metal flakes. In this way, the mass transfer, hydrodynamics, and the electrical field are influenced and create the specific gas–liquid interface, possibly including plasma-catalytic effects. A

thermofluidic analysis confirms a uniform temperature profile and a positive temperature effect on mass transfer. In this way, the research achieves process intensification, bringing the synthesis towards 1 g per day and maximising the intended performance and the photoluminescence intensity. Recycling further increases the mass yield via centrifugation. An analysis by optical emission spectroscopy reveals the formation of the plasma species from which a reaction mechanism is proposed.

The main contribution of this chapter is to achieve mass-based intensification by process design (the plasma jet-liquid distance, metal-plasma interaction, and recycling towards mass-based intensification).

Chapter 5. Rationally designed microplasma synthesis of N-doped carbon quantum dots for targeted applications. In this chapter, N-doped carbon quantum dots (NCQD) are rationally designed and synthesised, for the first time, from folic acid (Vitamin B9) by a non-thermal microplasma jet. The structural and analytical characterisation confirmed an average size of 3.1 nm for the synthesised NCQD with the multi-functional groups (-OH, –COOH, –NH2) on their surface. The TEM results indicated that the core of NCQD was a multilayered structure, including single-defected graphene sheets of graphitic nitrogen and pyrrolic nitrogen. In addition, the fluorescence performance and stability of the as-prepared NCQD were determined. The quantum yield of NCQD was 35%, which is relatively high, with a strong blue fluorescence.

The main contribution of this chapter is to provide a new conceptual strategy to rationally design and synthesise the desirable for three main applications (nanopesticides, water purification, and theranostic treatment).

Chapter 6. Insight into plasma-catalysis in triphasic microplasma synthesis for N-doped carbon quantum dots. In this chapter, as an analytical method, optical emission spectroscopy (OES) investigations are appropriate to investigate the mechanism of how a plasma(-heterogeneous) catalyst in a multiphase reaction may affect the fabrication of NCQD from Vitamin B9. Seven steps are proposed for the reaction mechanism to yield the N-doped quantum dots. The temperature at the plasma-liquid-catalyst interface was lower than 25 ^{0}C, as determined by IR imaging.

The contribution of this study is to understand the plasma-catalytic effect under the microplasma multiphase design and vice versa, to understand the multiphase design better. The key

of this research is to determine and advance multiphase hydrodynamics and reaction by shaping a characteristic surface profile via deep penetration of the plasma jet into the liquid volume.

Chapter 7. Stagnant Liquid Layer as "Microreaction System" in Submerged Plasma Micro-Jet for Formation of Carbon Quantum Dots. This study aims to improve reactivity in a plasma-activated three-phase catalyst system using bespoke transient hydrodynamics. Existing three-phase plasma systems are poorly designed, understood, and not commercially available. The study evaluated N-doped carbon quantum dots as fertilizers and wastewater treatment using a commercial plasma system generating a plasma microjet. The plasma can penetrate the catalyst bed via the stagnant thin liquid film and polarize the plasma-liquid interface, resulting in an increased reaction rate by reducing the solvent's viscosity and increasing liquid component diffusivity towards the catalyst bed.

The contribution of this study is to understand how the interface between the plasma and the liquid is deformed and how that might be utilised to increase mass transport. Then, this will be further studied in gas-liquid-solid microplasma process to investigate for catalytic activity to the synthesis reaction.

Chapter 8. Conclusion, challenges, and perspectives. This chapter provides the summary of this thesis by highlighting the main findings obtained from the results. Next, this chapter discusses the possible future directions for employing this work.

1.6. Budget and Research Funding

All costs of experiments, accessories, equipment, chemicals, conference and travel in this research were financially supported based on the Joint PhD Award between Adelaide and Warwick University under the umbrella of the project "Surface-COnfined fast-modulated Plasma for process and Energy intensification in small molecules conversion" (SCOPE).

1.7. Thesis Editing & Format

The thesis entitled "A new kind of microplasma for nitrogen-fixation multifunctional nanoparticle synthesis towards selected applications" has been prepared as a portfolio of

publications based on the requirements of The University of Adelaide. The printed and online versions of this thesis are identical.

1.8. References

1. Kah, M., N. Tufenkji, and J.C. White, Nano-enabled strategies to enhance crop nutrition and protection. Nature nanotechnology, 2019. 14(6): p. 532-540.
2. Shishoo, R., Introduction: trends in the global textile industry, in The global textile and clothing industry. 2012, Elsevier. p. 1-7.
3. Lellis, B., et al., Effects of textile dyes on health and the environment and bioremediation potential of living organisms. Biotechnology Research and Innovation, 2019. 3(2): p. 275-290.
4. Boretti, A. and L. Rosa, Reassessing the projections of the world water development report. NPJ Clean Water, 2019. 2(1): p. 1-6.
5. Baltes, N.J., J. Gil-Humanes, and D.F. Voytas, Genome engineering and agriculture: opportunities and challenges. Progress in molecular biology and translational science, 2017. 149: p. 1-26.
6. AL-Ahmadi, M.S., Pesticides, anthropogenic activities, and the health of our environment safety, in Pesticides-use and misuse and their impact in the environment. 2019, IntechOpen.
7. Crenna, E., T. Sinkko, and S. Sala, Biodiversity impacts due to food consumption in Europe. Journal of cleaner production, 2019. 227: p. 378-391.
8. Li, S., et al., Recent progress of plasma-assisted nitrogen fixation research: a review. Processes, 2018. 6(12): p. 248.
9. Fuller, J., et al., Reaction mechanism and kinetics for ammonia synthesis on the Fe (211) reconstructed surface. Physical Chemistry Chemical Physics, 2019. 21(21): p. 11444-11454.
10. Gafur, N.A., et al., A case study of heavy metal pollution in water of Bone River by Artisanal Small-Scale Gold Mine Activities in Eastern Part of Gorontalo, Indonesia. Water, 2018. 10(11): p. 1507.
11. Yaseen, D. and M. Scholz, Textile dye wastewater characteristics and constituents of synthetic effluents: a critical review. International journal of environmental science and technology, 2019. 16(2): p. 1193-1226.

12. Mudliar, R., et al., Energy efficient—Advanced oxidation process for treatment of cyanide containing automobile industry wastewater. Journal of Hazardous Materials, 2009. 164(2-3): p. 1474-1479.
13. Oturan, M.A. and J.-J. Aaron, Advanced oxidation processes in water/wastewater treatment: principles and applications. A review. Critical Reviews in Environmental Science and Technology, 2014. 44(23): p. 2577-2641.
14. Poyatos, J.M., et al., Advanced oxidation processes for wastewater treatment: state of the art. Water, Air, and Soil Pollution, 2010. 205(1): p. 187-204.
15. Fernández-Castro, P., et al., Insight on the fundamentals of advanced oxidation processes. Role and review of the determination methods of reactive oxygen species. Journal of Chemical Technology & Biotechnology, 2015. 90(5): p. 796-820.
16. Ou, R., et al., Improved photocatalytic performance of N-doped ZnO/graphene/ZnO sandwich composites. Applied Surface Science, 2022. 577: p. 151856.
17. Budak, M. and H. Segmen, Cancer Genes and Breast Cancers. 2022.
18. Song, J., et al., Effect of Nitrogen Doping on the Photoluminescence of Amorphous Silicon Oxycarbide Films. Micromachines (Basel), 2019. 10(10).
19. Li, O.L., et al., Selective nitrogen bonding states in nitrogen-doped carbon via a solution plasma process for advanced oxygen reduction reaction. RSC advances, 2016. 6(111): p. 109354-109360.
20. Sharma, A. and J. Das, Small molecules derived carbon dots: synthesis and applications in sensing, catalysis, imaging, and biomedicine. Journal of nanobiotechnology, 2019. 17(1): p. 1-24.
21. Gomez, I.J., et al., Nitrogen-doped carbon nanodots for bioimaging and delivery of paclitaxel. Journal of Materials Chemistry B, 2018. 6(35): p. 5540-5548.
22. Li, X., et al., Recent advances in carbon nanodots: properties and applications in cancer diagnosis and treatment. Journal of Analysis and Testing, 2019. 3(1): p. 37-49.
23. Huang, X., et al., Fast microplasma synthesis of blue luminescent carbon quantum dots at ambient conditions. Plasma Processes and Polymers, 2015. 12(1): p. 59-65.
24. Wang, J., C.F. Wang, and S. Chen, Amphiphilic egg-derived carbon dots: Rapid plasma fabrication, pyrolysis process, and multicolor printing patterns. Angewandte Chemie International Edition, 2012. 51(37): p. 9297-9301.

25. Lv, P., D. Xie, and Z. Zhang, Magnetic carbon dots based molecularly imprinted polymers for fluorescent detection of bovine hemoglobin. Talanta, 2018. 188: p. 145-151.
26. Ma, Z., et al., One-step ultrasonic synthesis of fluorescent N-doped carbon dots from glucose and their visible-light sensitive photocatalytic ability. New Journal of Chemistry, 2012. 36(4): p. 861-864.
27. Qu, D., et al., Highly luminescent S, N co-doped graphene quantum dots with broad visible absorption bands for visible light photocatalysts. Nanoscale, 2013. 5(24): p. 12272-12277.
28. Mehta, A., et al., Carbon quantum dots/TiO2 nanocomposite for sensing of toxic metals and photodetoxification of dyes with kill waste by waste concept. Materials & Design, 2018. 155: p. 485-493.
29. Manioudakis, J., et al., Effects of nitrogen-doping on the photophysical properties of carbon dots. Journal of Materials Chemistry C, 2019. 7(4): p. 853-862.
30. Lin, L. and Q. Wang, Microplasma: A New Generation of Technology for Functional Nanomaterial Synthesis. Plasma Chemistry and Plasma Processing, 2015. 35(6): p. 925-962.
31. Shah, J., et al., Ammonia synthesis by radio frequency plasma catalysis: revealing the underlying mechanisms. ACS Applied Energy Materials, 2018. 1(9): p. 4824-4839.
32. Rezaei, F., et al., Applications of plasma-liquid systems: A review. Materials, 2019. 12(17): p. 2751.
33. Weltmann, K.D., et al., The future for plasma science and technology. Plasma Processes and Polymers, 2019. 16(1): p. 1800118.
34. Lin, L., et al., Synthesis of metallic nanoparticles by microplasma. Physical Sciences Reviews, 2018. 3.
35. Lin, L., et al., Plasma-assisted nitrogen fixation in nanomaterials: fabrication, characterization, and application. Journal of Physics D: Applied Physics, 2020. 53(13): p. 133001.
36. Lin, L., et al., Plasma-electrochemical synthesis of europium doped cerium oxide nanoparticles. Frontiers of Chemical Science and Engineering, 2019. 13(3): p. 501-510.
37. Ma, X., et al., Synthesis of luminescent carbon quantum dots by microplasma process. Chemical Engineering and Processing - Process Intensification, 2019. 140: p. 29-35.

38. Lin, L., et al., Color-Tunable Eu3+ and Tb3+ Co-Doped Nanophosphors Synthesis by Plasma-Assisted Method. ChemistrySelect, 2019. 4(14): p. 4278-4286.
39. Lin, L., et al., Facile synthesis of lanthanide doped yttria nanophosphors by a simple microplasma-assisted process. Reaction Chemistry & Engineering, 2019. 4(5): p. 891-898.
40. Lin, L., et al., Synthesis of Ni nanoparticles with controllable magnetic properties by atmospheric pressure microplasma assisted process. AIChE Journal, 2018. 64(5): p. 1540-1549.
41. Lin, L., et al., Synthesis of metallic nanoparticles by microplasma. Physical Sciences Reviews, 2018. 3(10).
42. Reuter, S., T. Von Woedtke, and K.-D. Weltmann, The kINPen—A review on physics and chemistry of the atmospheric pressure plasma jet and its applications. Journal of Physics D: Applied Physics, 2018. 51(23): p. 233001.
43. Mariotti, D. and R.M. Sankaran, Microplasmas for nanomaterials synthesis. Journal of Physics D: Applied Physics, 2010. 43(32): p. 323001.
44. Patil, B.S., Plasma (catalyst) - assisted nitrogen fixation : reactor development for nitric oxide and ammonia production. 2017, Technische Universiteit Eindhoven.
45. Wang, W., et al., Nitrogen Fixation by Gliding Arc Plasma: Better Insight by Chemical Kinetics Modelling. ChemSusChem, 2017. 10(10): p. 2145-2157.
46. Priestley, J., Experiments and Observations on Different Kinds of Air: The Second Edition, Corrected. Cambridge Library Collection - Physical Sciences. Vol. 1. 2013, Cambridge: Cambridge University Press.
47. Cherkasov, N., A.O. Ibhadon, and P. Fitzpatrick, A review of the existing and alternative methods for greener nitrogen fixation. Chemical Engineering and Processing: Process Intensification, 2015. 90: p. 24-33.
48. Rusanov, V.D., A.A. Fridman, and G.V. Sholin, The physics of a chemically active plasma with nonequilibrium vibrational excitation of molecules. Soviet Physics Uspekhi, 1981. 24(6): p. 447.
49. Xu, X., et al., Electrophoretic analysis and purification of fluorescent single-walled carbon nanotube fragments. Journal of the American Chemical Society, 2004. 126(40): p. 12736-12737.

50. Sun, Y.-P., et al., Quantum-Sized Carbon Dots for Bright and Colorful Photoluminescence. Journal of the American Chemical Society, 2006. 128(24): p. 7756-7757.
51. Yan, Y., et al., Recent advances on graphene quantum dots: from chemistry and physics to applications. Advanced materials, 2019. 31(21): p. 1808283.
52. Liu, J., et al., Deep red emissive carbonized polymer dots with unprecedented narrow full width at half maximum. Advanced materials, 2020. 32(17): p. 1906641.
53. Jiang, K., et al., Facile, quick, and gram-scale synthesis of ultralong-lifetime room-temperature-phosphorescent carbon dots by microwave irradiation. Angewandte Chemie International Edition, 2018. 57(21): p. 6216-6220.
54. Dave, K. and V.G. Gomes, Carbon quantum dot-based composites for energy storage and electrocatalysis: mechanism, applications and future prospects. Nano Energy, 2019. 66: p. 104093.
55. Zhang, Z., et al., A minireview on doped carbon dots for photocatalytic and electrocatalytic applications. Nanoscale, 2020. 12(26): p. 13899-13906.
56. Behi, M., et al., Carbon dots: a novel platform for biomedical applications. Nanoscale Advances, 2022. 4(2): p. 353-376.
57. Guo, B., et al., The role of fluorescent carbon dots in crops: Mechanism and applications. SmartMat, 2022. 3(2): p. 208-225.
58. Guo, B., et al., The role of carbon dots in the life cycle of crops. Industrial Crops and Products, 2022. 187: p. 115427.
59. Sun, Y.-P., et al., Quantum-sized carbon dots for bright and colorful photoluminescence. Journal of the American Chemical Society, 2006. 128(24): p. 7756-7757.
60. Mu, X., et al., A sensitive “off-on” carbon dots-Ag nanoparticles fluorescent probe for cysteamine detection via the inner filter effect. Talanta, 2021. 221: p. 121463.
61. Huang, H., et al., Controllable synthesis of biocompatible fluorescent carbon dots from cellulose hydrogel for the specific detection of Hg2+. Frontiers in Bioengineering and Biotechnology, 2021. 9: p. 617097.
62. Wang, Y., Q. Zhuang, and Y. Ni, Facile microwave-assisted solid-phase synthesis of highly fluorescent nitrogen–sulfur-codoped carbon quantum dots for cellular imaging applications. Chemistry–A European Journal, 2015. 21(37): p. 13004-13011.

63. Li, D., et al., Far-red carbon dots as efficient light-harvesting agents for enhanced photosynthesis. ACS applied materials & interfaces, 2020. 12(18): p. 21009-21019.
64. Jana, J., et al., Blue emitting nitrogen-doped carbon dots as a fluorescent probe for nitrite ion sensing and cell-imaging. Analytica Chimica Acta, 2019. 1079: p. 212-219.
65. Qin, K., et al., Applications of hydrothermal synthesis of Escherichia coli derived carbon dots in in vitro and in vivo imaging and p-nitrophenol detection. Analyst, 2020. 145(1): p. 177-183.
66. Yuan, F., et al., Bright high-colour-purity deep-blue carbon dot light-emitting diodes via efficient edge amination. Nature Photonics, 2020. 14(3): p. 171-176.
67. Cao, Y., Y. Cheng, and M. Sun, Graphene-based SERS for sensor and catalysis. Applied Spectroscopy Reviews, 2023. 58(1): p. 1-38.
68. Liu, J., R. Li, and B. Yang, Carbon dots: A new type of carbon-based nanomaterial with wide applications. ACS Central Science, 2020. 6(12): p. 2179-2195.
69. Rabeya, R., et al., Structural defects in graphene quantum dots: A review. International Journal of Quantum Chemistry, 2022. 122(12): p. e26900.
70. Abbas, A., et al., High yield synthesis of graphene quantum dots from biomass waste as a highly selective probe for Fe3+ sensing. Scientific Reports, 2020. 10(1): p. 21262.
71. Chen, S., et al., Tuning the optical properties of graphene quantum dots by selective oxidation: a theoretical perspective. Journal of Materials Chemistry C, 2018. 6(25): p. 6875-6883.
72. Pho, Q.H., et al., Rational design for the microplasma synthesis from vitamin B9 to N-doped carbon quantum dots towards selected applications. Carbon, 2022. 198: p. 22-33.
73. Tao, S., et al., Confined-domain crosslink-enhanced emission effect in carbonized polymer dots. Light: Science & Applications, 2022. 11(1): p. 56.
74. Seliverstova, E., N. Ibrayev, and E. Menshova, Modification of structure and optical properties of graphene oxide dots, prepared by laser ablation method. Fullerenes, Nanotubes and Carbon Nanostructures, 2022. 30(1): p. 119-125.
75. Qin, J., L. Zhang, and R. Yang, Solid pyrolysis synthesis of excitation-independent emission carbon dots and its application to isoniazid detection. Journal of Nanoparticle Research, 2019. 21(3): p. 1-11.
76. Li, X., et al., Microwave synthesis of nitrogen and sulfur co-doped carbon dots for the selective detection of Hg2+ and glutathione. Optical Materials, 2020. 99: p. 109559.

77. Nguyen, V., et al., Double-pulse femtosecond laser ablation for synthesis of ultrasmall carbon nanodots. Materials Research Express, 2020. 7(1): p. 015606.
78. Nguyen, V., et al., Tuning photoluminescence of boron nitride quantum dots via surface functionalization by femtosecond laser ablation. Journal of Molecular Structure, 2021. 1244: p. 130922.
79. Wang, R., et al., Recent progress in carbon quantum dots: synthesis, properties and applications in photocatalysis. Journal of Materials Chemistry A, 2017. 5(8): p. 3717-3734.
80. Lu, S., et al., Near-infrared photoluminescent polymer–carbon nanodots with two-photon fluorescence. Advanced materials, 2017. 29(15): p. 1603443.
81. Liu, J., et al., One-step hydrothermal synthesis of nitrogen-doped conjugated carbonized polymer dots with 31% efficient red emission for in vivo imaging. Small, 2018. 14(15): p. 1703919.
82. Yuan, F., et al., Engineering triangular carbon quantum dots with unprecedented narrow bandwidth emission for multicolored LEDs. Nature communications, 2018. 9(1): p. 1-11.
83. Li, L., et al., Focusing on luminescent graphene quantum dots: current status and future perspectives. Nanoscale, 2013. 5(10): p. 4015-4039.
84. Sato, K., et al., Surface modification strategy for fluorescence solvatochromism of carbon dots prepared from p-phenylenediamine. Chemical Communications, 2020. 56(14): p. 2174-2177.
85. Mei, A., et al., Photocatalytic materials modified with carbon quantum dots for the degradation of organic pollutants under visible light: A review. Environmental Research, 2022. 214: p. 114160.
86. Mishra, V., et al., Carbon dots: emerging theranostic nanoarchitectures. Drug Discovery Today, 2018. 23(6): p. 1219-1232.
87. Xu, J., et al., Carbon dots as a luminescence sensor for ultrasensitive detection of phosphate and their bioimaging properties. Luminescence, 2015. 30(4): p. 411-415.
88. Liu, C., et al., Nano-carrier for gene delivery and bioimaging based on carbon dots with PEI-passivation enhanced fluorescence. Biomaterials, 2012. 33(13): p. 3604-3613.
89. Roy, P., et al., Photoluminescent carbon nanodots: synthesis, physicochemical properties and analytical applications. Materials Today, 2015. 18(8): p. 447-458.

90. Shi, Y., et al., Carbon dots: An innovative luminescent nanomaterial: Photovoltaics: Special Issue Dedicated to Professor Yongfang Li. Aggregate, 2022. 3(3): p. e108.
91. Cui, L., et al., Carbon Dots: Synthesis, Properties and Applications. Nanomaterials (Basel), 2021. 11(12).
92. Zhu, S., et al., Investigation of photoluminescence mechanism of graphene quantum dots and evaluation of their assembly into polymer dots. Carbon, 2014. 77: p. 462-472.
93. Kim, S., et al., Anomalous behaviors of visible luminescence from graphene quantum dots: interplay between size and shape. ACS nano, 2012. 6(9): p. 8203-8208.
94. Tang, J., et al., Influence of group modification at the edges of carbon quantum dots on fluorescent emission. Nanoscale Research Letters, 2019. 14(1): p. 1-10.
95. Pan, D., et al., Hydrothermal route for cutting graphene sheets into blue-luminescent graphene quantum dots. Advanced materials, 2010. 22(6): p. 734-738.
96. Zhu, S., et al., Strongly green-photoluminescent graphene quantum dots for bioimaging applications. Chemical communications, 2011. 47(24): p. 6858-6860.
97. Lin, L. and S. Zhang, Creating high yield water soluble luminescent graphene quantum dots via exfoliating and disintegrating carbon nanotubes and graphite flakes. Chemical communications, 2012. 48(82): p. 10177-10179.
98. Jin, S.H., et al., Tuning the photoluminescence of graphene quantum dots through the charge transfer effect of functional groups. ACS nano, 2013. 7(2): p. 1239-1245.
99. Wang, L., et al., Unraveling Bright Molecule-Like State and Dark Intrinsic State in Green-Fluorescence Graphene Quantum Dots via Ultrafast Spectroscopy. Advanced Optical Materials, 2013. 1(3): p. 264-271.
100. Lin, Z., et al., Classical oxidant induced chemiluminescence of fluorescent carbon dots. Chemical communications, 2012. 48(7): p. 1051-1053.
101. Wang, J. and J. Qiu, A review of carbon dots in biological applications. Journal of materials science, 2016. 51(10): p. 4728-4738.
102. Wang, R., X. Wang, and Y. Sun, One-step synthesis of self-doped carbon dots with highly photoluminescence as multifunctional biosensors for detection of iron ions and pH. Sensors and Actuators B: Chemical, 2017. 241: p. 73-79.
103. Bacon, M., S.J. Bradley, and T. Nann, Graphene quantum dots. Particle & Particle Systems Characterization, 2014. 31(4): p. 415-428.
104. Liu, H., T. Ye, and C. Mao, Fluorescent Carbon Nanoparticles Derived from Candle Soot Angewandte Chemie International EditionVolume 46. 2007, Issue.

105. Peng, J., et al., Graphene quantum dots derived from carbon fibers. Nano letters, 2012. 12(2): p. 844-849.
106. Zhao, P., et al., Facile One-Pot Conversion of Petroleum Asphaltene to High Quality Green Fluorescent Graphene Quantum Dots and Their Application in Cell Imaging. Particle & Particle Systems Characterization, 2016. 33(9): p. 635-644.
107. Li, X., et al., Preparation of carbon quantum dots with tunable photoluminescence by rapid laser passivation in ordinary organic solvents. Chemical Communications, 2010. 47(3): p. 932-934.
108. Hu, S.-L., et al., One-step synthesis of fluorescent carbon nanoparticles by laser irradiation. Journal of Materials Chemistry, 2009. 19(4): p. 484-488.
109. Kang, S.H., et al., Ultrafast method for selective design of graphene quantum dots with highly efficient blue emission. Scientific reports, 2016. 6(1): p. 1-7.
110. Ren, X., et al., Synthesis of N-doped micropore carbon quantum dots with high quantum yield and dual-wavelength photoluminescence emission from biomass for cellular imaging. Nanomaterials, 2019. 9(4): p. 495.
111. Zhuo, S., M. Shao, and S.-T. Lee, Upconversion and downconversion fluorescent graphene quantum dots: ultrasonic preparation and photocatalysis. ACS nano, 2012. 6(2): p. 1059-1064.
112. Zhou, S., et al., Graphene quantum dots: recent progress in preparation and fluorescence sensing applications. RSC advances, 2016. 6(112): p. 110775-110788.
113. Huang, H., et al., A one-step ultrasonic irradiation assisted strategy for the preparation of polymer-functionalized carbon quantum dots and their biological imaging. Journal of colloid and interface science, 2018. 532: p. 767-773.
114. Park, S.Y., et al., Photoluminescent green carbon nanodots from food-waste-derived sources: large-scale synthesis, properties, and biomedical applications. ACS applied materials & interfaces, 2014. 6(5): p. 3365-3370.
115. Li, L.L., et al., A facile microwave avenue to electrochemiluminescent two-color graphene quantum dots. Advanced Functional Materials, 2012. 22(14): p. 2971-2979.
116. Wang, Q., et al., Microwave-assisted synthesis of carbon nanodots through an eggshell membrane and their fluorescent application. Analyst, 2012. 137(22): p. 5392-5397.
117. Yao, Y.-Y., et al., Magnetofluorescent carbon dots derived from crab shell for targeted dual-modality bioimaging and drug delivery. ACS applied materials & interfaces, 2017. 9(16): p. 13887-13899.

118. Pires, N.R., et al., Novel and fast microwave-assisted synthesis of carbon quantum dots from raw cashew gum. Journal of the Brazilian Chemical Society, 2015. 26: p. 1274-1282.
119. Bandi, R., et al., Facile and green synthesis of fluorescent carbon dots from onion waste and their potential applications as sensor and multicolour imaging agents. RSC advances, 2016. 6(34): p. 28633-28639.
120. Zhao, Y., et al., A facile and high-efficient approach to yellow emissive graphene quantum dots from graphene oxide. Carbon, 2017. 124: p. 342-347.
121. Halder, A., et al., One-pot green synthesis of biocompatible graphene quantum dots and their cell uptake studies. ACS Applied Bio Materials, 2018. 1(2): p. 452-461.
122. Mehta, V.N., S. Jha, and S.K. Kailasa, One-pot green synthesis of carbon dots by using Saccharum officinarum juice for fluorescent imaging of bacteria (Escherichia coli) and yeast (Saccharomyces cerevisiae) cells. Materials Science and Engineering: C, 2014. 38: p. 20-27.
123. Lu, W., et al., Economical, Green Synthesis of Fluorescent Carbon Nanoparticles and Their Use as Probes for Sensitive and Selective Detection of Mercury(II) Ions. Analytical Chemistry, 2012. 84(12): p. 5351-5357.
124. Deng, Y., J. Qian, and Y. Zhou, Solvothermal Synthesis and Inkjet Printing of Carbon Quantum Dots. ChemistrySelect, 2020. 5(47): p. 14930-14934.
125. Zhu, S., et al., Strongly green-photoluminescent graphene quantum dots for bioimaging applications. Chemical Communications, 2011. 47(24): p. 6858-6860.
126. Tian, R., et al., Solvothermal method to prepare graphene quantum dots by hydrogen peroxide. Optical Materials, 2016. 60: p. 204-208.
127. Liu, W., et al., Green synthesis of carbon dots from rose-heart radish and application for Fe3+ detection and cell imaging. Sensors and Actuators B: Chemical, 2017. 241: p. 190-198.
128. Ma, C.-B., et al., A general solid-state synthesis of chemically-doped fluorescent graphene quantum dots for bioimaging and optoelectronic applications. Nanoscale, 2015. 7(22): p. 10162-10169.
129. Li, X., et al., Multicolour light emission from chlorine-doped graphene quantum dots. Journal of Materials Chemistry C, 2013. 1(44): p. 7308-7313.
130. Fan, L., et al., Direct Synthesis of Graphene Quantum Dots by Chemical Vapor Deposition. Particle & Particle Systems Characterization, 2013. 30(9): p. 764-769.

131. Vibhute, A., et al., Fluorescent carbon quantum dots: Synthesis methods, functionalization and biomedical applications. Applied Surface Science Advances, 2022. 11: p. 100311.
132. Carolan, D., et al., Environmentally friendly nitrogen-doped carbon quantum dots for next generation solar cells. Sustainable Energy & Fuels, 2017. 1(7): p. 1611-1619.
133. Li, O.L., et al., Synthesis of graphitic-N and amino-N in nitrogen-doped carbon via a solution plasma process and exploration of their synergic effect for advanced oxygen reduction reaction. Journal of Materials Chemistry A, 2017. 5(5): p. 2073-2082.
134. Bekeschus, S., et al., The plasma jet kINPen – A powerful tool for wound healing. Clinical Plasma Medicine, 2016. 4(1): p. 19-28.
135. Pho, Q.H., et al., Perspectives on plasma-assisted synthesis of N-doped nanoparticles as nanopesticides for pest control in crops. Reaction Chemistry & Engineering, 2020. 5(8): p. 1374-1396.
136. Anand, S.R., et al., Antibacterial Nitrogen-doped Carbon Dots as a Reversible "Fluorescent Nanoswitch" and Fluorescent Ink. ACS Omega, 2019. 4(1): p. 1581-1591.
137. Travlou, N.A., et al., S- and N-doped carbon quantum dots: Surface chemistry dependent antibacterial activity. Carbon, 2018. 135: p. 104-111.
138. Sharma, G., et al., Microwave assisted fabrication of La/Cu/Zr/carbon dots trimetallic nanocomposites with their adsorptional vs photocatalytic efficiency for remediation of persistent organic pollutants. Journal of Photochemistry and Photobiology A: Chemistry, 2017. 347: p. 235-243.
139. Wang, F., et al., Novel ternary photocatalyst of single atom-dispersed silver and carbon quantum dots co-loaded with ultrathin g-C3N4 for broad spectrum photocatalytic degradation of naproxen. Applied Catalysis B: Environmental, 2018. 221: p. 510-520.
140. Xie, Z., et al., Construction of carbon dots modified MoO3/g-C3N4 Z-scheme photocatalyst with enhanced visible-light photocatalytic activity for the degradation of tetracycline. Applied Catalysis B: Environmental, 2018. 229: p. 96-104.
141. Bruggeman, P. and C. Leys, Non-thermal plasmas in and in contact with liquids. Journal of Physics D: Applied Physics, 2009. 42(5): p. 053001.
142. Tang, J., et al., Carbon Nanodots Featuring Efficient FRET for Real-Time Monitoring of Drug Delivery and Two-Photon Imaging. Advanced Materials, 2013. 25(45): p. 6569-6574.

143. Cao, L., et al., Competitive performance of carbon "quantum" dots in optical bioimaging. Theranostics, 2012. 2(3): p. 295-301.
144. Kong, B., et al., Carbon Dot-Based Inorganic–Organic Nanosystem for Two-Photon Imaging and Biosensing of pH Variation in Living Cells and Tissues. Advanced Materials, 2012. 24(43): p. 5844-5848.
145. Molaei, M.J., Carbon quantum dots and their biomedical and therapeutic applications: a review. RSC Advances, 2019. 9(12): p. 6460-6481.
146. Kavitha, T. and S. Kumar, Turning date palm fronds into biocompatible mesoporous fluorescent carbon dots. Scientific Reports, 2018. 8(1): p. 16269.
147. Xu, Z.-Q., et al., Interactions between carbon nanodots with human serum albumin and γ-globulins: The effects on the transportation function. Journal of hazardous materials, 2015. 301: p. 242-249.
148. Wang, K., et al., Systematic safety evaluation on photoluminescent carbon dots. Nanoscale Res Lett, 2013. 8(1): p. 122.
149. Yoo, D., et al., Carbon Dots as an Effective Fluorescent Sensing Platform for Metal Ion Detection. Nanoscale Res Lett, 2019. 14(1): p. 272.
150. Yuan, F., et al., Shining carbon dots: Synthesis and biomedical and optoelectronic applications. Nano Today, 2016. 11(5): p. 565-586.

BLANK PAGE

Chapter 2

Literature review

After introducing the importance of nitrogen-fixation microplasma technology to generate advanced engineered multifunctional nanoparticles and their potential in agricultural applications to meet the high global food demand from the previous chapter. This second chapter will introduce a comprehensive overview and perspectives of promising applications of N-doped NPs as emerging nanopesticides and the opportunities which plasma-enabled NP technology offers for the scalable production of N-doped NPs based on a green, eco-friendly and sustainable approach.

The outcome of this chapter has been published as a review paper in "Reaction Chemistry & Engineering" journal as follows:

Pho, Q.H., Losic, D., Ostrikov, K.K., Tran, N.N. and Hessel, V., 2020. Perspectives on plasma-assisted synthesis of N-doped nanoparticles as nanopesticides for pest control in crops. *Reaction Chemistry & Engineering*, 5(8), pp.1374-1396. **(Q1, IF = 5.2)"** <Link>

Statement of Authorship

Title of Paper	Perspectives on plasma-assisted synthesis of N-doped nanoparticles as nanopesticides for pest control in crops
Publication Status	☑ Published ☐ Accepted for Publication ☐ Submitted for Publication ☐ Unpublished and Unsubmitted work written in manuscript style
Publication Details	Pho, Q.H., Losic, D., Ostrikov, K.K., Tran, N.N. and Hessel, V., 2020. Perspectives on plasma-assisted synthesis of N-doped nanoparticles as nanopesticides for pest control in crops. Reaction Chemistry & Engineering, 5(8), pp.1374-1396.

Principal Author

Name of Principal Author (Candidate)	Hue Quoc Pho		
Contribution to the Paper	Literature review, wrote, edited, and revised the manuscript.		
Overall percentage (%)	70%		
Certification:	This paper reports on original research I conducted during the period of my Higher Degree by Research candidature and is not subject to any obligations or contractual agreements with a third party that would constrain its inclusion in this thesis. I am the primary author of this paper.		
Signature		Date	28.01.2023

Co-Author Contributions

By signing the Statement of Authorship, each author certifies that:

i. the candidate's stated contribution to the publication is accurate (as detailed above);
ii. permission is granted for the candidate in include the publication in the thesis; and
iii. the sum of all co-author contributions is equal to 100% less the candidate's stated contribution.

Name of Co-Author	Dusan Losic		
Contribution to the Paper	Co-supervised and Writing- Review and Editing		
Signature		Date	2 feb 2023

Name of Co-Author	Kostya (Ken) Ostrikov		
Contribution to the Paper	Writing- Review and Editing		
Signature	on behalf of co-author	Date	30.01.2023

Please cut and paste additional co-author panels here as required.

Name of Co-Author	Nam Nghiep Tran		
Contribution to the Paper	Writing- Review and Editing		
Signature		Date	28.01.2023

Name of Co-Author	Volker Hessel		
Contribution to the Paper	Supervised, Conceptualisation, Writing – review & editing, and is the corresponding author.		
Signature		Date	28.01.2023

Please cut and paste additional co-author panels here as required.

Reaction Chemistry & Engineering

ROYAL SOCIETY OF CHEMISTRY

PERSPECTIVE

View Article Online
View Journal | View Issue

Check for updates

Cite this: *React. Chem. Eng.*, 2020, 5, 1374

Perspectives on plasma-assisted synthesis of N-doped nanoparticles as nanopesticides for pest control in crops

Quoc Hue Pho, [a] Dusan Losic, [ab] Kostya (Ken) Ostrikov, [c] Nam Nghiep Tran[ad] and Volker Hessel*[ae]

Received 20th February 2020,
Accepted 26th May 2020

DOI: 10.1039/d0re00069h

rsc.li/reaction-engineering

To enhance crop efficiency and meet the growing global demands for food, a new agri-tech revolution has recently been triggering. Engineered nanomaterials have the potential of lessening environmental impact and making agriculture more efficient, resilient, and sustainable. Nitrogen-doped nanoparticles (N-doped NPs) are a rising star toward the development of a new generation of nanopesticides for advanced green agriculture, providing improved efficiency, new concepts for pest control and reduced pesticide resistance, which are key limitations of conventional pesticides. The objectives of this paper are (1) to provide perspectives of promising applications of N-doped NPs as emerging nanopesticides and (2) to review the opportunities which plasma-enabled NP technology is offering for the scalable production of N-doped NPs based on a green, eco-friendly and sustainable approach. The main advantages of the N-doped NPs are their multifunctionality enabling them to provide enhanced adhesion to leaves or insect bodies and several different modes of action to kill insects, including physical, biochemical and catalytic, that are expected to considerably reduce the insect population. Apart from insects, these nanomaterials can inactivate phytopathogenic bacteria and fungi through various mechanisms and are therefore used for a broad spectrum of plant protection. In this review, N-doped ZnO and N-doped TiO_2 NPs will be introduced and reviewed as the first examples of these nanomaterials that have been successfully proven as nanopesticides. Following the first demonstration and the application of N-doped carbon dots (N-doped CDs), various agricultural applications such as nanopesticides, pesticide nanocarriers, disease detection, and pest targeting will be reviewed showing their enormous potential to be translated into real applications. The plasma technology comes into play when the focus is on the manufacturing process of these nanomaterials, since, in pest control, producing high-quality nanopesticides is indispensable and challenging. Plasma-chemical NP processing is a green, simple, and rapid approach compared to conventional methods and this review presents how this technology can be used to produce N-doped NPs in a high-quality, high-quantity, low-cost, energy-efficient and sustainable way with minimal waste and without the use of toxic chemicals. The implementation of this technology and introduction of N-doped NPs as new powerful pesticidal agents could make a significant impact on improved crop production.

1. Introduction

Along with the global economic expansion in the 21st century, the world population growth at an alarming rate has led to high demands on food and agriculture-based products. However, providing an adequately large amount of food from the agricultural sector becomes a challenging issue. Yet, there is also a threat from factors that influence adversely crop productivity such as pests, fungi, and weeds. Among these factors, fungi are considered to be the leading cause of 70% of frequent diseases.[1,2] For instance, *Magnaporthe oryzae* has been known as a fungus which causes rice blast – the most severe fungal infection in rice around the globe.[3–7] *Botrytis cinerea* has a negative impact in many agricultural regions because it exists in a wide range of hosts and causes severe damage, both pre- and post-harvest.[8–11] *Rhizoctonia crocorum* is a significant cause of the rot of various parts of vegetables such as leaf spot and stem rot.[12–14] The statistical results

[a] *School of Chemical Engineering and Advanced Materials, The University of Adelaide, Adelaide, SA 5005, Australia. E-mail: volker.hessel@adelaide.edu.au*
[b] *The ARC Graphene Research Hub, School of Chemical Engineering and Advanced Materials, The University of Adelaide, SA 5005, Australia*
[c] *School of Chemistry, Physics, and Mechanical Engineering, Queensland University of Technology, Brisbane, QLD 4000, Australia*
[d] *School of Chemical Engineering, Can Tho University, Can Tho City, 94000, Vietnam*
[e] *School of Engineering, University of Warwick, Library Rd, Coventry CV4 7AL, England, UK*

This journal is © The Royal Society of Chemistry 2020

View Article Online
Reaction Chemistry & Engineering Perspective

have indicated that multiple pathogens are one of the significant causes of crop losses, and this can be seen in a variety of plants such as rice, barley, wheat, grapevine, cotton, and groundnut.[12] Therefore, controlling pathogenic microbes that cause phytopathogenic diseases is a significant task for not only governmental bodies but also agricultural farmers and scientists to enhance crop productivity.

Over the past century, many chemically synthesized pesticides, such as insecticides, acaricides, rodenticides, nematicides, molluscicides, and fungicides, have been developed and used to improve agricultural crop efficiency as well as protect plants from unexpected damage, such as weeds, harmful insects, pathogenic bacteria and fungi. The pesticides made an enormous contribution to improving global food production especially in developing countries with a significant impact on the productivity of cultural heritage. However, there is still a need for improvement in the use of pesticides in agriculture as it is estimated that 20–40% of global agricultural crop loss is due to pathogens, animals, and weeds.[15–17] There are several challenging problems in conventional pesticides that need urgent solutions such as low efficiency. It is reported that 99% of utilized traditional pesticides are leaked into the groundwaters, contributing to the widespread eutrophication. Their high toxicity to humans and the environment with many disastrous examples can be seen in the past, which leads to "pesticide resistance" of pests that current pesticides could not deal with.[18] This issue has significantly increased production cost and heavily scrutinized the use of pesticides due to their environmental pollution as well as posing a risk to human well-being.

These problems with conventional pesticide formulations have motivated a new research direction in the nanotechnology application. In other words, new generations of advanced pesticides have demonstrated new solutions, which are more efficient and less toxic. Accordingly, nanotechnology has become an important driver for the impending agri-tech revolution.[19] In spite of being of concern only several decades ago, nanoscale-based science and technology have been paid more and more attention to provide innovative solutions to society and industrial and agricultural sectors.[20] The advanced applications of nanotechnology can sustainably contribute to the enhancement of crop efficiency. It is because they can protect plants against the impacts of phytopathogens and also monitor the development process of plants as well as guarantee the mass production of global food production.[19,21,22] They also enhance food quality and reduce the cost of food production as well as limit contaminants leaked into the surrounding environment.[23–28]

Although there are still few studies on nanotechnology applications for agriculture compared to biomedical sectors, researchers nowadays have paid more attention to the field because of tremendous benefits from this technology. Current nanoparticles (NPs) that have been used as nanopesticides in agriculture are silica NPs,[29–31] sulfur NPs,[32–34] silver NPs,[35–38] copper and copper oxide NPs,[39–41] zinc oxide NPs,[42–44] titanium dioxide NPs,[45–47] reduced graphene nanosheets,[48,49] and chitosan NPs.[50–52] All of these NPs have been proven to be capable of protecting cultural heritage from disease, fungi, weeds, and bacteria. The mechanism of the antifungal, antimicrobial, and antibacterial activity of these materials varies based on their intrinsic properties and structure. These mechanisms include reactive oxygen species (ROS) generation under UV and visible light irradiation, release of ions into cells, internalization of NPs into cells, and direct contact with the cell membrane *via* electrostatic force. Among these mechanisms, ROS generation is considered to be one of the main and most effective approaches that cause damage to pathogens.[53,54] In materials science and engineering applications, some of the typical nanomaterials such as TiO_2 (ref. 55) and ZnO (ref. 56) are capable of yielding ROS through photocatalysis. These ROS groups can decompose complex chemical compounds and inactivate a wide range of biological microorganisms.[57] However, most of these materials exhibit strong pesticidal properties only under UV exposure because of their broad energy gap, which limits their potential applications in pest control.

To overcome these drawbacks, scientists have recently focused on shifting the adsorption regions of these photocatalysts from UV light to visible light areas in order to enhance their intrinsic optical properties. One of the most effective and practical approaches is to dope heteroatoms on the surface of these materials.[58,59] Among heteroatoms, nitrogen doping into the surface of photocatalysts has been determined to be the most effective to narrow the energy gap. As a consequence, nitrogen doping results in a shift to a stronger absorption in the visible light region.[60] In addition, some scientific research has shown that nitrogen doping into photocatalytic nanoparticles not only enhances their optical properties but also increases antifungal and antimicrobial activity in

Hue Quoc Pho

Hue Quoc Pho received his bachelor's degree in chemical engineering in 2013 from Industrial University of Ho Chi Minh City, Vietnam. In 2014, he moved to Chung Yuan Christian University, Taiwan, to pursue a master's degree in biomedical engineering. He is currently pursuing his Ph.D. degree at the School of Chemical Engineering and Advanced Materials, the University of Adelaide, Australia, starting from August 2019. His research focuses on microplasma synthesis, multifunctional nanoparticles, biomedical and agricultural applications, and catalysts.

This journal is © The Royal Society of Chemistry 2020

agriculture because of more ROS generation.[61] However, these nitrogen-doped materials are not yet widely used to reduce damage from fungi, weeds, and plant pathogens. Therefore, in this paper, we will review the overall applications of these nitrogen-doped nanoparticles as nanopesticides until now.

There are many methods to fabricate nitrogen-doped nanoparticles, including microwave synthesis,[62–64] arc-discharge,[65–67] laser ablation,[68,69] electrochemical oxidation,[70] chemical oxidation,[71] ultrasonic synthesis,[72] hydrothermal treatment,[73,74] thermal decomposition,[75] and plasma treatment.[76–78] Compared to other conventional synthesis methods, plasma-assisted synthesis of nitrogen-doped nanoparticles offers some promise: (1) fast, environmentally friendly synthesis of high-quality and small-sized nanoparticles; (2) reduced starting materials and fewer steps of fabrication; (3) non-thermal controls over surface modification under atmospheric pressure with safety considerations. Additionally, the antimicrobial and antibacterial properties of nanoparticles are dependent on their size and shape.[79,80] Therefore, using a plasma-assisted synthesis system can generate high quality and size-controlled nanoparticles which can be applied widely to agriculture.

For these reasons, plasma-induced synthesis is a promising method to produce potential N-doped NPs to improve crop productivity. In this review, we will introduce an overview of nanoparticles used as antibacterial and

Dusan Losic

Dusan Losic is a professor at the School of Chemical Engineering and Advanced Materials, the University of Adelaide, South Australia. He pursued his Ph.D. degree at Flinders University in 2003. He was appointed as a postdoctoral researcher at Flinders University, Monash University, and the University of South Australia from 2003 to 2011. He has been appointed as an ARC Australian Future Fellow as well as a professor at the University of Adelaide since 2011. He is currently appointed as Director of ARC Research Hub for Graphene Enabled Industry Transformation. His research interest is involved in nanoscience, nanotechnology, nanomedicine, and graphene.

Kostya (Ken) Ostrikov

Kostya (Ken) Ostrikov is a professor with Queensland University of Technology, Australia, a founding leader of the CSIRO–QUT Joint Sustainable Processes and Devices Laboratory, and academician of the Academy of Europe and the European Academy of Sciences. His research focuses on nanoscale control of energy and matter contributing to the solution of the grand challenge of directing energy and matter at the nanoscale, to develop renewable energy and energy-efficient technologies for a sustainable future.

Nam Nghiep Tran

Nam Nghiep Tran pursued his BSc degree in chemical engineering from Can Tho University in 2006. He went to the University of Tokyo, Japan, to pursue his MSc in chemical system engineering with a prestigious Panasonic Scholarship in 2009. He started his Ph.D. study at the University of Adelaide in 2014 under the sponsorship of the Australian Awards Scholarship. Since 2018, he has been working as a researcher (postdoc) at the University of Adelaide, Australia. His research interests focus on process design and optimization, process simulation, renewable energy, and life cycle assessment.

Volker Hessel

Volker Hessel pursued his Ph.D. in organic chemistry at Mainz University in 1993. In 1994, he went to the Institut für Mikrotechnik Mainz GmbH. In 2002, Prof. Hessel was appointed as vice director of R&D at IMM and became director of R&D in 2007. From 2005 to 2011, Prof. Hessel was working at the Eindhoven University of Technology, the Netherlands. He has been working at the University of Adelaide, Australia, as deputy dean (research) at the ECMS faculty and professor in pharmaceutical engineering since 2018. His research interest focuses on chemical engineering design, bioprocessing, fertilisers and agrochemicals, industrial chemistry, manufacturing processes and technologies, medicinal chemistry, and organic green chemistry.

This journal is © The Royal Society of Chemistry 2020

View Article Online
Reaction Chemistry & Engineering Perspective

antifungal agents in pest control in section 2. Then, we will review N-doped NPs and their agricultural applications in section 3. Later on, we will give a new perspective to make N-doped NPs using plasma-induced synthesis methods in section 4. Next, plasma-induced production of N-doped NPs will be demonstrated as a part of a new agri-tech revolution in section 5. In section 6, we will conclude the key points of plasma-assisted synthesis of N-doped NPs for pesticidal applications in crops. Finally, we will sum up the pros and cons of plasma-assisted fabrication of N-doped NPs in pest control, and will discuss their future direction with a brief outlook in section 7.

2. The use of nanoparticles as nanopesticides

Various nanoparticle formulations have been demonstrated to be able to kill bacteria, fungi, and weeds as well as fight against plant pathogens in cultural heritage.[81,82] Based on the purpose of agricultural applications, nanopesticides are classified into various types, consisting of nanoherbicides,[83,84] nanofungicides,[85,86] and nanoinsecticides.[83,84] The focus in this review is on nanopesticides, which can be synthesized and modified by plasma-assisted fabrication.

2.1. Titanium dioxide (TiO_2) NPs as nanopesticides

These nanoparticles are well known as one of the most promising semiconductor catalysts in light of their physicochemical stability, cost-effectiveness, and high photocatalytic efficiency. TiO_2 NPs are non-toxic to humans and consequently have been investigated and licensed by the American Food and Drug Administration (FDA) for launching into the commercial market.[87] Also, extensive research on TiO_2 NPs has been carried out for the disinfection of different organisms such as viruses, bacteria, fungi, and algae. It is assumed that the antifungal and antibacterial activity of TiO_2 NPs is majorly owing to generation of ROS such as hydroxyl radicals ($^{\bullet}OH$), superoxide anions ($O^{\bullet}_2{}^{-}$), and hydrogen peroxide (H_2O_2) molecules.[88] On contact with microorganisms, these reactive

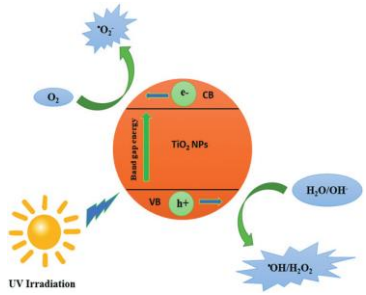

Fig. 1 Mechanism of ROS generation of TiO_2 NPs under UV irradiation (adapted from ref. 89 with permission from Springer Nature, 2015).

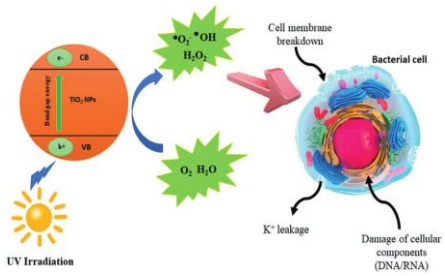

Fig. 2 Antimicrobial mechanism of TiO_2 nanotubes under UV irradiation *via* ROS generation (adapted from ref. 90 with permission from Elsevier, 2015).

redox species can damage their cell membrane. As a result, these microorganisms will be inactivated. The mechanism of TiO_2 generating reactive oxygen species under UV irradiation is described in Fig. 1.[89]

There are various pesticidal mechanisms of TiO_2 on different microorganisms, but the primary mechanism is explained by ROS generation under UV irradiation (Fig. 2).[90] Anatase nanoparticles are capable of inactivating *Rhipicephalus* (*Boophilus*) *microplus* larvae as well as adults of *Haemaphysalis bispinosa*.[91] The insecticidal activity of TiO_2 increased with the nanoparticle concentration in the interval of 4–20 mg l^{-1}.[91] It is reported that after 50 days of treatment, TiO_2 NPs can reduce a large amount of *Hypocrea lixii* (white rot) and *Nucor circibelloides* (brown rot) fungi, which can be observed on various types of wood such as Scots pine, silver fir, walnut, wild cherry, sessile oak, beech, and ash.[92,93] A scientific report about the pesticidal activity of TiO_2 NPs has concluded that TiO_2 sprayed at a low concentration can reduce the severity of foliar and pod diseases of cowpea.[94] Also, it has been reported that TiO_2 NPs could remarkably improve the growth of mung bean plant. The enhancement can be seen in different parts of the mung bean plant such as shoot length (17.02%), root length (49.6%), root area (43%), root nodule (67.5%), chlorophyll content (46.4%) and total soluble leaf protein (94%), when applied.[95,96] In another study, the enzyme alpha amylase was utilized as a reducing and capping substance for the synthesis of TiO_2 NPs. These nanomaterials can also suppress the activity of *Staphylococcus aureus* and *Escherichia coli* with a minimum inhibitory concentration (MIC) value of 62.50 μg ml^{-1} for both bacterial strains.[97] Another research indicated that TiO_2 inhibits the growth of various types of bacteria from *Aeromonas hydrophila* to *Escherichia coli*, *Staphylococcus aureus*, *Proteus mirabilis*, and *Pseudomonas aeruginosa*.[98] To improve their efficiency, TiO_2 NPs are used in combination with other nanoparticles to inhibit harmful fungi and bacteria. Specifically, silver-doped hollow TiO_2 nanoparticles with a concentration in the range of 0.02–0.52 mg per plate are effective against *Fusarium solani* and *Venturia inaequalis* in the presence of TiO_2.[46] The pesticidal properties of TiO_2 NPs are described in Table 1.

View Article Online
Perspective Reaction Chemistry & Engineering

Table 1 TiO_2 nanopesticides with antimicrobial performance against various types of microorganisms

Types	Microorganisms	Features	Ref.
Fungicides	*Candida albicans*	The concentration of TiO_2 NPs to inactivate *Candida albicans* fungi is 5.35 μg ml^{-1}	99
Fungicides	*Fusarium solani* and *Venturia inaequalis*	The antifungal activities of Ag-doped TiO_2 NPs are enhanced under visible light exposure	46
Bactericides and fungicides	*Bacillus*, *Klebsiella*, *Pseudomonas*, *Salmonella*, *Streptococcus*, *Aspergillus niger* and *Trichoderma reesei*	TiO_2 NPs exhibit excellent antimicrobial activity against both bacterial species and fungi	100
Bactericides	*Pseudomonas stutzeri*	*Pseudomonas stutzeri* is inactivated during irradiation with near-ultraviolet light	101
Bactericides	*Pseudomonas aeruginosa*	TiO_2 thin films can suppress *Pseudomonas aeruginosa* under longwave UV irradiation by ultrastructural damage on bacteria cells	92, 102, 103
Bactericides	*Staphylococcus aureus*	*Staphylococcus aureus* can survive under low irradiation of UVA but cannot resist when exposed to TiO_2 photocatalytic coatings	104
Bactericides	*Aeromonas hydrophila*, *Proteus mirabilis*, *Escherichia coli*, *Staphylococcus aureus* and *Pseudomonas aeruginosa*	TiO_2 NPs strongly inhibit the growth of these bacteria	98
Acaricide	*Rhipicephalus microplus* and *Haemaphysalis bispinosa*	TiO_2 NPs are demonstrated to be a highly stable nanomaterial, and remarkably inactivate the larvae of *Rhipicephalus microplus* and *Haemaphysalis bispinosa*	91

2.2. Zinc oxide (ZnO) NPs as nanopesticides

ZnO has been extensively used for various applications in industry because they of their typical properties such as optical properties,[105] chemical sensing,[106,107] semiconductivity,[107,108] electric conductivity,[109,110] *etc.* Also, a direct wide energy gap of ZnO NPs (3.3 eV) can be observed in the near-UV spectrum.[111,112]

Similar to TiO_2 NPs, research on the antibacterial and antifungal properties of ZnO NPs has taken a great interest from scientific communities. ZnO NPs exhibit attractive antibacterial activity since the surface reactivity can be improved when their specific surface area is increased. ZnO NPs have been known as photocatalytic agents that have significant impacts on chemical compounds and biological systems. Due to possessing high absorption under UV irradiation, ZnO NPs are often used in cosmetics in order to protect the skin from UV light.[113] As discussed in section 2.1, ROS groups are highly stable and able to oxidize; thus, they can suppress the growth of bacteria.[114,115]

The primary antibacterial mechanism of ZnO NPs has been determined to be due to ROS generation in various studies. It is also reported that ZnO antibacterial activity could be enhanced significantly when exposed to UV light because of the large number of generated ROS. ROS such as hydroxyl radicals ($^{\bullet}OH$), superoxide anions ($O^{\bullet}_2{}^{-}$), and hydrogen peroxide (H_2O_2) ultimately lead to cell death. One possible explanation is that these reactive groups are engaged in the decomposition of biological components in bacterial cells such as lipids, DNA, and proteins. The ROS generation of ZnO NPs is explained in Fig. 3.[116]

In particular, after release from ZnO NPs under UV irradiation, ROS species will accumulate on the cellular surface of bacteria. This induces oxidative stress in cells, leading to the decomposition of cellular components. Recently, a large number of studies revealed that the ROS of ZnO NPs also cause various processes such as lipid peroxidation, enzyme deactivation, and membrane destruction.

In addition to the ROS mechanism, there are other possible antibacterial mechanisms of ZnO as shown in Fig. 4,[117] including Zn^{2+} release, diffusion of ZnO into the bacteria, and subsequent electrostatic interactions.

ZnO NPs have been widely utilized in various applications, one of which is to control plant pathogens and other pathogenic microbial entities. It has been known that fruits are one of the major agricultural products for human consumption, and most of the plant diseases in fruit is caused by fungi.[118,119] Many severe phytopathogens are caused by various microbial organisms like fungus-like *B. cinerea* and *P. expansum*, and these plant pathogens can cause grey and blue mold on table grapes and rotting of stored apples and pears.[118,119] The ZnO NPs have inhibitory

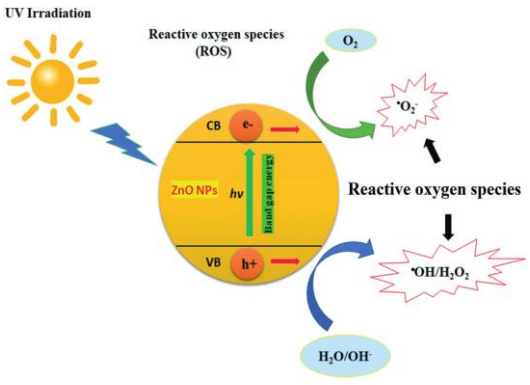

Fig. 3 Proposed mechanism of photo-triggered production of ROS by ZnO NPs (reproduced from ref. 116 with permission from the Royal Society of Chemistry 2018).

This journal is © The Royal Society of Chemistry 2020

View Article Online
Reaction Chemistry & Engineering Perspective

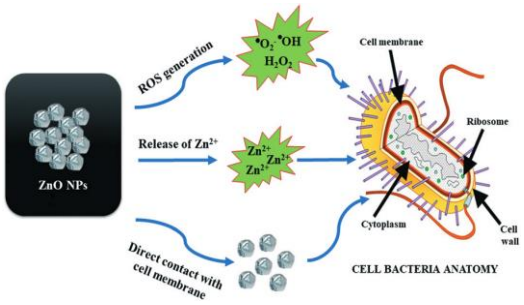

Fig. 4 Various antimicrobial mechanisms of ZnO NPs (reproduced from ref. 117 with permission from the Royal Society of Chemistry 2019).

effects on the growth of *Mucor plumbeus*, *Rhizopus stolonifer*, *F. oxysporum*, and *A. alternata*. Additionally, *Botrytis cinerea* and *Penicillium expansum* are inactivated when exposed to more than 3 mmol l^{-1} ZnO NPs.[120] ZnO also shows intense antifungal activity against plant pathogenic fungi such as *Fusarium oxysporum*, *Alternaria alternata*, *Mucor plumbeus*, and *Rhizopus stolonifer*.[121] The pesticide properties of ZnO NPs are depicted in Table 2.

3. N-doped nanoparticles as nanopesticides

The agricultural applications of nanoparticles as nanopesticides have been comprehensively reviewed in section 2.1. It has been considered that photo-catalysis is involved in the antibacterial and antifungal activity of these materials. However, their photocatalytic capacity is limited only under UV irradiation. It is also estimated that merely 10% of the solar spectrum can be used.[129] For this reason, it is of utmost importance to innovate novel nanomaterials that can express high photocatalytic activity under visible light exposure.

When the light adsorption is adjusted to the visible light region, the applications of these photocatalytic nanoparticles can be extended. The most effective and practical methodology is to engineer their surface by doping with heteroatoms.[130,131] In addition, it has been demonstrated that modifying the surface of nanoparticles by nitrogen doping could improve the photocatalytic properties, which leads to the enhancement of antifungal and antibacterial characteristics, compared to the original nanoparticles.[132,133] Although there are only a few studies of nitrogen-doped nanoparticles on pest control, their applications are expected to be promising for green agriculture. Therefore, we will summarize their current use in controlling phytopathogens and prove the impact of nitrogen doping on pesticide activity.

3.1. N-doped TiO_2 NPs as nanopesticides

As summarized in the previous sections, TiO_2 NPs have been extensively used in suppressing the growth of fungi, weed, bacteria, and other plant pathogens owing to their excellent photocatalytic property, which generates various reactive oxygen species (ROS). Also, by doping with nitrogen, this property has been improved significantly to kill some bacteria and fungi.

For example, nitrogen-doped metal oxide nanocatalysts such as TiO_2 achieved remarkable improvements in *E. coli* bacteria photodegradation efficiency.[134] In particular, an experiment was conducted about the interactions of TiO_2 and N-doped TiO_2 nanoparticles with *E. coli* bacteria in the dark. As a result, there is no detectable suppression of bacteria over all photocatalytic nanoparticles. Otherwise, N-doped TiO_2 shows a remarkable increase in the inactivation of *E. coli* bacteria after 120 min of solar light irradiation. Another experiment was carried out to compare different nitrogen sources in improving *E. coli* bacteria suppression. The results reveal that N-doped

Table 2 Antifungal and antibacterial properties of ZnO NPs on plant disease

Types	Microorganisms	Features	Ref.
Fungicides	*Botrytis cinerea* and *Penicillium expansum*	The development of *Botrytis cinerea* and *Penicillium expansum* can be inhibited at a concentration of more than 3 mmol l^{-1} of ZnO NPs	122
Fungicides	*Aspergillus fumigatus* and *Candida albicans* yeast	ZnO NPs have considerable antifungal activity	123
Fungicides	*Aspergillus niger*	ZnO nanopowders have biocidal activity against the fungus *Aspergillus niger*	124
Fungicides	*Fusarium oxysporum*, *Alternaria alternata*, *Mucor plumbeus*, and *Rhizopus stolonifera*	ZnO shows vigorous antifungal activity against plant pathogenic fungi	121
Fungicides	*Trichophyton mentagrophyte*, *Microsporum canis*, *Candida albicans* and *Aspergillus fumigatus*	ZnO exhibited an inhibitory effect on the growth of dermatophyte isolates	120
Fungicides	*Fusarium graminearum*	ZnO NPs possessed stronger inhibitory effects on fungal development than micro-sized ZnO particles	125
Bactericides	*Listeria monocytogenes*, *Salmonella enteritidis* and *Escherichia coli*	ZnO powder shows significant antimicrobial activities against all three pathogens in growth medium	126
Bactericides	*Escherichia coli*	*Escherichia coli* can survive in ZnO nanofluids. The antibacterial properties of ZnO nanofluids are based on their concentration and particle size	127
Bactericides	*Pseudomonas aeruginosa*, *Pseudomonas fluorescens*, *Salmonella enteritidis*, *Salmonella typhimurium*, *Staphylococcus aureus*, *Bacillus cereus*, *Escherichia coli*, and *Enterobacter cloacae*	Nanoscale particles of ZnO have stronger antibacterial properties than conventional powder	128

View Article Online
Perspective Reaction Chemistry & Engineering

TiO_2 nanoparticles using ethylenediamine as a precursor exhibited the best performance in inhibiting the growth of *E. coli* within 90 min.

Meanwhile, N-doped TiO_2 NPs derived from ethanolamine showed a moderate improvement in *E. coli* inhibition. This is attributed to the Ti–N bonds existing in N-doped TiO_2 NPs. Further, it is believed that the Ti–N bond mediates the electron coupling between the titanium of TiO_2 NPs and nitrogen in the doping, thus leading to a change of the electron structure at the valence band edge. As a consequence, the energy gap of TiO_2 is narrowed.[135,136] In particular, another evidence has been pointed out to explain the photocatalytic inactivation mechanism of *E. coli* using N-doped TiO_2.[137] Specifically, the inactivation process undergoes three stages. At the first stage, there is a relatively slower initial photo-degradation rate during the first 20 min because of the defense of *E. coli* against ROS penetration into the cell membrane. Next, more ROS is generated to overcome the defense of bacteria; consequently, the number of *E. coli* bacteria decreases rapidly. Lastly, the inactivation becomes slower due to the formation of by-products, such as acids or aldehydes. Similarly, recent research concluded that N-doped nitrogen exhibited antimicrobial activity against *E. coli* and ROS generation during 15 min of visible light irradiation.[138]

The fungicidal property of the photocatalytic N-doped TiO_2 has also been researched under visible light exposure.[61] In this research, it is demonstrated that nitrogen is successfully introduced into TiO_2, and the antifungal property exhibits actively due to stronger adsorption under visible light. Typically, the synthesized N-doped TiO_2 can completely suppress the development of *Helminthosporium maydis* fungi, while they can survive in pure TiO_2 NPs under the same condition. Biologically, *Helminthosporium maydis* is defined as a type of fungi that can cause plant pathogens *via* infection of the leaf, ear, and grain. It is reported that when their spores commenced germination in the first period, N-doped TiO_2 NPs can adhere to the cell membrane of *Helminthosporium maydis* with a negative charge. After inactivating the spores, the nanoparticles no longer adhered to the outer part of the cell membrane of *Helminthosporium maydis.*

Another study on the application of N-doped TiO_2 NPs has been conducted for inhibiting *Fusarium graminearum*, an agricultural pathogenic fungus.[139] *F. graminearum* has been classified as a pathogenic fungus on wheat, which could induce a considerable decrease in crop yield of grain. Additionally, it also generates various mycotoxins which can cause disease and death in both humans and animals. In a study, photocatalytic nitrogen-doped titanium oxide NPs modified with palladium is synthesized, which can be activated under visible light. It is demonstrated that modifying N-doped TiO_2 NPs with palladium oxide (TiON/PdO nanoparticles) could considerably enhance their photocatalytic disinfection on *F. graminearum*. It is investigated that these novel nanoparticles are capable of adhering onto the surface of macroconidia. This feature might facilitate the photocatalytic decomposition of these

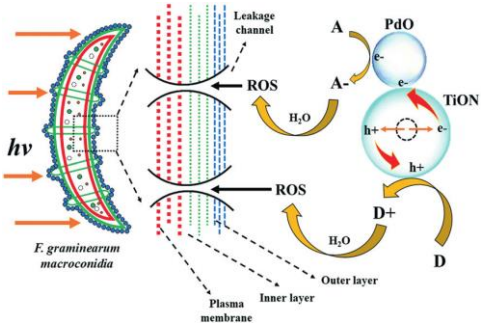

Fig. 5 Antifungal mechanism of TiON/PdO NPs on Fusarium graminearum (reproduced from ref. 139 with permission from the American Chemical Society 2013).

macroconidia, as shown in Fig. 5. It is also proposed that the photocatalytic antifungal mechanism of TiON/PdO nanoparticles on *F. graminearum* could be due to the invasion of generated ROS groups into their cell membrane, leading to disinfection of cellular components.

3.2. N-doped ZnO NPs as nanopesticides

Until now, only N-doped TiO_2 NPs have been applied to agricultural pathogenic control. Other N-doped nanoparticles such as nitrogen-doped ZnO and nitrogen-doped carbon dots, which possess similar photocatalytic disinfection on plant pathogens, are not widely used. This indicates a potential application of nitrogen-doped nanoparticles in pest control due to their excellent antibacterial and antifungal properties *via* photocatalysis.

Similar to the N-doped TiO_2 NPs, this type of nitrogen-doped ZnO nanoparticles typically exhibits stronger photocatalytic properties compared to the original ZnO.[140,141] In addition, it is demonstrated that doping nitrogen into ZnO NPs induces a shift of the light adsorption from UV to visible light, and finally, more ROS is generated. It is because the bandgap energy is narrowed as shown in Fig. 6.[140–143] Apart from that, ROS generation proves to be the primary

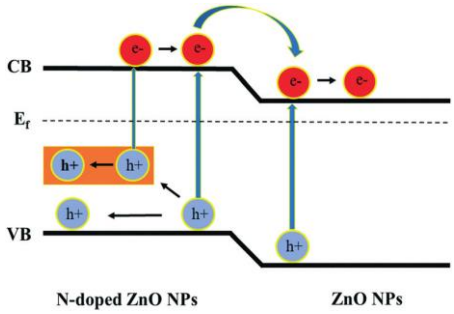

Fig. 6 Comparison of energy levels and charge transfer between ZnO and N-doped ZnO NPs (reproduced from ref. 141 with permission from the American Chemical Society 2013).

This journal is © The Royal Society of Chemistry 2020

View Article Online
Reaction Chemistry & Engineering Perspective

cause of inhibiting the growth of fungi and bacteria.[144] It can be concluded that utilizing N-doped TiO_2 NPs as a photocatalyst under visible light will pave a promising way for research on pest control.

3.3. N-doped carbon dots (N-doped CDs) as potential multifunctional nanopesticides

N-doped carbon dots or N-doped CDs are functionalized materials that derive from carbon dots (CDs).[145–147] Due to nitrogen doping along with available functional groups on the surface, N-doped CDs have been investigated to enhance remarkably their optical properties compared to CDs. Based on the unique features of N-doped CDs, their potential applications are summarized in Fig. 7.

3.3.1. N-doped CDs as potential nanopesticides. Carbon quantum dots (CQDs), also called carbon dots (CDs or C-dots) or carbon nanodots (CNDs), have been classified as one of the newest members of carbon-based materials.[148,149] CDs are defined as discrete and quasi-spherical carbon NPs with ultrasmall particle size ranging from 1 to 10 nm.[150–152] Their unique properties are the integration of typical fluorescence properties of quantum dots and excellent electronic properties of carbon nanomaterials.[153] As a result, this type of carbon nanomaterial becomes more dominant than conventional semiconductors in terms of fluorescence properties and particle size. In addition, CDs are more beneficial than other traditional materials in terms of cost-efficiency, non-toxicity, photoelectric nature, and capacity for generating $-/h^+$ pairs under UV light exposure.[154] CD-based photocatalysts are water soluble and non-toxic to the human body, while the majority of photocatalysts containing metals such as ZnO and TiO_2 NPs might result in a risk of water pollution after contaminants are degraded.[155] Additionally, C-dots also exhibit high intensity of fluorescence properties in the infrared and visible regions, as well as photochemical stability.[149] Like other conventional semiconductors (ZnO, TiO_2), CDs possess a typical energy gap between the valence and the conduction bands.[156] For this reason, they can cause photocatalytic redox reactions. It has been reported that the photocatalytic properties of CDs are size-dependent.[155] In addition, CDs as a photocatalyst can generate ROSs such as superoxide, shown in Fig. 8, and these groups can cause the decomposition of organic compounds and the death of hypoxic tumor cells.[157] Therefore, ROS generation of photocatalytic CDs under UV light can exhibit antibacterial and antifungal activity in controlling agricultural pathogens. It is also demonstrated that CDs could inhibit the activation of *E. coli* bacteria under ambient conditions.[158,159] Thus, this means that CDs exhibit significant bactericidal functions. Vitamin C is also used as a carbon source to fabricate degradable CDs with strong antibacterial and antifungal properties using a one-step electrochemical methodology.[160] These results reveal that CDs efficiently suppress the activation of bacteria like *Staphylococcus aureus*, *Bacillus subtilis*, *Escherichia coli*, the ampicillin-resistant *Escherichia coli*, *Rhizoctonia solani* and *Pyricularia grisea*. Various experiments have been carried out to prove the antibacterial and antifungal mechanism of CDs.[160] In particular, it is suggested that CDs could penetrate the bacterial cell membrane *via* a diffusion process. Next, these CDs can generate ROS groups to attack the bacterial cellular wall and attach to the DNA and RNA of bacteria. This might have negative impacts on their genetic process, leading to the death of bacteria and fungi at a very low concentration.

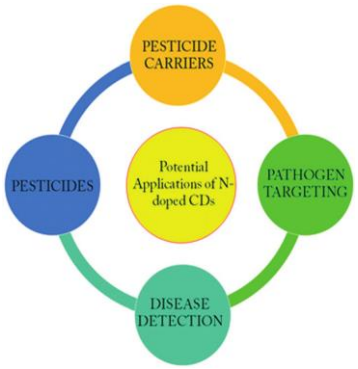

Fig. 7 Various possible applications of N-doped CDs in agriculture.

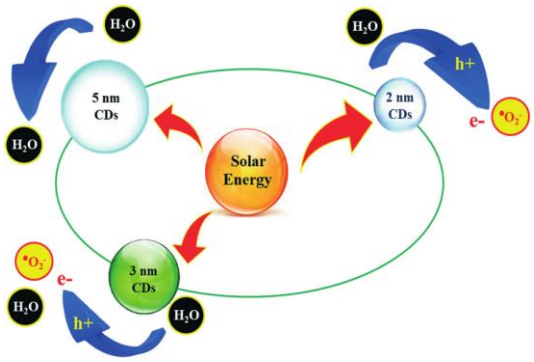

Fig. 8 Mechanism of size-dependent ROS generation from CDs (adapted from ref. 155 with permission from Elsevier, 2019).

Although CDs can express antifungal and bactericidal activity, these properties are not strong enough under visible light, which limits their potential applications in pest control. Therefore, nanotechnologists think of a novel solution to enhance this characteristic under visible light. One of the most efficient methods is to modify the surface of CDs by doping with nitrogen atoms to form nitrogen-doped CDs since the nitrogen atoms in CDs can provide excess electrons and inject into carbon dots, thus changing their photocatalytic and optical properties.[161] As a result, the light absorption of N-doped CDs can extend from UV to visible light. Therefore, N-doped CDs are more dominant than CDs in antibacterial and antifungal activity under visible light. It is showed that 25 and 75 μl ml^{-1} N-doped CDs could induce 100% antibacterial activity in the case of *E. coli* and *S. aureus*,

respectively.[146] It is concluded that nitrogen-containing groups such as amides and amines are of utmost importance to improve the antibacterial activity.[162] It is also believed that the causes of bacterial death involve an electrostatic force between protonated forms in nitrogen-containing groups and lipids in the cellular membrane of bacteria. Another explanation for bacterial and fungal death is that CDs can produce active oxygen species to damage the cellular components of bacteria and fungi. Though there are few studies on N-doped CDs, the evidence above strongly shows that this type of material could be a very promising candidate in inhibiting the growth of fungi- and bacteria-caused pathogens through photocatalysis under visible light in crops. The photocatalytic applications of N-doped CDs for bacterial and fungal inactivation is described in Fig. 9.

3.3.2. N-doped CDs as a biosensor for detecting agricultural pathogenic diseases. Apart from photocatalysis, N-doped CDs also exhibit powerful fluorescence properties which make them distinctive from other current nanomaterials.[163] It is believed that many nanomaterials with optical properties have been used as biosensors for detecting plant pathogens.[164] For example, quantum dots (QDs) have been extensively utilized to detect plant pathogens based on a fluorescence resonance energy transfer (FRET) mechanism.[165–168] The FRET mechanism relies on energy transfer between two light-reactive molecules. Some types of sensors based on QDs and FRET (QD-FRET-based sensors) have been designed to detect the witches' broom disease of lime.[169] The designed QD-FRET based sensor system exhibits a very high sensitivity to this kind of pathogens in lime. Apart from that, QD-FRET-based sensors are also investigated for the detection of pathogen vectors. In particular, they can detect the Beet necrotic yellow vein virus (BNYVV) and *Polymyxa betae* Keskin. This vector is determined to be a significant cause of rhizomania in sugar beets.[170] It has been demonstrated that N-doped CDs have been proved to have stronger and more stable fluorescence properties than QDs.[171] Therefore, N-doped CDs can be an alternative

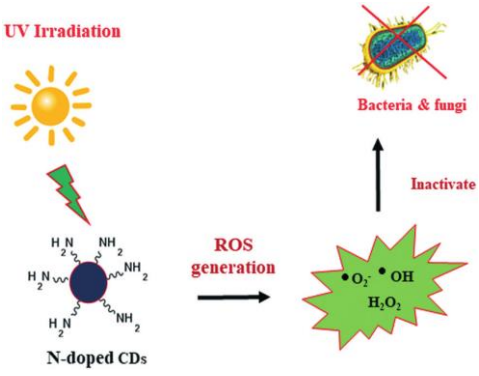

Fig. 9 Proposed application of N-doped CDs as a photocatalyst for antibacterial and antifungal activity to inactivate phytopathogenic microorganisms.

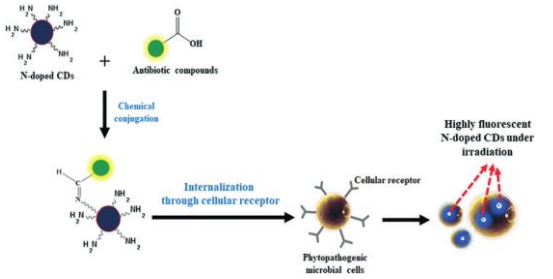

Fig. 10 Proposed application of N-doped CDs as biosensors for phytopathogenic detection.

nanomaterial as biosensors to detect harmful pathogenic fungi and bacteria in crops. The proposed application of N-doped CDs as biosensors for phytopathogenic detection is described in Fig. 10. Specifically, N-doped CDs are conjugated with targeting molecules such as antibiotic compounds, which can be recognized by specific cellular receptors. N-doped CDs can enter into phytopathogenic microbial cells through various cellular internalizations. After the internalization stage, these N-doped CDs in microbial cells can excite specific high fluorescence under irradiation.

3.3.3. N-doped CDs as a delivery carrier of pesticides. In addition to detecting phytopathogenic diseases based on their strong fluorescence properties, N-doped CDs can also be applied for smartly targeted nanopesticides like other nanoparticles. In this case, N-doped CDs are used as a nanocarrier for delivering pesticides with controlled release instead of being used as nanopesticides themselves. In fact, nanoparticles have been widely used to deliver drugs in biomedical applications such as metal oxide NPs,[172,173] polymeric nanoparticles,[174] and mesoporous NPs,[175] but comparatively few studies have focused on the agricultural applications of nanoparticles, especially N-doped CDs, for controlled release of pesticide compounds to target agricultural pathogens. Like other nanoparticles, the surface of N-doped CDs can be modified to conjugate with pesticide molecules for controlled release in crops. It is believed that most of the functional groups on the surface of N-doped CDs are $-NH_2$, –OH and –COOH.[176–180] Therefore, to enhance the loading efficiency of pesticides on N-doped CDs, these nanocarriers should undergo a carbodiimide crosslinking

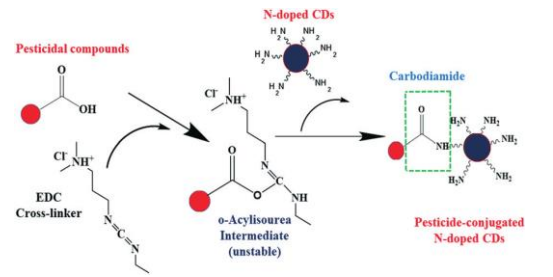

Fig. 11 Proposed crosslinking carbodiimide reaction of N-doped CDs for pesticide delivery.

This journal is © The Royal Society of Chemistry 2020

View Article Online
Reaction Chemistry & Engineering Perspective

reaction with pesticide reagents. This type of reaction is one of the most popular and effective methods to carry drugs or pesticides.[181–184] In principle, the carbodiimide reaction is a crosslinking reaction in which carboxyl-reactive chemical groups or carboxylic acids (–COOH) react directly with primary amines (–NH_2).[185] The scheme of the carbodiimide crosslinking reaction of N-doped CDs is described in Fig. 11.

This type of carbodiimide conjugate is believed to enhance the efficient use of pesticides and to prolong the release time of pesticides into pests, leading to a long-term pesticidal effect. In other words, it takes time to break the interaction between pesticidal molecules and N-doped CDs, resulting in a slow release rate. The concept of pesticide conjugated N-doped CDs can be described in Fig. 12. Recently, carrying some types of antibiotics such as streptomycin on CDs has been tried for pest control (Table 3).[186] Streptomycin has been determined to inhibit the spread of fire blight disease in apples and pears. However, overuse of these types of antibiotics for pest control is not favorable because this might lead to the development of other resistant bacterial phytopathogenic strains. Therefore, using CDs to load streptomycin can not only reduce the number of antibiotics used but also increase the pesticide efficiency of the streptomycin-CD conjugate.[187] The structure of streptomycin indicates that this type of antibiotic can be used to conjugate with N-CDs through the reaction between –NH_2 of N-doped CDs and –CHO of streptomycin. The reaction scheme is described in Fig. 13.

Adhesion to leaf and targeting delivery of N-doped CDs to pests depends on the structure of plants and pests. It is reported that the outermost layer of the leaf is called the cuticle, which is in direct contact with nanopesticides.[193] On the cuticle surface is a wax layer, which contains long hydrocarbon chains with various functional groups (alkanes, alcohols, aldehydes, and acids).[194] Therefore, the interaction between the nitrogen-containing functional groups and the wax layer is significantly enhanced due to the existence of –NH_2 groups on the surface of N-doped CDs. As a result, this will lead to the spread and adhesion of nanopesticide droplets to plants and pests.[195]

In comparison with other nanocarriers, N-doped CDs have a much smaller particle size of less than 10 nm.[145,196,197] Therefore, N-doped CDs with ultrasmall size can easily penetrate the cell membranes of pathogenic fungi, bacteria, and weeds.[198] This new way of delivery through cell membranes makes N-doped CDs more efficient and competitive than conventional pesticide delivery.

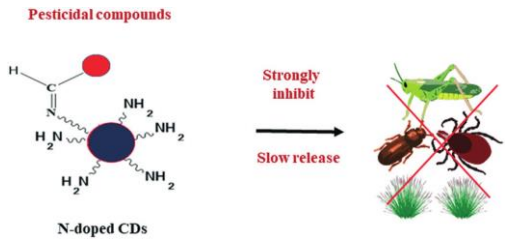

Fig. 12 Applications of N-doped CDs as a pesticide carrier for targeting pests.

The structure of targeted insects is another factor that needs to be considered when designing nanopesticides. It has been known that the insect body wall or exoskeleton – the external covering of the body – consists of the epidermis and cuticle. The cuticle is the outermost part of the insects' exoskeleton, which includes three sub-layers, shown in Fig. 14a.[199–201]

The major component of insect cuticle is nitrogenous polysaccharide and a polymer of *N*-acetylglucosamine, which has been called chitin fibers (Fig. 14b).[202] It cannot dissolve in water but is soluble in acids, alkalis, and organic solvents. Chemically, the structure of chitin contains many –OH and –C=O functional groups (Fig. 14b), which might have high affinity with N-containing functional groups on the surface of N-CDs. Apart from that, the outermost epicuticle is made of a non-water-soluble cement layer (wax layer). The composition of this layer varies from insect species such as alkanes, aldehydes, primary alcohols, free fatty acids, esters, and triterpenoids.[203] Therefore, nitrogen-doped nanopesticides like N-doped CDs can enhance their adhesion to the insect's exoskeleton due to the interaction of –CHO functional groups on the wax layer with nitrogen-containing groups on N-doped CDs. These morphological and chemical structures of the insect's skeleton will provide an enhanced intake of pesticides and also cause other problems, for example, the loss of water from the insect body that will impact their survival under harsh environmental conditions. The enhanced adhesion mechanism of the N-doped CDs to plants and insects is proposed in Fig. 15. In general, it can be concluded that knowing the precise chemical composition of the exoskeleton and the physiological properties of insects would provide a clue for researchers to design the corresponding targeted nanopesticides like N-doped CDs by surface modification.

4. Plasma synthesis of N-doped nanoparticles for agricultural applications

4.1. Principle of plasma synthesis of N-doped nanomaterials

The synthesis of nanomaterials has been of long-standing interest because of their wide range of applications ranging from agriculture, food industry, biomedical and environmental applications to energy. However, and in general for all nanomaterial syntheses, the effectiveness of their applications is based on their size- and shape-dependent properties. Hence, the production of high-quality nanoparticles with controllable properties becomes indispensable. Consequently, various nanomaterials synthesis methods have been developed, including wet chemical methods,[204] microwave technique,[205] laser ablation,[206] and hydrothermal method.[207,208] In comparison with the aforementioned conventional methods, plasma synthesis of nanomaterials has recently shown more

Table 3 List of antibiotics used to be delivered by N-doped CDs for pest control

Name	Properties	Applications in crops	Ref.
Streptomycin	An aminoglycoside antibiotic naturally produced by soil actinomycetes	It is used to inhibit the spread of fire blight disease in apples and pears	188, 189
Gentamicin	An aminoglycoside antibiotic that inhibits protein synthesis by binding to the bacterial ribosome	It is used to inhibit the spread of fire blight disease in apples and pears, and various phytopathogenic diseases caused by species of *Pectobacterium*, *Pseudomonas*, *Ralstonia*, and *Xanthomonas*	190
Oxytetracycline (terramycin)	A naturally produced tetracycline antibiotic of *Streptomyces rimosus*, with a spectrum of activity similar to that of chlortetracycline and tetracycline and remarkable thermostability	Controls *E. amylovora* on apples and diseases caused by *Pectobacterium* spp., *Pseudomonas* spp. and *Xanthomonas* spp. on several crops	189 and 191
Oxolinic acid	Oxolinic acid, a synthetic quinolone antibiotic, inhibits DNA replication and consequently bacterial growth	It is used to inhibit the spread of fire blight disease in apples, pears, and other related plants	192

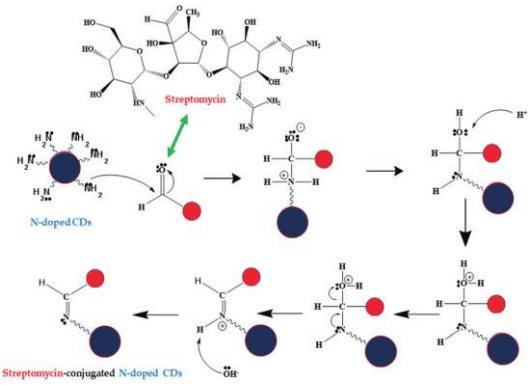

Fig. 13 Schematic illustration of the conjugation reaction of N-doped CDs with streptomycin.

dominance in terms of generating high-quality nanoparticles because of several reasons. First, plasma technology effectively fabricates or modifies various nanomaterials with fewer operating processes than conventional methods, hence, significantly reducing the labor costs.[209] The second tremendous benefit of plasma-assisted fabrication and modification system is that prepared nanomaterials possess rich functional groups such as $-NH_2$, –COOH, –CHO, *etc.* without using any initial chemicals for surface modifications.[210] Lastly, particle size along with morphological, structural, and fluorescence properties of the prepared nanomaterials is adjustable and tailorable.[211]

Plasma has been defined as the fourth state of matter, which can be characterized by a complex collective behavior.[211] It contains negatively and positively charged particles, electrons and free radicals, which can decompose various chemical compounds, and biological components.[212] One of the most significant advantages of plasma treatment or synthesis of N-doped nanomaterials is that it can properly introduce functional groups into the surface of nanomaterials. Based on this merit, nitrogen heteroatoms can be used to dope on the surface of nanomaterials by treating with ammonia or nitrogen gas. In summary, plasma fabrication of N-doped nanoparticles has been demonstrated to be a promising technology in pest control. An overall review of N-doped nanoparticles is shown in Table 4.

4.2. Plasma synthesis of N-doped TiO_2 NPs

Until now, plasma synthesis of N-doped TiO_2 NPs has not been widely applied in agricultural heritage, but it has been used for other applications. Therefore, we will discuss the overall summary of plasma synthesis of N-doped TiO_2 NPs because of their potential applications in pest control that we discussed in the previous sections.

In 2006, a Japanese research group used argon and nitrogen gas to generate plasma for fabricating N-doped TiO_2 particles. This plasma setup is described in Fig. 16.[213] In particular, discharge power and discharge time are adjusted in a range from 100 to 400 W and from 2–20 min, respectively. TiO_2 powders were used as a starting material. The results show that after nitrogen doping, Ti–N bonds are completely formed, which enhance their optical properties in the visible light range. From the results, it can be seen that this process is less time-consuming (2–20 min) and more energy-efficient (100–400 W) without using any toxic additives (only renewable nitrogen gas and argon plasma gas were used).

In 2007, a novel plasma-assisted fabrication process based on the atmospheric pressure plasma reactor was designed to produce photocatalytic N-doped TiO_2 particles using

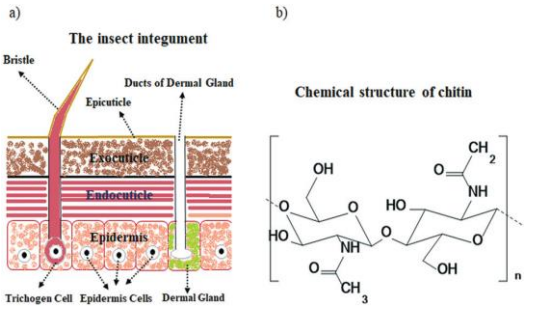

Fig. 14 (a) The structure of insects' exoskeleton (insect body wall) in crops. (b) Chemical structure of chitin in insect cuticle.

 This journal is © The Royal Society of Chemistry 2020

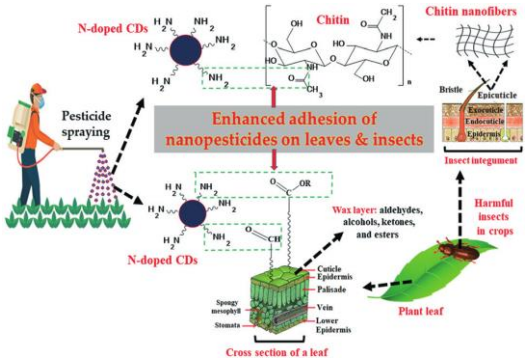

Fig. 15 Illustrative sketch of the proposed enhanced adhesion mechanism of N-doped CDs on plants and insects.

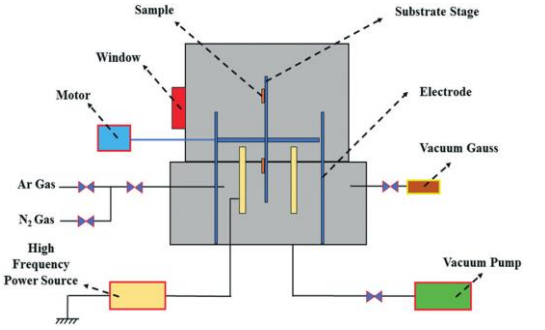

Fig. 16 Scheme of the setup of a bell jar-type plasma reactor for N–TiO_2 NPs (adapted from ref. 213 with permission from Elsevier, 2006).

$Ti[OCH(CH_3)_2]_4$ and water vapor as a source of starting materials, which is shown in Fig. 17.[214,215] The results depicted that the particle size of N-doped TiO_2 photocatalysts is around 22.0 nm. It is also demonstrated that N_2 plasma gas followed by air could generate nitrogen dopants. In this study, $Ti[OCH(CH_3)_2]_4$ and water vapor are used as precursors rather than raw TiO_2 (Fig. 16), indicating the flexibility of using starting materials. With a particle size of 22 nm, it is revealed that this process can produce well-defined nanoparticles using non-toxic materials such as N_2, H_2O, and $Ti[OCH(CH_3)_2]_4$. In particular, the synthesis process is carried out at atmospheric pressure in a closed system, showing that this system is in high-safety control.

Liquid-phase non-thermal plasma (LPNTP) is another plasma technology that can generate plasma under atmospheric pressure and temperature conditions. Plasma at the plasma–liquid interface can promote a complex mixture of reactions in solution. In 2010, LPNTP technology was applied to synthesize N-doped TiO_2 NPs for removal of azo dye (Fig. 18).[216] In particular, nanosized TiO_2 and NH_4Cl are used as starting materials. The bipolar pulse is utilized as a power supplier to produce pulsed irradiation in the range from 0 to 30 kV. The frequency rate is set up at 60 Hz with a high voltage discharge electrode (13.5 W), and a high-voltage probe and a pulsed current probe are used to measure the output of voltage and current. The influential parameters of discharge are adjusted and controlled using a digital oscilloscope. To generate a corona discharge in the water phase, an electrode in the form of a needle plate is put in the middle of a cylindrical quartz tube, and a discharge electrode is made from a stainless-steel hollow needle. The point electrode of the hollow needle is set up in the heart of the cylindrical reactor above the bottom of the vessel. Specifically, merely the tip of the point electrode is constructed to directly come in contact with the water phase. In addition, to make the ground electrode, a stainless-steel round plate with a diameter of 40 mm is used and put at the top of the reactor opposite to the needle-like discharge electrode. The temperature is modified in the range from 273 to 323 K at an airflow rate of 150 mL min^{-1}. The results show that this system is energy-efficient (13.5 W) in high safety control (a closed system at low temperature).

In Fig. 19, the plasma-assisted system is developed and combined with a particle-stirring system relying on the polygonal barrel-sputtering method to generate N-doped TiO_2.[217] This system includes an electrode for the gas supply and a vacuum chamber with a hexagonal barrel. N_2 gas is used to generate plasma for N-doped TiO_2 synthesis in a range of time from 30 to 180 min, and radio frequency (RF) is used as a power supply with a power of 25–300 W and frequency rate of 250 kHz. The results indicate that treatment time, RF power, and gas pressure directly influence the absorbance in the visible light range and the amount of

Table 4 Overall summary of plasma-induced synthesis of N-doped nanomaterials for potential pesticide applications

N-doped nanopesticides	Typical characteristics	Plasma process	Ref.
N-doped TiO_2	N_2 and Ar plasma	Bell jar-type plasma reactor	213
	N_2 and Ar plasma	Dielectric barrier discharge plasma	214, 215
	Corona discharge in water	Liquid-phase non-thermal plasma	216
	N_2 plasma treatment	RF plasma	217
	H_2 and Ar plasma	Arc discharge	218
	The formation of Arc plasma on the metal surface	Arc plasma	219
N-doped ZnO	N_2 and Ar plasma	DC thermal plasma	220
	Using Ar as a carrier gas	RF thermal plasma	221
N-doped CDs	He plasma	Indirect contact plasma–liquid system	222
	Using acrylonitrile and pyrazine as a source of nitrogen and carbon	Direct contact plasma–liquid system	223
	Using benzene and pyrazine as a source of nitrogen and carbon	Direct contact plasma–liquid system	224

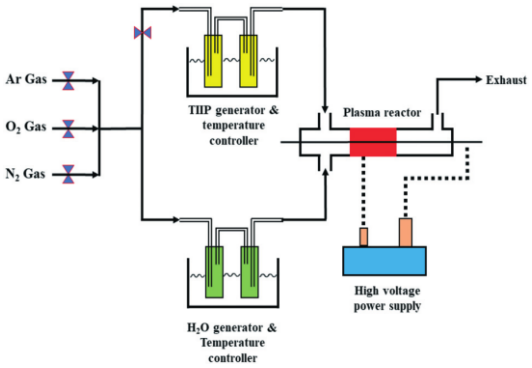

Fig. 17 Structure of the plasma-assisted fabrication process based on the atmospheric pressure plasma reactor for generating photocatalytic N-doped TiO_2 particles (reproduced from ref. 214 with permission from the American Chemical Society 2007).

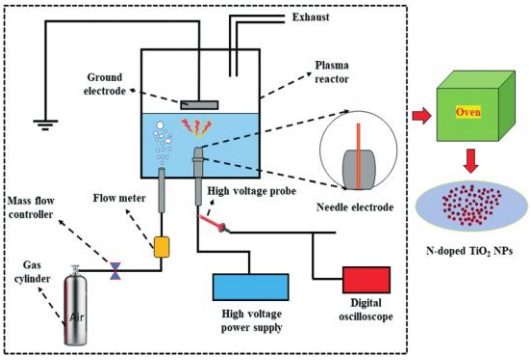

Fig. 18 Schematic drawing of the liquid-phase non-thermal plasma (LPNTP) system (adapted from ref. 216 with permission from Water Science and Technology, 2010).

nitrogen in plasma. It can be concluded that this system is a closed system with high-safety control and energy efficiency.

Another research group also developed a plasma system based on the arc-discharge method for mass production of N-doped TiO_2 NPs.[218] In particular, a pure titanium-made

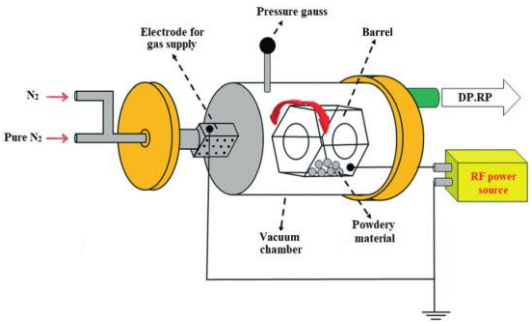

Fig. 19 Scheme of the plasma treatment system to fabricate N-doped TiO_2 (adapted from ref. 217 with permission from Elsevier, 2012).

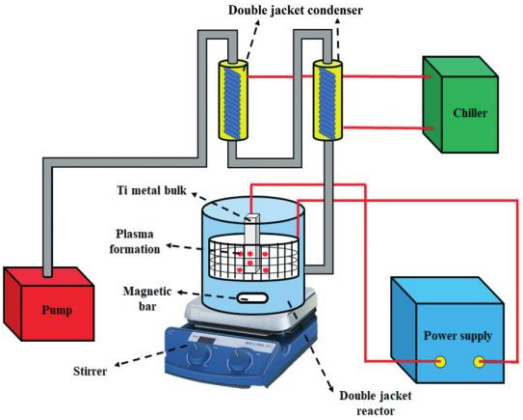

Fig. 20 Illustration of plasma-assisted fabrication based on electrolysis for N-doped TiO_2 NPs (adapted from ref. 219 with permission from Elsevier, 2018).

cylinder is set as the anode, and a tungsten needle is used as the cathode. The results depicted that most N-doped TiO_2 NPs show a disordered surface layer of 5 nm in thickness.

In 2018, a novel plasma-assisted fabrication of N-doped TiO_2 NPs was developed based on an electrolysis method using bulk titanium (Ti) as a source material and nitric acid as a nitrogen source (Fig. 20).[219] During the plasma-induced synthesis process, gaseous anionic species are generated to react with cationic Ti species to form N-doped TiO_2 NPs due to the formation of arc plasma on the metal surface. In this system, bulk titanium (Ti) is used as a source material instead of other materials like commercial TiO_2 or $Ti[OCH(CH_3)_2]_4$, indicating that plasma synthesis of N-doped TiO_2 is flexible about the use of starting materials.

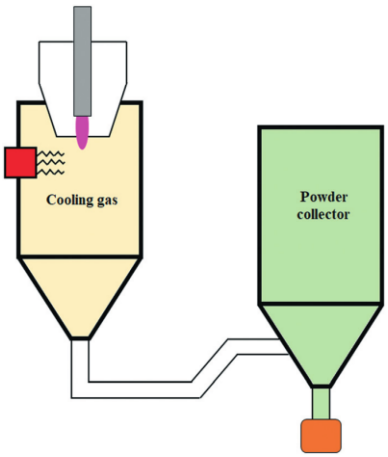

Fig. 21 Plasma synthesis reactor of N-doped ZnO NPs based on dc thermal plasma technology TiO_2 (adapted from ref. 220 with permission from Elsevier, 2012).

This journal is © The Royal Society of Chemistry 2020

View Article Online
Reaction Chemistry & Engineering Perspective

4.3. Plasma synthesis of N-doped ZnO NPs

Similar to the N-doped TiO_2 NPs, various studies on plasma synthesis of N-doped ZnO NPs have been developed. A novel dc thermal plasma reactor is designed to synthesize N-doped ZnO NPs with an average particle size of 31 nm.[220] Fig. 21 shows the plasma synthesis reactor of N-doped ZnO NPs based on dc thermal plasma technology. As a result, the adsorption of photocatalytic ZnO NPs under irradiation is obtained by doping several thousand ppm of nitrogen into ZnO. It is also demonstrated that N-doped ZnO NPs exhibit strongly photocatalytic decomposition of methylene blue and antimicrobial activity under visible light exposure. Once again, this result shows the potential applications of N-doped ZnO NPs in agricultural heritage. The power of the dc plasma-based reactor is determined at 70 kW under atmospheric pressure. The primary source of material is ZnO powder with a mean particle size of 10 μm. To dope nitrogen into ZnO particles, nitrogen gas is introduced into the plasma-forming and carrier gases.

In 2016, a RF thermal plasma process was introduced to mass produce N-doped ZnO NPs.[221] The scheme of the RF thermal plasma-assisted synthesis of N-doped ZnO NPs is shown in Fig. 22. First, the gas used to generate plasma is transferred to the torch, with the cooling water system. Later on, RF power is supplied to the induction coil. After introducing an electromagnetic field into the torch, the thermal plasma is formed. Finally, the precursors, along with carrier gas, are supplied to the thermal plasma to process vaporization and reactions. The fabrication conditions of the prepared N-doped ZnO NPs are adjusted to the power of 30 kW, with the frequency at 3.5 MHz, and the pressure at 150 torr. The cooling system is used to keep the temperature of the reactor's wall always at 300 K. The starting materials to be fed into the plasma flame are Zn powders. The results demonstrated that this system can perform mass production of N-doped NPs.

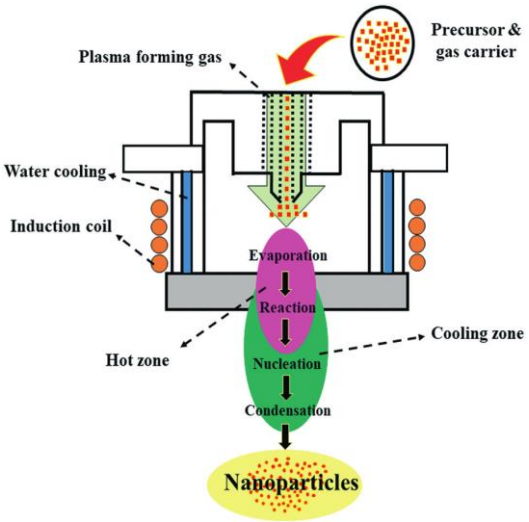

Fig. 22 Schematic procedure of the RF thermal plasma for the synthesis of N-doped ZnO NPs TiO_2 (adapted from ref. 221 with permission from Elsevier, 2016).

4.4. Plasma synthesis of N-doped CDs

In spite of being discovered in the past decades, N-CDs have become one of the most advanced materials which can be used for various applications. For this reason, many different fabrication methods have been tried to produce high-quality N-doped CDs. Recently, the microplasma system has shown its significant advantages in the production of N-doped CDs. Plasma-assisted nitrogen doping can also take place either in the form of an indirect contact plasma–liquid (ICPL) system or a direct contact plasma–liquid (DCPL) system due to the high flexibility of the plasma configuration. ICPL refers to the setting where plasma is generated in the gas phase above the surface of the electrolyte solution, while DCPL refers to the setting where plasma is formed within the bulk liquid volume.

Microplasma under atmospheric pressure generated in the form of ICPL is used to produce N-doped CDs using citric acid (CA) and ethylenediamine (EDA) as starting materials.[222] The microplasma synthesis procedure of N-doped CDs is shown in Fig. 23. Typically, a given amount of CA and EDA are dissolved in deionized water. Later on, a microplasma produced by a DC power supply under atmospheric pressure is set above the surface of the solution. The microplasma treatment is set up for 30 minutes as the anode, while the discharge current and discharge voltage are continuously kept at 6 mA and 13 kV, respectively.

Regarding DCPL, the addition of plasma gas is not necessary. Two types of the most well-known electrodes are pin-to-pin and pin-to-plate geometries. High voltage pulses are usually utilized to generate plasma as the corona. In

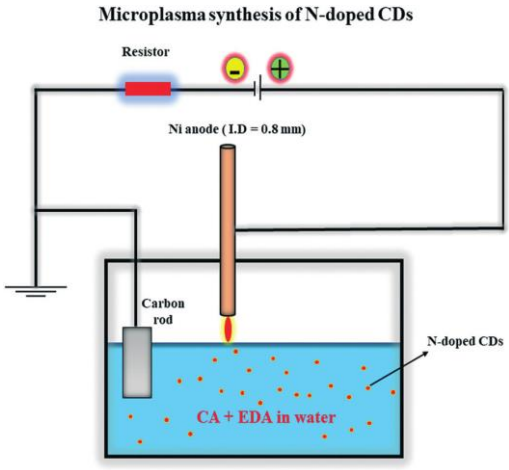

Fig. 23 Indirect microplasma–liquid interaction synthesis of nitrogen-doped carbon dots (N-doped CDs) from citric acid and ethylenediamine as initial precursors in water (from ref. 222 with permission from the Royal Society of Chemistry).

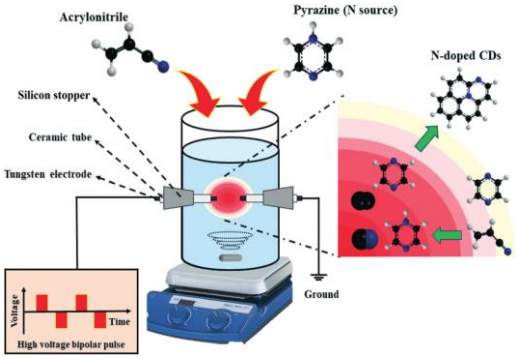

Fig. 24 Direct contact plasma–liquid (DCPL) system for the synthesis of N-doped CDs (from ref. 223 with permission from the Royal Society of Chemistry).

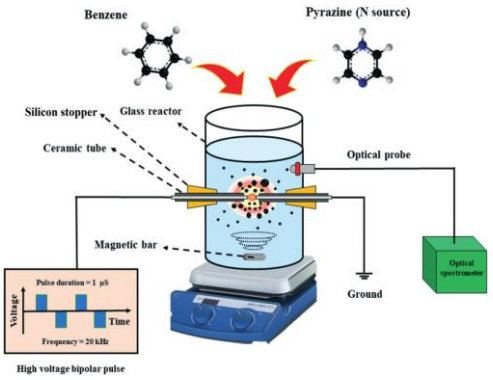

Fig. 25 Schematic illustration of the experimental setup for solution plasma synthesis of N-doped CDs (from ref. 224 with permission from the Royal Society of Chemistry).

Fig. 24, a solution plasma process is introduced to produce N-doped CDs using acrylonitrile and pyrazine as a precursor source.[223] Notably, approximately 100 mL of the solution of starting materials is used for solution plasma treatment. Microplasma treatment time is set at about 20 min under stirring. A tungsten wire is protected by a ceramic tube and designed as the electrode with a diameter of 1 mm. In the middle of a glass reactor, there is a pair of tungsten electrodes with a gap distance of 0.5 mm. A bipolar high voltage pulse with an intensity of 2.0 kV is applied to the tungsten electrodes, and the frequency is set at 20 kHz.

Similarly, another study has also been also conducted to fabricate N-doped CDs (Fig. 25), but the precursor sources for the synthesis are benzene and pyrazine.[224] In particular, a tungsten wire with a diameter of 1 mm is designed as the electrodes and shielded by a ceramic tube. In the middle of a glass reactor, a pair of tungsten electrodes is set with a distance of 1 mm. The intensity of the bipolar high voltage pulse used to apply to the tungsten electrodes is 1.5 kV, and the repetition frequency is adjusted to 20 kHz. The starting materials to synthesize N-doped CDs are benzene and pyrazine. Microplasma is introduced into 100 mL of the mixed starting materials under vigorous stirring for 20 min. When the microplasma is produced in between the electrodes, N-doped CDs are formed.

5. Green plasma-assisted production of N-doped NPs as part of the "agri-tech revolution"

Global warming,[225] degraded cultivating land,[226,227] and pesticide-resistant phytopathogens due to overuse of pesticides[228] are the primary causes of crop loss, leading to a remarkable decrease in biodiversity and impairment of ecosystem functions needed for a green agro-ecosystem.[229] With an alarming rate of population escalation, it has been estimated that the world's population has reached 7.7 billion in 2019, and is predicted to increase by more than 2 billion in 2050.[22] Therefore, an increase by 50–80% of crop production is estimated for food demand and agriculture-based products by 2050.[230] In addition, the lack of water resources and the global spread of phytopathogens are other factors that lead to deterioration of the current green agro-ecosystem.[230]

Based on such urgent needs and threats, a new agri-tech revolution has been recently proposed[19] with the aim of sustaining effective and efficient crop production to meet the demand of food in the future. This revolution, which is triggered by the advancement of information technology, novel materials, methods, and the use of plant-growth-promoting bacteria,[231] has potential advantages to make an improvement toward a more effective, efficient, resilient, green, sustainable agro-ecosystem.[19]

For many decades already the so-called "green revolution"[19] has brought considerable benefits for nitrogen fixation by advancing the Haber–Bosch (H–B) process, mechanization, agricultural irrigation, agrochemicals, *etc.*[19] Chemical nitrogen-fixation by the H–B process has played a crucial role in the green revolution and actually initiated it (Fig. 26). These technological advancements have led to considerably improved crop production efficiency. Nonetheless, the environmental impact has risen significantly

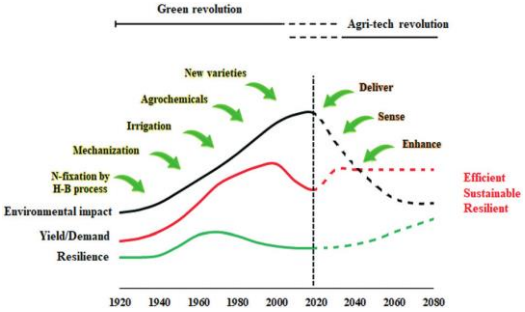

Fig. 26 Overall scheme of the green revolution and the new agri-tech revolution (from ref. 19 with permission from Nature 2019).

This journal is © The Royal Society of Chemistry 2020

from 1920 to 2020. This makes it clear that the green revolution alone cannot meet the demand for sustainability in the future due to the dynamics of the above-mentioned population growth and its assorted environmental burdens.[19] Rather, a declining resilience, increasing environmental damage, and increasing environmental impact is predicted, if simply moving on as in the past (Fig. 26). Consequently, this indicates that the green revolution may come to an end.

An entirely new approach is needed, the agri-tech revolution as defined above, to increase crop yields and resilience and to lessen the environmental impact. Its integral parts are the targeted delivery of pesticides, phytopathogenic detection, and enhanced management of plant diseases (Fig. 26). To the best of our knowledge, engineered nanomaterials (ENMs) are an excellent approach to meet those requirements. We have given evidence for that in this review: N-doped NPs are introduced and proven to be potential ENMs for enhancing crop production and also reducing the environmental effect. Existing industrial technology, including the ever-improving H–B process, will play its role in the agri-tech revolution. Yet, there is clearly a demand for alternative green technologies as well, and if it is only for reasons of complementary market provision, that is why plasma-based nitrogen fixation has been introduced in this review.

In the following, the greenness of the technology will be illustrated through four categories: (i) resource/waste on a reaction level, (ii) starting-material flexibility on a process level which translates to product flexibility, (iii) performance on a functional materials level, and (iv) process safety on a process level.

Seen from a resource/waste perspective, the plasma synthesis of N-doped NPs provides access to abundant, green, "renewable atmospheric nitrogen" as a precursor. This plasma technology is also a simple process, meaning that nitrogen can be easily fixed on the surface of nanoparticles without using any additive chemicals. The solvent itself can be used as a starting material[222–224] (see above for the solvents); which essentially makes the reaction "solvent (waste)-free".

Seen from a process-to-product perspective, an indication has been given in section 4 that the plasma manufacture of N-doped NPs is a flexible process in terms of starting material utilization. In particular, starting materials can be used in the liquid, solid, or gas phase, allowing a diversity of designs of ENMs to meet specific agricultural applications (*e.g.* delivery of pesticides, phytopathogenic detection, enhanced adhesion of pesticides *etc.*). To synthesize N-doped CDs, for example, starting carbon materials could be in the liquid phase,[222] reacting with nitrogen-containing gas in the plasma phase. As a process variant and to increase the nitrogen doping content in N-doped CDs, precursors could be selected from various mixtures of nitrogen and carbon sources such as benzene and pyrazine,[222] citric acid and ethylenediamine,[223] acrylonitrile and pyrazine.[224] There is also evidence showing that N-doped CDs can be synthesized from gaseous carbon-based-precursors. Another process variant may use solid precursors such as for N-doped TiO_2 NPs. Specifically, bulk titanium (Ti) was used as a solid starting material. During the plasma-induced synthesis process, gaseous anionic species are generated to react with cationic Ti species to form N-doped TiO_2 NPs due to the formation of arc plasma on the metal surface (Fig. 20).

Seen from a performance/function perspective, a noticeable learning from section 4 is that the plasma-assisted nitrogen fixation process has the potential to synthesize and modify high-quality engineered nanoparticles, especially N-doped NPs, as nanopesticides. These advanced materials largely fulfill the requirements part of the agri-tech revolution such as maximal use of starting materials, renewable precursors, reduced carbon footprint, energy efficiency, minimal toxicity to humans, maximal process safety, minimal solvent load, minimal waste, and flexible precursors.

Seen from a process safety perspective, the plasma-assisted synthesis of N-doped NPs is carried out in a closed system (reactor) under ambient conditions, which maximizes safety control as well as reduces unexpected accidents related to safety control.

To summarise, the plasma-based production of N-doped NPs has potential to maximize the use of renewable precursors, minimize waste production into environment and solvent load, as well as lessen toxicity and the carbon footprint to humans and the environment because no toxic additives were used or released. In addition, it fulfils the demands of the resilient and sustainable agri-tech revolution such as energy-effectiveness/carbon emission, high quality and quantity production, and maximal safety control. Finally, there is a quality argument. With its flexible designs, plasma-assisted production enables production of high-quality N-doped NPs with material properties fine-tuned to the purpose.

6. Conclusions

This review paper has studied and proved the recent achievements on using green plasma-based technology, compared to other conventional methods, to fabricate N-doped NPs and the pesticidal applications of these nanomaterials in pest control. Various plasma-assisted synthesis methods have been developed to fabricate N-doped NPs. The unique physiochemical characteristics of plasma-induced fabrication introduced active nitrogen species into the surface of nanoparticles (nanopesticides), which results in nitrogen-doped NPs. The existence of nitrogen heteroatoms on their surface also enhances the intrinsic properties of these nanopesticides, leading to potential multifunctional applications in agriculture such as pesticide nanocarriers, nanopesticides, phytopathogenic detection, and phytopathogen targeting. Some evidence has been given to prove the antibacterial and antifungal activities of N-doped NPs, paving a way for these nanomaterials to be applied widely in pest control. More importantly, plasma-induced synthesis is a flexible approach to develop various N-doped nanoparticles for targeting specifically harmful phytopathogens when the chemical structure and biological

View Article Online
Perspective Reaction Chemistry & Engineering

and physiological properties of these targeted pathogenic microorganisms are thoroughly understood. Finally, plasma-assisted production of N-doped NPs is considered as a part of the new agri-tech revolution because of their potential advantages for maximal use of starting materials, renewable precursors, reduced carbon footprint, energy efficiency, minimal toxicity to humans, maximal process safety, minimal solvent load, minimal waste, and flexible precursors.

7. Outlook

In this review, perspectives of promising applications of N-doped NPs as emerging nanopesticides and their synthesis using plasma-enabled NP technology as a green and eco-friendly and sustainable approach are presented. Several examples of N-doped NPs such as N-doped TiO_2 and N-doped ZnO evidently show their promising potential for the development of a new generation of nanopesticides based on their unique nanoscale size and active sites, catalytic performances, and new mode of pesticidal actions. Plasma-assisted synthesis of N-doped NPs to produce these materials in the future has been reviewed as an advanced technology due to its green, facile, low-cost and industry scalable capabilities. The presence of free radicals and negatively and positively charged ions in plasma is the primary reason that makes the plasma-based fabrication method suitable for N-doped NP synthesis. In comparison with traditional methods, this technique has potential to improve nanopesticide production in light of several reasons as follows:

(1) Plasma induced synthesis generates fine N-doped nanoparticles under atmospheric pressure and temperature conditions.

(2) Multi-steps of fabrication can be eliminated, leading to a more straightforward procedure without using addictive chemicals for conjugation.

(3) Safety and hazard conditions are of concern in this system as influential parameters are controllable.

(4) Plasma-generated N-doped NPs are eco-friendly and easy-to-produce nanomaterials and can be widely and effectively applied for cultural heritage.

The success of using plasma technology to produce high-quality multifunctional nanopesticides will provide new opportunities for pest control on an industrial scale. In order to deliver multifunctional NPs to large-scale agricultural production, our vision is to use smart spreaders. This seems to be a viable option, because spraying can deliver a pesticide over a large area. Due to the high pesticidal activity, targeted spraying systems can be employed for efficient dosing of chemicals (low concentration) and thus allow operation at low cost. In addition, multifunctional nanopesticides will be delivered in the form of suspension to the plants. As we discussed in this review paper, due to the advantages of plasma to modify the surface of ultra-small nanopesticides with –COOH and –OH groups, which make it more water soluble, therefore, these nanopesticides are easily dissolved in the form of suspension. The application of the new functionalized NPs has been indeed shown promising for the propagation in the field/greenhouses. For example, Ghafariyan *et al.* (2013) reported that magnetite nanoparticles were used in a greenhouse in order to investigate the impact of these functionalized NPs on soybean chlorophyll.[232]

However, in order to commercialize these pesticidal products, environmental and health risk assessment of these nanopesticides should be carried out. Unlike conventional pesticides, nanopesticides need a different approach for risk assessment (Rai S. Kookana *et al.*, 2014).[233] The Organisation for Economic Co-operation and Development (OECD) runs a large work program that is considering how test guidelines may need to be adapted in order to assess the hazard of nanopesticides. The particle number concentration and particle size distribution (PSD) as well as the ratio of "free" and nanoparticle-bound artificial intelligence are proposed for the determination of the pesticide bioavailability and toxicity. Approaches that are used to evaluate and reduce the NP health hazard could include scattering methods (*e.g.*, DLS), particle tracking methods (*e.g.*, NTA), centrifugal methods (*e.g.*, DCS), or fractionation methods (*e.g.*, FFF), the latter method allowing for determination of nanoparticle-bound artificial intelligence size when coupled with appropriate chemical selective detectors.

Although plasma-assisted synthesis of N-doped nanoparticles as nanopesticides is demonstrated as a promising technology, there are still some issues that need to be addressed. For instance, the influential parameters on synthesis conditions should be optimized depending on the properties and structure of N-doped NPs such as the design of the plasma reactor, types of plasma, precursor sources, types of power supply, *etc.* The mechanisms of N-doped NPs as nanopesticides in inactivating various pathogenic bacteria and fungi are still unanswered. Laboratory-scale plasma production of N-doped NPs has been successfully demonstrated, while industrial production for large-scale agricultural applications is also a challenge for future development.

In the long-term strategy, estimating the production cost needs to be considered as it plays a key point to further develop plasma production of nanopesticides in a large scale. Therefore, this is the main challenge for further development of plasma-assisted synthesis of N-doped nanoparticles as nanopesticides in pest control.

To the best of our knowledge, there are no cost studies on the feasibility of commercial manufacturing of nanopesticides. Yet, an analogy can be drawn to the commercial exploitation potential of plasma-based N-fixation processes for the manufacture of fertilisers, reported by us in the past years.[234,235] Anastasopoulou *et al.* have conducted a series of techno-economic feasibility studies on plasma-based fertiliser production, as an outcome of the industry-driven MAPSYN (microwave, ultrasonic and plasma assisted syntheses) European project.[234–240] These studies revealed that plasma-based fertiliser production of nitric acid, under the best assumptions (recycling, energy recovery), could have a better environmental profile than the conventional

 This journal is © The Royal Society of Chemistry 2020

process.[234] In terms of energy resources, the plasma-assisted fertilizer production is efficient in incorporating (local) renewable power supplies (solar, wind, *etc.*). The sustainability benefit of such a green-energy-powered plasma-based fertiliser production has been quantified compared to conventional natural gases. The global warming potential value is improved in the range of 68–91% with respect to a lignite-based energy supply.[234] Additionally, in terms of production process scale, the results showed that a 10 ton per day (t/d) plasma-assisted fertilizer production plant operated at 6% NO yield and with an energy consumption of 1396 KW per day.[235]

Motivated by this, a compact-plant ('container') based local fertiliser manufacture at the site of agricultural production has been envisioned ('Fertilising with the Wind', Evonik Company). The LEAP-Agri project AFRICA from the European Union currently aims to bring such a plasma technology to Africa on a small pilot scale.[241]

Apart from the aforementioned advantages, capital costs and energy costs are not yet in the range of a good industrial process.[238] For example, a plasma-assisted fertilizer production plant (10 t d^{-1}, with 6% NO yield) using the local solar and wind energy resources in Kenya would cost up to 155 and 312 million dollars, respectively.[235] Plasma-made nitric acid is calculated to be about 4 times more costly than conventionally made in terms of life-cycle costs.[239] As for electricity, this fertilizer plant will consume 10 155 706 (solar energy) and 21 720 846 (wind energy) kWh per year.[235]

It is hoped that this review could provide an insight into a novel plasma-assisted synthesis of N-doped NPs and the applications of these multifunctional NPs for agricultural pest control, paving a new way for more efficient, sustainable and environmentally friendly agriculture.

Author contributions

Mr. Hue Quoc Pho wrote and edited the draft of the manuscript. Prof. Volker Hessel, Prof. Dusan Losic, Prof. Kostya (Ken) Ostrikov, and Dr. Nam have revised the draft.

Conflicts of interest

The authors declare that they have no conflict of interest.

Acknowledgements

Mr. Hue Quoc Pho received the divisional ECMS and full-fee scholarships from the University of Adelaide, Australia. The authors acknowledge support from the ERC Grant Surface-Confined fast-modulated Plasma for process and Energy intensification (SCOPE) from the European Commission with grant number 810182.

References

1 H. C. J. Godfray, D. Mason-D'Croz and S. Robinson, *Philos. Trans. R. Soc., B*, 2016, **371**, 20150467.
2 A. Jain, S. Sarsaiya, Q. Wu, Y. Lu and J. Shi, *Bioengineered*, 2019, **10**, 409–424.
3 X. Yan and N. J. Talbot, *Curr. Opin. Microbiol.*, 2016, **34**, 147–153.
4 M. Osés-Ruiz and N. J. Talbot, *Commun. Integr. Biol.*, 2017, **10**, e1372067.
5 D. Saleh, J. Milazzo, H. Adreit, E. Fournier and D. Tharreau, *New Phytol.*, 2014, **201**, 1440–1456.
6 J. Fernandez and K. Orth, *Trends Microbiol.*, 2018, **26**, 582–597.
7 L. S. Ryder, Y. F. Dagdas, M. J. Kershaw, C. Venkataraman, A. Madzvamuse, X. Yan, N. Cruz-Mireles, D. M. Soanes, M. Oses-Ruiz, V. Styles, J. Sklenar, F. L. H. Menke and N. J. Talbot, *Nature*, 2019, **574**, 423–427.
8 B. Williamson, B. Tudzynski, P. Tudzynski and J. A. L. Van Kan, *Mol. Plant Pathol.*, 2007, **8**, 561–580.
9 K. Youssef, S. R. Roberto and A. G. de Oliveira, *Biomolecules*, 2019, **9**, 582.
10 C. Calvo-Garrido, J. Roudet, N. Aveline, L. Davidou, S. Dupin and M. Fermaud, *Front. Plant Sci.*, 2019, **10**, 105.
11 Y. H. Liu, S. K. Yuan, X. R. Hu and C. Q. Zhang, *Sci. Rep.*, 2019, **9**, 11644.
12 S. Rajeshkumar, in *Nanomaterials in Plants, Algae and Microorganisms*, Elsevier, 2019, pp. 197–217.
13 S. Rajeshkumar, in *Nanomaterials in Plants, Algae and Microorganisms*, ed. D. K. Tripathi, P. Ahmad, S. Sharma, D. K. Chauhan and N. K. Dubey, Academic Press, 2019, pp. 197–217, DOI: 10.1016/B978-0-12-811488-9.00010-X.
14 B. M. Duggar, *Ann. Mo. Bot. Gard.*, 1915, **2**, 403–458.
15 N. J. Baltes, J. Gil-Humanes and D. F. Voytas, in *Progress in molecular biology and translational science*, Elsevier, 2017, vol. 149, pp. 1–26.
16 M. S. AL-Ahmadi, in *Pesticides, Anthropogenic Activities and the Health of our Environment*, IntechOpen, 2019.
17 S. Savary, L. Willocquet, S. J. Pethybridge, P. Esker, N. McRoberts and A. Nelson, *Nat. Ecol. Evol.*, 2019, **3**, 430–439.
18 B. Huang, F. Chen, Y. Shen, K. Qian, Y. Wang, C. Sun, X. Zhao, B. Cui, F. Gao and Z. Zeng, *Nanomaterials*, 2018, **8**, 102.
19 G. V. Lowry, A. Avellan and L. M. Gilbertson, *Nat. Nanotechnol.*, 2019, **14**, 517–522.
20 R. Prasad, A. Bhattacharyya and Q. D. Nguyen, *Front. Microbiol.*, 2017, **8**, 1014.
21 L. Marchiol, *New Visions in Plant Science*, 2018, p. 121.
22 M. Kah, N. Tufenkji and J. C. White, *Nat. Nanotechnol.*, 2019, **14**, 532–540.
23 M. Kah, H. Walch and T. Hofmann, *Environ. Sci.: Nano*, 2018, **5**, 882–889.
24 F. Zulfiqar, M. Navarro, M. Ashraf, N. A. Akram and S. Munné-Bosch, *Plant Sci.*, 2019, **289**, 110270.
25 Y. Shang, M. Hasan, G. J. Ahammed, M. Li, H. Yin and J. Zhou, *Molecules*, 2019, **24**, 2558.
26 G. A. Achari and M. Kowshik, *J. Agric. Food Chem.*, 2018, **66**, 8647–8661.
27 X. He, H. Deng and H.-M. Hwang, *J. Food Drug Anal.*, 2019, **27**, 1–21.

This journal is © The Royal Society of Chemistry 2020

28 L. Li, Z. Xu, M. Kah, D. Lin and J. Filser, *Environ. Sci. Technol.*, 2019, **53**(14), 7923–7924.
29 A. Rastogi, D. K. Tripathi, S. Yadav, D. K. Chauhan, M. Živčák, M. Ghorbanpour, N. I. El-Sheery and M. Brestic, *3 Biotech.*, 2019, **9**, 90.
30 A. Derbalah, M. Shenashen, A. Hamza, A. Mohamed and S. El Safty, *Egypt. J. Basic Appl. Sci.*, 2018, **5**, 145–150.
31 H. A. Ayoub, M. Khairy, F. A. Rashwan and H. F. Abdel-Hafez, *J. Nanostruct. Chem.*, 2017, **7**, 91–100.
32 P. Paralikar, A. P. Ingle, V. Tiwari, P. Golinska, H. Dahm and M. Rai, *J. Environ. Sci. Health, Part A: Toxic/Hazard. Subst. Environ. Eng.*, 2019, **54**, 381–390.
33 S. Shankar and J.-W. Rhim, *Food Hydrocolloids*, 2018, **82**, 116–123.
34 S. Shankar, R. Pangeni, J. W. Park and J.-W. Rhim, *Mater. Sci. Eng., C*, 2018, **92**, 508–517.
35 S. Rajeshkumar, R. Santhiyaa and P. Veena, in *Exploring the Realms of Nature for Nanosynthesis*, Springer, 2018, pp. 109–145.
36 B. K. Mandal, in *Nano-Biopesticides Today and Future Perspectives*, ed. O. Koul, Academic Press, 2019, pp. 281–302, DOI: 10.1016/B978-0-12-815829-6.00012-7.
37 J. Chen, S. Li, J. Luo, R. Wang and W. Ding, *J. Nanomater.*, 2016, **2016**, 15.
38 S. B. Jaffri and K. S. Ahmad, *Artif. Cells, Nanomed., Biotechnol.*, 2018, **46**, 127–137.
39 J. Chen, S. Mao, Z. Xu and W. Ding, *RSC Adv.*, 2019, **9**, 3788–3799.
40 R. C. Kasana, N. R. Panwar, R. K. Kaul and P. Kumar, in *Nanoscience in Food and Agriculture 3*, Springer, 2016, pp. 129–143.
41 V. Sinisi, P. Pelagatti, M. Carcelli, A. Migliori, L. Mantovani, L. Righi, G. Leonardi, S. Pietarinen, C. Hubsch and D. Rogolino, *ACS Sustainable Chem. Eng.*, 2018, **7**, 3213–3221.
42 A. Singh, N. Singh, S. Afzal, T. Singh and I. Hussain, *J. Mater. Sci.*, 2018, **53**, 185–201.
43 Z. Luksiene, N. Rasiukeviciute, B. Zudyte and N. Uselis, *J. Photochem. Photobiol., B*, 2019, 111656.
44 S. Baker, S. Satish, N. Prasad and R. S. Chouhan, in *Industrial Applications of Nanomaterials*, Elsevier, 2019, pp. 341–363.
45 R. Rekha, M. Divya, M. Govindarajan, N. S. Alharbi, S. Kadaikunnan, J. M. Khaled, M. N. Al-Anbr, R. Pavela and B. Vaseeharan, *J. Photochem. Photobiol., B*, 2019, **199**, 111620.
46 S. S. Boxi, K. Mukherjee and S. Paria, *Nanotechnology*, 2016, **27**, 085103.
47 J. Li, M. Su, A. Wang, Z. Wu, Y. Chen, D. Qin and Z. Jiang, *Int. J. Mol. Sci.*, 2019, **20**, 5497.
48 X. Wang, H. Xie, Z. Wang and K. He, *Colloids Surf., B*, 2019, **173**, 632–638.
49 X. Wang, C. Liu, H. Li, H. Zhang, R. Ma, Q. Zhang, F. Yang, Y.-C. Liao, W. Yuan and F. Chen, *Environ. Sci.: Nano*, 2019, **6**, 3401–3421.
50 S.-C. Chun and M. Chandrasekaran, *Int. J. Biol. Macromol.*, 2019, **125**, 948–954.
51 S. Muthukrishnan, I. Murugan and M. Selvaraj, *Carbohydr. Polym.*, 2019, **212**, 169–177.
52 M. Malerba and R. Cerana, *Polymer*, 2019, **11**, 839.
53 Y. Wang, D. Ji, T. Chen, B. Li, Z. Zhang, G. Qin and S. Tian, *Int. J. Mol. Sci.*, 2019, **20**, 2994.
54 M. Ali, Z. Cheng, H. Ahmad and S. Hayat, *J. Plant Interact.*, 2018, **13**, 353–363.
55 H. Zhang, D. Meng, B. Fu, H. Fan, R. Cai, P. P. Fu and X. Wu, *J. Environ. Sci. Health, Part C: Environ. Carcinog. Ecotoxicol. Rev.*, 2019, 1–18.
56 H. Yin, P. S. Casey, M. J. McCall and M. Fenech, *Langmuir*, 2010, **26**, 15399–15408.
57 Y. Nosaka and A. Y. Nosaka, *Chem. Rev.*, 2017, **117**, 11302–11336.
58 L. K. Putri, B.-J. Ng, W.-J. Ong, H. W. Lee, W. S. Chang and S.-P. Chai, *ACS Appl. Mater. Interfaces*, 2017, **9**, 4558–4569.
59 Z. Song, M. Wang, Z. Wang, Y. Wang, R. Li, Y. Zhang, C. Liu, Y. Liu, B. Xu and F. Qi, *Environ. Sci. Technol.*, 2019, **53**(9), 5337–5348.
60 W. Wang, M. O. Tade and Z. Shao, *Prog. Mater. Sci.*, 2018, **92**, 33–63.
61 M. Li, Q. Z. Huang, D. F. Qiu, Z. J. Jiao, Z. H. Meng and H. Z. Shi, *Chin. Chem. Lett.*, 2010, **21**, 117–121.
62 N. Bundaleska, J. Henriques, M. Abrashev, A. M. B. do Rego, A. M. Ferraria, A. Almeida, F. M. Dias, E. Valcheva, B. Arnaudov, K. K. Upadhyay, M. F. Montemor and E. Tatarova, *Sci. Rep.*, 2018, **8**, 12595.
63 J. Xu, R. Zhang, S. Lu, H. Liu, Z. Li, X. Zhang and S. Ding, *Nanotechnology*, 2018, **29**, 305708.
64 S. Sudhakar, K. K. Jaiswal and A. P. Ramaswamy, *ChemistrySelect*, 2018, **3**, 8962–8972.
65 Y. Zhou, N. Wang, J. Muhammad, D. Wang, Y. Duan, X. Zhang, X. Dong and Z. Zhang, *Carbon*, 2019, **148**, 204–213.
66 Y. Zhou, N. Wang, X. Qu, F. Huang, Y. Duan, X. Zhang, X. Dong and Z. Zhang, *Nanoscale*, 2019, **11**, 19994–20005.
67 D. Zhang, K. Ye, Y. Yao, F. Liang, T. Qu, W. Ma, B. Yang, Y. Dai and T. Watanabe, *Carbon*, 2019, **142**, 278–284.
68 I. Novodchuk, M. Irannejad, B. Wales, K. Ibrahim, J. Sanderson, M. Bajcsy and M. Yavuz, *Mater. Res. Bull.*, 2019, **111**, 80–86.
69 I. Novoa-De León, J. Johny, S. Vázquez-Rodríguez, N. García-Gómez, S. Carranza-Bernal, I. Mendivil, S. Shaji and S. Sepúlveda-Guzmán, *Carbon*, 2019, **150**, 455–464.
70 J. Ding, P. Kannan, P. Wang, S. Ji, H. Wang, Q. Liu, H. Gai, F. Liu and R. Wang, *J. Power Sources*, 2019, **413**, 209–215.
71 A. Ghazitabar, M. Naderi and D. F. Haghshenas, *Ceram. Int.*, 2018, **44**, 23162–23171.
72 Y. Cui and J. D. Atkinson, *Mater. Chem. Phys.*, 2019, **221**, 29–33.
73 W. H. Abdelraheem, M. K. Patil, M. N. Nadagouda and D. D. Dionysiou, *Appl. Catal., B*, 2019, **241**, 598–611.
74 Y.-C. Shi, J.-J. Feng, X.-X. Lin, L. Zhang, J. Yuan, Q.-L. Zhang and A.-J. Wang, *Electrochim. Acta*, 2019, **293**, 504–513.
75 T. Zhang, Y. Guo, J. Li, Y. Guan, Z. Guo and H. Ma, *Propellants, Explos., Pyrotech.*, 2018, **43**, 1263–1269.
76 G. Panomsuwan, J. Chantaramethakul, C. Chokradjaroen and T. Ishizaki, *Mater. Lett.*, 2019, **251**, 135–139.

 This journal is © The Royal Society of Chemistry 2020

77 G. Ghanashyam and H. K. Jeong, *Chem. Phys. Lett.*, 2019, **725**, 31–37.
78 T. Zhu, S. Li, B. Ren, L. Zhang, L. Dong and L. Tan, *J. Mater. Sci.*, 2019, **54**, 9632–9642.
79 S. Rajeshkumar, L. Bharath and R. Geetha, in *Green Synthesis, Characterization and Applications of Nanoparticles*, Elsevier, 2019, pp. 429–444.
80 T. Gomathi, K. Rajeshwari, V. Kanchana, P. N. Sudha and K. Parthasarathy, in *Sustainable Polymer Composites and Nanocomposites*, ed. Inamuddin, S. Thomas, R. Kumar Mishra and A. M. Asiri, Springer International Publishing, Cham, 2019, pp. 313–336, DOI: 10.1007/978-3-030-05399-4_11.
81 M. Kah and T. Hofmann, *Environ. Int.*, 2014, **63**, 224–235.
82 C. G. Athanassiou, N. G. Kavallieratos, G. Benelli, D. Losic, P. Usha Rani and N. Desneux, *J. Pestic. Sci.*, 2018, **91**, 1–15.
83 A. Moreno, A. Jordana, R. Grillo, L. F. Fraceto and C. Jaime, *Colloids Surf., A*, 2019, **562**, 220–228.
84 A. B. Bombo, A. E. R. S. Pereira, M. G. Lusa, E. de Medeiros Oliveira, J. L. de Oliveira, E. V. R. Campos, M. B. de Jesus, H. C. Oliveira, L. F. Fraceto and J. L. S. Mayer, *J. Agric. Food Chem.*, 2019, **67**, 4453–4462.
85 P. Sharma, A. Sharma, M. Sharma, N. Bhalla, P. Estrela, A. Jain, P. Thakur and A. Thakur, *Global Challenges*, 2017, **1**, 1700041.
86 I. U. Haq and S. Ijaz, in *Nanobiotechnology in Bioformulations*, Springer, 2019, pp. 289–316.
87 J.-S. Hwang, J. Yu, H.-M. Kim, J.-M. Oh and S.-J. Choi, *Nanomaterials*, 2019, **9**, 1175.
88 M. G. Mendez Medrano, E. Kowalska, M. Endo Kimura, K. Wang, B. Ohtani, D. Bahena Uribe, J. L. Rodriguez Lopez and H. Remita, *ACS Appl. Bio Mater.*, 2019, **2**(12), 5626–5633.
89 J. Bogdan, A. Jackowska-Tracz, J. Zarzyńska and J. Pławińska-Czarnak, *Nanoscale Res. Lett.*, 2015, **10**, 57.
90 J. Podporska-Carroll, E. Panaitescu, B. Quilty, L. Wang, L. Menon and S. C. Pillai, *Appl. Catal., B*, 2015, **176**, 70–75.
91 S. Marimuthu, A. A. Rahuman, C. Jayaseelan, A. V. Kirthi, T. Santhoshkumar, K. Velayutham, A. Bagavan, C. Kamaraj, G. Elango and M. Iyappan, *Asian Pac. J. Trop. Med.*, 2013, **6**, 682–688.
92 J. Wang, C. Li, H. Zhuang and J. Zhang, *Food Control*, 2013, **34**, 372–377.
93 G. De Filpo, A. M. Palermo, F. Rachiele and F. P. Nicoletta, *Int. Biodeterior. Biodegrad.*, 2013, **85**, 217–222.
94 O. Owolade and D. Ogunleti, *J. Plant Prot. Res.*, 2008, **48**, 329–336.
95 R. Mahto, N. Chatterjee, T. Priya and R. K. Singh, in *Agronomic Crops: Volume 2: Management Practices*, ed. M. Hasanuzzaman, Springer Singapore, Singapore, 2019, pp. 605–636, DOI: 10.1007/978-981-32-9783-8_27.
96 R. Raliya, P. Biswas and J. C. Tarafdar, *Biotechnol. Rep.*, 2015, **5**, 22–26.
97 R. Ahmad, M. Mohsin, T. Ahmad and M. Sardar, *J. Hazard. Mater.*, 2015, **283**, 171–177.
98 T. Santhoshkumar, A. A. Rahuman, C. Jayaseelan, G. Rajakumar, S. Marimuthu, A. V. Kirthi, K. Velayutham, J. Thomas, J. Venkatesan and S.-K. Kim, *Asian Pac. J. Trop. Med.*, 2014, 7, 968–976.
99 F. Haghighi, S. Roudbar Mohammadi, P. Mohammadi, S. Hosseinkhani and R. Shipour, *Infect., Epidemiol. Microbiol.*, 2013, **1**, 33–38.
100 B. Durairaj, S. Muthu and T. Xavier, *Adv. Appl. Sci. Res.*, 2015, **6**, 45–48.
101 M. Biguzzi and G. Shama, *Lett. Appl. Microbiol.*, 1994, **19**, 458–460.
102 P. Amezaga-Madrid, R. Silveyra-Morales, L. Cordoba-Fierro, G. Nevarez-Moorillon, M. Miki-Yoshida, E. Orrantia-Borunda and F. Solıs, *J. Photochem. Photobiol., B*, 2003, **70**, 45–50.
103 K. Uboncholakate, L. Sikong and F. Saito, *Procedia Eng.*, 2012, **32**, 656–662.
104 A. Clemente, J. J. Ramsden, A. Wright, F. Iza, J. A. Morrissey, G. L. Puma and D. J. Malik, *J. Photochem. Photobiol., B*, 2019, **193**, 131–139.
105 C. Belkhaoui, N. Mzabi, H. Smaoui and P. Daniel, *Results Phys.*, 2019, **12**, 1686–1696.
106 E. Pargoletti, U. H. Hossain, I. Di Bernardo, H. Chen, T. Tran-Phu, J. Lipton-Duffin, G. Cappelletti and A. Tricoli, *Nanoscale*, 2019, **11**, 22932–22945.
107 V. S. Bhati, M. Hojamberdiev and M. Kumar, *Energy Rep.*, 2020, **6**, 46–62.
108 H. Gupta, J. Singh, R. N. Dutt, S. Ojha, S. Kar, R. Kumar, V. R. Reddy and F. Singh, *Phys. Chem. Chem. Phys.*, 2019, **21**, 15019–15029.
109 W. Han, J. Kim and H.-H. Park, *Sci. Rep.*, 2019, **9**, 6244.
110 G. Milano, M. Luebben, M. Laurenti, S. Porro, K. Bejtka, S. Bianco, U. Breuer, L. Boarino, I. Valov and C. Ricciardi, *Adv. Mater. Interfaces*, 2019, **6**, 1900803.
111 E. Ben Amara, A. Lebib, Z. Zaaboub and L. Beji, *RSC Adv.*, 2019, **9**, 25133–25141.
112 S. N. Nguyen, T. K. Truong, S.-J. You, Y.-F. Wang, T. M. Cao and V. V. Pham, *ACS Omega*, 2019, **4**, 12853–12859.
113 S. L. Schneider and H. W. Lim, *Photodermatol., Photoimmunol. Photomed.*, 2019, **35**, 442–446.
114 H. Zhang, X. Lv, Y. Li, Y. Wang and J. Li, *ACS Nano*, 2010, **4**, 380–386.
115 F. Zhao, W. Gu, J. Zhou, Q. Liu and Y. Chong, *J. Environ. Sci. Health, Part C: Environ. Carcinog. Ecotoxicol. Rev.*, 2019, **37**, 67–80.
116 P. Sivakumar, M. Lee, Y.-S. Kim and M. S. Shim, *J. Mater. Chem. B*, 2018, **6**, 4852–4871.
117 G. Yi, X. Li, Y. Yuan and Y. Zhang, *Environ. Sci.: Nano*, 2019, **6**, 68–74.
118 M. O. Moss, *J. Appl. Microbiol.*, 2008, **104**, 1239–1243.
119 D. Gong, Y. Bi, Y. Li, Y. Zong, Y. Han and D. Prusky, *Front. Plant Sci.*, 2019, **10**, 338.
120 E. M. El-Diasty, M. Ahmed, N. Okasha, S. F. Mansour, S. I. El-Dek, H. El-Khalek and M. H. Youssif, *Rom. J. Biophys.*, 2013, **23**, 191–202.
121 A. Wani and M. Shah, *J. Appl. Pharm. Sci.*, 2012, **2**, 4.

This journal is © The Royal Society of Chemistry 2020

122 L. He, Y. Liu, A. Mustapha and M. Lin, *Microbiol. Res.*, 2011, **166**, 207–215.
123 N. O. Jasim, *J. Nat. Sci. Res.*, 2015, **5**, 23–27.
124 S. Ruffolo, M. La Russa, M. Malagodi, C. O. Rossi, A. Palermo and G. Crisci, *Appl. Phys. A*, 2010, **100**, 829–834.
125 C. O. Dimkpa, J. E. McLean, D. W. Britt and A. J. Anderson, *BioMetals*, 2013, **26**, 913–924.
126 T. Jin, D. Sun, J. Su, H. Zhang and H. J. Sue, *J. Food Sci.*, 2009, **74**, M46–M52.
127 L. Zhang, Y. Jiang, Y. Ding, M. Povey and D. York, *J. Nanopart. Res.*, 2007, **9**, 479–489.
128 A. A. Tayel, W. F. El-Tras, S. Moussa, A. F. El-Baz, H. Mahrous, M. F. Salem and L. Brimer, *J. Food Saf.*, 2011, **31**, 211–218.
129 D. M. DeMarini, M. L. Shelton and L. F. Stankowski, *Mutat. Res., Fundam. Mol. Mech. Mutagen.*, 1995, **327**, 131–149.
130 J. Gomes, J. Lincho, E. Domingues, R. M. Quinta-Ferreira and R. C. Martins, *Water*, 2019, **11**, 373.
131 D. Ranjith Kumar, K. S. Ranjith, Y. Haldorai, A. Kandasami and R. T. Rajendra Kumar, *ACS Omega*, 2019, **4**, 11973–11979.
132 M. A. Ahmad, Y. Yuesuo, Q. Ao, M. Adeel, Z. Y. Hui and R. Javed, *Molecules*, 2019, **24**, 3916.
133 R. Javed, M. Usman, S. Tabassum and M. Zia, *Appl. Surf. Sci.*, 2016, **386**, 319–326.
134 Y. Liu, J. Li, X. Qiu and C. Burda, *J. Photochem. Photobiol., A*, 2007, **190**, 94–100.
135 R. Asahi, T. Morikawa, T. Ohwaki, K. Aoki and Y. Taga, *Science*, 2001, **293**, 269–271.
136 Z. Lin, A. Orlov, R. M. Lambert and M. C. Payne, *J. Phys. Chem. B*, 2005, **109**, 20948–20952.
137 M. Janus, E. Kusiak-Nejman, P. Rokicka-Konieczna, A. Markowska-Szczupak, K. Zając and A. W. Morawski, *Molecules*, 2019, **24**, 3026.
138 M. Iwatsu, T. Ogawa, T. Mokudai, H. Kanetaka, M. Kawashita, T. Watanabe and K. Sasaki, *Clin. Oral Implants Res.*, 2018, **29**, 242.
139 J. Zhang, Y. Liu, Q. Li, X. Zhang and J. K. Shang, *ACS Appl. Mater. Interfaces*, 2013, **5**, 10953–10959.
140 B. M. Rajbongshi, A. Ramchiary and S. Samdarshi, *Mater. Lett.*, 2014, **134**, 111–114.
141 H. Qin, W. Li, Y. Xia and T. He, *ACS Appl. Mater. Interfaces*, 2011, **3**, 3152–3156.
142 C. Shifu, Z. Wei, Z. Sujuan and L. Wei, *Chem. Eng. J.*, 2009, **148**, 263–269.
143 M. Samadi, M. Zirak, A. Naseri, E. Khorashadizade and A. Z. Moshfegh, *Thin Solid Films*, 2016, **605**, 2–19.
144 M. Y. Memar, R. Ghotaslou, M. Samiei and K. Adibkia, *Infect. Drug Resist.*, 2018, **11**, 567.
145 T. Nozaki, T. Kakuda, Y. B. Pottathara and H. Kawasaki, *Photochem. Photobiol. Sci.*, 2019, **18**, 1235–1241.
146 S. R. Anand, A. Bhati, D. Saini, Gunture, N. Chauhan, P. Khare and S. K. Sonkar, *ACS Omega*, 2019, **4**, 1581–1591.
147 V. Naik, P. Zantye, D. Gunjal, A. Gore, P. Anbhule, M. Kowshik, S. V. Bhosale and G. Kolekar, *ACS Appl. Bio Mater.*, 2019, **2**, 2069–2077.
148 K. O. Boakye-Yiadom, S. Kesse, Y. Opoku-Damoah, M. S. Filli, M. Aquib, M. M. B. Joelle, M. A. Farooq, R. Mavlyanova, F. Raza, R. Bavi and B. Wang, *Int. J. Pharm.*, 2019, **564**, 308–317.
149 V. Mishra, A. Patil, S. Thakur and P. Kesharwani, *Drug Discovery Today*, 2018, **23**, 1219–1232.
150 Q. Guan, R. Su, M. Zhang, R. Zhang, W. Li, D. Wang, M. Xu, L. Fei and Q. Xu, *New J. Chem.*, 2019, **43**, 3050–3058.
151 A. Sciortino, A. Cannizzo and F. Messina, *C*, 2018, **4**, 67.
152 S. Campuzano, P. Yáñez-Sedeño and J. M. Pingarrón, *Nanomaterials*, 2019, **9**, 634.
153 Q. Zhang, S. Deng, J. Liu, X. Zhong, J. He, X. Chen, B. Feng, Y. Chen and K. Ostrikov, *Adv. Funct. Mater.*, 2019, **29**, 1805860.
154 M. Han, S. Zhu, S. Lu, Y. Song, T. Feng, S. Tao, J. Liu and B. Yang, *Nano Today*, 2018, **19**, 201–218.
155 Y. Zhou, E. M. Zahran, B. A. Quiroga, J. Perez, K. J. Mintz, Z. Peng, P. Y. Liyanage, R. R. Pandey, C. C. Chusuei and R. M. Leblanc, *Appl. Catal., B*, 2019, **248**, 157–166.
156 F. Yuan, Z. Wang, X. Li, Y. Li, Z. A. Tan, L. Fan and S. Yang, *Adv. Mater.*, 2017, **29**, 1604436.
157 D.-W. Zheng, B. Li, C.-X. Li, J.-X. Fan, Q. Lei, C. Li, Z. Xu and X.-Z. Zhang, *ACS Nano*, 2016, **10**, 8715–8722.
158 F. Lin, Y.-W. Bao and F.-G. Wu, *C*, 2019, **5**, 33.
159 M. J. Meziani, X. Dong, L. Zhu, L. P. Jones, G. E. LeCroy, F. Yang, S. Wang, P. Wang, Y. Zhao and L. Yang, *ACS Appl. Mater. Interfaces*, 2016, **8**, 10761–10766.
160 H. Li, J. Huang, Y. Song, M. Zhang, H. Wang, F. Lu, H. Huang, Y. Liu, X. Dai and Z. Gu, *ACS Appl. Mater. Interfaces*, 2018, **10**, 26936–26946.
161 X. Liu, J. Liu, B. Zheng, L. Yan, J. Dai, Z. Zhuang, J. Du, Y. Guo and D. Xiao, *New J. Chem.*, 2017, **41**, 10607–10612.
162 N. A. Travlou, D. A. Giannakoudakis, M. Algarra, A. M. Labella, E. Rodríguez-Castellón and T. J. Bandosz, *Carbon*, 2018, **135**, 104–111.
163 D. Yoo, Y. Park, B. Cheon and M.-H. Park, *Nanoscale Res. Lett.*, 2019, **14**, 272.
164 A. C. Oluwaseun, P. Phazang and N. B. Sarin, *Biosensing Technologies for the Detection of Pathogens: A Prospective Way for Rapid Analysis*, 2018, p. 37.
165 S. Bhuckory, J. C. Kays and A. M. Dennis, *Biosensors*, 2019, **9**, 76.
166 P. T. Snee, *TrAC, Trends Anal. Chem.*, 2019, 115750, DOI: 10.1016/j.trac.2019.115750.
167 E. Bozkurt and Y. Onganer, *Synth. Met.*, 2018, **245**, 260–266.
168 J. Jiménez-López, S. S. M. Rodrigues, D. S. M. Ribeiro, P. Ortega-Barrales, A. Ruiz-Medina and J. L. M. Santos, *Spectrochim. Acta, Part A*, 2019, **212**, 246–254.
169 F. Rad, A. Mohsenifar, M. Tabatabaei, M. Safarnejad, F. Shahryari, H. Safarpour, A. Foroutan, M. Mardi, D. Davoudi and M. Fotokian, *J. Plant Pathol.*, 2012, **94**, 525–534.
170 H. Safarpour, M. R. Safarnejad, M. Tabatabaei, A. Mohsenifar, F. Rad, M. Basirat, F. Shahryari and F. Hasanzadeh, *Can. J. Plant Pathol.*, 2012, **34**, 507–515.
171 C. Xia, S. Zhu, T. Feng, M. Yang and B. Yang, *Adv. Sci.*, 2019, **6**, 1901316.

 This journal is © The Royal Society of Chemistry 2020

172 T. Yadavalli and D. Shukla, *Nanomed.: Nanotechnol., Biol. Med.*, 2017, **13**, 219–230.
173 T. Vangijzegem, D. Stanicki and S. Laurent, *Expert Opin. Drug Delivery*, 2019, **16**, 69–78.
174 E. Calzoni, A. Cesaretti, A. Polchi, A. Di Michele, B. Tancini and C. Emiliani, *J. Funct. Biomater.*, 2019, **10**, 4.
175 Y. Zhou, G. Quan, Q. Wu, X. Zhang, B. Niu, B. Wu, Y. Huang, X. Pan and C. Wu, *Acta Pharm. Sin. B*, 2018, **8**, 165–177.
176 Z. Ji, A. Sheardy, Z. Zeng, W. Zhang, H. Chevva, K. Allado, Z. Yin and J. Wei, *Molecules*, 2019, **24**, 152.
177 W. Liu, C. Li, Y. Ren, X. Sun, W. Pan, Y. Li, J. Wang and W. Wang, *J. Mater. Chem. B*, 2016, **4**, 5772–5788.
178 M. L. Liu, B. B. Chen, C. M. Li and C. Z. Huang, *Green Chem.*, 2019, **21**, 449–471.
179 M. Pan, Z. Xu, Q. Jiang, J. Feng, J. Sun, F. Wang and X. Liu, *Nanoscale Adv.*, 2019, **1**, 765–771.
180 B. Yao, H. Huang, Y. Liu and Z. Kang, *Trends Chem.*, 2019, 235–246.
181 O. Azie, Z. F. Greenberg, C. D. Batich and J. P. Dobson, *Int. J. Mol. Sci.*, 2019, **20**, 3190.
182 A. Baseer, A. Koenneke, J. Zapp, S. A. Khan and M. Schneider, *Macromol. Chem. Phys.*, 2019, **220**, 1900260.
183 S. Trombino, C. Servidio, F. Curcio and R. Cassano, *Pharmaceutics*, 2019, **11**, 407.
184 C. E. Campiglio, N. Contessi Negrini, S. Farè and L. Draghi, *Materials*, 2019, **12**, 2476.
185 M. P. Wickramathilaka and B. Y. Tao, *J. Biol. Eng.*, 2019, **13**, 63.
186 M. S. A. Mewada, in *Carbon Dots as Theranostic Agents*, 2018, pp. 209–240, DOI: 10.1002/9781119460435.ch6.
187 M. Thakur, S. Pandey, A. Mewada, V. Patil, M. Khade, E. Goshi and M. Sharon, *J. Drug Delivery*, 2014, 9.
188 F. Rezzonico, V. O. Stockwell and B. Duffy, *Antimicrob. Agents Chemother.*, 2009, **53**, 3173–3177.
189 A. K. Misra, *Agricultural Uses of Antibiotics*, Moats, WA, 1986.
190 I. Ahmad and F. M. Husain, *Biofilms in plant and soil health*, Wiley Online Library, 2017.
191 S. G. Aćimović, Q. Zeng, G. C. McGhee, G. W. Sundin and J. C. Wise, *Front. Plant Sci.*, 2015, **6**, 16.
192 D. Shtienberg, M. Zilberstaine, D. Oppenheim, Z. Herzog, S. Manulis, H. Shwartz and G. Kritzman, *Phytoparasitica*, 2001, **29**, 143–154.
193 D. Puppe and M. Sommer, *Advances in Agronomy*, 2018, vol. 152, pp. 1–49.
194 W. F. Tinto, T. O. Elufioye and J. Roach, "*Waxes.*" *Pharmacognosy*, Academic Press, 2017, pp. 443–455.
195 D. Fojtová, J. Vašíčková, R. Grillo, Z. Bílková, Z. Šimek, N. Neuwirthová, M. Kah and J. Hofman, *Environ. Chem.*, 2019, **16**, 470–481.
196 K. Jiang, S. Sun, L. Zhang, Y. Wang, C. Cai and H. Lin, *ACS Appl. Mater. Interfaces*, 2015, **7**, 23231–23238.
197 X. Ren, F. Zhang, B. Guo, N. Gao and X. Zhang, *Nanomaterials*, 2019, **9**, 495.
198 S. Bajpai, A. D. Souza and B. Suhail, *Int. Nano Lett.*, 2019, 1–10.
199 L.-Y. Wang, M. Jafarpour, C.-P. Lin, E. Appel, S. N. Gorb and H. Rajabi, *Soft Matter*, 2019, **15**, 8272–8278.
200 T. Falcon, D. G. Pinheiro, M. J. Ferreira-Caliman, I. C. Turatti, F. C. P. de Abreu, J. S. Galaschi-Teixeira, J. R. Martins, M. Elias-Neto, M. P. Soares and M. B. Laure, *PLoS One*, 2019, **14**, e0213796.
201 S. Mun, M. Young Noh, N. T. Dittmer, S. Muthukrishnan, K. J. Kramer, M. R. Kanost and Y. Arakane, *Sci. Rep.*, 2015, **5**, 10484.
202 R.-R. Yu, W.-M. Liu, X.-M. Zhao, M. Zhang, D.-Q. Li, R. Zuber, E.-B. Ma, K. Y. Zhu, B. Moussian and J.-Z. Zhang, *Insect Mol. Biol.*, 2019, **28**, 301–312.
203 E. Gorb, K. Haas, A. Henrich, S. Enders, N. Barbakadze and S. Gorb, *J. Exp. Biol.*, 2005, **208**, 4651–4662.
204 A. Nikam, B. Prasad and A. Kulkarni, *CrystEngComm*, 2018, **20**, 5091–5107.
205 S. D. Henam, F. Ahmad, M. A. Shah, S. Parveen and A. H. Wani, *Spectrochim. Acta, Part A*, 2019, **213**, 337–341.
206 A. S. H. Makhlouf and A. Barhoum, *Emerging Applications of Nanoparticles and Architectural Nanostructures: Current Prospects and Future Trends*, William Andrew, 2018.
207 Y. Yang, X. Wang, G. Yi, H. Li, C. Shi, G. Sun and Z. Zhang, *Nanomaterials*, 2019, **9**, 1599.
208 M. Shandilya, R. Rai and J. Singh, *Adv. Appl. Ceram.*, 2016, **115**, 354–376.
209 N. K. Kaushik, N. Kaushik, N. N. Linh, B. Ghimire, A. Pengkit, J. Sornsakdanuphap, S.-J. Lee and E. H. Choi, *Nanomaterials*, 2019, **9**, 98.
210 S. Nemoto, T. Ueno, A. Watthanaphanit, J. Hieda, M. A. Bratescu and N. Saito, *Jpn. J. Appl. Phys.*, 2017, **56**, 096202.
211 L. Lin, S. Li, V. Hessel, S. A. Starostin, R. Lavrijsen and W. Zhang, *AIChE J.*, 2018, **64**, 1540–1549.
212 F. Rezaei, P. Vanraes, A. Nikiforov, R. Morent and N. De Geyter, *Materials*, 2019, **12**, 2751.
213 K. Yamada, H. Nakamura, S. Matsushima, H. Yamane, T. Haishi, K. Ohira and K. Kumada, *C. R. Chim.*, 2006, **9**, 788–793.
214 C. Chen, H. Bai, S.-M. Chang, C. Chang and W. Den, *J. Nanopart. Res.*, 2007, **9**, 365–375.
215 C. Chen, H. Bai and C. Chang, *J. Phys. Chem. C*, 2007, **111**, 15228–15235.
216 H.-H. Cheng, S.-S. Chen, Y.-W. Cheng, W.-L. Tseng and Y.-H. Wang, *Water Sci. Technol.*, 2010, **62**, 1060–1066.
217 K. Matsubara, M. Danno, M. Inoue, Y. Honda and T. Abe, *Chem. Eng. J.*, 2012, **181**, 754–760.
218 P. Si, W. Jiang, H. Wang, Z. Li, J. Liu, J. Lee and C. Choi, *Mater. Lett.*, 2012, **68**, 161–163.
219 T. H. Kim, G.-M. Go, H.-B. Cho, Y. Song, C.-G. Lee and Y.-H. Choa, *Front. Chem.*, 2018, **6**, 458.
220 H.-F. Lin, S.-C. Liao and S.-W. Hung, *J. Photochem. Photobiol., A*, 2005, **174**, 82–87.
221 Y. Hiragino, T. Tanaka, H. Takeuchi, A. Takeuchi, J. Lin, T. Yoshida and Y. Fujita, *Solid-State Electron.*, 2016, **118**, 41–45.
222 D. Carolan, C. Rocks, D. B. Padmanaban, P. Maguire, V. Svrcek and D. Mariotti, *Sustainable Energy Fuels*, 2017, **1**, 1611–1619.

This journal is © The Royal Society of Chemistry 2020

223 O. L. Li, S. Chiba, Y. Wada, H. Lee and T. Ishizaki, *RSC Adv.*, 2016, **6**, 109354–109360.
224 P. Gasidit, *J. Mater. Chem. A*, 2014, **2**(43), 18677–18686.
225 B. Sultan, D. Defrance and T. Iizumi, *Sci. Rep.*, 2019, **9**, 12834.
226 D. Pimentel and M. Burgess, *Agriculture*, 2013, **3**, 443–463.
227 *Summary Report: 2015 National Resources Inventory*, US Department of Agriculture, 2018.
228 K. Dietzel, D. Valle, N. Fierer, J. M. U'Ren and A. Barberán, *Front. Ecol. Evol.*, 2019, **7**, 304.
229 E. Crenna, T. Sinkko and S. Sala, *J. Cleaner Prod.*, 2019, **227**, 378–391.
230 E. National Academies of Sciences and Medicine, *Science breakthroughs to advance food and agricultural research by 2030*, National Academies Press, 2019.
231 D. Lyu, R. Backer, W. G. Robinson and D. L. Smith, *Front. Microbiol.*, 2019, **10**, 1761.
232 M. H. Ghafariyan, M. J. Malakouti, M. R. Dadpour, P. Stroeve and M. Mahmoudi, *Environ. Sci. Technol.*, 2013, **47**(18), 10645–10652.
233 Rai S. Kookana, A. B. A. Boxall, P. T. Reeves, R. Ashauer, S. Beulke, Q. Chaudhry, G. Cornelis, T. F. Fernandes, J. Gan, M. Kah, I. Lynch, J. Ranville, C. Sinclair, D. Spurgeon, K. Tiede and P. J. V. D. Brink, *J. Agric. Food Chem.*, 2014, **62**(19), 4227–4240.
234 A. Anastasopoulou, S. Butala, J. Lang, V. Hessel and Q. Wang, *Ind. Eng. Chem. Res.*, 2016, **55**(29), 8141–8153.
235 A. Anastasopoulou, S. Butala, B. Patil, J. Suberu, M. Fregene, J. Lang, Q. Wang and V. Hessel, *Processes*, 2016, **4**(4), 54.
236 V. Hessel, *et al.*, *Chem. Eng. Process.: Process Intesif.*, 2013, **71**, 19–30.
237 V. Hessel, *et al.*, *Catal. Today*, 2013, **211**, 9–28.
238 A. Anastasopoulou, *et al.*, *Processes*, 2014, **2**, 694–710.
239 A. Anastasopoulou, *et al.*, *J. Phys. D: Appl. Phys.*, 2020, **53**, 234001.
240 European Comission, *MAPSYN (Microwave, Ultrasonic and Plasma assisted Syntheses)*, Accessed April 2020, (https://cordis.europa.eu/project/id/309376/reporting).
241 European Union, *A long term EU-Africa research and innovation partnership on food and nutrition security and sustainable agriculture*, Accessed April 2020, (https://leap.iamb.it/?page_id=281).

 This journal is © The Royal Society of Chemistry 2020

BLANK PAGE

Chapter 3

Sustainability assessment of various large-scale synthesis processes of NCQDs

In this chapter, a comprehensive literature review of the up-to-date gram-scale synthesis methods of N-doped carbon quantum dots to collect operational parameters for analysis. Then, green chemistry and circular and EcoScale/Good-Manufacturing-Practice metrics were used to compare all synthesis methods comprehensively. Along with this study, the advantages and disadvantages of each method are depicted in manifold sustainability facets. It is shown how recycling/reuse of unconverted starting materials and solvents can improve the sustainability profile. In addition, safety constraints, cost analysis, and energy consumption are considered.

This chapter has been published as a research paper in "*ACS Sustainable Chemistry and Engineering*" journal as follows:

Pho, Q.H., Escriba-Gelonch, M., Losic, D., Rebrov, E.V., Tran, N.N. and Hessel, V., 2021. Survey of synthesis processes for N-doped carbon dots assessed by green chemistry and circular and EcoScale metrics. *ACS Sustainable Chemistry & Engineering*, 9(13), pp.4755-4770. <Link>

Statement of Authorship

Title of Paper	Survey of Synthesis Processes for N-Doped Carbon Dots Assessed by Green Chemistry and Circular and EcoScale Metrics
Publication Status	☑ Published ☐ Accepted for Publication ☐ Submitted for Publication ☐ Unpublished and Unsubmitted w ork w ritten in manuscript style
Publication Details	Pho, Q.H., Escriba-Gelonch, M., Losic, D., Rebrov, E.V., Tran, N.N. and Hessel, V., 2021. Survey of synthesis processes for N-doped carbon dots assessed by green chemistry and circular and EcoScale metrics. ACS Sustainable Chemistry & Engineering, 9(13), pp.4755-4770.

Principal Author

Name of Principal Author (Candidate)	Hue Quoc Pho		
Contribution to the Paper	Literature review, Conceptualization, Methodology, Formal analysis, Investigation, Data curation, Writing – original draft		
Overall percentage (%)	65%		
Certification:	This paper reports on original research I conducted during the period of my Higher Degree by Research candidature and is not subject to any obligations or contractual agreements with a third party that would constrain its inclusion in this thesis. I am the primary author of this paper.		
Signature		Date	28.01.2023

Co-Author Contributions

By signing the Statement of Authorship, each author certifies that:

i. the candidate's stated contribution to the publication is accurate (as detailed above);
ii. permission is granted for the candidate in include the publication in the thesis; and
iii. the sum of all co-author contributions is equal to 100% less the candidate's stated contribution.

Name of Co-Author	Marc Escriba-Gelonch		
Contribution to the Paper	Methodology, Formal analysis, Investigation, Data curation, Writing – original draft		
Signature		Date	01.02.2023

Name of Co-Author	Dusan Losic		
Contribution to the Paper	Co-supervised and Writing- Review and Editing.		
Signature		Date	2 feb 2023

Please cut and paste additional co-author panels here as required.

Name of Co-Author	Evgeny V. Rebrov		
Contribution to the Paper	Writing- Review and Editing.		
Signature		Date	06.02.2023

Name of Co-Author	Nam Nghiep Tran		
Contribution to the Paper	Writing- Review and Editing.		
Signature		Date	28.01.2023

Name of Co-Author	Volker Hessel		
Contribution to the Paper	Supervised (scientific ideas, concepts, objectives, assessment of achievement degree, societal impact), Conceptualised, Writing – review & editing, and is the corresponding author.		
Signature		Date	28.01.2023

Please cut and paste additional co-author panels here as required.

ACS Sustainable Chemistry & Engineering

pubs.acs.org/journal/ascecg

Research Article

Survey of Synthesis Processes for N-Doped Carbon Dots Assessed by Green Chemistry and Circular and EcoScale Metrics

Quoc Hue Pho, Marc Escriba-Gelonch, Dusan Losic, Evgeny V. Rebrov, Nam Nghiep Tran, and Volker Hessel*

Cite This: *ACS Sustainable Chem. Eng.* 2021, 9, 4755−4770

Read Online

ACCESS | Metrics & More | Article Recommendations

ABSTRACT: Six of the most promising lab-scale synthesis process methodologies for N-doped carbon dots (NCDs) are selected and compared in terms of green chemistry and circular and EcoScale/Good-Manufacturing-Practice metrics. We compare a new innovative route, the low-temperature plasma-enabled synthesis of carbon dots, e.g., from citric acid and monoethanolamine, to more-established literature processes, such as thermochemical processes, from the same or other materials. Along with this study, the advantages and disadvantages of each method are depicted in manifold sustainability facets. It is shown how recycling/reuse of nonconverted starting materials and solvents can improve the sustainability profile. In addition, safety constraints, cost analysis, and energy consumption are considered. The analysis showed that the thermal process from citric acid and monoethanolamine gives the best performance with regard to the sustainability assessment chosen here. It has a material circularity indicator of 0.971, with an EcoScale factor of 56% and an E-factor of 5.56. In continuation of those results, the paper shows how the low-temperature plasma using the same materials and the same recycling strategy can be improved to come closer to the performance of its thermal counterpart. It has the best energy efficiency, while lacking so far in mass efficiency. From this study, we learned more about which of these methods are most promising for scaling-up and industrial manufacturing of N-doped carbon dots.

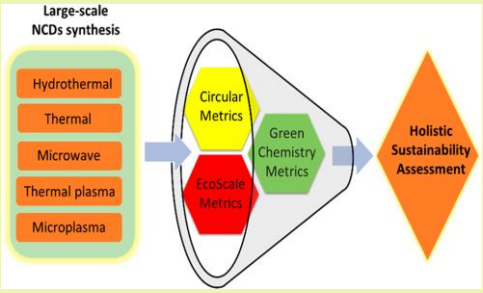

KEYWORDS: *Green chemistry, Circular and EcoScale metrics, Laboratory-scale synthesis, Large-scale synthesis, Nitrogen-doped carbon dots*

INTRODUCTION

Carbonic nanomaterials such as nanodiamonds, fullerenes, carbon nanotubes, graphene sheets, and fluorescent carbon nanoparticles (Carbon Dots: CDs) have strongly emerged during recent years thanks to their many exciting properties. One of the key features of these novel nanomaterials is their optical properties, which can be customized by the nanoparticle size and shape.[1] Consequently, this typical characteristic of these nanomaterials leads to a variety of important applications in medicine,[2] agriculture,[3] electronics,[4] environment,[5] etc. However, despite being discovered serendipitously by Xu et al. in 2004,[6] carbon dots (CDs) have been considered as a stronger candidate for various applications due to their smaller particle size ranging from 1 to 10 nm in comparison with these carbon nanomaterials.[7] This class of fluorescent CDs is, apart from that, not only interesting due to their optical properties[8] but also because of their high aqueous solubility, electronic properties, as well as excellent biocompatibility and functionalizability.[8−13] Thanks to these outstanding characteristics, CDs have manifold uses as sensors (including chemo and biosensors),[14] catalysts, pesticides and fertilizers, chemical and biosensing, bioimaging, drug/gene delivery,[15−17] and optoelectronic devices applications.[7,18]

In an agri-tech context, CDs have been used as nanopesticides to enhance crop efficiency throughout various functionalities such as pesticide nanocarriers, pesticides, pathogen targeting, and phytopathogen detecting.[19] This underlines the above-mentioned arguments (pros/cons of CDs) as a real-life example of eminent importance for humankind, which we have compiled in a review paper.[20] Pesticides are extensively used in modern agriculture and are an effective and economical way to enhance the yield quality and quantity of vegetables, ensuring consequently food security

Received: December 23, 2020
Revised: March 3, 2021
Published: March 23, 2021

ACS Publications © 2021 American Chemical Society

https://doi.org/10.1021/acssuschemeng.0c09279
ACS Sustainable Chem. Eng. 2021, 9, 4755−4770

for the ever-growing population around the globe.[21] The application of chemical pesticides is still preferred over all other alternatives to protect crops from yield loss.[22,23] Presently, throughout the globe approximately 2 million tonnes of pesticides are used, from which 47.5% are herbicides, 29.5% insecticides, 17.5% fungicides and 5.5% other types.[21,24] The top ten pesticide consuming countries in the world are China, the USA, Argentina, Thailand, Brazil, Italy, France, Canada, Japan, and India. Moreover, it has been estimated that by the year 2020, the global pesticide usage will increase up to 3.5 million tonnes.[21,25,26] The downside of the extensive use of pesticides is soil and water pollution, as well as remaining contaminants in the crops, which finally enter the food chain. This poses threats to humans and the environment.[27] In order to tackle this issue, new research initiatives have developed new technologies and new materials (e.g., well-engineered CDs) to promote the development of safe and sustainable agro-systems.[20,28]

In comparison with the first-generation metal quantum dots (QDs) (e.g., cadmium quantum dots) with regard to agriculture applications, CDs, considered as the second generation of quantum dots, have proved to be less toxic and more environmentally friendly.[8] In terms of the fabrication process, CDs synthesis is simpler than the (high-temperature) routes described for metal QDs, with the potential to lower production costs, keeping comparable optical properties and versatility for chemical modification and surface passivation.[29] Importantly, to enhance the typical properties of CDs, surface modification and passivation is one of the most effective functionalization approaches. Among surface functionalization strategies, doping of CDs with nitrogen (N-doped carbon dots, NCDs) has proven to be the most effective for tuning catalytic activity and electronic and optical properties.[30] Yet, the need for doping may increase the process complexity, costs, and toxicity.[31] Thus, as a complementary bioapproach, different procedures for the synthesis of NCDs have been described using natural precursors such as milk[32] and soy milk,[33] peanut[34] and prawn shells,[35] grass,[36] silk,[37] seaweed,[38] mushroom[39] and Prunusavium fruit,[40] or biomass waste (orange peels,[41] lemon peels,[42] rice residue,[43] coffee ground,[44] etc.), but with limited production and quantum yields. Besides the mentioned performance functions of CDs and NCDs, those natural precursor based-nanomaterials have resistance to photobleaching, superior electron transfer ability, versatile surface engineering properties, and outstanding colloidal stability, which limits their potentials in agri-tech applications.

The key to that is chemical process technology, which is also suitable at an industrial scale. Yang et al.[45] first synthesized CDs by facile, economical microwave pyrolysis in a household microwave oven within 7 min, with a production efficiency yield of 30%. Chen et al.[46] synthesized CDs at gram scale with a high yield (42%) by carbonization of sucrose with oil acid in one-step synthesis. Similarly, Hu et al.[47] developed a rapid thermal synthesis of NCDs from citric acid with a yield of 15% in 10 min. Hydrothermal methods have been also developed to increase CDs' production rate, e.g., Zhang et al.[48] conducted a green, versatile, and scalable route to prepare CDs at a large scale from commercial bee pollens with a high production yield of 30%. Other references use ultrasonic baths at 300 W and 40 kHz for 24 h at room temperature.[49] The latter uses a combined effect of ultrasounds with thermal, since the temperature of the bath is also increased along 24 h sonication. Yet, in this case, no extra heating energy is needed.

Other more sophisticated methodologies, such as thermal plasma, have been considered to produce CDs on a large scale; concerning the needs of the specialty functional materials (with many grams or few kilograms being "large"). In this context, Kim et al.[50] carried out a size-controllable and low-cost fabrication method of graphene quantum dots (GQDs), using a thermal plasma jet with a production rate of 4 g/h. Microplasma, with its much smaller reaction volumes, has been considered as well, as process miniaturization might help to conduct a process in a more controlled way. Ma et al.[51] demonstrated the synthesis of NCDs via a microplasma-assisted process at atmospheric pressure, yet with a low yield of 0.4%.

This analysis makes clear that the yield and productivity rate has to be improved, if CDs syntheses should become industrial and be considered green. Otherwise, they produce much more waste relatively than a normal chemical process. Besides the yield, the use of environmentally friendly starting materials and process conditions is demanded; yet a high yield is even for those mandatory. Seeing the above state of the art, yield should be, at least, larger than 50%. The Circular Economy (CE) concept goal aims to reuse all compounds in a process and manufacturing lifecycle, while concurrently increasing their usage and reducing their waste. The European Commission has filed the EU Circular Economy Action Plan[52] (EU CEAP) as a top priority, with the aim of "closing loops" by greater reuse and recycling of materials. To quantify how close a process is to true circularity, circular metrics have been introduced by the Ellen MacArthur Foundation's CE100 program, where the Material Circular Indicator (MCI) has been used as a central metric.[53]

While CDs have so far hardly reached industrial scale, other nanomaterials have. True sustainability studies, beyond using bioapproaches or similar, are largely missing. This CDs process engineering study wants to close this missing link. Green chemistry and circularity metrics are used to assess the sustainability of thermal, microwave-assisted, hydrothermal, thermal plasma, and microplasma methods for the synthesis of CDs (Figure 1). In this study, all processes were considered as closed systems, so secondary manufacturing or landfill costs were not considered to avoid the complexity of the study and not introduc too many possible alternatives to the proposed production circular loops.

EXPERIMENTAL SECTION

The vast majority of the literature relevant for this paper is scientifically curiosity oriented regarding the design and synthesis of new nanomaterials and do not head for process-sustainability information concerning future industrial processes as we give. They investigate the use of various precursors, synthesis methods, characterization of synthesized CDs, and new applications of CDs. All of those studies were conducted at laboratory-scale, while the possibility to produce CDs at a large scale is hardly explored; thus, the combination of lab-scale and higher scale publications could deliver leverages in working conditions due to scale-up.[54] All of those research papers lack process data which are essential for this study (e.g., initial mass of starting materials, mass of products, production yields, etc.) and do not allow conclusions to be made for a large-scale production of CDs. Tables 1 and 2 show the information underlined above and explain the reasons why selected papers are used in our manuscript.

Raw data from each scenario are collected from the literature, including the masses of starting materials and products, cost of materials, energy consumption, and reaction time. Based on that, a comparison of the calculation of green chemistry and circularity

https://doi.org/10.1021/acssuschemeng.0c09279
ACS Sustainable Chem. Eng. 2021, 9, 4755−4770

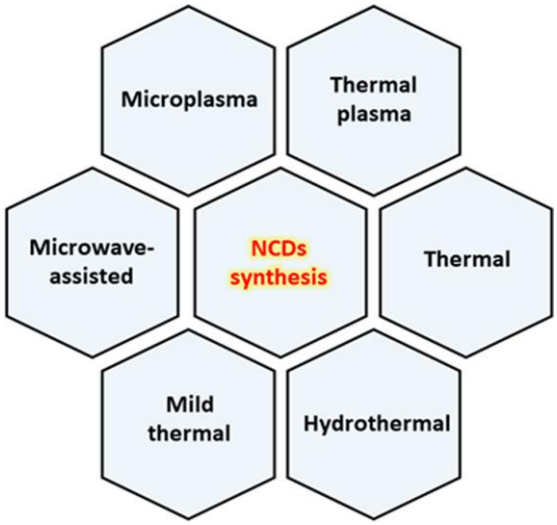

Figure 1. Potential synthesis pathways of N-doped carbon dots (NCDs).

metrics is performed. As CDs and other nanomaterials do not have a defined molecular structure, as low-molecular weight compounds have, and typically do not react by just one defined reaction mechanism, a yield as a percentage value of mole product per mole reactant cannot be defined, as common in chemical engineering. Rather a mass-rated yield, termed mass-yield, is used in the following, meaning the mass of nanomaterial produced per mass of key reactant. The latter is the one providing the carbon (and nitrogen) atoms and is not used in excess to other reactants. The list of six selected synthesis methodologies with specific parameters is shown in Table 3.

NCDs Process Chemistry Methodologies. NCDs process chemistry methodologies from the literature review (including hydrothermal, thermal, microwave, thermal plasma, and microplasma) are briefly described with a fabrication process diagram in the following sections.

Hydrothermal NCDs Synthesis Process (Scenario 1). In this method (Figure 2), commercial bee pollen is well-dispersed into water under sonication.[48] Then, the resulting pollen solution is transferred into a Teflon-lined stainless-steel autoclave, heated to 180 °C for 24 h, and cooled to room temperature before undergoing vacuum filtration. Finally, the synthesized carbon dots are stored at 4 °C for characterization and applications. A total of 1 g of bee pollen costs about 0.07 Chinese yuan, equivalent to about 0.01 U.S. dollars. At least 3 g of CDs can be prepared from 10 g input of the raw material, giving a mass yield of ∼30% (w/w).

Thermal NCDs Synthesis Process (Scenario 2). In this method (Figure 3), precursors are heated without using water as a solvent during reaction, since oleic acid acts as a solvent.[46] Sucrose and oleic acids are rapidly mixed and transferred into a three-neck flask at 215 °C to allow 5 min reaction. Thereafter, the mixture is purified and extracted by using water and hexane. Finally, the extracted products are dialyzed using a 0.5 kDa membrane before freeze-drying, giving a mass-yield of 42%.

Thermal NCDs Synthesis Process (Scenario 3). In this method (Figure 4), citric acid and monoethanolamide (MEA) are mixed under mechanical stirring and then heated to 170 °C.[47] Soon after, the mixture becomes a transparent solution, turning also from colorless to yellow, indicating the generation of NCDs. The solvent removal is conducted under a vacuum oven to obtain 40 g of products.

Microwave-Assisted NCDs Synthesis Process (Scenario 4). This method (Figure 5) uses household microwave equipment for heating.[45] 4,7,10-Trioxa-1,13-tridecane-diamino (TTDDA) and glu-

Table 1. References of N-Doped Carbon Dots with and without Process Information

	our collected references	other references with similar protocols		
name of methodologies	name of collected reference	relevant process information for this assessment	refs	missing process information for this assessment
hydrothermal	Zhang et al. (2015)	After synthesis, 0.3 g of CDs are obtained out of 1 g of starting materials.	55	This report does not reveal the mass of obtained CDs.
			56	This report does not reveal the mass of obtained CDs.
			57	This report does not reveal the mass of obtained CDs.
microwave	Yang et al. (2017)	After synthesis, 3 g of synthesized CDs are obtained.	58	This report does not reveal the mass of obtained CDs.
			59	This report does not reveal the mass of obtained CDs.
			60	This report does not reveal the mass of obtained CDs.
thermal	Chen et al. (2013)	After synthesis, 8.36 g of synthesized CDs are obtained.	61	This report does not reveal the mass of obtained CDs.
			62	This report does not reveal the mass of obtained CDs.
			63	This report does not reveal the mass of obtained CDs.
	Hu et al. (2015)	After synthesis, 40.0 g of synthesized CDs are obtained.	64	This report does not reveal the mass of obtained CDs.
thermal plasma	Kim et al. (2019)	After synthesis, 4 g of synthesized CDs are obtained.	65	This report does not reveal the mass of obtained CDs.
microplasma	Ma et al. (2020)	The yield of the reaction is 0.42%.	66	This report does not reveal the mass of obtained CDs.
			67	This report does not reveal the mass of obtained CDs.
			68	This report does not reveal the mass of obtained CDs.

https://doi.org/10.1021/acssuschemeng.0c09279
ACS Sustainable Chem. Eng. 2021, 9, 4755−4770

Table 2. References of N-Doped Carbon Dots Made by Thermal Methods with and without Process Information

compounds	yield	volumes	process	working conditions	purification and NCD's features	fluorescence	refs
o-phenylenediamine	n/a	108 mg	thermal	180 °C	+ Purification by scratching the crucible and washing with water	365 nm	69
2,6-pyridinedicrboxylic acid		167 mg		4 h	+ Particle size 4.9 nm	QY = 34%	
carboxymethyl cellulose	n/a	100 mg	hydrothermal	260 °C	+ Purification in three steps: (i) centrifugation 10 000 rpm 12 min, (ii) filtration 0.22 μm, (iii) dialysis membrane (1 kDa)	465 nm	70
polyethylenimine		1 mg		2 h	+ Particle size 3.4 nm	QY = 44%	
pulp-free grapefruit juice	n/a	20 mL	hydrothermal	180 °C	+ Purification in three steps: (i) centrifugation 5000 rpm 15 min, (ii) dialysis 3.4 kDa 48 h, (iii) freeze-drying	365 nm	71
urea		1.82 mL		6 h			
water		20 mL			+ Particle size 6.34 nm		
silk	n/a	160 mg	hydrothermal	200 °C	+ Purification in three steps: (i) centrifugation 11 000 rpm 15 min, (ii) dialysis 0.5 kDa 12 h, (iii) freeze and vacuum drying	360 nm	72
citric acid		160 mg		3.5 h		QY = 61%	
water		4 mL			+ Particle size 5.6 nm		
4-aminophenol	n/a	500 mg	hydrothermal	200 °C	+ Purification in three steps: (i) centrifugation 14 000 rpm 20 min, (ii) $CHCl_3$ addition and organic layer separation, (iii) dialysis 1 kDa 24 h	340 nm	73
water		20 mL		20 h	+ Particle size 2.25 nm	QY = 45%	
gum tragacanth	n/a	1000 mg	hydrothermal	180 °C	+ Purification in two steps: (i) centrifugation 20 000 rpm 15 min, (ii) freeze-drying of the liquid fraction	436 nm	74
ethylenediamine		3.12 mg		10 h		QY = 66.7%	
water		60 mL			+ Particle size 2 nm		
$Ti(SO_2)_2$	60%	240 mg	hydrothermal	180 °C	+ Crystals washed with water and ethanol	n/a	75
$H_2C_2O_2{\cdot}2H_2O$		252 mg		72 h			
N-ethylpiperazine		83 μL			+ Particle size 4 nm		
citric acid	63%	2 g	hydrothermal	110 °C	+ Water and methanol added for purification	365 nm	76
ethylenediamine		0.7 mL		4 h		QY = 73%	
water		0.5 mL			+ Particle size 2.5 nm		
L-citrulline	n/a	500 mg	hydrothermal	220 °C	+Purification in two steps: (i) centrifugation 17 000 rpm 40 min, (ii) filtration 0.22 μm.	350 nm	77
water		25 mL		12 h	+ Particle size 2.7 nm	QY = 33%	
ammonium citrate triethylenetetramine	n/a	2.43 g	microwave pyrolysis	800 W	+ For each cycle, 5 mL water addition	350 nm	78
		1.46 mL		2 min (three cycles of 1 min 800 W)	+ Purification in three steps: (i) centrifugation 15 000 rpm 10 min, (ii) filtration 0.22 μm, (iii) dialysis 1 kDa 48 h	QY = 30%	
water		10 mL			+ Particle size 7 nm		

Table 3. Methodologies for NCDs Process Synthesis

scenario	precursors	cost (Sigma-Aldrich)	density (kg/dm^3)	M_w (g/mol)	power/heat	purification method	reaction time (min)	QY (%)	particle size (nm)	mass of product (g)	reference
1	rapeseed flower bee pollen (1 g)	$12.58/kg	n/a	180.2	180 °C	vacumm filtration	1440 (24 h)	9.1	from 1 to 2	0.3	Zhang et al.
	40 mL (H2O)	0	1.0	18.0							
2	oleic acid (40 mL)	$32.14/L	0.895	282.5	215 °C	solvent extraction	5	21.6	1.84	8.36	Chen et al.
	20 g Sucrose	$52.46/kg	1.59	342.3							
	40 mL (H2O)	0	1.0	18.0							
	Hexane (*Extraction solvent*)	$94.84/L	0.659	86.2							
3	30 g of citric acid	$67.22/kg	1.66	192.1	170 °C	vacumm distillation	10	40.3	3.5	39.96	Hu et al.
	230 mL of MEA	$42.96/L	1.01	61.1							
4	glucose (5 g)	$42.18/kg	1.56	180.2	800 W	dialysis	7	n/a	7	3	Yang et al.
	TTDDA (5 g)	$159.83/kg	1.005	220.3							
	H_2O (80 mL)	0	1.0	18.0							
5	ethylene gas (150 L) 177 g	$20.77/kg	1.18	28.1	600 kW h	ethanol isolation	60	13.5	10	4	Kim et al.
6	citric acid (1 g)	$67.21/kg	1.66	192.1	30 W	dialysis	20	9.9	5.98	0.007	Ma et al.
	EDA (0.6 mL)	$37.69/kg	0.9	60.0							
	water (10 mL)	0	1.0	18.0							

cose are mixed well in distilled water under sonication. Then, the obtained solution is heated for 7 min, obtaining an aqueous solution with a concentration of CDs of 20 mg/mL, which is freeze-dried. The mass-yield is 30%.

https://doi.org/10.1021/acssuschemeng.0c09279
ACS Sustainable Chem. Eng. 2021, 9, 4755−4770

ACS Sustainable Chemistry & Engineering pubs.acs.org/journal/ascecg Research Article

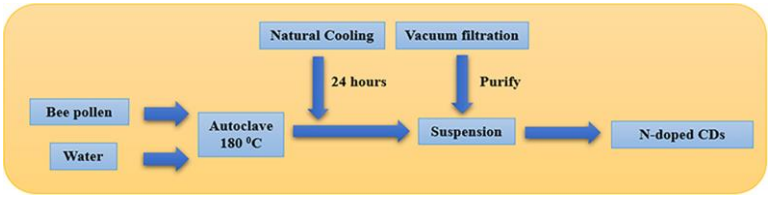

Figure 2. Hydrothermal NCDs synthesis process from bee pollen.

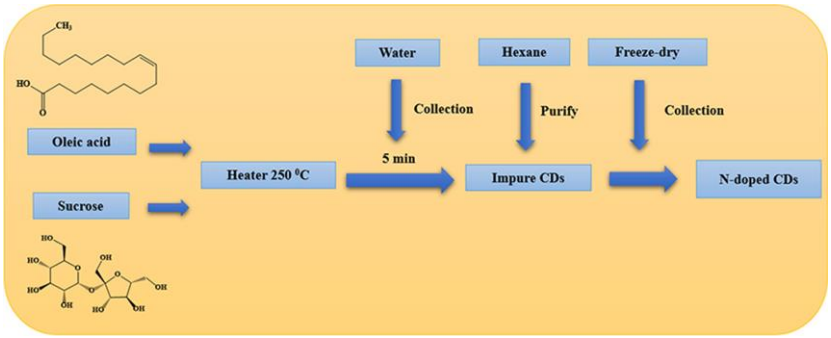

Figure 3. Thermal NCDs synthesis process from oleic acid and sucrose.

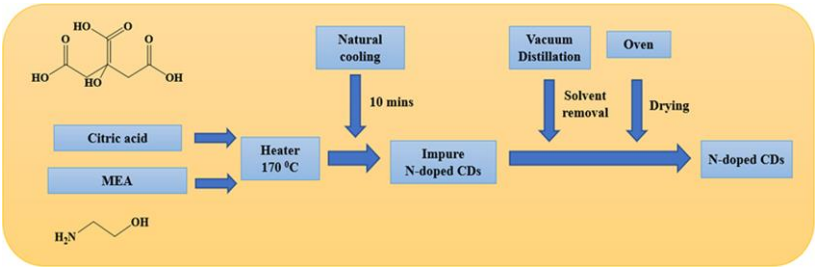

Figure 4. Thermal NCDs synthesis process from citric acid and monoethanolamide.

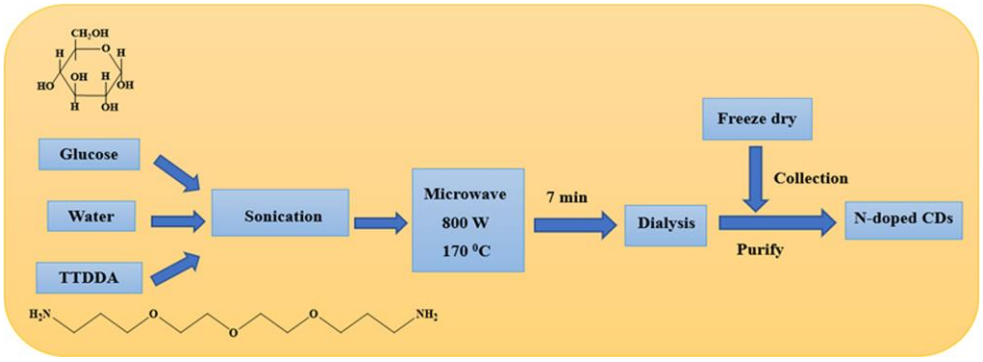

Figure 5. Microwave-assisted NCDs synthesis process from glucose and 4,7,10-trioxa-1,13-tridecane-diamino (TTDDA).

Thermal Plasma NCDs Synthesis Process (Scenario 5). Thermal plasma is generated by applying a high voltage of 3 kV between a zirconium-containing tungsten cathode and a copper anode (Figure 6).[50] The thermal plasma jet is operated by a direct voltage with a current of 200 A. A carbon atomic beam is generated by injecting a large amount (2.5 L/min) of ethylene gas continuously into an argon plasma. The beam flows then through a carbon tube (5, 10, or 20 cm in length depending on the desired size of CDs) attached to the anode and then is dispersed into a chamber. The CDs are made by gas-phase reaction. The production rate of the carbon soot is 40 g/h at a 2.5 L/min injection rate. While the carbon soot is dispersed in ethanol by sonication, isolated CDs are dispersed in ethanol by stirring.

https://doi.org/10.1021/acssuschemeng.0c09279
ACS Sustainable Chem. Eng. 2021, 9, 4755−4770

ACS Sustainable Chemistry & Engineering pubs.acs.org/journal/ascecg Research Article

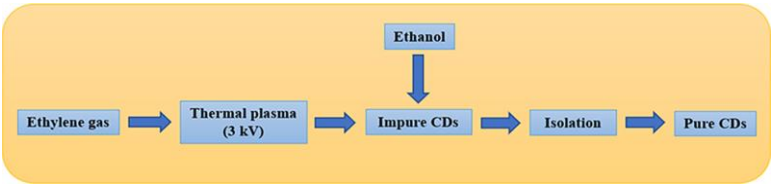

Figure 6. Thermal NCDs synthesis process from ethylene.

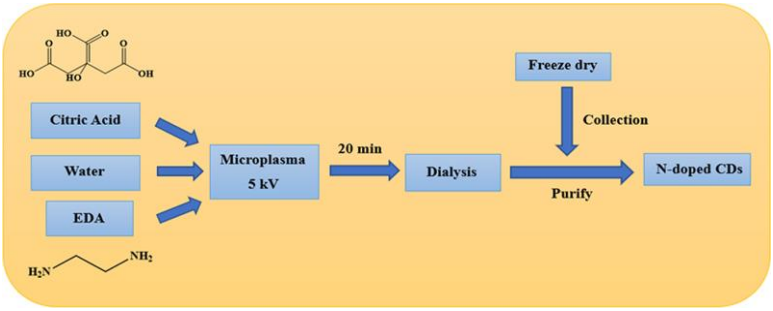

Figure 7. Microplasma-assisted NCDs synthesis process from citric acid and ethylenediamine (EDA).

Low-Temperature Microplasma–Assisted NCDs Synthesis Process (Scenario 6). A second low-temperature plasma-assisted method uses citric acid and ethylene diamine dissolved in deionized H_2O (Figure 7).[51] The resulting solution is transferred into a self-designed quartz reactor, where microplasma is applied to the solution for 20 min. The product is purified by dialysis and freeze-dried. This procedure has a mass-yield of 0.4%.

Green Chemistry Metrics Studies. Roschangar et al.[79] proposed a way to group green chemistry (GC) metrics. Following this, herewith the GC metrics are grouped along with the four reaction mixture ingredients: NCDs raw material, auxiliary reagent(s), solvent, and water. Particularly, PMI and PME are considered to be related to "water" assessment, while MI, MP, and E-factor are relevant to "solvent" ingredient.[79] RMI and EMY are used to assess "auxiliary reagents", while RME, AE, and CE are related to "raw material" assessment.[79]

GC Metrics for NCDs Raw Materials. *Reaction Mass Efficiency (RME).* Reaction mass efficiency (RME) measures the mass of product divided by the total mass of raw materials, expressed as a percentage. RME does not account for the solvent used.[80,81]

$$\text{RME}(\%) = \frac{\text{mass of product} \times 100}{\text{total mass of raw materials}} \quad (1)$$

Carbon Economy (CE). Carbon economy is the mass of carbon in the product divided by the total mass of carbon in the raw materials, expressed as a percentage.[80]

$$\text{carbon economy}(\text{CE}\%) = \frac{\text{carbon in product} \times 100}{\text{total carbon in raw materials}} \quad (2)$$

Atom Economy (AE). Atom economy is the metrics, which relates the molecular weight of the product to that of the reactants, expressed as a percentage. Thus, it is a measure of the relative loss of molecular weight (atoms) of the process, which generates waste.

$$\text{atom economy}(\text{AE}\%) = \frac{\text{MW}_{\text{product}} \times 100}{\text{MW}_{\text{reagents}} + \text{MW}_{\text{raw materals}}} \quad (3)$$

GC Metrics Related to Solvents. *E-Factor (E).* The E-factor is the amount of waste produced considering all process components, including reactants, catalysts, and solvent, yet excluding water, relative to the mass of the final product.[52,82] A higher E-factor means more waste is generated; the ideal E-factor is zero.

$$\text{E-factor}(E) = \frac{\text{total mass of waste}}{\text{mass of final product}} \quad (4)$$

Mass Productivity (MP). Mass Productivity relates the mass of the product to the mass of all input materials. The latter would include reactants, catalysts, solvent, and even water.

$$\text{mass productivity}(\text{MP}\%) = \frac{m_{\text{product}} \times 100}{m_{\text{input materials}}} \quad (5)$$

Mass Intensity (MI). Linked with the previous metrics, Mass Intensity is an inversely defined metrics as to the Mass Productivity.

$$\text{mass intensity}(\text{MI kg kg}^{-1}) = \frac{m_{\text{input materials}}}{m_{\text{product}}} \quad (6)$$

Solvent Intensity (SI). Solvent intensity is the mass intensity only considering solvent flows.

$$\text{solvent intensity}(\text{SI kg kg}^{-1}) = \frac{m_{\text{solvents}}}{m_{\text{product}}} \quad (7)$$

GC Metrics Related to Water consumption. *Process Mass Intensity (PMI).* Process mass intensity is the ratio of total input of materials, as detailed above and, in addition, including water.[80,83] PMI focuses on reducing the costs of the raw materials input.

$$\text{process mass index}(\text{PMI kg kg}^{-1}) = \frac{\text{total mass in process}(\text{incl } H_2O)}{\text{mass of product}} \quad (8)$$

Process Mass Efficiency (PME). Process mass efficiency is linked with process mass intensity, but the inverse definition.

$$\text{process mass efficiency}(\text{PME}\%) = \frac{m_{\text{product}} \times 100}{m_{\text{input materials including water}}} \quad (9)$$

Wastewater Intensity (WWI). Wastewater intensity is linked with Mass Intensity, but only considering process water flows.

$$\text{waste water intensity}(\text{WWI } kg \text{ kg}^{-1}) = \frac{m_{\text{process water}}}{m_{\text{product}}} \quad (10)$$

https://doi.org/10.1021/acssuschemeng.0c09279
ACS Sustainable Chem. Eng. 2021, 9, 4755−4770

ACS Sustainable Chemistry & Engineering pubs.acs.org/journal/ascecg Research Article

Table 4. Green Metrics Calculation by 1 kg of Products for Different Synthesis Processes of N-Doped CDs

metric	equation	unit	sc.1	sc.2	sc.3	sc.4	sc.5	sc.6	ideal value
CY		%	30	42	42	30	2.2	0.5	100
RME	1	%	30	42	15	30	2.3	0.44	100
CE	2	%	37	n/a	26	34	n/a	n/a	100
AE	3	%	100	100	100	90	102	100	100
E-factor	4	kg kg^{-1}	2.3	1.4	5.6	2.3	43	228	0
MP	5	%	30	15	15	30	2.3	0.44	100
MI	6	kg kg^{-1}	3.3	6.7	6.6	3.3	44	229	1
PMI	8	kg kg^{-1}	137	11	6.6	30	44	1657	1
PME	9	%	0.73	8.7	15.2	3.3	2.3	0.06	100
EMY	11	%	30	15	15	30	2.3	0.44	100
RMI	12	kg kg^{-1}	3.3	6.7	6.6	3.3	44	229	1
SI	7	kg kg^{-1}	0	0.10	0	0	0	0	0
WWI	10	kg kg^{-1}	133	4.8	0.0	27	0.0	1429	0
E. Cons.		kW h kg^{-1}	14 688	n/a	84 688	2286	150 000	1429	0

GC Metrics Related to Reagent Consumption. *Effective Mass Yield (EMY).* Effective mass yield is the ratio of the mass of product to raw materials and reagents.

$$\text{effective mass yield(EMY\%)} = \frac{m_{\text{products}} \times 100}{m_{\text{raw materials}} + m_{\text{reagents}}} \quad (11)$$

Reaction mass intensity (RMI). Reaction Mass Intensity is linked with effective mass intensity, but the inverse definition.

$$\text{reaction mass intensity(RMI kg kg}^{-1}) = \frac{m_{\text{raw materials}} + m_{\text{reagents}}}{m_{\text{products}}} \quad (12)$$

Other Relevant GC Metrics. *Energy Consumption.* The energy consumption from the different synthesis process methodologies in this study is calculated based on heat-transfer principles.[84] In eq 11, Q [W] refers to the heat added (or being removed) from the object, m [kg] is the mass (weight), Cp [J/kg C] is the specific heat capacity, and t [s] is the time required for cooling (or heating).

$$Q = \frac{mC_p\Delta T}{t} \quad (13)$$

Volume–Time–Output (VTO). VTO is defined as the volume of all reactors (V_r) (in m^3) multiplied by the residence time (rt) per batch, divided by the whole amount of product per batch in kg. In this context, the chemical process is acceptable for VTO values below 1; otherwise the process still needs to be improved.

$$\text{VTO} = \frac{V_r[\text{m}^3]\text{rt[h]}}{\text{products[kg]}} \quad (14)$$

Circular Metric Studies for N-Doped CDs Synthesis Scenarios. The research here follows the Material Circularity Indicator (MCI) methodology of the Ellen MacArthur Foundation (EMA) CE100 program.[85] Seeing that the processes proposed have a low yield, recycling is mandatory.

Therefore, as described by Escriba-Gelonch et al.,[86] a peculiarity of chemical processes is that the recovered or recycled chemical species remain the same with equal performance as the virgin ones. Using this methodology, it is possible to probe the high challenges of low-yielded processes to be circular, since the amount of unreacted materials strictly demands the recycling/reuse by circular loops. In the context of CDs, the quantum yield was taken as the utility value, as luminescence is a major characteristic of CDs exploited in several of their performances; following a similar replacement approach as described in ref 86. In the case of scenario 4, where no value is provided, the utility value was considered as 1.

RESULTS AND DISCUSSION

Comparison of the NCDs Synthesis Process Methodologies. The processes given (Table 3) differ in their amount of use of raw materials, solvents, and/or water. They also differ in energy consumption, since they use different sources for heating (heat, radio waves, and ionized gases). For example, the NCDs process using hydrothermal methodology has a higher energy demand, which is mainly due to the higher residence time. That means productivity in terms of material produced per time is an issue. The thermal (scenario 3) method produces the highest product mass of almost 40 g, while the microplasma method (scenario 6) produces the least amount with only 7 mg. That spans nearly 4 orders of magnitude.

Finally, the selected scenarios also include the purification process (Figures 2–7). In this context, dialysis, freeze-drying, vacuum distillation, and solvent extraction are used for NCDs purification, which again differs in material and energy consumption as well as in their processing time. The mass of the product, and thus productivity, varies for the different methods. The reaction time of our synthesized CDs by microplasma treatment is approximately 1 h, while the dialysis time is much longer and roughly 72 h. There is obviously a major mismatch in the essential time constants, and as now, the productivity would be determined by purification. For several CD applications and assuming optimization of productivity, this might be still commercially sufficient, as we might produce 200–500 mg per week, e.g., theranostic nanoparticles in medicinal treatment. Yet, for others such as water purification, we may need to make gram amounts and beyond. Our main limitation sits on the dialysis side. To increase the purified mass yield, we suggest increasing the volume of dialysis bags as well as the number of dialysis batches. We expect to increase dialysis productivity by a factor of 10 this way, leaving another factor of 10 to match the plasma-synthesis productivity. If that is the goal, probably another faster purification approach needs to be developed.

In addition to the above-mentioned process parameters, the circularity metrics, different from the green chemistry metrics, consider functionality, meaning the performance per mass of the product, which is the quantum yield in the context of this research.[87] Table 3 shows high differences in terms of the quantum yield of produced NCDs. Thermal methods described in scenarios 2 and 3 results in the highest quantum yield of 22 and 40%, respectively.

https://doi.org/10.1021/acssuschemeng.0c09279
ACS Sustainable Chem. Eng. 2021, 9, 4755–4770

Thus, concerning sustainability the use of materials and energy as opposed to productivity and its performance are to be considered; with a view on the full process, covering both the nanomaterials synthesis and purification.

Green Metrics Calculation. The green chemistry metrics were calculated following eqs 1−12 for a functional unit of 1 kg product, see Table 4.

Reaction Mass Efficiency (RME). The results of this first metric related to raw materials revealed that scenarios not related to plasma showed values between 15 and 42, being the highest the thermal procedure described in scenario 2. Plasma-linked procedures showed much lower RME values (scenarios 5 and 6) due to the low reaction yield. Here, the reuse of raw materials is mandatory as discussed below in order to keep the process economically feasible.

Carbon and Atom Economy (CE and AE). The carbon economy of the available hydrothermal (scenario 1), microwave (scenario 4) and thermal (scenario 3) synthesis were in the same range, performing the first the highest value: 37. These results suggest that the hydrothermal process described in scenario 1 is the best in converting carbon atoms from starting materials into the product. All results concerning atom economy (AE) showed also to be highly efficient.

Process Mass Intensity (PMI). The process mass intensity of scenarios 1 and 6 showed values much above the others (Figure 8). Especially the PMI of scenario 6 (microplasma)

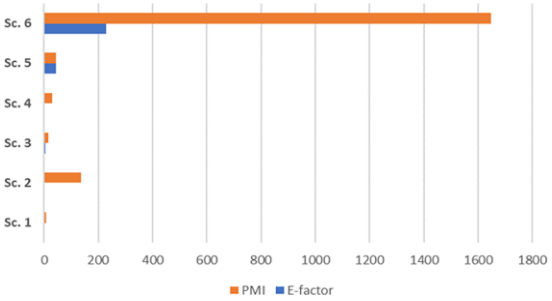

Figure 8. Comparison of process mass intensity (PMI) and E-factor of various NCDs synthesis process methods.

was 1657, due to a large amount of water used, i.e., the high reactant dilution, and the low mass-yield of the product (0.007 g). The second highest PMI value is given for the hydrothermal process with 137, which is again due to a large amount of water used as well as the relatively low yield.

E-Factor. The E-factors of scenarios 1 to 4 were low, with a minimum value of 1.4 for scenario 2, see Figure 8. The higher mass-yield of scenarios 1 to 4 decreases the E-factor because of the higher efficiency. The mass-yield and the use of materials are guiding parameters for the E-factor, which penalizes scenarios 5 and 6 where the factor achieves nonadvantageous high values, especially in scenario 6 where this value amounts 228.

Waste Water and Solvents Intensity. Concerning parameters related to solvents (SI) and wastewater (WWI) intensity, most scenarios do not use solvents, and therefore this parameter comes to 0. Only scenario 2 computes 0.10 kg/kg, due to the hexane needed for the extraction process after the reaction in order to recover the oleic acid used for the reaction. This situation is not the same with water, since most the scenarios use water, and especially scenario 6 uses a lot (1429 kg/kg). Scenario 1 also needs a considerable amount of water (133 kg/kg), which penalizes in terms of green metrics. Scenarios 3 and 5 show good performance on this index, since they use neither water nor solvent, as stated before.

Operation Temperature. Operating temperature is also an essential parameter that needs to be considered in large-scale production. Operating synthesis processes at high temperatures lead to an increase in energy consumption and pose a risk to the safety of a process. As a result, It might significantly increase the production cost and make the product less competitive in comparison to the other synthesis routes that can be operated at room temperatures. Working in a high-temperature environment also causes a hazard risk to operators of synthesis processes. For this reason, the low (room) temperature-based synthesis process is ideally considered as a green process. As a result, the operating temperature in scenarios 1, 2, and 3 are estimated around 180, 215, and 170 °C, respectively. Scenario 5 performs an extremely high operating temperature, up to nearly 10 000 °C, due to the temperature of electrons flow in thermal plasma, while the operating temperatures of scenarios 4 and 6 are only 100 and 20 °C, respectively. It can be seen that nonthermal plasma synthesis of NCDs in scenario 6 is considered to be the greenest method in terms of operating temperature as it can be operated at room temperature (20 °C). Therefore, the total cost of production might decrease significantly.

Energy Consumption. In terms of energy consumption, the scenarios linked with thermal procedures (1, 3, and 5) have obviously higher energy demands (Figure 9). Foremost among

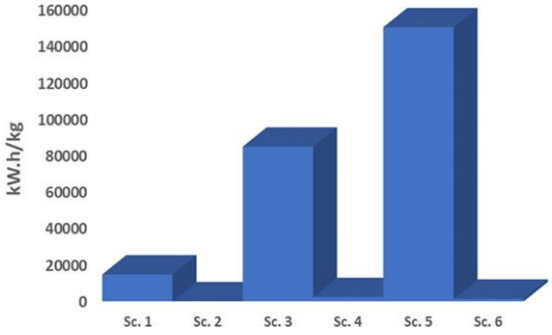

Figure 9. Energy consumption of the NCDs synthesis process methods.

these is the thermal plasma method (scenario 5). The latter, consuming 150 000 (kW.h/kg product), is in the range of 2 orders of magnitude higher than the demands of low-temperature microplasma method (scenario 6). Nonetheless, the energy consumption is still high in other thermal procedures, being 84,668 and 14,688 (kW.h/kg product) for the thermal (scenario 3) and hydrothermal (scenario 1) methods, respectively. Interesting to mention that microwave and microplasma consume the least energy with 2,286 and 1,429 (kW h/kg product) respectively, due to the lower working temperatures.

Cost Analysis of Precursors. To enable a proper uniform prices scale pattern, which eliminates all confounding factors derived from managing different suppliers with different criteria, taxes and interests, we assumed that all chemicals

https://doi.org/10.1021/acssuschemeng.0c09279
ACS Sustainable Chem. Eng. 2021, 9, 4755−4770

used are at the same class and purchased from Sigma-Aldrich. Therefore, we used the prices listed on the company's Web site for the calculation of chemical costs. A cost analysis for the production of 1 kg of NCDs was performed for each synthesis scenario taking the simple data records from Table 3. The results are shown in Figure 10, where high differences can be

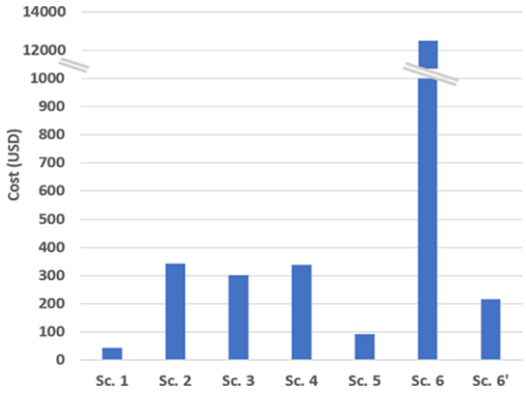

Figure 10. Costs of starting materials for the production of 1 kg of NCDs in different synthesis scenarios. No recycling loops are considered except for Sc.6′.

appreciated. First, scenario 1 appears to be the cheapest thanks to the inexpensive starting bee pollen, followed by scenario 5, where the fact of working with just one reactant (ethylene gas) is an advantage. Yet, scenarios 2 to 4 appear to be in the same range of costs. This is because of two reasons: first, all three methodologies are in the same range of mass-yield, which means that the amount of raw materials is also in the same order of magnitude. Second, despite being most of the reactants inexpensive, each methodology has one expensive reactant which is also in the same range of price, making comparable the production costs in different scenarios. In this connection, scenario 2 uses hexane ($284.53/3L), scenario 3 uses monoethylene amine ($250.05/5.82 kg), and scenario 4 uses TTDDA ($266.92/1.67 kg). Scenario 6 results to be the most expensive not because of the costly materials, but because of the lowest mass-yield, which demands a much higher amount of starting materials per kilo of final compound ($12,509 per kg of product). The materials are inexpensive in this scenario (see Table 3), and in the way that for the cost analysis recycling was not considered, the process becomes costly. Yet, one advantage of this process is the absence of side reactions, which enables the reuse of the starting materials in a circular context, as discussed below. Therefore, the real cost of the materials would be much lower if, in the end, all of the starting materials can be transformed to NCDs after successive reuse loops. Sc.6′ in Figure 10 shows the hypothetical costs in a cumulative yield scenario of 30% mass-yield after successive recycling loops. As shown, incomparable mass-yield conditions with scenarios 2−4, the cost of scenario 6 would be even lower than those for scenarios 2−4. This is an example where circularity becomes a key point in a process design.

Apart from using the above-mentioned precursors, using waste materials to synthesize CDs is an approach to reduce the cost of starting materials. Solid waste materials from agriculture and industrial activities such as banana peels commonly go to landfill. Atchudan et al. used the peels of Dwarf banana fruits from the food market to synthesize CDs by the hydrothermal method with a particle size of 5 nm.[88] Similarly, other waste materials (orange peels,[41] lemon peels,[42] rice residue,[43] coffee ground,[44] etc.) were also used to synthesize CDs at a low cost of starting materials.[89]

Overall Green Metrics Ratios. Figure 11 shows a comparative picture of all relative parameters (in %) for each scenario. The optimal value of them is 100, so the more open the plot is, the better it is. In the picture, scenarios 1, 3, and 4 show the overall best performance in green metrics. Apparently, the worst scenarios in this context are 5 and 6, where besides AE, all parameters are close to 0.

Circular Metrics. Being different from the green chemistry metrics, in CE reuse of the starting materials is considered and measured, using so-called circular transition indicators with the MCI as a central metric.[53] In this way, even the low mass-yield processes can achieve high MCI values through recycling/reuse strategies, which can deliver also interesting economical results as illustrated in the costs analysis of scenario 6. To meet this objective, a recycling/reuse design was performed and evaluated for each scenario, according to the process parameters obtained from the literature. In this context, Figure 12 shows a flowchart of the material loops for the purification and recycling operation proposed for scenario 2 as an example. Such engineering of the purification of nanomaterials is hardly discussed so far in the literature. Yet this analysis shows the importance of that for the sustainability and circularity of nanomaterial syntheses.

Tables 5 and 6 show the results of the circular metrics calculated for each scenario. Tables 5 and 6 show the circular metrics in the current linear fashion and those for the proposed looped scenarios (assuming recycling) respectively. Partial analysis of the key reactants was also performed when possible. In Table 5, the virgin amounts are considered to be equal to M, and obviously $F_R = C_R = 0$. Additionally, waste (W) has the same value of Wo, and appears to be at least 1 order of magnitude higher than the corresponding scenario in Table 6. Processes in Table 5 do consider neither composting nor reuse/recycling/recovery operations. Due to the low mass-yield of most of the processes, LFI appears to be above 0.8 in all scenarios, being the lowest for scenarios 2 and 4 because of the higher yield and the subsequent lower waste. Concerning MCI, scenarios 1 and 6 have low values around 0.1, being the highest scenarios 2 and 4, yet with very poor MCI values around 0.250.

Table 6 calculates the circular metrics assuming reuse of the process materials (reactants and solvent), meaning to assume recycle-looped processes for each scenario. Where available (scenario 1), documented material loss is subtracted from the unreacted starting material, i.e., the initial starting material by mass minus the mass-yield. Where not available (other scenarios than 1), a complete recovery of the unreacted starting material is assumed. The same approach was taken for the solvent (please note that this is the dominating factor in combined reactant-solvent based metrics as the mass of the solvent is much higher). As expected, this can drastically decrease the use of virgin materials (V), waste production (W), and lost fractions (C_C). As shown in Table 6, the loops would increase the MCI and therefore the circularity, as compared to Table 5. The recycling fraction of the process scenarios under study (F_R) would be above 60% in Table 6, as well as the efficiency of the extraction process of the starting nanomaterials (E_F) in the range of 90%.

https://doi.org/10.1021/acssuschemeng.0c09279
ACS Sustainable Chem. Eng. 2021, 9, 4755−4770

ACS Sustainable Chemistry & Engineering pubs.acs.org/journal/ascecg Research Article

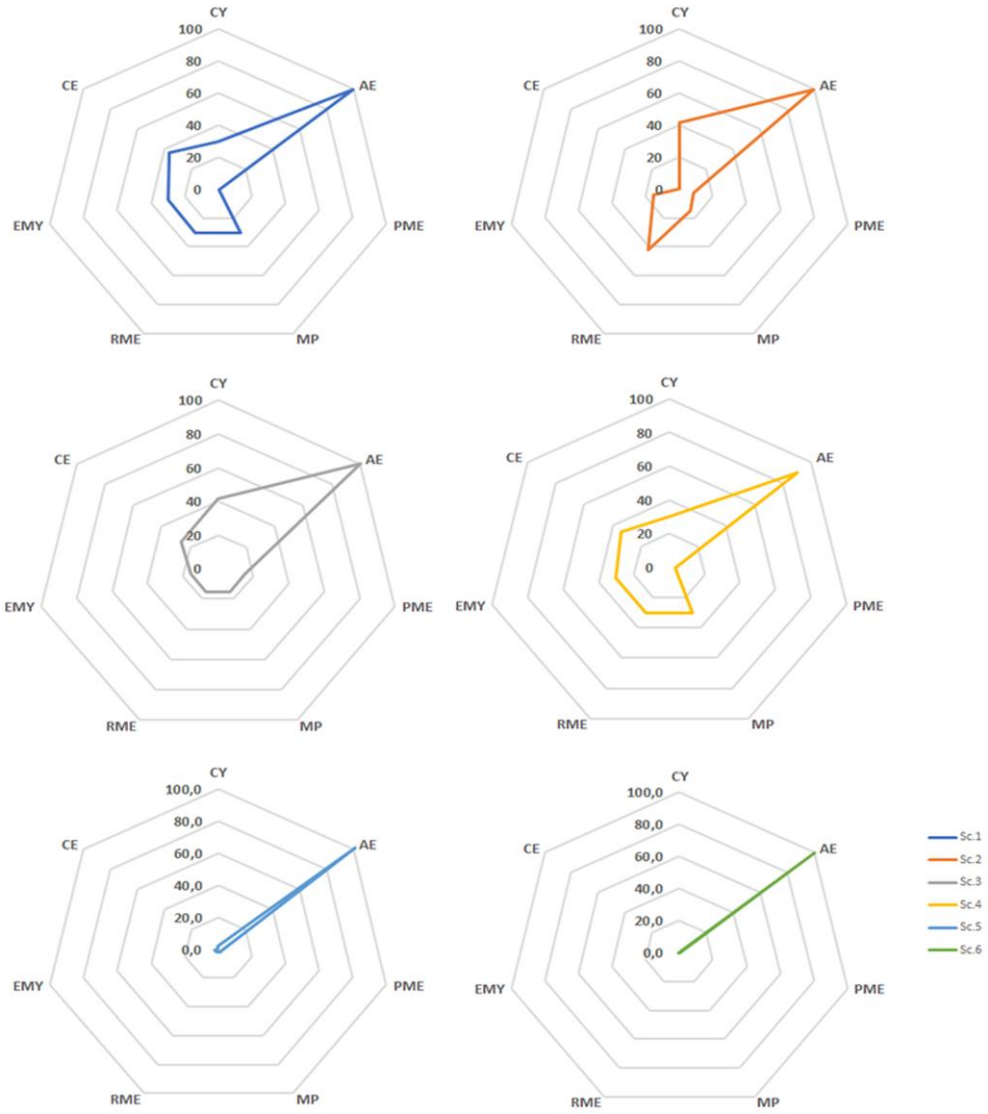

Figure 11. Comparative plots of green chemistry metrics for the different scenarios of NCDs synthesis.

Scenario 1, as said, is different from the other scenarios, since it has 28% loss (C_C) requiring to refresh the process by 60% virgin materials in the next loop, allowing only for a recycling fraction (F_R) of 40%. This fact penalises also the rest of the results, because it increases the amount of waste (showing the highest W value) giving a linear flow index (LFI) of 0.55, meaning above 50%. This is the reason why the MCI value for the bee pollen is the lowest (0.509) of all scenarios. Nevertheless, the MCI of the whole process is much higher (0.971), because of the recycling of most of the water used in the process (operation at low concentration). Bee pollen is the cheapest reactant of all scenarios.

As utility values X, quantum yields (QY) are taken as this luminescent property is a key performance parameter of the NCDs and widely documented (see Table 3). This "utility" X is normalized by the $F(X)$ function as described by EMA-CE100.[85] Therefore, a high QY increases MCI as shown in scenarios 2 and 3 and, with lower impact, in scenario 5. The utility factor for scenario 3 shows the highest increase to 4.42 due to high QY. Therefore, scenario 3 has the highest MCI value. The opposite is given in scenario 4, which at the end appears to be the most linear process. No QY is available in the literature, keeping X to 1. Hence, even having good recycling parameters such as 60% of F_R and waste generation 1.71 kg/60 kg of starting materials, scenario 4 is penalised by the absence of performance values, which decreases the MCI to 0.838.

Overall, the MCI values of the NCDs synthesis process methodologies with recycling added are all above 80% and a major part being 90% or higher, meaning close to circular; with the exception of the mentioned bioreactant (pollen)-based scenario 1, and scenario 4 due to the absence of performance values. Scenarios 1 and 3 score the same highest value 0.971,

https://doi.org/10.1021/acssuschemeng.0c09279
ACS Sustainable Chem. Eng. 2021, 9, 4755−4770

ACS Sustainable Chemistry & Engineering pubs.acs.org/journal/ascecg Research Article

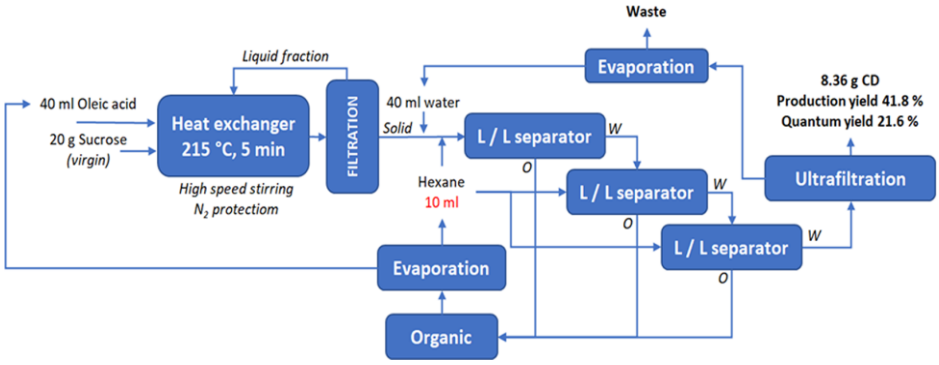

Figure 12. Proposed flowchart of the circular scenario 2.

Table 5. Circular Metrics Calculation for the NCDs Synthesis Process Methodologies, in Their Current Linear Fashion

	sc. 1		sc. 2	sc. 3	sc. 4		sc. 5	sc. 6	
	pollen	overall	sucrose	overall	Glu + TTDDA	overall	ethylene	citric acid	overall
M (kg)	10	810.0	20	233	10	60	2.95	1	11.54
W (kg)	6.8	806.8	12.06	222	6.126	41.13	2.28	0.999	10.49
LFI	0.84	0.998	0.802	0.922	0.8063	0.843	0.887	0.999	0.955
MCI	0.244	0.102	0.279	0.170	0.274	0.242	0.201	0.100	0.141

Table 6. Circular Metrics Calculation for the NCDs Synthesis Process Methodologies in an Assumed Circular Fashion, Using the Looped Processes Proposed in This Paper

	sc. 1		sc. 2	sc. 3	sc. 4		sc. 5	sc. 6	
	pollen	overall	sucrose	overall	Glu + TTDDA	overall	ethylene	citric acid	overall
M (kg)	10	810	20	263	10	60	3	1	12
FR	0.40	0.97	0.60	0.79	0.60	0.67	0.77	0.90	0.90
V (kg)	6.0	23.0	8.0	55.0	4.0	20.0	0.67	0.10	1.1
CC	0.280	0.024	0.003	0.053	0.013	0.019	0.002	0.100	0.100
CR	0.400	0.972	0.600	0.791	0.600	0.667	0.773	0.896	0.905
EF	0.300	0.975	0.995	0.933	0.979	0.972	0.997	0.889	0.890
W (kg)	7.47	29.96	0.09	21.51	0.19	1.71	0.01	0.16	1.80
W0 (kg)	2.80	19.80	0.06	14.00	0.13	1.13	0.01	0.10	1.15
WF (kg)	9.33	20.31	0.06	15.01	0.13	1.16	0.01	0.11	1.30
LFI	0.55	0.03	0.20	0.14	0.21	0.18	0.12	0.13	0.12
F(X)	0.90	0.90	0.38	0.20	0.90	0.90	0.61	0.83	0.83
X	1.00	1.00	2.37	4.42	1.00	1.00	1.48	1.09	1.09
MCI	0.509	0.971	0.923	0.971	0.812	0.838	0.930	0.896	0.899

followed by scenario 5. The latter achieves this position due to the good performance in QY (13%) which delivers a utility factor of 1.48, the high recycling fraction (F_R = 0.77) and the low waste generation (0.01 kg/3 kg of ethylene).

Safety Concerns for NCDs Synthesis. Nanomaterials pose hazards and risks concerning human health, and the environment.[88] Particularly, food science and engineering demand for safety control and risk assessment[90] and use as nanopesticides is one of our target applications.[20] The toxicity of conventional QDs depends on the size, concentration, charge, outer coating, bioactivity, and photolytic, oxidative, and mechanical stability.[91] It is generally high due to the content of cadmium or other heavy metals. Yet, hardly any health or environmental constraints have been reported for CDs.[92−95] CDs have good biocompatibility, and no significant toxic effect is observed at different doses. They cause neither any abnormality nor damage in organs, and specifically do not exhibit gene toxicity.[96] NCDs, as shown in this paper, can be synthesized from natural and harmless raw materials, such as sugars and pollen bees. Nevertheless, the use of highly toxic and flammable solvents in some cases such as ethylene (scenario 5) and ethylenediamine (scenario 6) is still a drawback concerning safety constraints.

In addition, cold plasma, herewith described as microplasma in scenario 6, has been described as an advantageous nonthermal treatment even suitable to be used to chemically modify food surfaces at room temperature (~20 °C) and atmospheric pressure (14.7 psi) in safety conditions.[97]

Good Manufacturing Indicators. To apply a circularity assessment means to assume that the CDs synthesis processes can be brought to industrial capacity, i.e., a scale-up from laboratory to pilot scale. This involves developments concerning the process and analytical chemistry, process engineering, and safety and regulatory requirements.[54]

In this context, Dach et al.[98] propose a methodology package in order to define the degree of good manufacturing of

https://doi.org/10.1021/acssuschemeng.0c09279
ACS Sustainable Chem. Eng. 2021, 9, 4755−4770

a process to compare different pathways to the same chemical compound. Eight evaluation criteria or Good Manufacturing Indices (GMI) are applied to three main stages: chemical development, process development, and chemical production.

Economic Factors. Criterion 1. Material Cost. A high cost of raw materials, availability, and required quantities penalizes good manufacture. The use of natural resources in most of the assessed scenarios may reduce costs. In the scenarios under study, the costs of raw-materials per kilo are in the range of $70 for scenarios 1 and 5, $300 for scenarios 2 to 4 and more than $12k for scenario 6, the latter due to the low mass-yield.

Process Efficiency Factors (Criteria 2–5). Criterion 2: Atom Economy (AE). Hardly any data exist for nanomaterial syntheses and their lack of atomic stoichiometry set limits to the application of a criterion based on AE. Generally, raw materials with major contents of carbon and nitrogen atoms should be favorable; as oxygen and hydrogen atoms reduce the "AE". In the scenarios herewith assessed, AE was higher than 90%.

Criterion 3: Yield. For the above-mentioned lack of stoichiometry, no yield can be defined; yet a mass-yield is the right surrogate. Thermal methods have a comparatively high mass-yield for NCDs and nanomaterials in general, being up to 50%. Plasma- and solvent-based methodologies have typically lower mass-yields, yet there is no theoretical reason why those could not be higher. Meaning more development is demanded here.

Criterion 4: Volume–Time–Output (VTO). Thermal methods are reasonably fast at good mass-yields; meaning they achieve good productivity or VTO. Plasma methods are fast, yet their mass yields need to be improved, as showed in Table 4, scenario 5.

Criterion 5: Environmental Factor (E-Factor)/Process Mass Intensity (PMI). The recycling strategies presented in this paper improve significantly the E-factor and PMI of NCD syntheses shown in Figure 8, which are very low typically when done in a linear fashion.

Process Reproducibility Factors (Criteria 6–7). Criterion 6: Quality Service Level (QSL). For the scenarios considered here, no data in terms of reproducibility and robustness are provided by the sources. This gap may be filled by future studies.

Criterion 7: Process Excellence Index (PEI). This paper highlights the importance of recycling and reuse; not only their efficiency is important, but also the cycle time of these operations. This index could not be calculated with the data provided by the sources.

Ecoscale Definition. Criterion 8: Modified EcoScale. This procedure, developed by van Aken et al.,[99] provides a so-called EcoScore by cumulating penalty points in the case non-sustainable measures have been used. This procedure has been applied for each scenario as described in Table 7. According to Table 7, scenario 2 has the best score mainly because of the lower mass-yield penalty points. Scenario 6 looks also very promising, having in most categories very low penalty values; yet the safety and yield of this process needs to be improved.

The GMI can be quantified with the methodology described by Dach et al.,[98] based on research performed at Boehringer Ingelheim Pharma GmbH. Here, this methodology is applied for quantifying and comparing the good manufacturing performance of the 6 scenarios assessed in this paper. Table 8 summarizes the values obtained for each criterion and each scenario accordingly. This table is distributed in two sections:

Table 7. Ecoscale Calculation for the Different NCDs Synthesis Scenarios (sc. = scenario)

EcoScale parameter	sc. 1	sc. 2	sc. 3	sc. 4	sc. 5	sc. 6
1. yield	35	29	29	35	39	50
2. price of reaction components	3	5	5	5	5	0
3. safety (hazard warning symbols)	0	0	5	5	10	10
4. technical setup	3	1	0	2	2	0
5. temperature/time	3	2	2	2	0	1
6. workup and purification	0	3	3	0	0	0
total penalty points	44	40	44	49	56	61
EcoScale score	56	60	56	51	45	39

Section A shows the values obtained for each criterion per parameter, section B shows the good manufacturing scores obtained for each value in section A. The final GMI for each scenario is the sum of section B values. Process reproducibility factors (criterions 6 and 7) could not be applied because of the absence of data in the literature. Each criterion has a weight or relative importance in the assessment for the calculation of GMI, which can vary for different process optimization objectives and by company priorities. Here the relative importance is assigned to evaluate the capability of the scenario to be brought to industrial capacity. To meet this goal, Dach et al.[98] propose to take VTO as the most impactful criterion and use it predominantly as shown in Table 8.

Concerning the price (first criteria), scenarios 1 and 5 scored the highest followed by scenarios 2–4. The high costs per kg penalized scenario 6. Criterion 2 is not conclusive since the available values score in the same range. The quantification of atom economy in nanotechnology is difficult, and most of the data in this context are not provided. That is the reason because the weight of criterion 2 was only 5%. Scenario 6 is also very penalised in eco-efficiency (criterion 5) due to the low concentration used as well as the low mass-yield. Scenarios 3 and 4 are the procedures, which meet all criteria with the weights proposed in the literature, with a GMI of 97.2 and 95.9% respectively. These procedures correspond to the thermal process (citric acid with MEA) and microwave (glucose with TTDDA). The worst scenario is scenario 6 (microplasma) with a value of 45.9%. This value is obtained because of the high price and the environmental factors scored due to the low concentration. The second worst scenario is scenario 1 (pollen bee) with a value of 56.5%, which is very penalised by the high VTO factor, which weighs 40% of the total amount. It is worth noting that thermal plasma (ethylene) scored an interesting GMI of 87.2%, despite being still penalized by the low yield.

CONCLUSIONS

This study uses single-criterion and multiple-criteria assessments for scenarios for judging the sustainability of six selected process synthesis methodologies for N-doped carbon dots (NCDs), including hydrothermal, thermal, microwave, thermal plasma, and microplasma. The single-criterion assessment has been performed through green chemistry metrics and circular transition indicators, and the multiple-criteria assessment by the Good Manufacturing Practice, developed by the Boehringer-Ingelheim Company, which includes the EcoScale index. This paper wants to make a hot-spot analysis and shows weaknesses in sustainability, and show the way out.

https://doi.org/10.1021/acssuschemeng.0c09279
ACS Sustainable Chem. Eng. 2021, 9, 4755–4770

Table 8. Good Manufacturing Index Calculation for the Different NCDs Synthesis Scenarios

		criterion 1	criterion 2	criterion 3	criterion 4	criterion 5		criterion 8
	scenario	price (USD)	AE	mass-yield (%)	VTO	E-factor	PMI	EcoScale
section A	1	41.89	37	30.0	4.2857	2.33	136.67	56
	2	341.29	n/a	41.8	0.0005	1.39	11.46	60
	3	300.46	26	41.8	0.0010	5.56	6.56	56
	4	337.37	34	30.0	0.0019	2.33	30.00	51
	5	91.91	n/a	23.0	0.0622	43.25	44.25	45
	6	12 509.70	n/a	0.4	0.0714	227.57	1657.14	39
				partial GMI values				GMI (%)
	weights (%)	15	5	5	40	10	15	10	final
section B	1	14.9	5.0	3.6	0.0	9.9	13.8	9.3	56.5
	2	14.6	n/a	5.0	40.0	9.9	14.9	10.0	94.4
	3	14.6	3.5	5.0	40.0	9.8	14.9	9.3	97.2
	4	14.6	4.6	3.6	40.0	9.9	14.7	8.5	95.9
	5	14.9	n/a	2.8	39.4	8.1	14.6	7.4	87.2
	6	0.0	n/a	0.1	39.3	0.0	0.0	6.5	45.9

Scenario 3, the synthesis of NCDs using citric acid with monoethanolamine, shows the most promise when all assessments are considered. Scenario 3 is circular with the highest material circularity indicator (MCI) of 0.971 and has the second-best EcoScale index of 56%. In the latter, scenario 2, using oleic acid and sucrose for NCDs synthesis, scores best with 60%.

The assessment of the six synthesis process methodologies for N-doped carbon dots nanoparticles determines that scenarios 1, 3, and 4 score best in terms of green metrics, while scenarios 2, 3, and 5 do likewise with circular metrics. Finally, concerning good manufacturing criteria, scenarios 2, 3, and 4 show the best performance. In addition, NCDs produced from hydrothermal (scenario 1), microwave (scenario 4), and thermal method (scenario 2) need a purification process for good sustainability performance.

In view of all metrics considered, scenario 3 (citric acid with MEA) ranks best, followed by scenario 4 (microwave with glucose). Interesting to note that thermal plasma (scenario 5) shows good indices despite of the high-energy consumption. The latter is overcompensated by the fact that scenario 5 (as well as scenario 3) does use neither water nor solvent, which reduces the waste generation. Therefore, any improvement in energy consumption for the thermal plasma would let it jump up to even the best scenario. This gives also hope for future use of nonthermal plasma and its miniaturized version (scenario 6), which is also known as an energy-consuming technology, yet with considerable improvements over the years. It needs fewer operating processes than conventional methods, hence has profits from process simplicity. Yet this is not paid off so far in terms of green chemistry and circularity.

Finally, it is worth mentioning that "utility" constitutes a strong point to enhance circularity in the sense of the Ellen MacArthur definition. The plasma prepared nanomaterials are rich in functional groups such as $-NH_2$, $-COOH$, $-CHO$, etc. without the need for chemicals for surface modification. Those surface groups are key to the NCD functionality, *i.e.* their photoluminescent properties.[100]

AUTHOR INFORMATION

Corresponding Author

Volker Hessel − *School of Chemical Engineering and Advanced Materials, North Terrace Campus, The University of Adelaide, Adelaide, SA 5005, Australia; School of Engineering, University of Warwick, Coventry CV4 7AL, United Kingdom;* orcid.org/0000-0002-9494-1519; Email: volker.hessel@adelaide.edu.au

Authors

Quoc Hue Pho − *School of Chemical Engineering and Advanced Materials, North Terrace Campus, The University of Adelaide, Adelaide, SA 5005, Australia; School of Engineering, University of Warwick, Coventry CV4 7AL, United Kingdom;* orcid.org/0000-0002-2257-6401

Marc Escriba-Gelonch − *Laboratoire de Génie des Procédés Catalytiques (LPGC), Centre National de la Recherche Scientifique (CNRS), CPE-Lyon, 69100 Villeurbanne, France;* orcid.org/0000-0003-0540-7232

Dusan Losic − *The ARC Graphene Research Hub, School of Chemical Engineering and Advanced Materials, North Terrace Campus, The University of Adelaide, Adelaide, SA 5005, Australia;* orcid.org/0000-0002-1930-072X

Evgeny V. Rebrov − *School of Engineering, University of Warwick, Coventry CV4 7AL, United Kingdom;* orcid.org/0000-0001-6056-9520

Nam Nghiep Tran − *School of Chemical Engineering and Advanced Materials, North Terrace Campus, The University of Adelaide, Adelaide, SA 5005, Australia; School of Chemical Engineering, Can Tho University, Can Tho city, Vietnam*

Complete contact information is available at: https://pubs.acs.org/10.1021/acssuschemeng.0c09279

Notes

The authors declare no competing financial interest.

ACKNOWLEDGMENTS

The authors acknowledge support from the ERC Grant Surface-COnfined fast modulated Plasma for process and Energy intensification (SCOPE) from the European Commission with the Grant No. 810182.

LIST OF ABBREVIATIONS

F_R fraction from recycled sources
C_C fraction of mass to go into a composting process
C_R fraction of mass to go into a recycling process

https://doi.org/10.1021/acssuschemeng.0c09279
ACS Sustainable Chem. Eng. 2021, 9, 4755−4770

E_F	efficiency of the recycling process
W	mass [kg] of unrecoverable waste associated with a product
W_0	unrecoverable end-of-life waste [kg] through a product's material
W_F	unrecoverable waste [kg] generated when recycling
LFI	material flowing in a linear fashion
$F(X)$	utility factor built as a function of the utility X of a product
MCI	material circularity indicator

REFERENCES

(1) https://www.nanosysinc.com/quantum-dot-basics/ (last access October 2020).

(2) Nair, A.; Haponiuk, J. T.; Thomas, S.; Gopi, S. Natural carbon-based quantum dots and their applications in drug delivery: A review. *Biomed. Pharmacother.* **2020**, *132*, 110834.

(3) Wang, A.; Kang, F.; Wang, Z.; Shao, Q.; Li, Z.; Zhu, G.; Lu, J.; Li, Y. Y. Facile Synthesis of Nitrogen-Rich Carbon Dots as Fertilizers for Mung Bean Sprouts. *Adv. Sustain. Syst.* **2019**, *3* (3), 1800132.

(4) Segkos, A.; Sakellis, I.; Boukos, N.; Drivas, C.; Kennou, S.; Kordatos, K.; Tsamis, C. Patterned carbon dot-based thin films for solid-state devices. *Nanoscale* **2020**, *12* (18), 10254−10264.

(5) Tadesse, A.; RamaDevi, D.; Hagos, M.; Battu, G.; Basavaiah, K. Synthesis of nitrogen doped carbon quantum dots/magnetite nanocomposites for efficient removal of methyl blue dye pollutant from contaminated water. *RSC Adv.* **2018**, *8* (16), 8528−8536.

(6) Xu, X.; Ray, R.; Gu, Y.; Ploehn, H. J.; Gearheart, L.; Raker, K.; Scrivens, W. A. Electrophoretic analysis and purification of fluorescent single-walled carbon nanotube fragments. *J. Am. Chem. Soc.* **2004**, *126* (40), 12736−12737.

(7) Zhang, J.; Yu, S.-H. Carbon dots: large-scale synthesis, sensing and bioimaging. *Mater. Today* **2016**, *19* (7), 382−393.

(8) Lim, S. Y.; Shen, W.; Gao, Z. Carbon quantum dots and their applications. *Chem. Soc. Rev.* **2015**, *44* (1), 362−381.

(9) Chen, B. B.; Liu, M. L.; Li, C. M.; Huang, C. Z. Fluorescent carbon dots functionalization. *Adv. Colloid Interface Sci.* **2019**, *270*, 165−190.

(10) Chen, B. B.; Liu, M. L.; Huang, C. Z. Carbon dot-based composites for catalytic applications. *Green Chem.* **2020**, *22* (13), 4034−4054.

(11) Liu, M. L.; Chen, B. B.; Li, C. M.; Huang, C. Z. Carbon dots: synthesis, formation mechanism, fluorescence origin and sensing applications. *Green Chem.* **2019**, *21* (3), 449−471.

(12) Chen, B. B.; Liu, M. L.; Huang, C. Z. Recent advances of carbon dots in imaging-guided theranostics. *TrAC, Trends Anal. Chem.* **2021**, *134*, 116116.

(13) Liu, M.-L.; Chen, B.-B.; Li, C.-M.; Huang, C.-Z. Carbon dots prepared for fluorescence and chemiluminescence sensing. *Sci. China: Chem.* **2019**, 968−981.

(14) Esteves da Silva, J. C.G.; Goncalves, H. M.R. Analytical and bioanalytical applications of carbon dots. *TrAC, Trends Anal. Chem.* **2011**, *30* (8), 1327−1336.

(15) Das, P.; Bhattacharyya, S. K.; Banerji, P.; Das, N. C. Acoustic cavitation assisted synthesis and characterization of photoluminescent carbon quantum dots for biological applications and their future prospective. *Nano-Struct. Nano-Objects* **2021**, *25*, 100641.

(16) Bhattacharyya, S. K.; Dule, M.; Paul, R.; Dash, J.; Anas, M.; Mandal, T. K.; Das, P.; Das, N. C.; Banerjee, S. Carbon dot cross-linked gelatin nanocomposite hydrogel for pH-sensing and pH-responsive drug delivery. *ACS Biomater. Sci. Eng.* **2020**, *6* (10), 5662−5674.

(17) Ganguly, S.; Das, P.; Das, S.; Ghorai, U.; Bose, M.; Ghosh, S.; Mondal, M.; Das, A. K.; Banerjee, S.; Das, N. C. Microwave assisted green synthesis of Zwitterionic photolumenescent N-doped carbon dots: an efficient 'on-off'chemosensor for tracer Cr (+ 6) considering the inner filter effect and nano drug-delivery vector. *Colloids Surf., A* **2019**, *579*, 123604.

(18) Shen, L.-M.; Liu, J. New development in carbon quantum dots technical applications. *Talanta* **2016**, *156*, 245−256.

(19) Li, Y.; Xu, X.; Wu, Y.; Zhuang, J.; Zhang, X.; Zhang, H.; Lei, B.; Hu, C.; Liu, Y. A review on the effects of carbon dots in plant systems. *Mater. Chem. Front* **2020**, *4* (2), 437−448.

(20) Pho, Q. H.; Losic, D.; Ostrikov, K. K.; Tran, N. N.; Hessel, V. Perspectives on plasma-assisted synthesis of N-doped nanoparticles as nanopesticides for pest control in crops. *React. Chem. Eng.* **2020**, *5* (8), 1374−1396.

(21) Sharma, A.; Kumar, V.; Shahzad, B.; Tanveer, M.; Sidhu, G. P. S.; Handa, N.; Kohli, S. K.; Yadav, P.; Bali, A. S.; Parihar, R. D. Worldwide pesticide usage and its impacts on ecosystem. *SN Appl. Sci.* **2019**, *1* (11), 1−16.

(22) Aktar, W.; Sengupta, D.; Chowdhury, A. Impact of pesticides use in agriculture: their benefits and hazards. *Interdiscip. Toxicol.* **2009**, *2* (1), 1−12.

(23) Popp, J.; Pető, K.; Nagy, J. Pesticide productivity and food security. A review. *Agron. Sustainable Dev.* **2013**, *33* (1), 243−255.

(24) Hassaan, M. A.; El Nemr, A. Pesticides pollution: Classifications, human health impact, extraction and treatment techniques. *Egypt. J. Aquat. Res.* **2020**, *46* (3), 207−220.

(25) Zhang, W. Global pesticide use: Profile, trend, cost/benefit and more. *Proc. Int. Acad. Ecol. Environ. Sci.* **2018**, *8* (1), 1.

(26) Maluin, F. N.; Hussein, M. Z. Chitosan-based agro-nanochemicals as a sustainable alternative in crop protection. *Molecules* **2020**, *25* (7), 1611.

(27) Özkara, A.; Akyıl, D.; Konuk, M. Pesticides, environmental pollution, and health. *Environmental Health Risk-Hazardous Factors to Living Species*; IntechOpen: 2016.

(28) Lowry, G. V.; Avellan, A.; Gilbertson, L. M. Opportunities and challenges for nanotechnology in the agri-tech revolution. *Nat. Nanotechnol.* **2019**, *14* (6), 517−522.

(29) Li, L.; Dong, T. Photoluminescence tuning in carbon dots: surface passivation or/and functionalization, heteroatom doping. *J. Mater. Chem. C* **2018**, *6* (30), 7944−7970.

(30) Xu, Q.; Kuang, T.; Liu, Y.; Cai, L.; Peng, X.; Sreenivasan Sreeprasad, T.; Zhao, P.; Yu, Z.; Li, N. Heteroatom-doped carbon dots: synthesis, characterization, properties, photoluminescence mechanism and biological applications. *J. Mater. Chem. B* **2016**, *4* (45), 7204−7219.

(31) Atchudan, R.; Edison, T. N. J. I.; Aseer, K. R.; Perumal, S.; Karthik, N.; Lee, Y. R. Highly fluorescent nitrogen-doped carbon dots derived from Phyllanthus acidus utilized as a fluorescent probe for label-free selective detection of Fe3+ ions, live cell imaging and fluorescent ink. *Biosens. Bioelectron.* **2018**, *99*, 303−311.

(32) Wang, L.; Zhou, H. S. Green synthesis of luminescent nitrogen-doped carbon dots from milk and its imaging application. *Anal. Chem.* **2014**, *86* (18), 8902−8905.

(33) Zhu, C.; Zhai, J.; Dong, S. Bifunctional fluorescent carbon nanodots: green synthesis via soy milk and application as metal-free electrocatalysts for oxygen reduction. *ChemComm.* **2012**, *48* (75), 9367−9369.

(34) Xue, M.; Zhan, Z.; Zou, M.; Zhang, L.; Zhao, S. Green synthesis of stable and biocompatible fluorescent carbon dots from peanut shells for multicolor living cell imaging. *New J. Chem.* **2016**, *40* (2), 1698−1703.

(35) Yuan, C.; Liu, B.; Liu, F.; Han, M.-Y.; Zhang, Z. Fluorescence "turn on" detection of mercuric ion based on bis (dithiocarbamato) copper (II) complex functionalized carbon nanodots. *Anal. Chem.* **2014**, *86* (2), 1123−1130.

(36) Liu, S.; Tian, J.; Wang, L.; Zhang, Y.; Qin, X.; Luo, Y.; Asiri, A. M.; Al-Youbi, A. O.; Sun, X. Hydrothermal treatment of grass: a low-cost, green route to nitrogen-doped, carbon-rich, photoluminescent polymer nanodots as an effective fluorescent sensing platform for label-free detection of Cu (II) ions. *Adv. Mater.* **2012**, *24* (15), 2037−2041.

(37) Wu, Z. L.; Zhang, P.; Gao, M. X.; Liu, C. F.; Wang, W.; Leng, F.; Huang, C. Z. One-pot hydrothermal synthesis of highly luminescent nitrogen-doped amphoteric carbon dots for bioimaging

https://doi.org/10.1021/acssuschemeng.0c09279
ACS Sustainable Chem. Eng. 2021, 9, 4755−4770

from Bombyx mori silk—natural proteins. *J. Mater. Chem. B* **2013**, *1* (22), 2868−2873.
(38) Godavarthi, S.; Mohan Kumar, K.; Vazquez Velez, E.; Hernandez-Eligio, A.; Mahendhiran, M.; Hernandez-Como, N.; Aleman, M.; Martinez Gomez, L. Nitrogen doped carbon dots derived from Sargassum fluitans as fluorophore for DNA detection. *J. Photochem. Photobiol., B* **2017**, *172*, 36−41.
(39) Wang, W.-J.; Xia, J.-M.; Feng, J.; He, M.-Q.; Chen, M.-L.; Wang, J.-H. Green preparation of carbon dots for intracellular pH sensing and multicolor live cell imaging. *J. Mater. Chem. B* **2016**, *4* (44), 7130−7137.
(40) Edison, T. N. J. I.; Atchudan, R.; Shim, J.-J.; Kalimuthu, S.; Ahn, B.-C.; Lee, Y. R. Turn-off fluorescence sensor for the detection of ferric ion in water using green synthesized N-doped carbon dots and its bio-imaging. *J. Photochem. Photobiol., B* **2016**, *158*, 235−242.
(41) Prasannan, A.; Imae, T. One-pot synthesis of fluorescent carbon dots from orange waste peels. *Ind. Eng. Chem. Res.* **2013**, *52* (44), 15673−15678.
(42) Tyagi, A.; Tripathi, K. M.; Singh, N.; Choudhary, S.; Gupta, R. K. Green synthesis of carbon quantum dots from lemon peel waste: applications in sensing and photocatalysis. *RSC Adv.* **2016**, *6* (76), 72423−72432.
(43) Qi, H.; Teng, M.; Liu, M.; Liu, S.; Li, J.; Yu, H.; Teng, C.; Huang, Z.; Liu, H.; Shao, Q.; Umar, A.; Ding, T.; Gao, Q.; Guo, Z. Biomass-derived nitrogen-doped carbon quantum dots: highly selective fluorescent probe for detecting Fe3+ ions and tetracyclines. *J. Colloid Interface Sci.* **2019**, *539*, 332−341.
(44) Wang, L.; Li, W.; Wu, B.; Li, Z.; Wang, S.; Liu, Y.; Pan, D.; Wu, M. Facile synthesis of fluorescent graphene quantum dots from coffee grounds for bioimaging and sensing. *Chem. Eng. J.* **2016**, *300*, 75−82.
(45) Yang, Y.; Lin, X.; Li, W.; Ou, J.; Yuan, Z.; Xie, F.; Hong, W.; Yu, D.; Ma, Y.; Chi, Z.; Chen, X. One-pot large-scale synthesis of carbon quantum dots: efficient cathode interlayers for polymer solar cells. *ACS Appl. Mater. Interfaces* **2017**, *9* (17), 14953−14959.
(46) Chen, B.; Li, F.; Li, S.; Weng, W.; Guo, H.; Guo, T.; Zhang, X.; Chen, Y.; Huang, T.; Hong, X.; You, S.; Lin, Y.; Zeng, K.; Chen, S. Large scale synthesis of photoluminescent carbon nanodots and their application for bioimaging. *Nanoscale* **2013**, *5* (5), 1967−1971.
(47) Hu, Y.; Yang, J.; Tian, J.; Yu, J.-S. How do nitrogen-doped carbon dots generate from molecular precursors? An investigation of the formation mechanism and a solution-based large-scale synthesis. *J. Mater. Chem. B* **2015**, *3* (27), 5608−5614.
(48) Zhang, J.; Yuan, Y.; Liang, G.; Yu, S. H. Scale-up synthesis of fragrant nitrogen-doped carbon dots from bee pollens for bioimaging and catalysis. *Adv. Sci.* **2015**, *2* (4), 1500002.
(49) Ma, Z.; Ming, H.; Huang, H.; Liu, Y.; Kang, Z. One-step ultrasonic synthesis of fluorescent N-doped carbon dots from glucose and their visible-light sensitive photocatalytic ability. *New J. Chem.* **2012**, *36* (4), 861−864.
(50) Kim, J.; Suh, J. S. Size-controllable and low-cost fabrication of graphene quantum dots using thermal plasma jet. *ACS Nano* **2014**, *8* (5), 4190−4196.
(51) Ma, X.; Li, S.; Hessel, V.; Lin, L.; Meskers, S.; Gallucci, F. Synthesis of N-doped carbon dots via a microplasma process. *Chem. Eng. Sci.* **2020**, *220*, 115648.
(52) European Commission, a. C. f. t. C. t. t. E. P., the Council, the European Economic and Social Committee and the Committee of the Regions 'Closing the Loop - An EU Action Plan for the Circular Economy'. COM (2015) 614. Available at http://www.circularocean.eu/circularnews/circular-economy-cut-carbon-emissions-europe-70-percent/ (Last access November 2020).
(53) The Ellen MacArthur Foundation, C. I. A. a.; https://www.ellenmacarthurfoundation.org/resources/apply/circularity-indicators, L. a. N., 2020).
(54) Escribà-Gelonch, M.; de Leon Izeppi, G. A.; Kirschneck, D.; Hessel, V. Multistep Solvent-Free 3 m2 Footprint Pilot Miniplant for the Synthesis of Annual Half-Ton Rufinamide Precursor. *ACS Sustainable Chem. Eng.* **2019**, *7* (20), 17237−17251.
(55) Zheng, Y.; Zhang, H.; Li, W.; Liu, Y.; Zhang, X.; Liu, H.; Lei, B. Pollen derived blue fluorescent carbon dots for bioimaging and monitoring of nitrogen, phosphorus and potassium uptake in Brassica parachinensis L. *RSC Adv.* **2017**, *7* (53), 33459−33465.
(56) Han, Z.; He, L.; Pan, S.; Liu, H.; Hu, X. Hydrothermal synthesis of carbon dots and their application for detection of chlorogenic acid. *Luminescence* **2020**, *35* (7), 989−997.
(57) Wang, Y.; Chang, X.; Jing, N.; Zhang, Y. Hydrothermal synthesis of carbon quantum dots as fluorescent probes for the sensitive and rapid detection of picric acid. *Anal. Methods* **2018**, *10* (23), 2775−2784.
(58) Liang, Y.; Liu, Y.; Li, S.; Lu, B.; Liu, C.; Yang, H.; Ren, X.; Hou, Y. Hydrothermal growth of nitrogen-rich carbon dots as a precise multifunctional probe for both Fe3+ detection and cellular bio-imaging. *Opt. Mater.* **2019**, *89*, 92−99.
(59) Gul, U.; Kanwal, S.; Tabassum, S.; Gilani, M. A.; Rahim, A. Microwave-assisted synthesis of carbon dots as reductant and stabilizer for silver nanoparticles with enhanced-peroxidase like activity for colorimetric determination of hydrogen peroxide and glucose. *Mikrochim. Acta* **2020**, *187* (2), 1−8.
(60) Lopez, C.; Zougagh, M.; Algarra, M.; Rodriguez-Castellon, E.; Campos, B.B.; Esteves da Silva, J.C.G.; Jimenez-Jimenez, J.; Rios, A. Microwave-assisted synthesis of carbon dots and its potential as analysis of four heterocyclic aromatic amines. *Talanta* **2015**, *132*, 845−850.
(61) Rimal, V.; Shishodia, S.; Srivastava, P. Novel synthesis of high-thermal stability carbon dots and nanocomposites from oleic acid as an organic substrate. *Appl. Nanosci.* **2020**, *10* (2), 455−464.
(62) Ma, C. a.; Yin, C.; Fan, Y.; Yang, X.; Zhou, X. Highly efficient synthesis of N-doped carbon dots with excellent stability through pyrolysis method. *J. Mater. Sci.* **2019**, *54* (13), 9372−9384.
(63) Wei, X.; Li, L.; Liu, J.; Yu, L.; Li, H.; Cheng, F.; Yi, X.; He, J.; Li, B. Green Synthesis of Fluorescent Carbon Dots from Gynostemma for Bioimaging and Antioxidant in Zebrafish. *ACS Appl. Mater. Interfaces* **2019**, *11* (10), 9832−9840.
(64) Dong, X.; Su, Y.; Geng, H.; Li, Z.; Yang, C.; Li, X.; Zhang, Y. Fast one-step synthesis of N-doped carbon dots by pyrolyzing ethanolamine. *J. Mater. Chem. C* **2014**, *2* (36), 7477−7481.
(65) Li, C.-X.; Yu, C.; Wang, C.-F.; Chen, S. Facile plasma-induced fabrication of fluorescent carbon dots toward high-performance white LEDs. *J. Mater. Sci.* **2013**, *48* (18), 6307−6311.
(66) Carolan, D.; Rocks, C.; Padmanaban, D. B.; Maguire, P.; Svrcek, V.; Mariotti, D. Environmentally friendly nitrogen-doped carbon quantum dots for next generation solar cells. *Sustain. Energy Fuels* **2017**, *1* (7), 1611−1619.
(67) Wang, Z.; Lu, Y.; Yuan, H.; Ren, Z.; Xu, C.; Chen, J. Microplasma-assisted rapid synthesis of luminescent nitrogen-doped carbon dots and their application in pH sensing and uranium detection. *Nanoscale* **2015**, *7* (48), 20743−20748.
(68) Huang, X.; Li, Y.; Zhong, X.; Rider, A. E.; Ostrikov, K. Fast microplasma synthesis of blue luminescent carbon quantum dots at ambient conditions. *Plasma Processes Polym.* **2015**, *12* (1), 59−65.
(69) Bandi, R.; Kannikanti, H. g.; dadigala, R.; Gangapuram, B. r.; Vaidya, J. r.; Guttena, V. One step synthesis of hydrophobic carbon dots powder with solid state emission and application in rapid visualization of latent fingerprints. *Opt. Mater.* **2020**, *109*, 110349.
(70) Issa, M. A.; Abidin, Z. Z.; Sobri, S.; Rashid, S. A.; Mahdi, M. A.; Ibrahim, N. A. Fluorescent recognition of Fe 3+ in acidic environment by enhanced-quantum yield N-doped carbon dots: optimization of variables using central composite design. *Sci. Rep.* **2020**, *10* (1), 1−18.
(71) Huo, X.; He, Y.; Ma, S.; Jia, Y.; Yu, J.; Li, Y.; Cheng, Q. Green Synthesis of Carbon Dots from Grapefruit and Its Fluorescence Enhancement. *J. Nanomater.* **2020**, *2020*, 8601307 DOI: 10.1155/2020/8601307.
(72) Liu, H.; Zhang, Y.; Liu, J. H.; Hou, P.; Zhou, J.; Huang, C. Z. Preparation of nitrogen-doped carbon dots with high quantum yield from Bombyx mori silk for Fe (III) ions detection. *RSC Adv.* **2017**, *7* (80), 50584−50590.

https://doi.org/10.1021/acssuschemeng.0c09279
ACS Sustainable Chem. Eng. 2021, 9, 4755−4770

(73) Omer, K. M.; Sartin, M. Dual-mode colorimetric and fluorometric probe for ferric ion detection using N-doped carbon dots prepared via hydrothermal synthesis followed by microwave irradiation. *Opt. Mater.* **2019**, *94*, 330−336.
(74) Rahmani, Z.; Ghaemy, M. One-step hydrothermal-assisted synthesis of highly fluorescent N-doped carbon dots from gum tragacanth: Luminescent stability and sensitive probe for Au3+ ions. *Opt. Mater.* **2019**, *97*, 109356.
(75) Yang, P.; Zhang, Z.-W.; Zou, G.-D.; Huang, Y.; Li, N.; Fan, Y. Template Thermolysis to Create a Carbon Dots-Embedded Mesoporous Titanium-Oxo Sulfate Framework for Visible-Light Photocatalytic Applications. *Inorg. Chem.* **2020**, *59* (3), 2062−2069.
(76) Ding, H.; Xiong, H.-M. Exploring the blue luminescence origin of nitrogen-doped carbon dots by controlling the water amount in synthesis. *RSC Adv.* **2015**, *5* (82), 66528−66533.
(77) Zhang, Q.; Xie, S.; Yang, Y.; Wu, Y.; Wang, X.; Wu, J.; Zhang, L.; Chen, J.; Wang, Y. A facile synthesis of highly nitrogen-doped carbon dots for imaging and detection in biological samples. *Journal of analytical methods in chemistry* **2018**, *2018*, 7890937 DOI: 10.1155/2018/7890937.
(78) Liu, W.; Zhang, R.; Kang, Y.; Zhang, X.-y.; Wang, H.-j.; Li, L.-h.; Diao, H.-p.; Wei, W.-l. Preparation of nitrogen-doped carbon dots with a high fluorescence quantum yield for the highly sensitive detection of Cu^{2+} ions, drawing anti-counterfeit patterns and imaging live cells. *New Carbon Mater.* **2019**, *34* (4), 390−402.
(79) Roschangar, F.; Sheldon, R.; Senanayake, C. Overcoming barriers to green chemistry in the pharmaceutical industry−the Green Aspiration Level concept. *Green Chem.* **2015**, *17* (2), 752−768.
(80) Sheldon, R. A. Metrics of green chemistry and sustainability: past, present, and future. *ACS Sustainable Chem. Eng.* **2018**, *6* (1), 32−48.
(81) Dicks, A. P.; Hent, A. Atom economy and reaction mass efficiency. *Green Chemistry Metrics*; Springer: 2015; pp 17−44 DOI: 10.1007/978-3-319-10500-0_2.
(82) Reid, B. T.; Reed, S. M. Improved methods for evaluating the environmental impact of nanoparticle synthesis. *Green Chem.* **2016**, *18* (15), 4263−4269.
(83) Monteith, E. R.; Mampuys, P.; Summerton, L.; Clark, J. H.; Maes, B. U.; McElroy, C. R. Why we might be misusing process mass intensity (PMI) and a methodology to apply it effectively as a discovery level metric. *Green Chem.* **2020**, *22* (1), 123−135.
(84) Welty, J.; Rorrer, G. L.; Foster, D. G. *Fundamentals of momentum, heat, and mass transfer*; John Wiley & Sons: 2014.
(85) MacArthur, E. Towards the circular economy. *J. Ind. Ecol.* **2013**, *2*, 23−44.
(86) Escriba-Gelonch, M.; Bricout, J.; Hessel, V. Circular Economy Metrics for the Photo-High-p, T Continuous Multistep Synthesis of Vitamin D3. *ACS Sustainable Chem. Eng.* **2021**, *9* (4), 1867.
(87) Bagheri, Z.; Ehtesabi, H.; Rahmandoust, M.; Ahadian, M. M.; Hallaji, Z.; Eskandari, F.; Jokar, E. New insight into the concept of carbonization degree in synthesis of carbon dots to achieve facile smartphone based sensing platform. *Sci. Rep.* **2017**, *7* (1), 1−11.
(88) Atchudan, R.; Edison, T. N. J. I.; Shanmugam, M.; Perumal, S.; Somanathan, T.; Lee, Y. R. Sustainable synthesis of carbon quantum dots from banana peel waste using hydrothermal process for in vivo bioimaging. Physica E Low Dimens. *Syst. Nanostruct.* **2021**, *126*, 114417.
(89) Lead, J. R.; Valsami-Jones, E. *Nanoscience and the Environment*; Elsevier: 2014.
(90) Luo, X.; Han, Y.; Chen, X.; Tang, W.; Yue, T.; Li, Z. Carbon dots derived fluorescent nanosensors as versatile tools for food quality and safety assessment: A review. *Trends Food Sci. Technol.* **2020**, *95*, 149−161.
(91) Hardman, R. A toxicologic review of quantum dots: toxicity depends on physicochemical and environmental factors. *Environ. Health Perspect.* **2006**, *114* (2), 165−172.
(92) Wang, Y.; Anilkumar, P.; Cao, L.; Liu, J.-H.; Luo, P. G.; Tackett, K. N.; Sahu, S.; Wang, P.; Wang, X.; Sun, Y.-P. Carbon dots of different composition and surface functionalization: cytotoxicity issues relevant to fluorescence cell imaging. *Exp. Biol. Med.* **2011**, *236* (11), 1231−1238.
(93) Yang, S.-T.; Cao, L.; Luo, P. G.; Lu, F.; Wang, X.; Wang, H.; Meziani, M. J.; Liu, Y.; Qi, G.; Sun, Y.-P. Carbon dots for optical imaging in vivo. *J. Am. Chem. Soc.* **2009**, *131* (32), 11308−11309.
(94) Cao, L.; Wang, X.; Meziani, M. J.; Lu, F.; Wang, H.; Luo, P. G.; Lin, Y.; Harruff, B. A.; Veca, L. M.; Murray, D.; Xie, S.-Y.; Sun, Y.-P. Carbon dots for multiphoton bioimaging. *J. Am. Chem. Soc.* **2007**, *129* (37), 11318−11319.
(95) Yang, S.-T.; Wang, X.; Wang, H.; Lu, F.; Luo, P. G.; Cao, L.; Meziani, M. J.; Liu, J.-H.; Liu, Y.; Chen, M.; Huang, Y.; Sun, Y.-P. Carbon dots as nontoxic and high-performance fluorescence imaging agents. *J. Phys. Chem. C* **2009**, *113* (42), 18110−18114.
(96) Wang, K.; Gao, Z.; Gao, G.; Wo, Y.; Wang, Y.; Shen, G.; Cui, D. Systematic safety evaluation on photoluminescent carbon dots. *Nanoscale Res. Lett.* **2013**, *8* (1), 1−9.
(97) López, M.; Calvo, T.; Prieto, M.; Múgica-Vidal, R.; Muro-Fraguas, I.; Alba-Elías, F.; Alvarez-Ordóñez, A. A review on non-thermal atmospheric plasma for food preservation: Mode of action, determinants of effectiveness, and applications. *Front. Microbiol.* **2019**, *10*, 622.
(98) Dach, R.; Song, J. J.; Roschangar, F.; Samstag, W.; Senanayake, C. H. The eight criteria defining a good chemical manufacturing process. *Org. Process Res. Dev.* **2012**, *16* (11), 1697−1706.
(99) Van Aken, K.; Strekowski, L.; Patiny, L. EcoScale, a semi-quantitative tool to select an organic preparation based on economical and ecological parameters. *Beilstein J. Org. Chem.* **2006**, *2* (1), 3.
(100) Wei, X.; Mei, S.; Yang, D.; Zhang, G.; Xie, F.; Zhang, W.; Guo, R. Surface states induced photoluminescence enhancement of nitrogen-doped carbon dots via post-treatments. *Nanoscale Res. Lett.* **2019**, *14* (1), 1−9.

https://doi.org/10.1021/acssuschemeng.0c09279
ACS Sustainable Chem. Eng. 2021, 9, 4755−4770

BLANK PAGE

Chapter 4

Process intensification for gram scale synthesis of NCQDs

The results from Chapter 3 indicate that microplasma is one of the most sustainable methods in terms of energy efficiency while lacking mass efficiency. Chapter 4 focuses on mass-based intensification by process design to overcome this research gap. First, the distance of the tip of the microplasma jet to the water surface is changed in three steps, named distant, contact, and deflection modes. As a further variation, the liquid volume is either stirred or unstirred and may contain glass beads or metal flakes. In this way, the mass transfer, hydrodynamics, and the electrical field are influenced and create the specific gas–liquid interface, possibly including plasma-catalytic effects. A thermofluidic analysis confirms a uniform temperature profile and a positive temperature effect on mass transfer. By doing this way, the research achieves process intensification.

This chapter has been published as a research paper in "Chemical Engineering Journal" as follows:

Pho, Q.H., Lin, L., Rebrov, E.V., Sarafraz, M.M., Tran, T.T., Tran, N.N., Losic, D. and Hessel, V., 2023. Process intensification for gram-scale synthesis of N-doped carbon quantum dots immersing a microplasma jet in a gas-liquid reactor. Chemical Engineering Journal, 452, p.139164. **<Link>**

Statement of Authorship

Title of Paper	Process intensification for gram-scale synthesis of N-doped carbon quantum dots immersing a microplasma jet in a gas-liquid reactor
Publication Status	☑ Published ☐ Accepted for Publication ☐ Submitted for Publication ☐ Unpublished and Unsubmitted w ork w ritten in manuscript style
Publication Details	Pho, Q.H., Lin, L., Rebrov, E.V., Sarafraz, M.M., Tran, T.T., Tran, N.N., Losic, D. and Hessel, V., 2023. Process intensification for gram-scale synthesis of N-doped carbon quantum dots immersing a microplasma jet in a gas-liquid reactor. Chemical Engineering Journal, 452, p.139164.

Principal Author

Name of Principal Author (Candidate)	Quoc Hue Pho		
Contribution to the Paper	Conceptualization, Methodology, Formal analysis, Investigation, Data curation, Writing – original draft		
Overall percentage (%)	65%		
Certification:	This paper reports on original research I conducted during the period of my Higher Degree by Research candidature and is not subject to any obligations or contractual agreements with a third party that would constrain its inclusion in this thesis. I am the primary author of this paper.		
Signature		Date	28.01.2023

Co-Author Contributions

By signing the Statement of Authorship, each author certifies that:

i. the candidate's stated contribution to the publication is accurate (as detailed above);
ii. permission is granted for the candidate in include the publication in the thesis; and
iii. the sum of all co-author contributions is equal to 100% less the candidate's stated contribution.

Name of Co-Author	LiangLiang Lin		
Contribution to the Paper	Investigation and Writing- Review and Editing.		
Signature		Date	30.01.2023

Name of Co-Author	Evgeny V. Rebrov		
Contribution to the Paper	Formal analysis, Writing- Review and Editing.		
Signature		Date	06.02.2023

Please cut and paste additional co-author panels here as required.

Name of Co-Author	Mohammad Mohsen Sarafraz		
Contribution to the Paper	Formal analysis, Data curation, Writing- Review and Editing.		
Signature	Digitally signed by Dr Mohammad Mohsen Sarafraz DN: cn=Dr Mohammad Mohsen Sarafraz, o=Deakin University, ou=FATE Thermofluids Group, email=Mason.Sarafraz@gmail.com, c=AU Date: 2023.02.03 10:42:19 +11'00'	Date	03.02.2023

Name of Co-Author	Thanh Tung Tran		
Contribution to the Paper	Formal analysis, Writing- Review and Editing.		
Signature		Date	1.2.2023

Name of Co-Author	Nam NghiepTran		
Contribution to the Paper	Writing- Review and Editing.		
Signature		Date	28.01.2023

Name of Co-Author	Dusan Losic		
Contribution to the Paper	Co-supervised andss Writing- Review and Editing.		
Signature		Date	2 feb 2023

Name of Co-Author	Volker Hessel		
Contribution to the Paper	Supervised (scientific ideas, concepts, objectives, assessment of achievement degree, societal impact) Conceptualised, Writing – review & editing, and is the corresponding author.		
Signature		Date	28.01.2023

Please cut and paste additional co-author panels here as required.

Chemical Engineering Journal 452 (2023) 139164

Contents lists available at ScienceDirect

Chemical Engineering Journal

journal homepage: www.elsevier.com/locate/cej

Process intensification for gram-scale synthesis of *N*-doped carbon quantum dots immersing a microplasma jet in a gas-liquid reactor

Quoc Hue Pho [a,e], LiangLiang Lin [d], Evgeny V. Rebrov [e], Mohammad Mohsen Sarafraz [c], Thanh Tung Tran [a,b], Nam Nghiep Tran [a], Dusan Losic [a,b], Volker Hessel [a,e,*]

[a] School of Chemical Engineering and Advanced Materials, The University of Adelaide, Adelaide, SA 5005, Australia
[b] The ARC Graphene Research Hub, School of Chemical Engineering and Advanced Materials, The University of Adelaide, SA 5005, Australia
[c] School of Engineering, Deakin University, Waurn Ponds Campus, Geelong, Victoria 3216, Australia
[d] School of Chemical and Material Engineering, Jiangnan University, Wuxi 214122, People's Republic of China
[e] School of Engineering, University of Warwick, Library Rd, Coventry CV4 7AL, England, UK

ARTICLE INFO

Keywords:
N-doped carbon dots
Microplasma jet
Gas–liquid reactor
Process intensification
Gram-scales
Vitamin B9

ABSTRACT

N-doped carbon quantum dots are synthesised by immersing a microplasma jet into a gas–liquid reactor of the size of a microwell, containing an aqueous solution of folic acid (Vitamin B9). The distance of the tip of the microplasma jet to the water surface is changed in three steps, named distant, contact, and deflection modes. As a further variation, the liquid volume is either stirred or unstirred and may contain glass beads or metal flakes. In this way, the mass transfer, hydrodynamics, and the electrical field are influenced and create the specific gas–liquid interface, possibly including plasma-catalytic effects. A thermofluidic analysis confirms a uniform temperature profile and a positive temperature effect on the mass transfer. In this way, the research achieves process intensification, bringing the synthesis towards 1 g per day and maximising the intended performance, the photoluminescence intensity. Recycling further increases the mass yield via centrifugation. An analysis by optical emission spectroscopy reveals the formation of the plasma species from which a reaction mechanism is proposed.

1. Introduction

The key issue around plasma catalysis, or any multi-phase plasma processing, is the short lifetime of the active species [1,2]. This hampers the effectiveness of any conventional matter transport from one phase to the other, even when intensified. At best, the plasma phase is in direct contact with the catalyst or other phase, rendering superfluous any matter transport. Yet that may deteriorate the catalyst by thermal action or cause abrasion, and even then, a major part of the plasma phase will remain as unused bulk volume [3]. Rather than using a pure plasma gas phase, a solution may add a liquid volume and benefit from plasma-multiphase interactions. The liquid volume may be the only reaction medium towards a catalyst (heterogeneous or homogeneous) or contain a reactant molecule (to be converted with or without a catalyst). Here, we consider a gas–liquid reaction without a catalyst or with metal particles of potential catalytic nature.

It is known that plasma-liquid interaction can bring additional benefits compared to pure gas-phase plasmas. Those benefits are enhanced chemical diversity (e.g·H_2O_2, OH·, H_2O^+, H*, etc.), increased fluidic cooling rate, wider precursor choice, and reduced nanoparticle aggregation [4]. The high heat capacity of a liquid phase would likely avoid the thermal hassle (ensuring good thermal transport).

Concerning the distant (non-penetrating) contact mode, one class of plasma gas–liquid reactors have been developed, with applications ranging from nanomaterials synthesis and surface modification to wastewater treatment, VOC decomposition, and antibacterial purpose. Several design variations of this concept are known. For instance, a hollow-cathode microplasma system was proposed by Sankaran et al. for the rapid synthesis of colloidal metal nanoparticles in aqueous solutions (Fig. 1A) [5,6]. A similar method was also applied to prepare silver nanoparticles and their coverage with a surfactant [7]. Julien et al. used a microfluidic chip to generate plasma within microchannels to evaluate the safety and selectivity of an oxidation reaction converting liquid cyclohexane to form a mixture of cyclohexanol, cyclohexanone and cyclohexyl hydroperoxide [8]. Lin et al. fabricated gold nanoparticles using a one-pot microplasma-induced approach, applying the obtained products for surface-enhanced Raman spectroscopic detection of methylene blue [9]. By integrating plasma-liquid interactions with

* Corresponding author at: School of Chemical Engineering and Advanced Materials, The University of Adelaide, Adelaide, SA 5005, Australia.
E-mail address: volker.hessel@adelaide.edu.au (V. Hessel).

https://doi.org/10.1016/j.cej.2022.139164
Received 14 March 2022; Received in revised form 3 August 2022; Accepted 8 September 2022
Available online 13 September 2022
1385-8947/© 2022 Elsevier B.V. All rights reserved.

microfluidics in a T-type capillary, they further synthesised Au-Ag nanoalloys with tunable composition (Fig. 1B) [10].

Another class of plasma gas–liquid reactor with more vigorous contact can cause gas dispersion (e.g. by jet penetration), thus forming the discharges within the bulk liquid. A "needle-to-needle" plasma-liquid interaction configuration was proposed by Jung et al. to fabricate tin and tin oxide (Fig. 1**C**). Through process control over pH, plasma exposure time, and precursor concentration, the size and composition of the products can be flexibly tuned [11]. Another plasma-liquid system is reported by Suehiro et al. [12], where plasma discharges are formed between two electrodes (wire-to-plane system) immersed in water, used for carbon nanotube surface modification (Fig. 1**D**). Due to the formation of strongly oxidative species like H_2O_2, OH·, O· to the surface of the carbon nanotubes, their water solubility was significantly enhanced.

Gas-liquid plasma equipment with gas-dispersion is even commercially available, such as the Leap100 reactor from Plasma-Leap Technologies. This is a non-thermal plasma bubble column reactor of dual reactor configurations with multiple discharge schemes and dynamic bubble control [13]. This scalable reactor works in continuous mode and has shown a high production rate of ammonia [13], organic pollutant degradation [14], food sanitisation [15], and inactivation of tumour - cells [16].

In this research, however, we like to perform fundamental investigations, which follow the principles of chemical reactor design and allow us to make some critical variations easily. Therefore, we have chosen to use simple equipment, the commercially available KINPen®IND reactor, providing a cold atmospheric-pressure microplasma jet with noble gases such as argon. The KINPen®IND microplasma jet reactor has found large usage and considerable literature documentation [17–22].

This paper explores the KINPen®IND microplasma jet reactor to synthesise *N*-doped carbon nanodots from folic acid (Vitamin B9) in an aqueous solution. We like to revisit processing with it from the chemical engineering viewpoint. This concern mainly the interaction of the jet with a liquid volume (which may contain a catalyst). Our preliminary work shows that metal flakes can act as an electrocatalyst in the decomposition of folic acid. To the best of our knowledge, the inner electrons of the alloys tend to move from nickel to copper in the electrochemical series. In this case, Cu acts as a strong oxidant (electron receptors) while Ni acts as a reduction (electron donors). As a result, more reactive electrons are on the surface of the catalysts. When electrons and ionised species from microplasma colloid with the surface of the catalysts, the electrons on the surface can be more reactive and removed from the surface to colloid with folic acid molecules. As a result, it causes more folic acid molecules to be decomposed.

By varying the jet-liquid distance in this way, the plasma jet can be turned vigorous in its interaction with a liquid volume due to its high velocities, which can induce turbulence in small liquid volumes, facilitating mass transport. In that mode, the liquid surface is constantly deformed and renewing. In the strongest interaction, it is expected that plasma gas bubbles may form with a favourably small interface for mass transfer. The latter effect would also increase residence time, besides mass transfer. As an option, we load the liquid volume with solid particles, increasing the mixing effect by impulse transfer and may even act as reaction-promoting material. The latter might also happen by changing the electric field when the particles are electrically conductive.

2. Materials and methodologies

2.1. Reactor system configuration

Our experimental design is inspired by the concept of high-intensity gas–liquid reactors using vigorous gas jets, which are known to enhance phase mixing. Wild et al. developed a high velocity impinging stream reactor entering a small reactor volume, moving in a counter-current fashion. Guided by tiny nozzles, gas and liquid feed streams collide in a small reactor volume, resulting in a highly turbulent gas-phase dispersion into the liquid. The mass transfer rate is intensified, supported by bubble formation and breakup. Another design of a high-intensity gas–liquid reactor consists of a pump, an orifice, a vertical tube coaxial to the orifice and an impinging plate. The pump generates a downward vertical liquid jet through the orifice generating gas–liquid

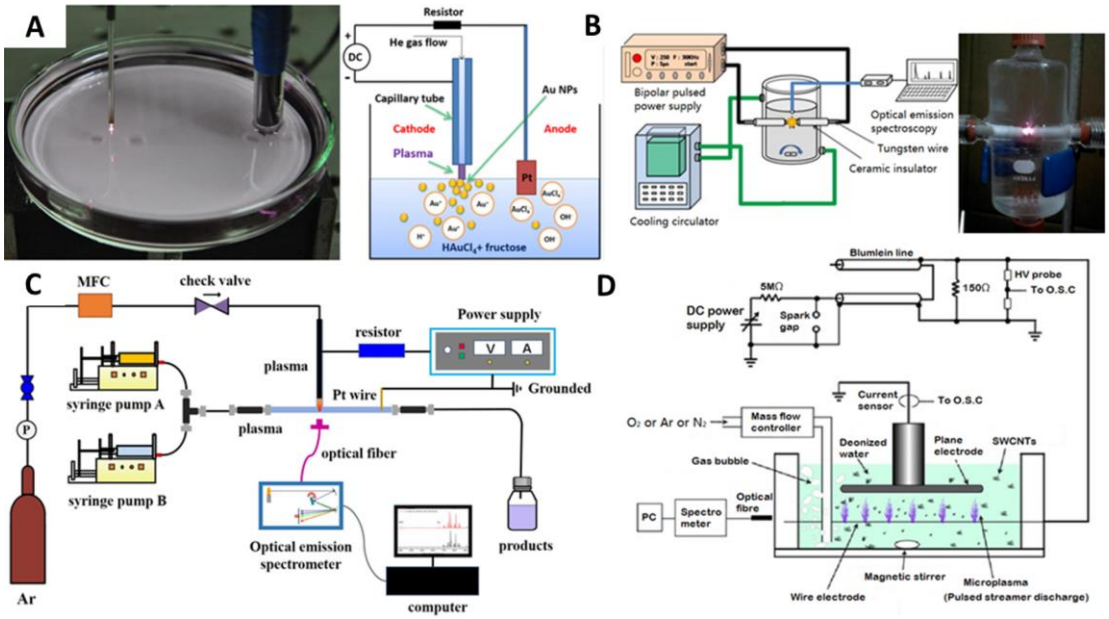

Fig. 1. Various plasma-liquid interaction systems for nanomaterials synthesis with non-dispersive or dispersive multi-phase interaction: (A) "Hollow-cathode" microplasma system; (B) Microfluidic plasma system; (C) Needle-to-needle plasma system; (D) Wire-to-plane plasma system.

dispersion in a tube. The two-phase jet is directed towards an impinging plate near the bottom of the tank and dispersed in the volume of the liquid. The liquid is withdrawn below the impinging plate and recycled [23]. Our experimental design follows the concept of those high-intensity gas–liquid reactors, but we need to simplify it. It would mean having a plasma gas phase over a long length, which is difficult to achieve. Instead, we use a microplasma jet directed towards a liquid **(**Fig. 2**).** We also refrain from flow recycling for repeated gas–liquid interaction, as a single contact will show us better the fundamentals governing the process intensification [24].

The reactor configuration and experimental synthesis process was adapted from our previous study [24]. In brief, the synthesis reactors include two parts: (1) a kINPen®IND microplasma jet with a dimension of 105 × 180 × 330 mm (H × W × D) was purchased from Neoplas GmbH, Germany and (2) an open glass reactor was designed and fabricated in our laboratory with a 9 mm × 15 mm (W × H) dimension. A 110 VAC power supply (50 Hz) was used to connect with the kINPen®IND microplasma jet. A continuous Ar (99.9 %) gas stream was connected to the microplasma jet. A stable microplasma stream with a length of 1 cm was formed under an Ar gas stream (2 sccm) and a regulated pressure of 3 Bar. To understand the reaction mechanism, an optical fibre was set up in the plasma-liquid interaction region to detect reactive species generated from microplasma. The general synthesis process was also described in Fig. 2**.** Briefly, folic acid (FA) solution (0.1 g/mL) as a starting carbon source was prepared by dissolving 2 g of folic acid (98 %) in 20 ml of $NaHCO_3$ (0.5 M) as a solvent under stirring until the resulting orange solution was homogeneously mixed. 1 ml of FA solution (0.1 mg/mL) was then transferred to the open reactor and then treated under microplasma.

To operate in the non-dispersive and dispersive mode, we chose three generic configurations of positioning the plasma jet relative to the liquid surface **(**Fig. 3**A).** In the "distant" position, we emulate many plasma reactor configurations reported in the literature, following the design shown in Fig. 1**A**. The most eminent part of the microplasma jet (assumed to be the tip) is brought in contact with the liquid surface. One would assume hardly any impact on the liquid phase hydrodynamics and mass transfer. In the "contact" position, we emulate the high-intensity gas–liquid reactors of Wild et al. This may force the adjacent region of the liquid phase into motion, yet likely may leave the bulk liquid volume still unaffected. In the "deflection" position, we emulate the Botes plasma reactor configuration of the 'high velocity impinging stream reactors'. The shape and velocity of microplasma has changed significantly when changing the mode from distant to contact and deflection. The term "contact" here means the tip of the microplasma is in contact right in the bottom of the reactor. The term "deflection" here means the microplasma will reflect back due to convection effect when the distance is shorter than the contact position. By deflecting the plasma jet on the floor of the reactor well, momentum is transferred into the whole liquid bulk volume. The expectation is to generate a highly turbulent system with constant renewal of interfaces, potentially with the generation and breakup of plasma droplets.

In one step further, an experimental set is conducted when glass beads (100 μm) or metal flakes (copper-nickel) (500 μm) are added to the liquid volume or a mixing bar for stirring (1000 rpm) **(**Fig. 3**B).** In this way, reactor engineering is changed fundamentally. First, mass transfer is enhanced, both by the bar and the particles, which can pick up the impulse of the jet. Second, the plasma may interact with the particles, driven both by their material properties and geometry (size, shape), as known from literature and our investigations. The presence of a material can change the plasma and electric field intensity and presumably the nature and concentration of the plasma excited species.

2.2. Recycling and purification

The recycling and purification process is based on precipitation, centrifugation and dialysis. After the first treatment of folic acid solution under microplasma, the resulting solution is diluted into water and then precipitated by HCl (0.5 M) under stirring. Afterwards, the resulting mixture is separated by centrifugation (4000 rpm) for 30 min. After centrifugation, the supernatant is used for dialysis against water for three days. The residue of unreacted folic acid is washed with water and dissolved back to $NaHCO_3$ for the second synthesis. This process will be repeated ten times of recycling. The dialysed N-doped carbon dots are freeze-dried to obtain solid N-doped carbon dots.

2.3. Analysis

2.3.1. Photoluminescence and UV–vis

Fluorescence spectra were carried out on a photoluminescence Spectrometer (FLS 1000, United Kingdom). The system is a modular fluorescence and phosphorescence spectrometer for measuring ultraviolet (UV) spectra to the mid-infrared spectral range. Firstly, Photoluminescence 3D colour mapping was investigated to determine the as-prepared *N*-doped carbon dots' maximal excitation and emission wavelength. The excitation and emission spectra were set from 300 to 700 nm and plotted in photoluminescence 3D colour mapping. After

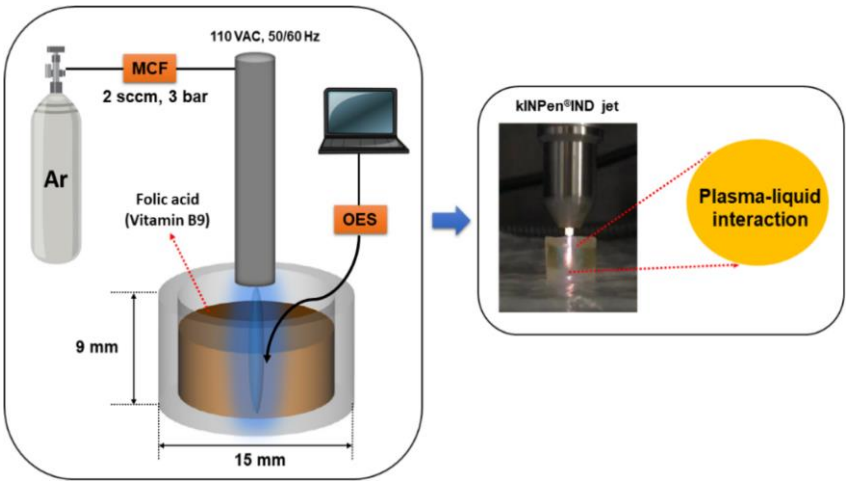

Fig. 2. Reactor configurations and experimental synthesis process setup of *N*-doped CDs.

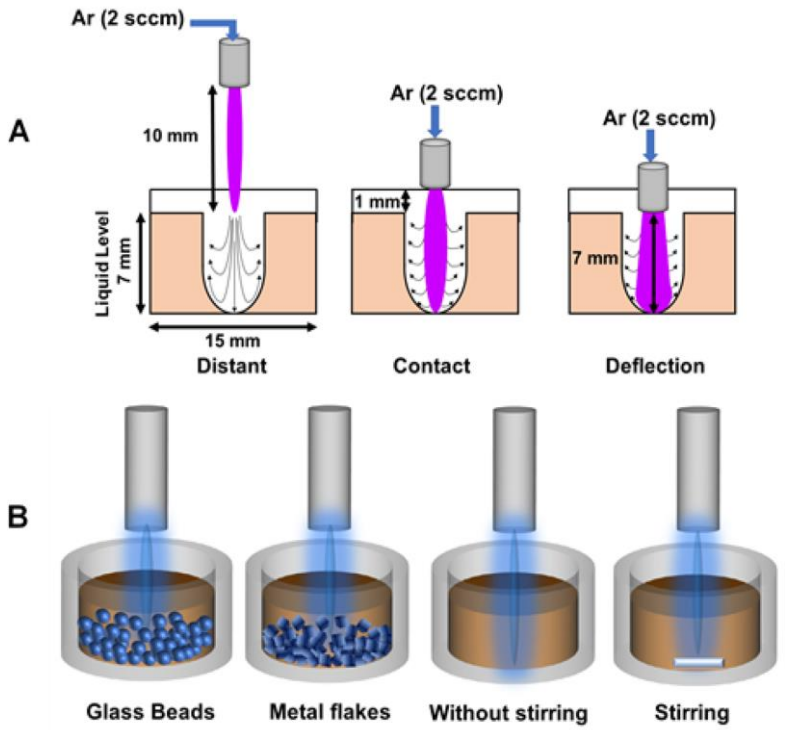

Fig. 3. **A:** Generic configurations of the microplasma jet-liquid system as a function of the distance between the jet and liquid phase. **B:** Various operational modes of kINPen®IND ®IND jet-based synthesis reactors. *Glass beads* (100 μm), metal flakes (copper-nickel) (500 μm), stirring bar (1000 rpm).

investigating the excitation and emission wavelength, these parameter values are used for further photoluminescence intensity tests. 1 ml of the as-prepared *N*-doped carbon dots (1 μg/mL) is inserted into the FLS1000 under the investigated excitation light source to determine the photoluminescence curve at the maximal wavelength.

UV–vis spectra are another important optical parameter that needs to investigate. Briefly, 1 ml of the as-prepared *N*-doped carbon dots (1 μg/mL) is inserted into Cary 60 UV–vis Agilent Technologies to record the spectra to determine the maximal absorbance wavelength. Based on this data, further absorbance tests are carried out.

2.3.2. SEM/edx

FEI Quanta 450 FEG Environmental Scanning Electron Microscope (ESEM) ascertained *N*-doped carbon dots' elemental co mposition and structural purity. Briefly, 10 mg of *N*-doped carbon dots were dispersed into ethanol under sonication to ensure the *N*-doped carbon dots dissolved well and homogeneously. Later on, the *N*-doped carbon dots solution is drop-wised into a carbon tape and put on the ESEM holder. Then, the ESEM sample is dried up in the oven at 50 ^{0}C to remove solvents. Finally, the samples are tested with FEI Quanta 450 FEG Environmental Scanning Electron Microscope (ESEM) to record EDX data.

2.3.3. Elemental distribution (HAADF)

To determine the elemental distribution (HAADF) and HRTEM, the as-prepared N-doped carbon dots were tested with FEI Titan Themis 80–200. Briefly,10 mg of *N*-doped carbon dots were dispersed into water under sonication. Then, the *N*-doped carbon dots solution is drop-wised into the TEM grid. Afterwards, the grid is dried up naturally at a certain time. Finally, the prepared sample is tested for elemental distribution (HAADF).

2.3.4. Optical emission spectroscopy

The optical emission spectrum was measured using an HR2000 + ES spectrometer (Ocean Optics, Inc.). An optical fibre outside the reactor collected the emitted light from the plasma gas–liquid interactions. The OES fibre was inserted into the liquid-plasma interaction where the reaction occurs and then transmitted to a computer to record the emission.

2.4. Thermofluidic modelling

To assess the thermal performance of the microplasma and its suitability for process intensification, the thermophysical properties of the argon gas, including density (ρ), thermal conductivity (k) and heat capacity (c_p), were evaluated at operating temperatures ranging from 300 K to 343 K using HYSYS properties. The Peng-Robinson and Uniquac activity coefficient model was used to describe the thermodynamics of the model. An atmospheric feed stream of argon was defined, and a sensitivity analysis was carried out to evaluate the effect of the temperature of the bulk of gas on the thermophysical properties.

3. Results and discussion

3.1. Microplasma jet thermofluidics

Often overlooked in chemical engineering literature is that plasma can promote physical properties and fluid transport. Micro-scale phenomena such as Brownian motion (gas–liquid) [25] and thermophoresis [26] can play a vital role in plasma chemistry. The issue here, using a microplasma jet, is that heat transfer in a multi-phase plasma requires efficient localised and on-spot thermal energy in the form of sensible heat to be released on the surface/inside the folic acid precursor

solution. Short-lived reactive species must be created at the right position, ensuring they are reactive enough. These short-living plasma species include but are not limited to spinning, fast-travelling excited species, charged particles, surficial or gas bulk atomic or molecular radicals, and highly reactive molecules. Likewise, Ion species can be traced and measured in the effluent of the kINPen®IND jet microplasma reactor. The calculated quasi-neutral density is ~ 10^{12} cm^{-3} when created by kINPen®IND at 20 W [27]. This is a sufficient density number for fast and highly localised electron impact reactions to generate and drive any surface reactions in the gas/liquid [28]. The kINPen®IND microplasma jet reactor can preheat the plasma up to 70 °C (343 K, Fig. 4).

While the gas temperature is less than 313 K, at a frequency of ~ 1 MHz, the kINPen®IND 's nominal exergy power is approximately 1 W once a power throughput of 20 W is applied to the plasma driver. The discharge pathway from the tip of the KINPen®IND follows the air impurity distribution in the argon jet effluent demonstrated by [27]. The calculated thermal conductivity k and heat capacity C_p for argon in the kINPen®IND microplasma jet are given as a function of temperature (Fig. 5). When increasing the temperature from 298 K to 348 K, k increases by only ~ 10 %, while C_p changes by 0.1 %.

As represented in Fig. 4, the heat capacity (Cp) value slightly changes with the temperature of the plasma gas (0.4 %), which in turn shows that there is no non-uniformity in the spatiotemporal temperature profile of the plasma gas due to the variation in the heat capacity and sensible heat gradient. It is also worth mentioning that the reactivity of the plasma is a strong function of the distribution and formation of the radical species, which is spatially non-uniform and scattered within the reactor. Accordingly, as opposed to conventional reactors, in plasma, the only variation in the energy profile is sourced from radical species rather than sensible heat transfer. Notably, conventional reactors (e.g., continuous stirred-tank reactor, CSTR) have technical challenges associated with the relatively slow kinetics (magnitude of few seconds) compared to plasma (magnitude of microseconds). Also important is the formation of dead zones that suppress the chemical performance of the reactors; however, in plasma jets, there is no dead zone formation as the reactor's gap is a few millimetres.

Concerning the thermal conductivity, the second positive finding is that the kINPen®IND reactor is not energy-intensive but is process-intensive. The power source is used to excite plasma chemistry and, to an extent, increase transport properties by increasing the thermal conductivity. Improving the thermal conductivity is necessary for better chemical performance, faster response, and faster reactions. This is because improving the thermal conductivity of a gas is proportional to its thermal diffusivity. The thermal diffusivity is defined as the ratio of thermal conductivity (k) to the products of gas bulk density and heat capacity, referred to as $\alpha = (\frac{k}{\rho C_p})$. The value of α is enormously intensified by increasing thermal conductivity and accordingly affects the time required for the plasma reactor to reflect the effect of the temperature. The higher the thermal diffusivity, the smaller the response time and more uniform thermal transport. This clarifies that the plasma chemistry of argon at T < 343 K is coping with reaction characteristics of the fast plasma (microseconds) and is energetically symmetric and uniform.

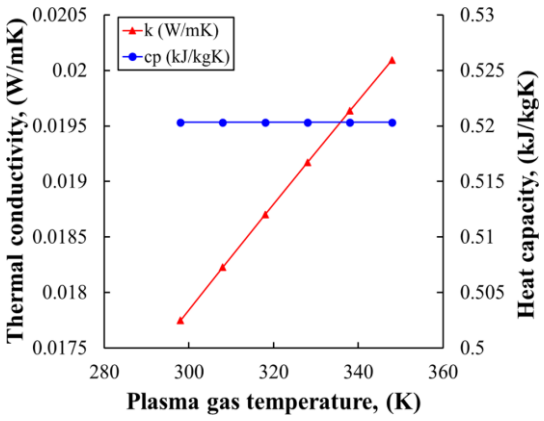

Fig. 4. Variation of the thermal conductivity (red line) and heat capacity of the argon (blue line) with plasma gas temperature calculated via Uniquac thermodynamic models.

3.2. Microplasma jet-microagitation and –materials confinement

The following experiments were made with this contact concept to conclude that the deflection mode is most effective for mass transfer in terms of turbulence and plasma volume extension. The question is if the plasma jet, now able to penetrate the liquid surface partly, can stir the liquid volume enough to avoid mass transfer limitation. Thus, we installed a benchmark experiment with a mixing bar. We used glass beads to intensify the jet impulse for mixing (and to be able to form a trickle bed at a high filling degree). Metal flakes served the same purpose but with the additional hope that they might act as catalysts for the nanoreaction and/or modify the electrical field.

Rather than analysing the quantum dots' size, morphology, crystallinity, etc., we take photoluminescence as a gross performance parameter, which plays a crucial role in applying carbon quantum does for wastewater purification and health care (theranostic agents). We ranked the different plasma gas–liquid reactor configurations in their reaction performance with these metrics.

Fig. 5A shows the UV–vis spectra of the different reactor configurations. A steady increase in absorption is observed from the processing without stirring, using the impulse transfer to the (inert) glass beads, mixing with a bar and metal flakes. When reviewing photoluminescence, the same order of impact is confirmed, yet showing a much stronger effect of the last reactor concept, i.e. the use of metal flakes. It seems that stirring the liquid volume is advantageous. Likely, the mixing bar is more effective than the jet impulse transfer to the glass beads, which might be too heavy and large for the effect chosen. Thus, it might be doubtful if the metal flake effect is alone due to a stirring effect, as metal flakes and glass beads have similar size and mass. Instead, it might be guessed if the flakes act catalytically or interact with the plasma-electrical field. An indication of that is the liquid solution's darkening, forming during the plasma exposure and reaction.

Fig. 5B shows that the deflection mode is better than the contact or distant mode. In terms of photoluminescence, the performance outcome is triple compared to the distant mode. This demonstrates that learning from high-intensification gas–liquid processing is effective for microplasma gas–liquid processing. Fig. 5C also confirms that using metal flakes is superior to stirring throughout; because of impact-driven mixing and a possible catalytic-electric effect.

3.3. Suitability of performance and composition to applications of the quantum dots

Process intensification of quantum materials does not end in achieving a synthesis with a maximised product output; rather, maximising the performance of the nanomaterial must be the goal. Nanomaterials are 'performance chemicals' in the sense of specialty chemicals, and customers are willing to pay for their function and not for their mass.

In this lieu, Fig. 6**A** demonstrates the performance of the obtained *N*-doped carbon dots in terms of their main functional parameter, photoluminescence. The obtained emission wavelengths of 454 nm, absorbance wavelength at 310 nm, and excitation wavelength of 360 nm suit applications in wastewater processing regarding photocatalysis [29,30],

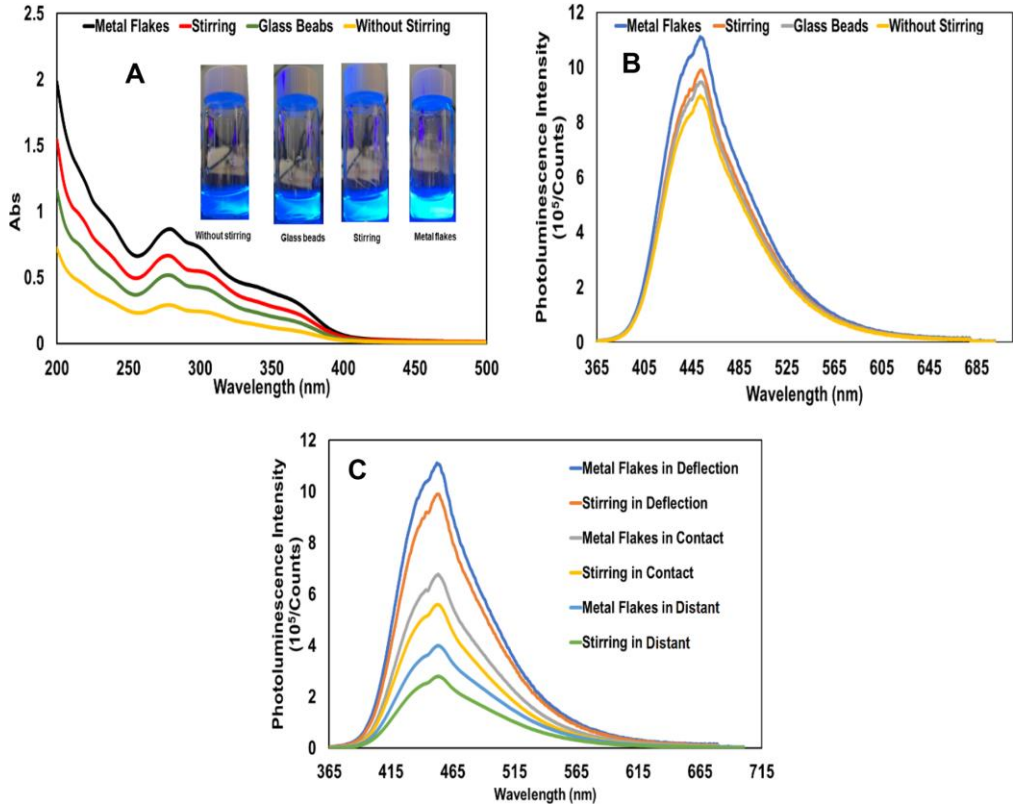

Fig. 5. UV–vis (A) and photoluminescence (B) of N-doped carbon dots synthesised for different operational modes, i.e. partly penetrating the liquid volume (deflection mode, kINPen®IND microplasma jet, 25 °C, 0.1 g/mL folic acid solution, 0.5 g metal flakes, 99.99 % Ar gas). Photoluminescence comparison of metal flakes and stirring mode at various positions of microplasma jet (C).

nanopesticides [31] and health theranostics [32] regarding photoluminescence.

Photocatalysis and photoluminescence of *N*-doped carbon dots are "golden properties" that make it widely applicable in wastewater processing and medical theranostics. With regard to the former application, CDs play a role in the photocatalytic degradation of organic compounds or microorganisms [29,33–35]. *N*-doped carbon dots absorb the light at a wavelength of 310 nm to generate e^-/h^+ pairs. Under the excitation of 360 nm, e-/h^+ pairs are separated and transferred to generate reactive oxygen species. Finally, the ROS groups cause subsequent photocatalytic reactions to decompose the structure of organic compounds or microorganisms [36,37].

Regarding the latter, *N*-doped carbon dots with surfaces modified by receptors such as folate will internalise into tumour cells [35,38]. Then, CDs exhibit strong blue fluorescence under suitable illumination when imaging tumour cells [39–41]. In parallel, ROS groups are also generated from *N*-doped carbon dots under UV exposure to kill tumour cells [39,42,43]. Many studies have used C-dots for bioimaging under UV irradiation. For example, Smriti Sri et al. synthesized zwitterionic carbon dots as a novel approach for bioimaging applications in cancerous cells [44]. In addition, many studies reported that *N*-doped CDs could be used as a nanocarrier to load drugs as a therapeutic medicine [45]. Therefore, the authors believe that *N*-doped CDs can be utilised for theranostic applications under UV irradiation. The as-prepared *N*-doped CDs can emit a blue fluorescence (454 nm) under an excitation of 360 nm. This indicates that our *N*-doped CDs can be excited under (near UV) UVA, which is less harmful than UVB and UVC.

A point beam EDX analysis of *N*-doped carbon dots in Fig. 6**B** shows that the C-represents only three significant peaks of carbon (44.6 %), oxygen (29.8 %), and nitrogen (25.5 %) in terms of atomic mass. This indicates that the as-prepared *N*-doped carbon dots are highly pure without the elemental signature of any foreign impurities other than carbon and oxygen, and nitrogen. Several peaks are not labelled in the EDX spectra. These peaks are attributed to the substrate, which is carbon tape. In the chemical composition of carbon tape, except for carbon which is the main component, silicon and aluminium are also found. For this reason, several peaks have been detected in the EDX spectra. Regarding our purification methodology, the mixed solution includes *N*-doped CDs, NaCl, and H_2O before dialysis. Therefore, the EDX spectra in our study show no presence of NaCl, and the phrase "the elemental signature of any foreign impurities other than carbon, oxygen, and nitrogen" means that no NaCl was found after dialysis.

While not quantitative, the elemental distribution given in Fig. 6**C** shows that all elements are distributed relatively uniform in the nanomaterial. C and N are the expected, name-giving constituents, and O is an unwanted side-constituent. Still, a spread in colour intensity is visible. For example, the left-down side of the C elemental distribution is more intense, maybe because of a higher quantum dot thickness rather than a higher presence of carbon. It is also evident that nitrogen and oxygen have lower contents than carbon, in a similar amount, yet seemingly with somewhat more oxygen than nitrogen. This result also agrees with EDX, confirming the high purity of the as-prepared *N*-doped carbon dots. Apart from the above characterisation, the XRD, XPS, FTIR, and ^{1}H NMR reported from our previous studies revealed that the core

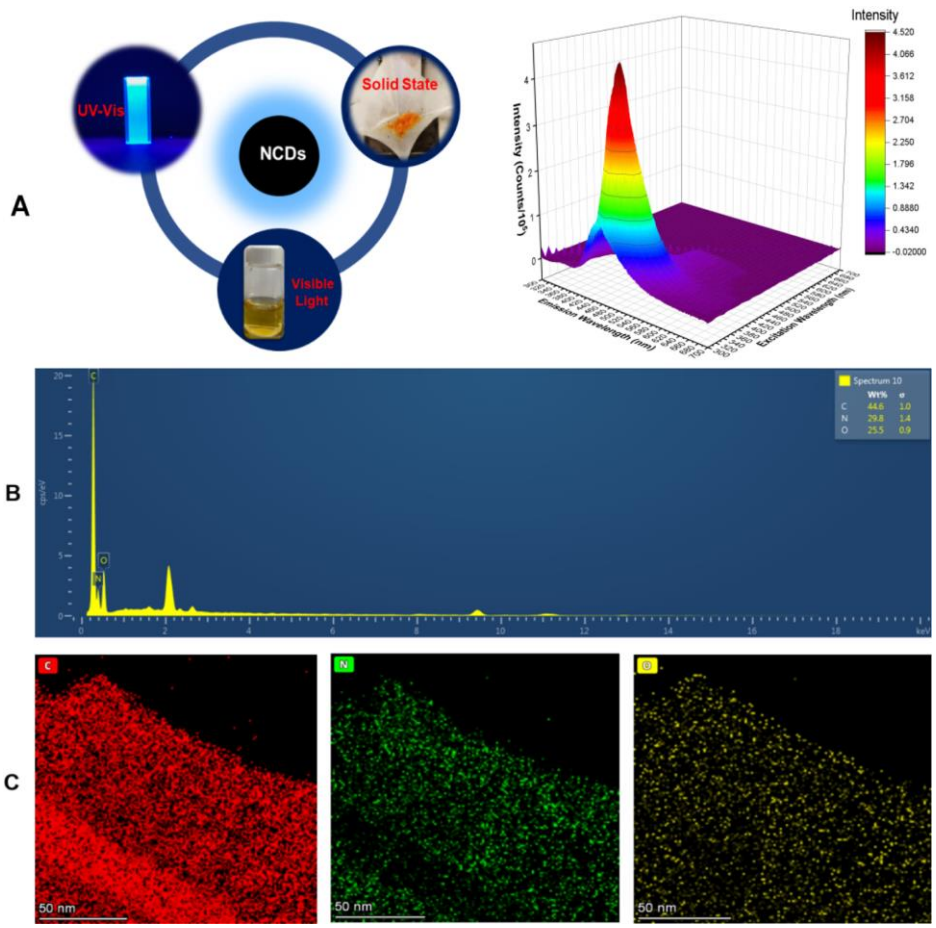

Fig. 6. A: The as-prepared *N*-doped carbon dots in solid-state and liquid-state; and their photoluminescence 3D colour at 1 μg/mL. B, C: EDX elemental analysis and elemental distribution (HAADF) of *N*-doped carbon dots after 20 min synthesis (deflection mode, metal flakes, kINPen®IND microplasma jet, 25 °C, 0.1 g/mL folic acid solution, 0.5 g metal flakes, 99.99 % Ar gas).

structure of *N*-doped CDs was in the form of a crystalline with multi-layered graphitic- and pyrrolic-nitrogen defected graphene sheets. The surface of *N*-doped CDs was decorated by $–NH_2$, –OH, and –COOH functional groups. The resulting *N*-doped CDs had an intensely blue fluorescence performance with a QY of 35 % [46].

3.4. Process intensification

Having identified that the deflection mode and addition of metal flakes are best for the quantum dot formation, a small reaction engineering study shall reveal the productivity of the reaction concept and if process intensification is found, which is usually synonymously quoted with the use of emerging technologies. Process intensification means maximising the performance obtained, either relative to the same plasma reactor system or other technologies giving the same quantum dot product, with the ambition to be significantly better, e.g. order of magnitude.

The approach is trifold. i) operating at best kinetical parameters by varying reaction time and concentration; ii) determining mass reaction efficiency of best conditions; iii) increasing reaction mass efficiency by recycling and repeated reaction with the same starting material.

3.4.1. Operating at best kinetic parameters

Photoluminescence intensity is the performance considered, relating to a high mass yield of our plasma process. A molecular yield cannot be defined for a nanomaterial (having no molecular mass). Rather than making a comprehensive study in an optimisation fashion, we focus here on varying two key process parameters, which are the reaction time and reactant concentration, as central process engineering parameters. Thereafter, we perform process optimisation by varying the process itself, adding agitation and reaction-promoting materials to the blank plasma gas–liquid process.

Fig. 7 plots the emitted fluorescence (photoluminescence) intensity, which is equivalent to nanodot concentration, which is a function of reaction time; the concentration scales with the mass yield as we keep the reaction volume constant. Fig. 7A shows a linear increase in the fluorescence intensity when processing from 0 to 20 min. After that, the emitted photoluminescence intensity grows hardly, reaching saturation. At 20 min, about 90 % of the maximal photoluminescence intensity is reached. Thus a chemical manufacturing process would likely be operated here, as any other time would have a lower rate (while giving a little bit more concentration/mass yield). This classifies the microplasma jet process as fast according to the terminology of process intensification, and the reaction time is similarly short as for typical flow

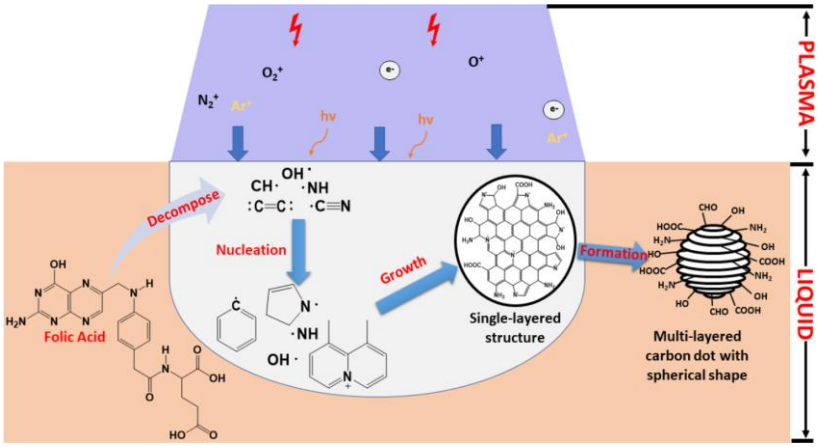

Fig. 11. Proposed mechanism of the microplasma synthesis of *N*-doped CDs.

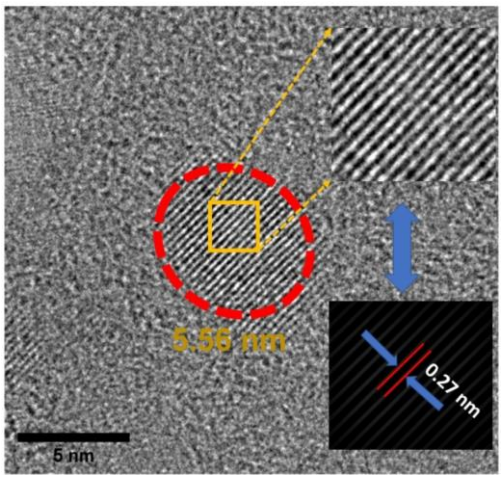

Fig. 12. Morphology of *N*-doped CDs with a multi-layer structure characterised by HRTEM.

microplasma jet into a gas–liquid reactor of the size of a microwell, containing an aqueous solution of folic acid (Vitamin B9). An initial experiment investigated the effect of the distance of the tip of the microplasma jet to the water surface. The closer it came, the more the plasma was deformed and spread out into the whole gaseous reaction volume. In the contact and deflection mode, the jet penetrated the liquid volume down to the reaction well floor. From then onwards, we investigated only the deflection mode. As a further process variation, it was shown that stirred microwell operation delivers higher photoluminescence than unstirred one. The addition of glass beads results in higher photoluminescence, demonstrating the impulse transfer-based mass transfer improvement than the unstirred mode but cannot reach the quality of the stirred plasma operation.

In contrast, adding metal flakes is superior to all modes of operation. It is assumed that this cannot be alone because of better mass transfer and hydrodynamics but may be due to changing the electrical field and possibly plasma-catalytic effects. A thermofluidic analysis confirms a uniform temperature profile and a positive temperature effect on the mass transfer. In this way, the research demonstrated we achieved process intensification. The intended performance for the foreseen applications of the nanomaterial, the photoluminescence intensity, was maximised. In addition, we could reach a productivity of 1 g per day. This is much more than many reported plasma-based and other process-based nanomaterial syntheses in literature and is even quoted to be on the way to production (as nanomaterials most often are only needed in minute volumes). We reported in the paper a synthesis, which in one run makes about 51 mg of product (in 60 min).

Meanwhile, several collaboration partners have requested our material for use in their studies. We have just shipped a sample of about 1 g to India, which is the combined outcome of 20 process runs with about 51 mg each. As this could be elegantly done within one day of work, we think we can claim a gram-scale synthesis if we would work for several days. Recycling further increases the mass yield via precipitation and centrifugation. An analysis by optical emission spectroscopy reveals the formation of the plasma species from which a reaction mechanism is proposed. This analysis also clearly shows the increased reactive excited plasma intermediates when adding the metal flakes.

5. Outlook

Thus, we could conduct a comprehensive chemical engineering study, targeting hydrodynamics, heat and mass transfer, and reactivity in the way of traditional reactor engineering and process design. We added the viewpoint of process intensification by following the concept of high-intensity gas–liquid reactors reported in the literature. Such consequent chemical engineering guidance is largely missing in the operation of plasma reactors. We could show the benefit of adding a liquid phase to the plasma gas, besides just carrying a reactant. For better recycling, we propose combining dialysis and precipitation to remove both large and medium-sized particles. Precipitation does remove only large ones.

CRediT authorship contribution statement

Quoc Hue Pho: Conceptualization, Methodology, Formal analysis, Investigation, Data curation, Writing – original draft. **Liangliang Lin:** Writing – review & editing. **Mohammad Mohsen Sarafraz:** Writing – review & editing. **Evgeny V. Rebrov:** Writing – review & editing. **Thanh Tung Tran:** Conceptualization, Writing- Review and Editing. **Nam Nghiep Tran:** Writing – review & editing. **Dusan Losic:** Writing – review & editing, Supervision. **Volker Hessel:** Conceptualization, Writing – review & editing, Supervision.

Declaration of Competing Interest

The authors declare that they have no known competing financial interests or personal relationships that could have appeared to influence the work reported in this paper.

Data availability

Data will be made available on request.

Acknowledgements

Hue Quoc Pho received the divisional ECMS and full-fee scholarships from the University of Adelaide, Australia. Liangliang Lin thanks the financial support from the Natural Science Foundation of Jiangsu Province (BK20190605) and the National Natural Science Foundation of China (22078125, 52004102). All authors acknowledge support from the ERC Grant Surface-Confined fast-modulated Plasma for process and Energy intensification (SCOPE) from the European Commission with grant number 810182.

References

[1] K. Sklias, J. Santos Sousa, P.-M. Girard, Role of Short- and Long-Lived Reactive Species on the Selectivity and Anti-Cancer Action of Plasma Treatment In Vitro, Cancers 13 (2021) 615.
[2] C. Du, Y. Liu, Y. Huang, Z. Li, R. Men, Y. Men, J. Tang, Qualitation and Quantitation on Microplasma Jet for Bacteria Inactivation, Sci. Rep. 6 (2016) 18838.
[3] A. Bogaerts, X. Tu, J.C. Whitehead, G. Centi, L. Lefferts, O. Guaitella, F. Azzolina-Jury, H.-H. Kim, A.B. Murphy, W.F. Schneider, T. Nozaki, J.C. Hicks, A. Rousseau, F. Thevenet, A. Khacef, M. Carreon, The 2020 plasma catalysis roadmap, J. Phys. D Appl. Phys. 53 (2020), 443001.
[4] L. Lin, H. Quoc Pho, L. Zong, S. Li, N. Pourali, E. Rebrov, N. Nghiep Tran, K. Ostrikov, V. Hessel, Microfluidic plasmas: Novel technique for chemistry and chemical engineering, Chem. Eng. J. 417 (2021), 129355.
[5] W.-H. Chiang, C. Richmonds, R.M. Sankaran, Continuous-flow, atmospheric-pressure microplasmas: a versatile source for metal nanoparticle synthesis in the gas or liquid phase, Plasma Sources Sci. Technol. 19 (2010), 034011.
[6] X. Huang, Y. Li, X. Zhong, Effect of experimental conditions on size control of Au nanoparticles synthesized by atmospheric microplasma electrochemistry, Nanoscale Res. Lett. 9 (2014) 572.
[7] L. Lin, X. Li, J. Zhou, J. Zou, J. Lai, Z. Chen, J. Shen, H. Xu, Plasma-aided green and controllable synthesis of silver nanoparticles and their compounding with gemini surfactant, J. Taiwan Inst. Chem. Eng. 122 (2021) 311–319.
[8] J. Wengler, S. Ognier, M. Zhang, E. Levernier, C. Guyon, C. Ollivier, L. Fensterbank, M. Tatoulian, Microfluidic chips for plasma flow chemistry: application to controlled oxidative processes, React. Chem. Eng. 3 (2018) 930–941.
[9] X. Li, L. Lin, W.-H. Chiang, K. Chang, H. Xu, Microplasma synthesized gold nanoparticles for surface enhanced Raman spectroscopic detection of methylene blue, React. Chem. Eng. 7 (2) (2022) 346–353.
[10] L. Lin, X. Li, H. Gao, H. Xu, S.A. Starostin, K.K. Ostrikov, V. Hessel, Microfluidic Plasma-Based Continuous and Tunable Synthesis of Ag–Au Nanoparticles and Their SERS Properties, Ind. Eng. Chem. Res. 61 (5) (2022) 2183–2194.
[11] H. Lee, S.H. Park, S.J. Kim, Y.K. Park, B.H. Kim, S.C. Jung, Synthesis of tin and tin oxide nanoparticles using liquid phase plasma in an aqueous solution, Microelectron. Eng. 126 (2014) 153–157.
[12] K. Imasaka, Y. Kato, J. Suehiro, Enhancement of microplasma-based water-solubilization of single-walled carbon nanotubes using gas bubbling in water, Nanotechnology 18 (2007), 335602.
[13] J. Sun, D. Alam, R. Daiyan, H. Masood, T. Zhang, R. Zhou, P.J. Cullen, E.C. Lovell, A.(. Jalili, R. Amal, A hybrid plasma electrocatalytic process for sustainable ammonia production, Energy Environ. Sci. 14 (2) (2021) 865–872.
[14] T. Zhang, R. Zhou, P. Wang, A. Mai-Prochnow, R. McConchie, W. Li, R. Zhou, E. W. Thompson, K. Ostrikov, P.J. Cullen, Degradation of cefixime antibiotic in water by atmospheric plasma bubbles: Performance, degradation pathways and toxicity evaluation, Chem. Eng. J. 421 (2021), 127730.
[15] K. Hadinoto, J.B. Astorga, H. Masood, R. Zhou, D. Alam, P.J. Cullen, S. Prescott, F. J. Trujillo, Efficacy optimization of plasma-activated water for food sanitization through two reactor design configurations, Innovative Food Sci. Emerg. Technol. 74 (2021), 102867.
[16] J. Wanigasekara, C. Barcia, P.J. Cullen, B. Tiwari, J.F. Curtin, Plasma induced reactive oxygen species-dependent cytotoxicity in glioblastoma 3D tumourspheres, Plasma Processes Polym. 19 (4) (2022) 2100157.
[17] S. Bekeschus, A. Schmidt, K.-D. Weltmann, T. von Woedtke, The plasma jet kINPen–A powerful tool for wound healing, Clinical Plasma Medicine 4 (1) (2016) 19–28.
[18] S. Bekeschus, E. Freund, C. Spadola, A. Privat-Maldonado, C. Hackbarth, A. Bogaerts, A. Schmidt, K. Wende, K.-D. Weltmann, T. von Woedtke, Risk assessment of kINPen plasma treatment of four human pancreatic cancer cell lines with respect to metastasis, Cancers 11 (2019) 1237.
[19] E. Freund, L. Miebach, R. Clemen, M. Schmidt, A. Heidecke, T. von Woedtke, K.-D. Weltmann, S. Kersting, S. Bekeschus, Large volume spark discharge and plasma jet-technology for generating plasma-oxidized saline targeting colon cancer in vitro and in vivo, J. Appl. Phys. 129 (2021), 053301.
[20] A. Quade, K. Fricke, K.-D. Weltmann, Atmospheric pressure plasma treatments inside meander-like cavities, International Conference on Plasma Surface Engineering (2012) 291–294.
[21] L. Bundscherer, S. Nagel, S. Hasse, H. Tresp, K. Wende, R. Walther, S. Reuter, K.-D. Weltmann, K. Masur, U. Lindequist, Non-thermal plasma treatment induces MAPK signaling in human monocytes, Open Chemistry 13 (2015).
[22] L. Bundscherer, K. Wende, K. Ottmüller, A. Barton, A. Schmidt, S. Bekeschus, S. Hasse, K.-D. Weltmann, K. Masur, U. Lindequist, Impact of non-thermal plasma treatment on MAPK signaling pathways of human immune cell lines, Immunobiology 218 (10) (2013) 1248–1255.
[23] F.G. Botes, L. Lorenzen, J.S.J. Van deventer, The development of high intensity gas-liquid jet reactors, Chem. Eng. Commun. 170 (1) (1998) 217–244.
[24] R. Botton, D. Cosserat, S. Poncin, G. Wild, A simple gas-liquid mass transfer jet system, 8th World Congress of, Chem. Eng. (2009) pp. CDrom du congrès.
[25] K. Arkar, M.M. Vasiliev, O.F. Petrov, E.A. Kononov, F.M. Trukhachev, Dynamics of active brownian particles in plasma, Molecules 26 (2021) 561.
[26] N. Lee, S. Wiegand, Thermophoretic micron-scale devices: practical approach and review, Entropy (Basel) 22 (2020) 950.
[27] S. Reuter, T. von Woedtke, K.-D. Weltmann, The kINPen—a review on physics and chemistry of the atmospheric pressure plasma jet and its applications, J. Phys. D Appl. Phys. 51 (2018), 233001.
[28] L. Taghizadeh, A. Nikiforov, R. Morent, J. van der Mullen, C. Leys, Determination of the electron temperature of atmospheric pressure argon plasmas by absolute line intensities and a collisional radiative model, Plasma Processes Polym. 11 (8) (2014) 777–786.
[29] K. Akbar, E. Moretti, A. Vomiero, Carbon dots for photocatalytic degradation of aqueous pollutants: recent advancements, Adv. Opt. Mater. 9 (17) (2021) 2100532.
[30] N. Basavaraj, A. Sekar, R. Yadav, Review on green carbon dot-based materials for the photocatalytic degradation of dyes: fundamentals and future perspective, Mater. Adv. 2 (2021) 7559–7582.
[31] Q.H. Pho, D. Losic, K.(. Ostrikov, N.N. Tran, V. Hessel, Perspectives on plasma-assisted synthesis of N-doped nanoparticles as nanopesticides for pest control in crops, React. Chem. Eng. 5 (8) (2020) 1374–1396.
[32] S.K. Bhunia, A.R. Maity, S. Nandi, D. Stepensky, R. Jelinek, Imaging cancer cells expressing the folate receptor with carbon dots produced from folic acid, ChemBioChem 17 (7) (2016) 614–619.
[33] S. Zhang, X. Fan, R. Guan, Y. Hu, S. Jiang, X. Shao, S. Wang, Q. Yue, Carbon dots as metal-free photocatalyst for dye degradation with high efficiency within nine minutes in dark, Opt. Mater. 123 (2022), 111914.
[34] N. Yadav, K.H. Adolfsson, M. Hakkarainen, Carbon dot-triggered photocatalytic degradation of cellulose acetate, Biomacromolecules 22 (5) (2021) 2211–2223.
[35] M. Zaib, A. Akhtar, F. Maqsood, T. Shahzadi, Green synthesis of carbon dots and their application as photocatalyst in dye degradation studies, Arabian Journal for Science and Engineering 46 (1) (2021) 437–446.
[36] J. Li, R. Chen, W. Cui, X.a. Dong, H. Wang, K.-H. Kim, Y. Chu, J. Sheng, Y. Sun, F. Dong, Synergistic Photocatalytic Decomposition of a Volatile Organic Compound Mixture: High Efficiency, Reaction Mechanism, and Long-Term Stability, ACS Catalysis 10 (2020) 7230-7239.
[37] W. Abou Saoud, A.A. Assadi, M. Guiza, A. Bouzaza, W. Aboussaoud, I. Soutrel, A. Ouederni, D. Wolbert, S. Rtimi, Abatement of ammonia and butyraldehyde under non-thermal plasma and photocatalysis: Oxidation processes for the removal of mixture pollutants at pilot scale, Chem. Eng. J. 344 (2018) 165–172.
[38] J. Zhang, X. Zhao, M. Xian, C. Dong, S. Shuang, Folic acid-conjugated green luminescent carbon dots as a nanoprobe for identifying folate receptor-positive cancer cells, Talanta 183 (2018) 39–47.
[39] L.M.T. Phan, A.R. Gul, T.N. Le, M.W. Kim, S.K. Kailasa, K.T. Oh, T.J. Park, One-pot synthesis of carbon dots with intrinsic folic acid for synergistic imaging-guided photothermal therapy of prostate cancer cells, Biomaterials, Science 7 (12) (2019) 5187–5196.
[40] H. Saljoughi, F. Khakbaz, M. Mahani, Synthesis of folic acid conjugated photoluminescent carbon quantum dots with ultrahigh quantum yield for targeted cancer cell fluorescence imaging, Photodiagn. Photodyn. Ther. 30 (2020), 101687.
[41] S. Roy, Y. Bobde, B. Ghosh, C. Chakraborty, Targeted bioimaging of cancer cells using free folic acid-sensitive molybdenum disulfide quantum dots through fluorescence "turn-off", ACS Applied Bio Materials 4 (3) (2021) 2839–2849.
[42] B. Perillo, M. Di Donato, A. Pezone, E. Di Zazzo, P. Giovannelli, G. Galasso, G. Castoria, A. Migliaccio, ROS in cancer therapy: the bright side of the moon, Exp. Mol. Med. 52 (2) (2020) 192–203.
[43] X. Wang, C. Hu, Z. Gu, L. Dai, Understanding of catalytic ROS generation from defect-rich graphene quantum-dots for therapeutic effects in tumor microenvironment, J. Nanobiotechnol. 19 (2021) 340.
[44] S. Sri, R. Kumar, A.K. Panda, P.R. Solanki, highly biocompatible, fluorescence, and zwitterionic carbon dots as a novel approach for bioimaging applications in cancerous cells, ACS Appl. Mater. Interfaces 10 (44) (2018) 37835–37845.
[45] S. Bayda, E. Amadio, S. Cailotto, Y. Fríón-Herrera, A. Perosa, F. Rizzolio, Carbon dots for cancer nanomedicine: a bright future, Nanoscale Advances 3 (18) (2021) 5183–5221.
[46] Q.H. Pho, L. Lin, N.N. Tran, T.T. Tran, A.H. Nguyen, D. Losic, E.V. Rebrov, V. Hessel, Rational design for the microplasma synthesis from vitamin B9 to N-

doped carbon quantum dots towards selected applications, Carbon 198 (2022) 22–33.
[47] D.J.C. Constable, A.D. Curzons, V.L. Cunningham, Metrics to 'green' chemistry—which are the best? Green Chem. 4 (6) (2002) 521–527.
[48] R.A. Sheldon, Metrics of Green Chemistry and Sustainability: Past, Present, and Future, ACS Sustainable Chem. Eng. 6 (1) (2018) 32–48.
[49] Q.H. Pho, M. Escriba-Gelonch, D. Losic, E.V. Rebrov, N.N. Tran, V. Hessel, Survey of synthesis processes for N-doped carbon dots assessed by green chemistry and circular and ecoscale metrics, ACS Sustainable Chem. Eng. 9 (13) (2021) 4755–4770.
[50] D. Kurniawan, R.-J. Weng, O. Setiawan, K. Ostrikov, W.-H. Chiang, Microplasma nanoengineering of emission-tuneable colloidal nitrogen-doped graphene quantum dots as smart environmental-responsive nanosensors and nanothermometers, Carbon 185 (2021) 501–513.
[51] X. Ma, S. Li, V. Hessel, L. Lin, S. Meskers, F. Gallucci, Synthesis of N-doped carbon dots via a microplasma process, Chem. Eng. Sci. 220 (2020), 115648.
[52] X. Ma, S. Li, V. Hessel, L. Lin, S. Meskers, F. Gallucci, Synthesis of luminescent carbon quantum dots by microplasma process, Chemical Engineering and Processing - Process Intensification 140 (2019) 29–35.
[53] B.S. Truscott, M.W. Kelly, K.J. Potter, M. Johnson, M.N.R. Ashfold, Y. A. Mankelevich, Microwave plasma-activated chemical vapor deposition of nitrogen-doped diamond. I. N2/H2 and NH3/H2 plasmas, The Journal of Physical Chemistry A 119 (52) (2015) 12962–12976.
[54] M. Ferus, P. Kubelík, A. Knížek, A. Pastorek, J. Sutherland, S. Civiš, High Energy Radical Chemistry Formation of HCN-rich Atmospheres on early Earth, Sci. Rep. 7 (2017) 6275.
[55] P.T. Snee, The Role of Colloidal Stability and Charge in Functionalization of Aqueous Quantum Dots, Acc. Chem. Res. 51 (11) (2018) 2949–2956.

BLANK PAGE

Chapter 5

Rationally designed microplasma synthesis of NCQDs for targeted applications

After successfully achieving the mass-based intensification for the microplasma synthesis of N-doped carbon quantum dots, the innovative contribution of this chapter is to provide a new conceptual strategy to rationally design and synthesise the desirable for three main applications (nanopesticides, water purification, and theranostic treatment). N-doped carbon quantum dots (NCQD) were rationally designed and synthesised, for the first time, from folic acid (Vitamin B9) by a non-thermal microplasma jet. Then, the morphology, size, crystallographic structure, and photoluminescence of the as-prepared NCQD, which plays a key role in selected applications, were investigated by various analytical characterisations such as HR, TEM, XPS, ^{1}HNMR, XRD, FTIR, UV-Vis, Raman spectroscopy, etc. Finally, The Derjaguin, Landau, Vervey, and Overbeek (DLVO) theory is conducted to understand their colloidal behaviours.

This chapter has been published as a research paper in "Carbon" journal as follows:

Pho, Q.H., Lin, L., Tran, N.N., Tran, T.T., Nguyen, A.H., Losic, D., Rebrov, E.V. and Hessel, V., 2022. Rational design for the microplasma synthesis from vitamin B9 to N-doped carbon quantum dots towards selected applications. *Carbon*, 198, pp.22-33. <Link>

Statement of Authorship

Title of Paper	Rational design for the microplasma synthesis from vitamin B9 to N-doped carbon quantum dots towards selected applications
Publication Status	☑ Published ☐ Accepted for Publication ☐ Submitted for Publication ☐ Unpublished and Unsubmitted w ork w ritten in manuscript style
Publication Details	Pho, Q.H., Lin, L., Tran, N.N., Tran, T.T., Nguyen, A.H., Losic, D., Rebrov, E.V. and Hessel, V., 2022. Rational design for the microplasma synthesis from vitamin B9 to N-doped carbon quantum dots towards selected applications. Carbon, 198, pp.22-33.

Principal Author

Name of Principal Author (Candidate)	Quoc Hue Pho		
Contribution to the Paper	Conceptualization, Methodology, Formal analysis, Investigation, Data curation, Writing – original draft		
Overall percentage (%)	65%		
Certification:	This paper reports on original research I conducted during the period of my Higher Degree by Research candidature and is not subject to any obligations or contractual agreements with a third party that would constrain its inclusion in this thesis. I am the primary author of this paper.		
Signature		Date	28.01.2023

Co-Author Contributions

By signing the Statement of Authorship, each author certifies that:

i. the candidate's stated contribution to the publication is accurate (as detailed above);
ii. permission is granted for the candidate in include the publication in the thesis; and
iii. the sum of all co-author contributions is equal to 100% less the candidate's stated contribution.

Name of Co-Author	LiangLiang Lin		
Contribution to the Paper	Conceptualization, Writing- Review and Editing		
Signature		Date	30.01.2023

Name of Co-Author	Nam Nghiep Tran		
Contribution to the Paper	Writing- Review and Editing		
Signature		Date	28.01.2023

Please cut and paste additional co-author panels here as required.

Name of Co-Author	Thanh Tung Tran		
Contribution to the Paper	Formal analysis, Writing- Review and Editing		
Signature		Date	1.2.2023

Name of Co-Author	An Hoa Nguyen		
Contribution to the Paper	Data curation		
Signature		Date	28.01.2023

Name of Co-Author	Dusan Losic		
Contribution to the Paper	Co-supervised and Writing- Review and Editing.		
Signature		Date	2 feb 2023

Name of Co-Author	Evgeny V.Rebrov		
Contribution to the Paper	Writing- Review and Editing.		
Signature		Date	06.02.2023

Name of Co-Author	Volker Hessel		
Contribution to the Paper	Supervised (scientific ideas, concepts, objectives, assessment of achievement degree, societal impact), conceptualised, Writing – review & editing, and is the corresponding author.		
Signature		Date	28.01.2023

Please cut and paste additional co-author panels here as required.

Carbon 198 (2022) 22–33

Contents lists available at ScienceDirect

Carbon

journal homepage: www.elsevier.com/locate/carbon

Rational design for the microplasma synthesis from vitamin B9 to N-doped carbon quantum dots towards selected applications

Quoc Hue Pho [a,d], LiangLiang Lin [c,e], Nam Nghiep Tran [a], Tung T. Tran [a,b], An Hoa Nguyen [a], Dusan Losic [a,b], Evgeny V. Rebrov [d], Volker Hessel [a,d,*]

[a] School of Chemical Engineering and Advanced Materials, The University of Adelaide, Adelaide, SA, 5005, Australia
[b] The ARC Graphene Research Hub, School of Chemical Engineering and Advanced Materials, The University of Adelaide, SA, 5005, Australia
[c] School of Chemical and Material Engineering, Jiangnan University, Wuxi, People's Republic of China
[d] School of Engineering, University of Warwick, Library Rd, Coventry, CV4 7AL, England, UK
[e] Key Laboratory of Nanodevices of Jiangsu Province, Suzhou, People's Republic of China

ARTICLE INFO

Keywords:
Nonthermal microplasma
NCQD
Rational design
Quantum materials
Quantum dots

ABSTRACT

N-doped carbon quantum dots (NCQD) are rationally designed and synthesised, for the first time, from folic acid (Vitamin B9) by a non-thermal microplasma jet. A new conceptual design was developed to synthesise the desirable NCQD for three main applications (nanopesticides, water purification, and theranostic treatment). The structural and analytical characterisation confirmed an average size of 3.1 nm for the synthesised NCQD with the multi-functional groups (-OH, –COOH, $–NH_2$) on their surface. The TEM results indicated that the core of NCQD was a multilayered structure, including single defected graphene sheets of graphitic-nitrogen and pyrrolic-nitrogen. In addition, fluorescence performance and stability of the as-prepared NCQD were determined. The quantum yield of NCQD was 35%, which is relatively high, with a strong blue fluorescence. A basis for predicting colloidal behaviours based on balancing molecular attractive and repulsive forces was elucidated by applying the Derjaguin, Landau, Vervey, and Overbeek (DLVO) theory. Finally, compared with other similar microplasma-assisted synthesis processes, this developed method has proven the ability to provide a tailored and scalable synthesis process of high-quantum-yield NCQD at gram-scale production.

1. Introduction

After the first discovery in 2004, carbon dots (CD) have attracted considerable attention in exploring various potential applications because of their outstanding properties, including their low toxicity [1], biocompatibility [2], water-solubility [3] and excellent optical properties [4].

A broad range of starting materials as carbon sources, from organic compounds (ethylenimine [5], citric acid [6], urea [7], chitosan [8], sucrose [9], cystine [10], etc.) and biomass materials (orange peels [11], banana peels [12], bamboo leave [13], prawn shells [14], etc.), has been explored over the last decade for CD synthesis [15]. As a result, an extensive library of CD with diverse structures and properties has been created using various synthetic techniques, including laser ablation [16], arc discharge [17], hydrothermal [18], pyrolysis [19], solvothermal [20], ultrasonic [21], etc. Most of these CD synthesis strategies can be classified as the trial-and-error approach in searching for suitable applications [22]. It is a time-consuming journey with cost- and process inefficiency to create CD with suitable structure and properties available for a specific application.

Instead, another alternative approach to producing a high-quality CD for a target application is to focus on "design-for purpose" before carrying out the synthesis processes, which is called "a rational design approach" [23]. In principle, the first step of this approach is to scientifically define the problems that need to be solved using CD with specific properties.

Based on the precise problem definition, a conceptual design of CD solution can be proposed in response to the defined problems for the scientific check.

It can be repeated many times and improved until the rationally designed nanomaterials meet the requirements to solve the defined problems. Therefore, defining problems in applications will give us information on which properties of CD need to be created and adjusted to establish final strategic synthetic pathways.

* Corresponding author. School of Chemical Engineering and Advanced Materials, The University of Adelaide, Adelaide, SA, 5005, Australia.
E-mail address: volker.hessel@adelaide.edu.au (V. Hessel).

https://doi.org/10.1016/j.carbon.2022.07.004
Received 1 April 2022; Received in revised form 30 May 2022; Accepted 2 July 2022
Available online 8 July 2022
0008-6223/© 2022 Elsevier Ltd. All rights reserved.

This study aims at a rational design strategy that combines the synthesis of CD with specific properties and their applications for nanopesticides, water purification, and theranostic treatment (Table 1). One of the critical problems of CD in these applications is to enhance the high-quality intrinsic properties of CD, including water solubility, stability, and intensity of fluorescence. Therefore, we proposed a conceptual design approach to address these problems and achieve these desired properties, targeting to create CD with the required modification of bulk/size, surface, and morphology of CD (Fig. 1). Based on the literature, the size of CD from 2 to 3 nm exhibits an excellent photocatalytic activity [24]. In addition, it has been reported that carbon quantum dots have a spherical morphology with quantum confinement and high crystal structure [25], which exhibit a stable system in an aqueous solution. Besides, heteroatom doping is one of the most effective approaches for modulating CD's bulk/size, surface, and morphology [26]. It is revealed that the photoluminescence of CD was enhanced by introducing amide (-NH_2) functional groups into the surface [27]. A synergistic effect of graphitic N and pyrrolic N in graphene for the enhanced photocatalytic performance of CD is confirmed [28]. In addition, for improved water solubility and stability, introducing –OH and –COOH functional groups on the surface of CD is one of the easiest and most effective strategies [29,30].

With the aforementioned evidence in Table 1, we proposed a conceptual design of NCQD guided by three molecular targets (Fig. 1): (1) surface functional group control (characterised by HNMR, FTIR, XPS, UV–Vis and fluorescein isothiocyanate); (2) crystallographic control (characterised by XRD and Raman spectroscopy); (3) bulk/size control (characterised by TEM and HR-TEM). In addition, gross-product property targets concerning fluorescence and stability were determined.

After the conceptual design of N-doped carbon quantum dots, a suitable synthesis strategy is required to ensure that the rationally designed NCQD is obtained in higher quantity and quality. In this rational design concept, bottom-up synthesis approaches are more dominant than these top-down counterparts to meet the requirements of the proposed conceptual design [31]. First, it is more flexible by using various starting materials with different functional groups [32]. Second, these approaches do not undergo further surface passivation, and heteroatoms are easily introduced into NCQD [33]. For this reason, we aim to follow the bottom-up synthesis approach to produce NCQD.

Table 1
Types of applications of rationally designed NCQD synthesised from kINPen®IND plasma jet.

Applicable fields	Specific applications	Targeted properties of NCQD	Rational design approaches
Agriculture	Nanopesticides	Antifungal and antibacterial by photocatalysis [34]	-Functional –NH_2 group control -Crystallography: graphitic N and pyrrolic N control
	Plant growth stimulus	Water solubility [35]	-Functional –OH group control
Environment	Water purification	Photocatalysis [36–40]	-Functional –NH_2 group control -Crystallography: graphitic N and pyrrolic N control
Medical	Theranostic treatment	Photoluminescence [41]	-Functional –NH_2 group control -Crystallography: graphitic N and pyrrolic N control
		Photocatalysis [41]	-Functional –NH_2 group control -Crystallography: graphitic N and pyrrolic N control
		Stability [42]	-Functional –OH group control -Functional –NH_2 group control

Yet, the current challenges of conventional bottom-up synthesis processes are the high temperature [43], high pressure [44], and strong acids [45], which lead to energy inefficiency, multiple processes, and unavoidable harm to the environment. To avoid this problem, we use the kINPen®IND plasma jet for the first time as a new synthesis method of bottom-up approaches to design NCQD rationally. However, the critical issue in microplasma synthesis of NCQD is low mass-production yield and productivity [46]. In this case, process miniaturisation might help conduct a more controlled process to enhance productivity [47]. Thus, the second goal of this paper is to use kINPen®IND plasma to produce rationally designed NCQD using folic acid as a green and non-toxic source of nitrogen and carbon in NCQD synthesis [48].

After the synthesis of rationally designed NCQD is implemented, the performance of this material will be tested with photoluminescence. Technically, the safety of NCQD in applications is related to their stability. This study has finished at the safety stage, with DLVO theory being used to understand more of their colloidal behaviours. For this reason, economics and circularity research has not been done yet at this stage. Nonetheless, our previous study reported using green chemistry and circular and EcoScale metrics to evaluate various synthesis approaches to NCQD fabrication. As a result, this study has pointed out that the microplasma-assisted synthesis approach might have much higher sustainable potential than its counterparts. Therefore, our current study on using the kINPen®IND microplasma jet to synthesise NCQD is conducted to explore that potential [47].

2. Materials and methodologies

2.1. Materials

Sodium hydrogen carbonate, folic acid, hydrochloric acid, quinine sulphate, sulfuric acid (98%), and fluorescein 5(6)-isothiocyanate were purchased from Sigma-Aldrich, which were of analytical grades and used without further purification. kINPen®IND microplasma jet was purchased from Neoplas GmbH, Germany.

2.2. Experimental setup for the synthesis of NCQD

NCQD were synthesised in an open reactor with a 9 mm × 15 mm (W x H) dimension under kINPen®IND-induced microplasma. The microplasma jet with a dimension of 105 x 180 × 330 mm (H x W x D) was connected with a 110 VAC power supply (50 Hz). A continuous Ar (99.9%) gas stream with a flow rate of 2 sccm was injected into the jet at the pressure of 3 bar to form microplasma. An optical fibre was inserted into the plasma-liquid interaction region to detect reactive species formed from microplasma. The length of the formed microplasma was about 1 cm. The synthesis procedure was described in Fig. 2. Briefly, folic acid (FA) solution as a starting carbon source was prepared by dissolving in $NaHCO_3$ (0.5 M) as a solvent under stirring until the resulting orange solution was homogeneously mixed. The FA solution was then transferred to the open reactor with 0.5 g of metal flakes (500–1000 μm) to intensity the electrical field with plasma-catalytic effects for enhanced photoluminescence of NCDQ. Afterwards, the microplasma formed by the kINPen®IND jet was applied to treat the solution for a given time. After completing the treatment, the resulting solution turned dark brown. To collect NCQD, the treated solution was transferred to a beaker and precipitated by HCl 0.5 M. After precipitation, the mixture was centrifugated (10,000 rpm) for 30 min. The unreacted FA pellet was removed, while the supernatant liquid was then dialysed against water in a dialysis bag (1000 Da) for three days. Finally, pure NCQD were obtained in power by a freeze dryer.

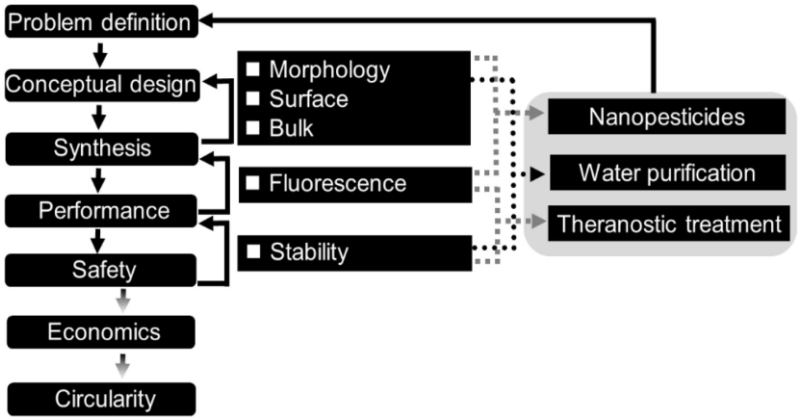

Fig. 1. Rational design of NCQD synthesised from kINPen®IND plasma jet.

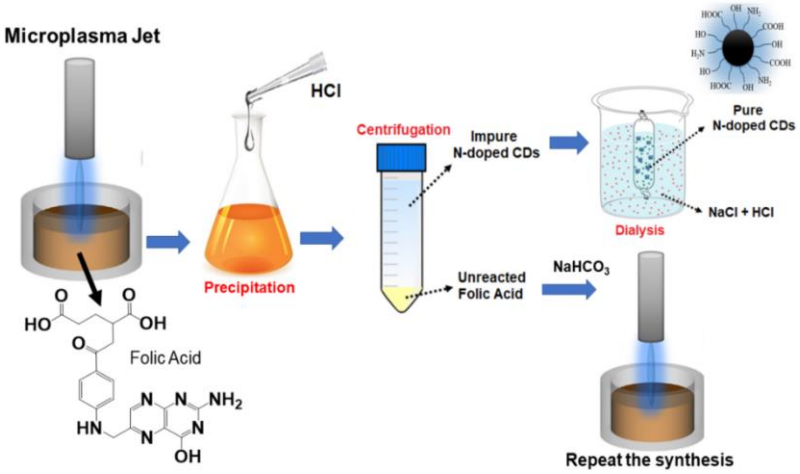

Fig. 2. Schematic of the synthesis of NCQD using folic acid by using the kINPen®IND microplasma.

2.3. Characterisation of NCQD

2.3.1. High resolution - transmission electron microscopy (HR-TEM)

The transmission electron microscopy measurements on FEI Titan Themis 80-200 operated at 200 kV is a powerful technique with high resolution, which was used to investigate the structure, particle size and distribution, and morphology of the rationally designed NCQD. Briefly, 10 mg of NCQD were dispersed into water under sonication until NCQD became homogeneously. Later on, the NCQD solution was dropped into a TEM grid. Then, the resulting TEM grid was dried entirely in a convection oven at 60 °C to remove solvents. Finally, the grid was measured with FEI Titan Themis 80-200 to analyse the as-prepared NCQD material.

2.3.2. X-ray photoelectron spectroscopy (XPS)

X-ray photoelectron spectroscopy (XPS) from SPECS Sage XPS was a technique for analysing the surface chemistry of NCQD. The preparation of XPS samples was similar to TEM preparation (10 mg/ml). Later on, the NCQD solution was drop-casted into a silicon wafer. Then, the resulting silicon wafer was dried up in the oven at 50 °C to remove water. Finally, the silicon wafer was investigated by SPECS Sage XPS to record data.

2.3.3. X-ray powder diffraction (XRD) and Raman spectroscopy

The degree of crystallinity structure of NCQD was measured/characterised by X-ray Powder Diffraction (XRD)-Rigaku MiniFlex 600. Cu-$K_{\alpha 1}$ radiation with a wavelength of 1.54056 Å was used in the diffractometer. The samples were scanned at a speed of 0.2°/min from 10 to 90°.

Raman spectroscopy-HORIBA LabRAM HR Evolution is a chemical analysis device that does not destroy the components of samples, which was used to investigate NCQD's chemical structure and crystallinity. The measurement was carried out using the 512 nm-wavelength laser as the excitation.

2.3.4. ^{1}HNMR spectroscopy and Fourier transform infrared (FTIR)

Fourier transform infrared (FTIR): The Nicolet 6700 FTIR spectrometer was employed to obtain an infrared spectrum of absorption of NCQD. From the spectrum, functional groups on the surface of NCQD were characterised.

Proton nuclear magnetic resonance (^{1}HNMR): The Agilent 600 MHz NMR spectrometer was used for molecular structure characterisation of NCQD. 20 mg of the sample was dissolved into DMSO-d_6 solvent overnight to ensure that all samples were well-dissolved. Finally, the samples were inserted into The Agilent 600 MHz NMR spectrometer for recording data.

2.3.5. UV–vis and photoluminescence

The fluorescence spectrum was carried out on a photoluminescence Spectrometer (FLS 1000, United Kingdom). Firstly, photoluminescence 2D colour mapping was investigated to determine the as-prepared NCQD's maximal excitation and emission wavelength. The excitation and emission spectra were set from 300 to 700 nm and plotted in photoluminescence 2D colour mapping. After investigating the excitation and emission wavelength, these parameter values were used for further photoluminescence intensity tests. 1 mL of the as-prepared NCQD (1 μg/mL) was inserted into the FLS1000 under the investigated excitation light source to determine the photoluminescence curve at the maximal wavelength.

UV–Vis spectra are another important optical parameter that needs to investigate. Briefly, 1 mL of the as-prepared NCQD (1 μg/mL) was inserted into Cary 60 UV–Vis Agilent Technologies to record the spectra to determine the maximal absorbance wavelength. Based on this data, further absorbance tests are carried out.

2.3.6. Fluorescein isothiocyanate (FTIC) assay

Fluorescein isothiocyanate (FTIC) assay has been widely used to attach amine groups. The isothiocyanate groups in FTIC can react with primary amines to form isothiourea conjugate. To determine $-NH_2$ functional groups on the surface of NCQD, fluorescein-5-isothiocyanate (1 μg/mL) was used to react with NCQD (1 μg/mL). The resulting mixture was tested with photoluminescence spectroscopy (FSL1000).

2.4. Quantum yield calculation

The quantum yield of fluorescent NCQD was measured based on UV–Vis and photoluminescence spectroscopy. Quinine sulphate in 0.1 M H_2SO_4 aqueous solution has a similar intense blue fluorescence of carbon dots. Thus, it was used as a standard fluorescent agent with a fluorescence quantum yield of 0.54. The quantum yield of NCQD was calculated as following equation (1):

$$\Phi_{CD} = \Phi_{QS} \times \left(\frac{Grad_{CD}}{Grad_{QS}}\right) \times \left(\frac{\eta_{CD}}{\eta_{QS}}\right)^2 \quad (1)$$

where Φ_{CD} and Φ_{QS} are the quantum yield of NCQD and quinine sulphate, respectively; Grad is the gradient from the linear regression of NCQD and quinine sulphate; η is the solution's refractive index; The subscripts "QS" and "CD" refer to the standard fluorescent agent (quinine sulphate) and NCQD accordingly; The ratio of the refractive index of solvent (η) is 1; The absorbance of NCQD and quinine sulphate is controlled under 0.1 at the 360 nm excitation.

2.5. The colloidal behaviours in aqueous solutions by using Derjaguin, Landau, Vervey, and Overbeek (DLVO) theory

In agricultural applications, the colloidal behaviour of the as-prepared NCQD in water plays a vital role in hydrophilic nanopesticides. For this reason, Derjaguin, Landau, Vervey, and Overbeek (DLVO) theory was studied in this research. In principle, the DLVO theory is the total effect of van der Waals interactions (V_H) and electrical double layer interactions (V_D), as shown in equations (2)–(4):

$$V_T = V_H + V_D \quad (2)$$

van der Waals interactions (V_H) are calculated in the following equation:

$$V_H = -\frac{A_{12}r}{12hkT} \quad (3)$$

And electrical double layer interactions (V_D) are used in the following equation:

$$V_D = \frac{2\pi e_0 \varepsilon \rho^2 \ln\left(1 + e^{1(h/k^{-1})}\right)}{k_B.T} \quad (4)$$

where r (nm) is the radius of NCQD; h (nm) is the distance from the surface to surface between two NCQD; A_{12} is the Hamaker constant, 6.26×10^{-21} J; kT is the Boltzmann temperature, e_0 is the permittivity of free space; e is electron charge; k_B is Boltzmann constant; ε is dielectric constant; ρ is zeta potential (mV); k^{-1} is the Debye length.

Three key influential parameters on the behaviour of NCQD in water include particle size, temperature, and potential with surface charges. Table 2 showed different scenarios for studying colloidal behaviours of NCQD in water. In this study, the mean particle size was calculated as 3.13 ± 0.65 nm, and the environment temperature was 298.15 (^{0}K). Therefore, the only influential parameter on their behaviours is the zeta potential with charge, as shown in Table 2.

2.6. Influence of pH and water solubility on photoluminescence of NCQD

Various NCQD solutions were prepared with pH values (2, 4, 6, 8, 10, 12, 14) and various solvents (ethanol, acetone, acetonitrile, and water) for dissolving NCQD. All the solution samples were characterised by photoluminescence spectroscopy (FLS1000).

3. Results and discussion

3.1. Rational design strategy for the synthesis of NCQD

A portable atmospheric-pressure plasma device, known as kINPen®IND, was explored here to synthesise N-CQDs, which has not been explored before [49]. For the first time, our study has demonstrated its potential in fabricating NCQD. This study selected various starting materials for the synthesis process, including urea, vitamin C, and folic acid. The strategy for this synthesis was the miniaturisation process, where a reactor with a small volume was designed to maximise plasma-liquid interaction. Thus, various reactors were used to optimise the synthesis process based on plasma-liquid interaction, consisting of the Petri dish, Eppendorf, glass beaker, and our reactors.

The initial results in Table 3 showed that citric acid/urea and vitamin C could not produce NCQD under microplasma, though these precursors are available for other synthesis methods [[50,51]]. In contrast, folic acid shows good performance when exposed to microplasma [48]. In addition, we also tested folic acid under various types of reactors. The results revealed that our container with an optimal dimension results in the best performance of the synthesis process. Thus, this reactor was used for fabricating NCQD. The mass reaction efficiency of the described-above reaction conditions was 17%, which is very high for a nanomaterial product. Those or related efficiencies, being usually much lower, are rarely mentioned in nanomaterials literature. This research achieves process intensification, bringing the synthesis to 1 g per day. The formation of NCQD was confirmed by optical emission spectroscopy (OES) in Fig. 3 where various reactive species were detected. The OES results indicates that folic acid was decomposed by microplasma jet to form various reactive species such as OH·, CH·, :C═C:, ·CN, and NH·. Reactive species like CH· and :C═C: are considered as intermediates which may conjugates each other to form graphite-like structure. In contrast, ·CN and NH· can react with CH· and :C═C: to form nitrogen

Table 2
Influential parameters on colloidal behaviours in water.

Scenario	Mean size (nm)	Potential (φ)	Temperature (^{0}K)
1	3.13 ± 0.65	±5	298.15
2		±10	
3		±20	
4		±40	

Table 3
Strategies for synthesis of NCQD using kINPen®IND microplasma jet.

Chemicals	Types of reactors			
	Petri dish (35 mm)	Eppendorf (2 mL)	Glass beaker (10 mL)	Our container 9 mm × 15 mm (W x H)
Citric acid/ Urea	N/A	N/A	N/A	N/A
Vitamin C	N/A	N/A	N/A	N/A
Folic acid	N/A	N/A	N/A	Available

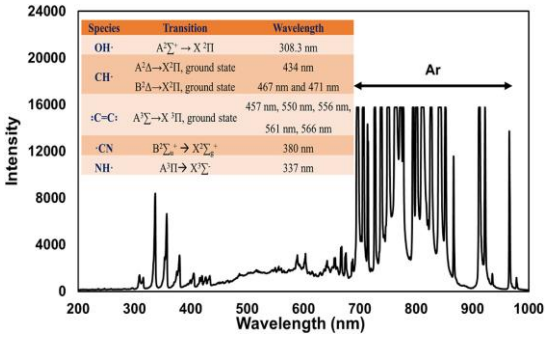

Fig. 3. Optical emission spectroscopy of N-doped carbon dots reaction for the processing of immersing an argon plasma jet into folic acid solution with metal flakes.

defects (graphitic and pyrrolic N) in graphite-like structure. Finally, OH· and NH· can conjugate with graphite-like structure on the surface to form –OH and $–NH_2$ functional groups.

3.2. Size and morphology of the as-prepared NCQD

The TEM image (Fig. 4A) showed spherical NCQD with a particle size of 3.13 ± 0.65 nm. In addition, the synthesised NCQD also showed a narrow size distribution ranging from 1 to 10 nm, indicating a well-distributed particle size. Based on the definition and classification from Valcárcel et al. (2016) [25], the as-prepared carbon dots in our study are classified as carbon quantum dots with multilayered graphene sheets. Table S1 compared TEM images from various types of carbon dots in terms of structure and morphology. More specifically, the HR-TEM pattern (Fig. 4B) showed spherical quantum dots with a lattice spacing of 0.27 nm, indicating the high crystallinity of NCQD with graphite structure. The interlayer spacing of NCQD was about 0.27 nm, which corresponds to the (002) plane of the graphite structure. The lattice spacing of 0.27 nm (calculated by performing Fast Fourier Transform (FFT) from Image J software) means the spacing between two graphene layers [52]. In addition, the XRD and Raman spectroscopy results in our study also revealed that the as-prepared NCQD are highly crystalline (see section 3.3.1).

3.3. Crystallographic structure of NCQD

3.3.1. Crystalline structure

The Raman spectrum in Fig. 5A showed two distinctive peaks at 1338 cm^{-1} and 1558 cm^{-1}, attributed to the D and G bands [46]. This result indicates that NCQD has a crystalline structure. The G peak results from stretching vibrations of sp^2 carbon atoms in both rings and chains, whereas the D peak represents some structural defects in graphene structure due to the breathing modes of sp^2 atoms in rings. A D band peak at 1338 cm^{-1} indicated that the addition of nitrogen elements could contribute to the defect in the graphitic structure of carbon dots.

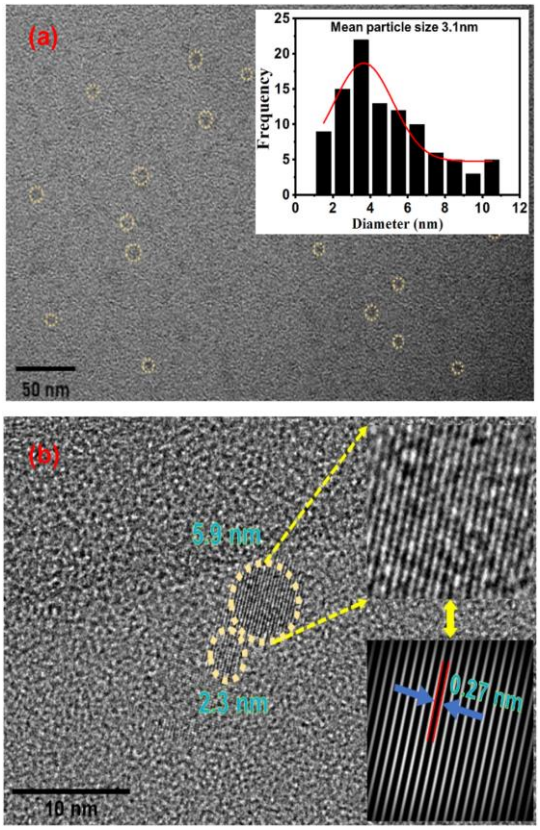

Fig. 4. HR-TEM characterised the morphology of NCQD synthesised from kINPen®IND microplasma jet: (a) size distribution (b) morphology and structure.

The ratio of the intensity of D/G peaks is an important parameter, revealing the defects in the structure of NCQD. D/G ratio is relevant to the ratio of the number of sp^3 to sp^2 carbon atoms. Based on the Raman spectroscopy, the value of I_D/I_G was 0.26, implying that more sp^2-hybridized carbons were formed in a two-dimension hexagonal lattice. Apart from two distinctive peaks attributed to the D and G bands, another two peaks were observed at 1129 cm^{-1} and 1234 cm^{-1}. These two typical peaks are attributed to *trans*-polyacetylene (*trans*-PA), which is an alternate chain of sp^2 carbon atoms, with single hydrogen bonded to each carbon [53].

In agreement with the Raman spectrum, the XRD pattern of NCQD (Fig. 5B) showed a broad peak at 25.5°. The results indicate that the crystalline structure of folic acid has been decomposed by microplasma to form crystalline carbon dots. The broad peak at 25.5° corresponds to the (002) surface. This result reveals that the interlayer spacing (d) of the NCQD (0.27 nm) was lower than that of the interlayer spacing of graphene structure (0.33 nm). Thus, in agreement with HR-TEM, XRD patterns and Raman spectroscopy confirm carbon dots' high crystalline nature, attributing to the generation of oxygen and nitrogen-containing groups with multiple-layered structures in the core.

3.3.2. The pyrrolic-and graphitic-nitrogen structure of NCQD

^{1}HNMR spectra in Fig. 6 provide more evidence for the chemical structure of NCQD. The chemical shift at 11.39 ppm, 6.93 ppm, and 6.62 ppm corresponded to –COOH and Ph-OH protons on the surface of NCQD. These functional groups majorly contribute to the water-soluble properties of NCQD. The peak at 9.86 ppm was associated with Ph-CHO

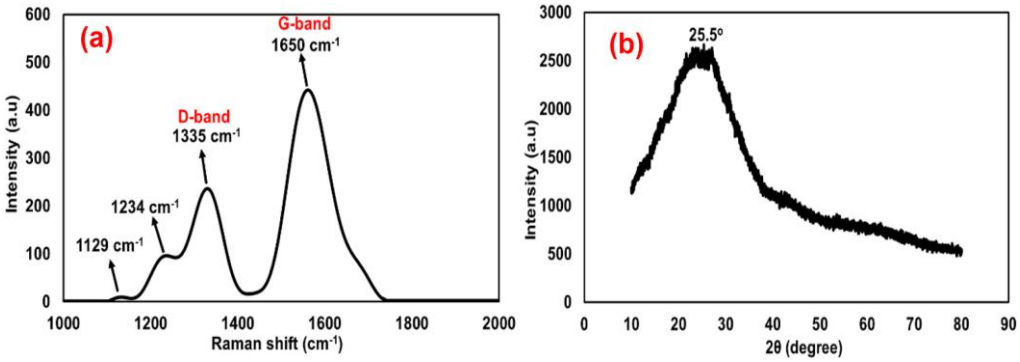

Fig. 5. (a) Raman spectroscopy and (b) XRD pattern of NCQD synthesised from kINPen®IND microplasma jet.

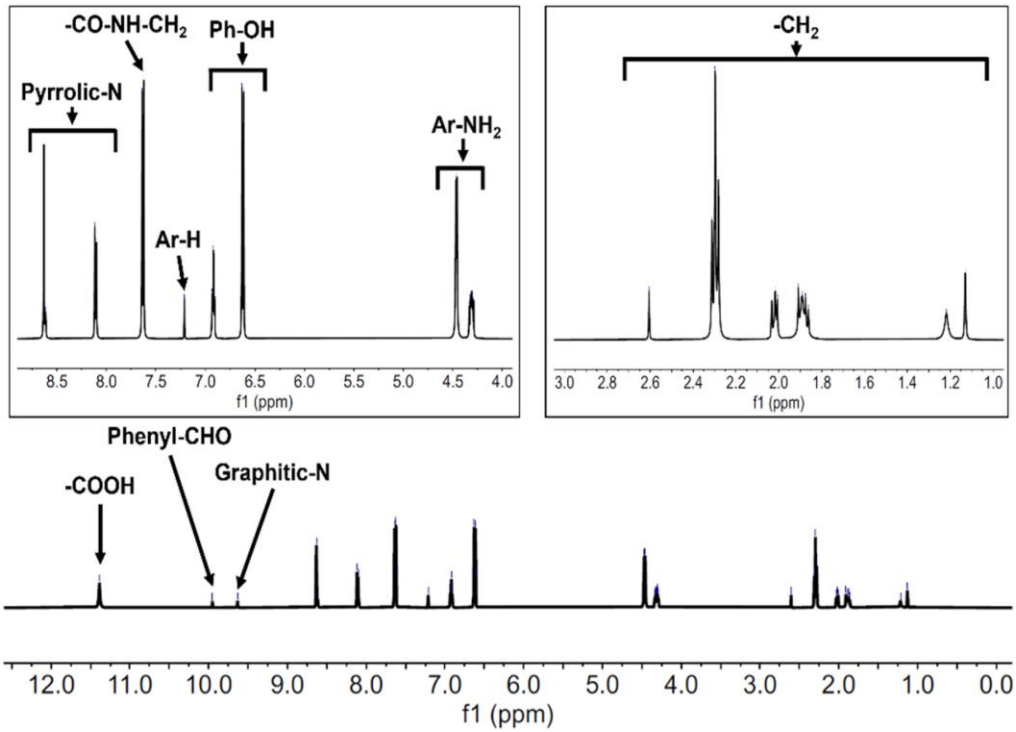

Fig. 6. *^{1}HNMR spectra of NCQD synthesised from* kINPen®IND microplasma jet.

protons. A typical peak at 4.29 ppm–4.50 ppm was assigned to protons in Ar-NH_2. The chemical shifts in the regions from 7.62 to 7.64 ppm indicated the presence of protons in –CO–NH-CH_2 bonding. The chemical shift at 7.21 ppm was related to Ar–H protons in graphitic structure. The typical peaks at 9.05 ppm–9.63 ppm reveal protons' existence in graphitic-N structure, while chemical shifts at 8.26 ppm, and 8.63 ppm are attributed to protons in pyrrolic-N structure. Lastly, peaks from 1.13 ppm to 2.61 ppm represent protons in methylene –CH_2 moieties.

3.4. Multi-functional surface groups control of the as-prepared NCQD

3.4.1. Confirmation of –OH and NH_2 functional groups by FTIR and XPS

The full XPS spectrum presented in Fig. 7a showed three peaks at 285.5 eV, 400.3 eV, and 532.8 eV, suggesting that NCQD consisted of C, N, O elements, and the atomic percentages were calculated to 57%, 13%, and 30%, respectively [54]. In Fig. 7b, the high-resolution XPS spectra of C 1s were divided into three peaks at 288.6 eV, 286.3 eV, and 285.1 eV, corresponding to -O-C═O, C–N/-C═N, and C–C/C═C, respectively. The N 1s band in Fig. 7c exhibits two typical peaks at 400.1 eV and 401.4 eV, respectively, corresponding to pyrrolic-N (70%) and graphitic-N structures (30%). These two high-resolution bands indicate the successful doping of N into carbon dots. The O 1s band (Fig. 7d) revealed two specific peaks at 532.6 eV and 533.5 eV, attributing to C═O/O–C═O and C–OH.

The FTIR spectrum was obtained to determine the NCQD's surface functional groups. In Fig. 8, the FTIR spectra revealed the presence of functional groups including –OH (3527 cm^{-1}), –NH bending in amides (3300 cm^{-1} and 1602 cm^{-1}), different vibration modes of –C═N and C–N (1334 cm^{-1} and 1286 cm^{-1}, respectively), the stretching of >C═O at 1688 cm^{-1}, sp^3 C–H stretching (2917 cm^{-1} and 2846 cm^{-1}), sp^2 C–H

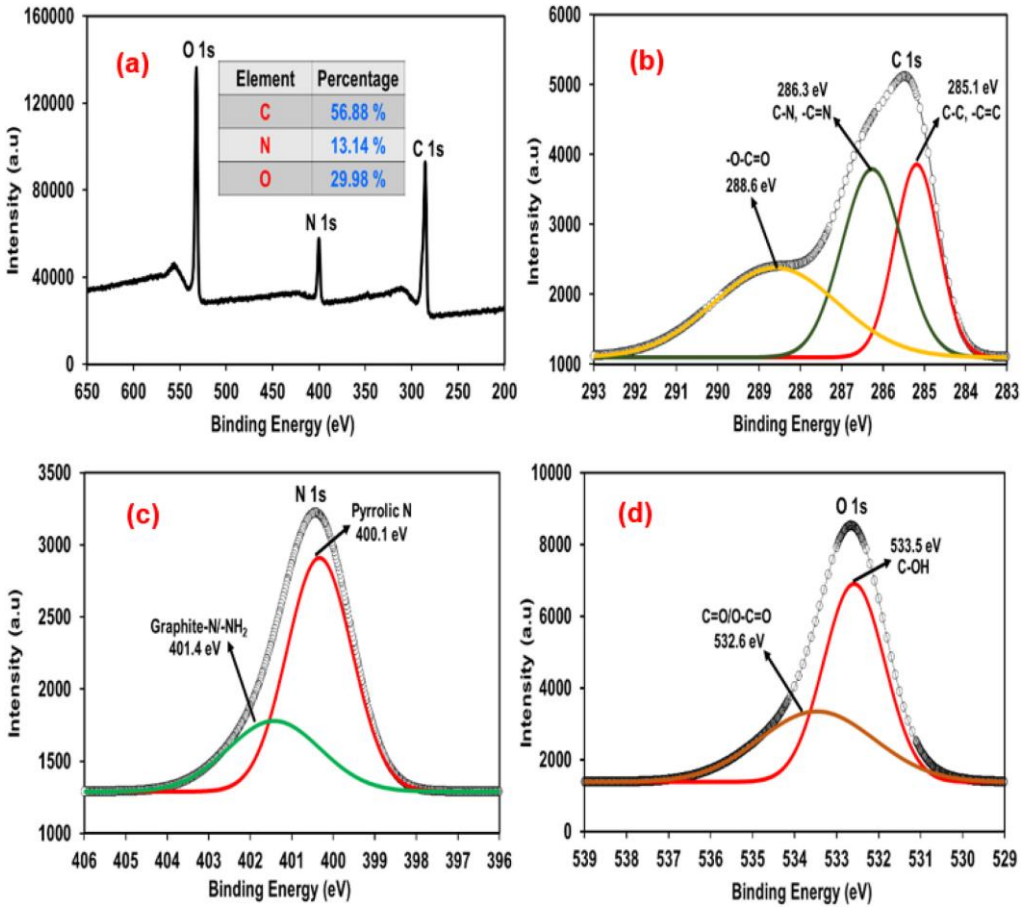

Fig. 7. XPS analysis of NCQD synthesised from kINPen®IND microplasma jet: (a) full XPS spectra (b) XPS spectra of C1s spectrum (c) XPS spectra of N1s spectrum (d) XPS spectra of O1s spectrum.

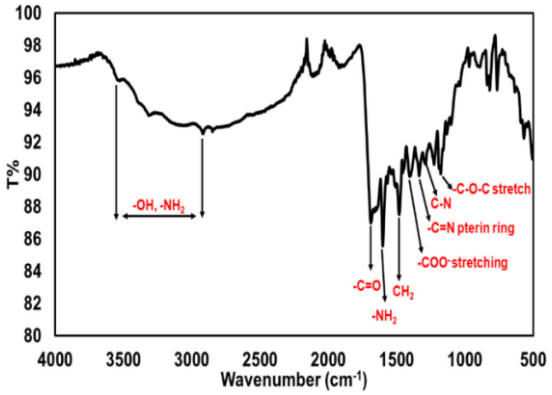

Fig. 8. FTIR spectrum of NCQD synthesised from kINPen®IND microplasma jet.

stretching of aromatic rings (1906 cm^{-1}).

3.4.2. Determine -NH2 functional groups by fluorescein isothiocyanate (FTIC) assay

Multi-functional groups on the surface of NCQD play an essential role in defining their applications. Therefore, it is necessary to prove the existence of $–NH_2$, –OH, and –COOH via FTIR, XPS, and NMR. In nanopesticides and theranostic applications, NCQD could function as a fluorescence for bioimaging and as a nanocarrier of active ingredients/drugs. To be an effective and efficient nanocarrier, NCQD should be able to be chemically conjugated with active ingredients/drugs. To prove this concept, Fluorescein-5-isothiocyanate (FTIC), one of the most widely used assays for detecting rich-NH_2 compounds, was selected to conjugate with $–NH_2$ on the surface of NCQD.

The principle lies in the reaction between fluorescein-5-isothiocyanate and $–NH_2$ functional groups of NCQD. The reaction is relevant to the central, electrophilic carbon of fluorescein-5-isothiocyanate attacking the nucleophile. As a result, a thiourea conjugation is formed due to the electron shift and proton loss [55]. Fig. 9 depicted the photoluminescence of fluorescein-5-isothiocyanate, NCQD, and fluorescein-5-isothiocyanate-conjugated NCQD. There was a significant decrease in photoluminescence at an emission wavelength of 522 nm [56] and 454 nm [57], compared to the original fluorescein-5-isothiocyanate. In addition, a new peak appeared at 443 nm, confirming the formation of isothiourea conjugation as the products

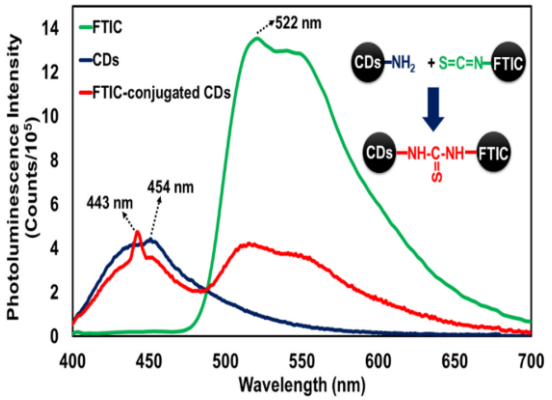

Fig. 9. Comparison of photoluminescence of fluorescein-5-isothiocyanate, NCQD, and fluorescein-5-isothiocyanate-conjugated NCQD in determining $–NH_2$ functional groups.

between $–NH_2$ on the surface of NCQD and 5-isothiocyanate.

3.5. Fluorescence performance of the as-prepared NCQD

From Fig. 10a, the UV–visible absorption spectrum of NCQD showed two peaks at 280 nm and 310 nm, while there was only a typical peak at 280 nm for folic acid [58]. A new strong peak at 310 nm indicated the formation of NCQD due to the decomposition of folic acid from microplasma [59]. Specifically, the absorbance peak at around 280 nm can be attributed to $\pi \rightarrow \pi^*$ transitions, revealing the absorbance by aromatic structure (C═C bond) of folic acid. Under microplasma treatment, the aromatic system of folic acid was damaged to form NCQD with graphitic nitrogen structure and the introduction of nitrogen and oxygen functional groups at the surface [54,60]. As a result, a new intense absorbance at 310 nm assigned to $n \rightarrow \pi^*$ transition has appeared in the UV–Vis spectrum of NCQD.

The UV–visible spectra also explained the influence of nitrogen doping on the optical properties of NCQD. Fig. 10b showed that NCQD absorbs the UV–Vis light at 310 nm under excitation of 360 nm to emit an enormously intense blue fluorescence at a wavelength of 454 nm. It was explained that the graphitic nitrogen structure has a lone pair of electrons, which donate to the carbon structure. As a result, NCQD has a positively charged surface, thus increasing the carbon density and reducing the bandgap [54,60].

Quantum yield is an important parameter to evaluate the photoluminescence of NCQD, which is known as the efficiency of converting absorbed light into emitted light in fluorescence [61]. Ideally, a quantum yield of 1.0 means that 100% of absorbed photons are converted to emitted photons. However, compounds with quantum yields above 0.10 are still considered a strong fluorescence in practical terms. In this study, the quantum yield of the as-prepared NCQD was 35%, which is relatively high and good enough for various applications in water purification, nanopesticides, and theranostic treatment. Table 4 compares the quantum yield of NCQD synthesised from various microplasma. The results showed that our current microplasma technology showed a considerable improvement in quantum yield. Most of the microplasma methods produced NCQD with a low quantum yield (less than 10%), while only NCQD in this study and Kurniawan's study are qualified with a quantum yield above 30 [62].

3.6. Stability of NCQD

The photoluminescence intensity of NCQD is relatively sensitive to pH values [67]. Thus, it is crucial to study how stable the fluorescence of NCQD is in various pH values, which provides more information for target applications. Deprotonation and protonation are typical mechanisms to explain the pH-dependent fluorescence of NCQD. Remarkably, these mechanisms can change the property and the rate of transition processes, thus affecting the PL spectrum and intensity of the NCQD [68]. Therefore, $-COO^-$, –OH, and $–NH_2$ functional groups on the surface of NCQD may undergo protonation and deprotonation processes [67]. Fig. 11a showed the difference in photoluminescence against pH values from 2 to 14. The intensity of photoluminescence increased significantly when the pH increased gradually from 2 to 8. However, when the pH

Table 4
Quantum yield comparison of NCQD synthesised from various types of microplasma.

Types of microplasma	Precursors	Fluorescence	QY%	References
Ar	Folic acid	Blue	35%	This study
Ar	Citric acid and ethylenediamine	Blue	9.9%	[46]
Ar	Isopropanol	Blue	1.5%	[63]
Ar	Ethylenediamine	Blue	5.1%	[64]
Ar	Sodium dodecyl sulphate	Blue	1.5%	[65]
Ar	Chitosan/Acetic acid	Blue	30%	[62]
He	D-Fructose/NaOH	Blue	1.55%	[66]

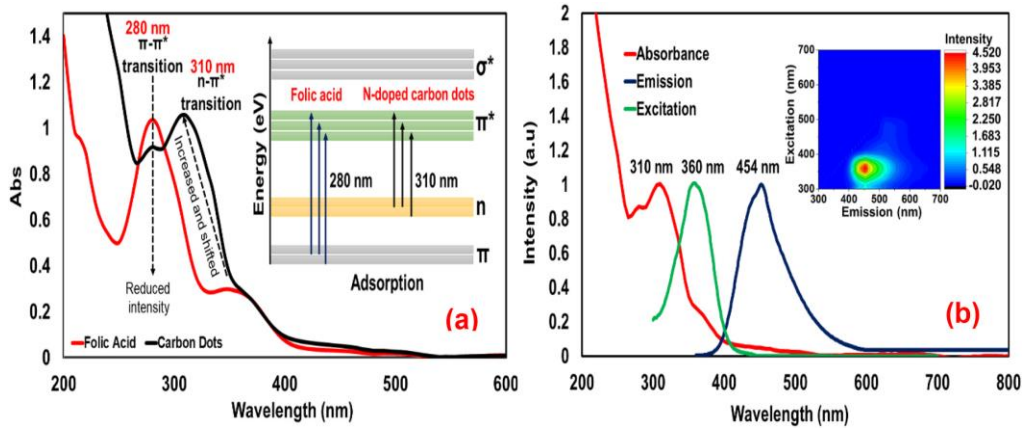

Fig. 10. (a) UV–Vis spectrum of folic acid and NCQD, (b) absorbance, excitation, and emission spectra of NCQD.

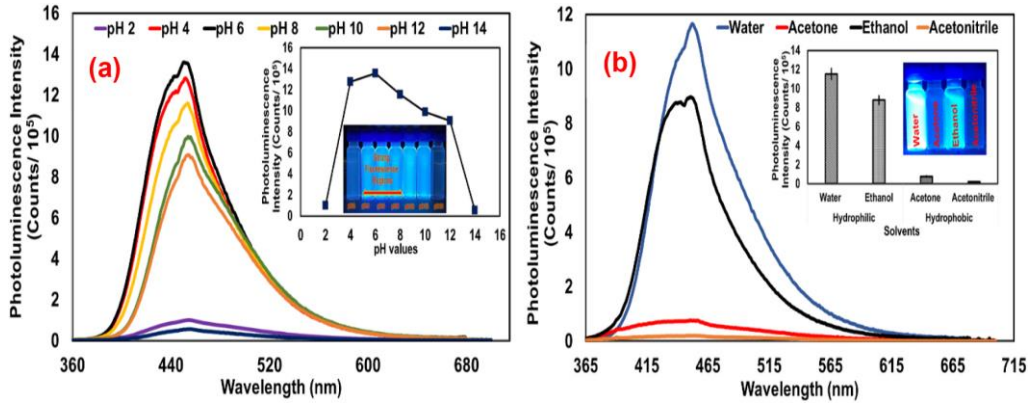

Fig. 11. *Influence of* pH *(a) and solvents (b) on photoluminescence of NCQD.*

value gradually increased from 8 to 14, the photoluminescence intensity decreased significantly. It was explained that the carboxyl group could cause hydrogen bonds intramolecularly and intermolecularly. This result showed the intense vibrational coupling of the OH functional groups in the surface state of NCQD, thus which induce the broadness of energy level and bands of the absorption spectra of NCQD at a low pH value.

Once increasing the pH values from 2 to 8, the carboxyl group's proton dissociation process was more dominant, thus decreasing the effect of intramolecular and intermolecular hydrogen bonds significantly. As a result, there was an increase in photoluminescence intensity without changing the photoluminescence spectrum. In contrast, the hydroxyl group interacted with emission sites, and a new surface state in NCQD with a lower bandgap was formed due to its deprotonation process. When the pH values increase from 8 to 14, the carboxyl groups become deprotonated. On the other hand, the hydroxyl groups undergo a slow deprotonation process, which leads to a decrease in photoluminescence intensity.

Solvents are also one of the most critical parameters in the multifunctional applications of the as-prepared NCQD [69]. In this study, NCQD were dissolved into hydrophilic (water and ethanol) and hydrophobic solvents (acetone and acetonitrile). Fig. 11b indicated that NCQD dissolved well in water or ethanol to perform the intense blue photoluminescence. In contrast, hydrophobic solvents (acetone and acetonitrile) showed low solubility performance with weak blue photoluminescence. In water or ethanol, NCQD undergoes the swelling and the changing of proton donor-acceptor properties in the carbon core, which changes their conformation. Thus, NCQD can express excitation wavelength-dependent behaviour. More specifically, in polar solvents such as water or ethanol, pyrrolic- and graphitic-nitrogen in the core of NCQD can enhance the charge-carrier density by interacting with the surrounding molecules in solvents.

Additionally, by changing the dipole direction of the surrounding solvent molecules, excited electrons from the ground state can be stabilised. It is required more energy to change the dipole direction of the solvent molecules when increasing the polarity of solvents. For this reason, exciting electrons in a high polar solvent (water or ethanol) lose more energy to emit a strong blue fluorescence at 454 nm. Otherwise, low polar solvents like acetone and acetonitrile did not exhibit intense blue fluorescence at the emission wavelength of 454 nm.

Overall, the as-prepared NCQD has shown the potential in various applications) water treatment, hydrophilic pesticides and theranostic medicine) with the strongest blue photoluminescence in water.

3.7. DLVO theory on colloidal behaviours

The DLVO theory is a model to describe the behaviour of colloidal dispersion [70]. In this theory, the zeta potential and particle size are used to interpret how two nanoparticles interact in an aqueous solution [71,72]. According to DLVO, the zeta potential of nanoparticles is the key to the stability of nanofluids. From this principle, the DLVO model can predict the optimal conditions of zeta potential to obtain the most stable NCQD in an aqueous solution. Therefore, the motivation for using the DLVO model in this study is to understand the colloidal behaviours in an aqueous solution with various zeta potentials to create stable NCQD. This study showed four scenarios with different zeta potentials in Table 2 and Fig. 12. The DLVO models of NCQD dispersed in water are plotted with a mean particle size of 3.13 nm at 298.15 0K, and the distance between two NCQD was hypothesised from 0 to 10 nm. V_D and V_H represent dispersion and attraction forces between two NCQD. Therefore, the colloidal behaviours of NCQD rely on the total energy of V_D and V_H, known as V_T.

In scenario 1 (Fig. 12a), at a zeta potential of ±5 mV, the electrical double layer interactions (V_D) were lower than 0.05 and reached 0 at the distance of 3 nm, while the energy force of van der Waals interactions (V_H) was by far higher than that of V_D. As a result, when increasing the distance from 0 to 10 nm, NCQD' total energy force (V_T) was below 0, indicating a tendency to congregate NCQD in an aqueous solution. This result was explained that in NCQD, there was a lack of functional groups (-NH_2 and –OH) on the surface leading to low absorption of water molecules to form the electrical double layers. In other words, NCQD interacted majorly via van der Waals interactions, resulting in a tendency to aggregation.

When increasing the zeta-potential to ±10 and ± 20 mV in scenarios 2 (Figs. 12b) and 3 (Fig. 12c), electrical double layer interactions of NCQD in water increase significantly. This result explained that the number of functional groups (-NH_2, –COOH, and –OH) on the surface of NCQD in these two models increased significantly, leading to enhanced electrical double layer interactions. However, the total energy curve of NCQD in water still shows a negative curve, meaning that at this condition, NCQD were still not stable in water, giving the chances of aggregation.

Compared with scenarios 1, 2, and 3, the DLVO model in scenario 4 (Fig. 12d) depicted the most stable NCQD with zeta potential ±40 mV. At this condition, the electrical double layer interactions of NCQD were by far higher than in the other three scenarios, resulting in the total energy of the curve being positive. This result means that the as-prepared NCQD are stable in the form of suspension with a distance of 0.6 nm. Finally, the prediction from DLVO theory provided vital information that increasing the zeta potential value may lead to more stable

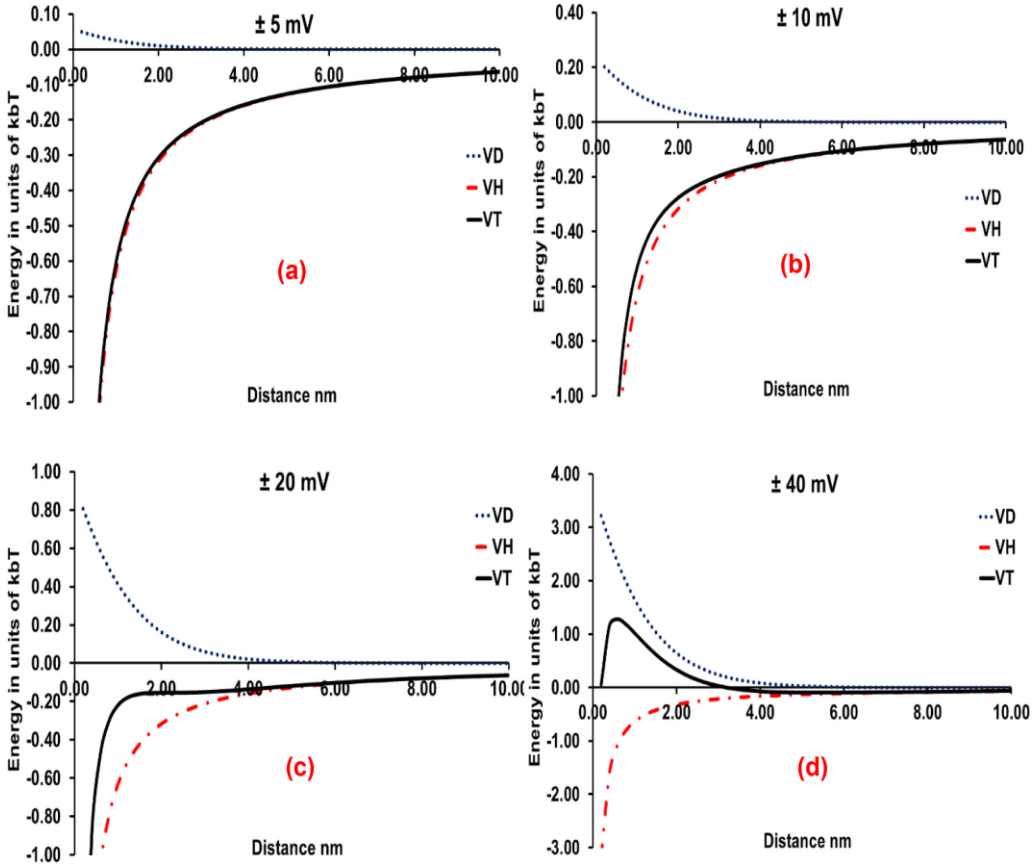

Fig. 12. *NCQD on colloidal* behaviours in water based on DLVO theory.

NCQD, which can be used in the targeting applications (nanopesticides, water purification, and theranostics).

4. Conclusions

N-doped carbon quantum dots (NCQD) are rationally designed and synthesised by the kINPen®IND microplasma jet with properties required for three main applications, including nanopesticides, water purification, and theranostics. The results indicate that three molecular targets guiding the rational designs have been achieved in a proof of principle fashion. The NCQD were monodispersed with a mean particle size of 3.13 nm. The core structure of NCQD was in the form of a crystalline. It consisted of multilayered graphitic- and pyrrolic-nitrogen defected graphene sheets, while their surface was decorated by $–NH_2$, –OH, and –COOH functional groups. The resulting NCQD had an intensely blue fluorescence performance with a QY of 35%, which was the highest among other plasma synthesis approaches and the best of all methods applied.

Regarding fluorescence stability, NCQD showed the most intense fluorescence in the range of pH values of 6–8. By performing the strongest fluorescence in water, the NCQD was considered hydrophilic, which is in line with the presence of protic and polar surface groups. DLVO theory predicts that at a potential of ±40 mV, NCQD may have the most stable colloidal behaviour in water.

As said and being critical, we have explored many steps, and this study was proof of concept. This already has advanced literature and considerably in some relevant properties. The outcome of this study was to provide a valuable contribution to this field, introducing a new synthetic approach with microplasma for NCQD with appropriate properties. Yet, the ambition was to molecularly tailor nanoparticles in the sense of (1) having only one functional group on the surface instead of several, at a defined and controllable surface density, (2) having only one bulk-constituting material with definition on the molecular level, and (3) excluding undesired atomic inclusions such as oxygen where possible. Finally, we aim to make nanomaterial products distinct from being a ‘performance chemical’ for an envisaged application.

5. Outlook

This study is a part of our research series on the N-doped carbon quantum dots. Our first literature review has pointed out the potential applications of this material in agriculture as nanopesticides [34]. At the same time, some literature also proved their applicability in water purification [36] and theranostic treatment [41]. Due to its outstanding properties, which are applicable for various applications, it is a driving force for us to survey and comprehensively assess NCQD synthesis processes using green chemistry and circular and Ecoscale metrics [47]. This survey indicates that microplasma is one of the most sustainable methods in terms of energy efficiency while lacking mass efficiency. Another study has been carried out to improve the mass efficiency of NCQDs by a process intensification to obtain gram-scale production. Future work is underway to characterise the efficiency of our rationally designed NCQD for applications as nanopesticides, water purification, and theranostic treatment.

After demonstrating the potential applications of the as-prepared NCQD, industrial-scale production is another challenge in bringing this outstanding NCQD to the market. Microplasma jet has lower power generation than other plasma reactors, which might result in low mass

efficiency. However, the microplasma jet is way more advanced than other plasma reactors in terms of safety, process efficiency, simple operation, economical, and high-quality product. The authors believe that mass production efficiency is significant in industrial production. Still, other factors such as safety, process efficiency, simple operation, economics, and high-quality product should be highly considered in terms of sustainable production, which will define the total cost of industrial production. Especially in biomedical applications, an excellent fine product is required.

Several ideas have been proposed to mitigate large-scale production issues: (1) an array of microplasma jets can be developed to up-scale the production of high-quality NCQD in an energy-efficient, eco-friendly, and safe manner while still ensuring high mass efficiency; (2) another device that could be used for further study is PlasmaLeap, where bubble microplasma is formed. It is believed that these two proposed approaches can enhance the large-scale production of NCQD.

CRediT authorship contribution statement

Quoc Hue Pho: Conceptualization, Methodology, Software, Data curation, Writing – original draft. **LiangLiang Lin:** Writing – review & editing. **Nam Nghiep Tran:** Writing – review & editing. **Tung T. Tran:** Conceptualization, Writing – review & editing. **An Hoa Nguyen:** Validation. **Dusan Losic:** Writing – review & editing, Supervision. **Evgeny V. Rebrov:** Writing – review & editing. **Volker Hessel:** Conceptualization, Writing – review & editing, Supervision.

Declaration of competing interest

The authors declare that they have no known competing financial interests or personal relationships that could have appeared to influence the work reported in this paper.

Acknowledgements

Mr. Hue Quoc Pho received the divisional ECMS and full-fee scholarships from the University of Adelaide, Australia. The authors acknowledge support from the ERC Grant Surface-Confined fast-modulated Plasma for process and Energy intensification (SCOPE) from the European Commission with grant number 810182.

Appendix A. Supplementary data

Supplementary data to this article can be found online at https://doi.org/10.1016/j.carbon.2022.07.004.

References

[1] H. Belkahla, R. Boudjemaa, V. Caorsi, D. Pineau, A. Curcio, J. Lomas, P. Decorse, A. Chevillot-Biraud, T. Azaïs, C. Wilhelm, Carbon dots, a powerful non-toxic support for bioimaging by fluorescence nanoscopy and eradication of bacteria by photothermia, Nanoscale Adv. 1 (7) (2019) 2571–2579.
[2] S. Pandiyan, L. Arumugam, S.P. Srirengan, R. Pitchan, P. Sevugan, K. Kannan, G. Pitchan, T.A. Hegde, V. Gandhirajan, Biocompatible carbon quantum dots derived from sugarcane industrial wastes for effective nonlinear optical behavior and antimicrobial activity applications, ACS Omega 5 (47) (2020) 30363–30372.
[3] Y. Liu, J. Zhang, X. Zhao, W. Li, J. Wang, Y. Gao, Y. Cui, S. Xu, X. Luo, Water-soluble carbon dots with blue, yellow and red emissions: mechanism investigation and array-based fast sensing application, Chem. Commun. 56 (29) (2020) 4074–4077.
[4] J. Wan, X. Zhang, K. Fu, X. Zhang, L. Shang, Z. Su, Highly fluorescent carbon dots as novel theranostic agents for biomedical applications, Nanoscale 13 (41) (2021) 17236–17253.
[5] X. Liu, S. Zhang, H. Xu, R. Wang, L. Dong, S. Gao, B. Tang, W. Fang, F. Hou, L. Zhong, A. Aldalbahi, Nitrogen-doped carbon quantum dots from poly (ethyleneimine) for optical dual-mode determination of Cu2+ and l-cysteine and their logic gate operation, ACS Appl. Mater. Interfaces 12 (42) (2020) 47245–47255.
[6] S. Chahal, N. Yousefi, N. Tufenkji, Green synthesis of high quantum yield carbon dots from phenylalanine and citric acid: role of stoichiometry and nitrogen doping, ACS Sustain. Chem. Eng. 8 (14) (2020) 5566–5575.
[7] J.D. Stachowska, A. Murphy, C. Mellor, D. Fernandes, E.N. Gibbons, M. J. Krysmann, A. Kelarakis, E. Burgaz, J. Moore, S.G. Yeates, A rich gallery of carbon dots based photoluminescent suspensions and powders derived by citric acid/urea, Sci. Rep. 11 (1) (2021), 10554.
[8] S. Pawar, U.K. Togiti, A. Bhattacharya, A. Nag, Functionalized chitosan–carbon dots: a fluorescent probe for detecting trace amount of water in organic solvents, ACS Omega 4 (6) (2019) 11301–11311.
[9] S. Fatimah, S.M. Bilqis, D. Tahir, Luminescence properties of carbon dots synthesis from sugar for enhancing glows in paints, Mater. Res. Express 6 (9) (2019), 095006.
[10] S.S. Suner, M. Sahiner, R.S. Ayyala, V.R. Bhethanabotla, N. Sahiner, Versatile fluorescent carbon dots from citric acid and cysteine with antimicrobial, anti-biofilm, antioxidant, and AChE enzyme inhibition capabilities, J. Fluoresc. 31 (6) (2021) 1705–1717.
[11] X. Hu, Y. Li, Y. Xu, Z. Gan, X. Zou, J. Shi, X. Huang, Z. Li, Y. Li, Green one-step synthesis of carbon quantum dots from orange peel for fluorescent detection of Escherichia coli in milk, Food Chem. 339 (2021), 127775.
[12] R. Atchudan, T.N. Jebakumar Immanuel Edison, M. Shanmugam, S. Perumal, T. Somanathan, Y.R. Lee, Sustainable synthesis of carbon quantum dots from banana peel waste using hydrothermal process for in vivo bioimaging, Phys. E Low-dimens. Syst. Nanostruct. 126 (2021), 114417.
[13] X. Yang, D. Wang, N. Luo, M. Feng, X. Peng, X. Liao, Green synthesis of fluorescent N,S-carbon dots from bamboo leaf and the interaction with nitrophenol compounds, Spectrochim. Acta Mol. Biomol. Spectrosc. 239 (2020), 118462.
[14] G. Gedda, C.-Y. Lee, Y.-C. Lin, H.-f. Wu, Green synthesis of carbon dots from prawn shells for highly selective and sensitive detection of copper ions, Sensor. Actuator. B Chem. 224 (2016) 396–403.
[15] C. He, P. Xu, X. Zhang, W. Long, The synthetic strategies, photoluminescence mechanisms and promising applications of carbon dots: current state and future perspective, Carbon 186 (2022) 91–127.
[16] A. Kaczmarek, J. Hoffman, J. Morgiel, T. Mościcki, L. Stobiński, Z. Szymański, A. Małolepszy, Luminescent carbon dots synthesized by the laser ablation of graphite in polyethylenimine and ethylenediamine, Materials 14 (4) (2021) 729.
[17] Y. Su, M. Xie, X. Lu, H. Wei, H. Geng, Z. Yang, Y. Zhang, Facile synthesis and photoelectric properties of carbon dots with upconversion fluorescence using arc-synthesised carbon by-products, RSC Adv. 4 (10) (2014) 4839–4842.
[18] Z. Han, L. He, S. Pan, H. Liu, X. Hu, Hydrothermal synthesis of carbon dots and their application for detection of chlorogenic acid, Luminescence 35 (7) (2020) 989–997.
[19] C.a. Ma, C. Yin, Y. Fan, X. Yang, X. Zhou, Highly efficient synthesis of N-doped carbon dots with excellent stability through pyrolysis method, J. Mater. Sci. 54 (13) (2019) 9372–9384.
[20] D. Zhang, D. Chao, C. Yu, Q. Zhu, S. Zhou, L. Tian, L. Zhou, One-step green solvothermal synthesis of full-color carbon quantum dots based on a doping strategy, J. Phys. Chem. Lett. 12 (37) (2021) 8939–8946.
[21] C. Qi, H. Wang, A. Yang, X. Wang, J. Xu, Facile fabrication of highly fluorescent N-doped carbon quantum dots using an ultrasonic-assisted hydrothermal method: optical properties and cell imaging, ACS Omega 6 (48) (2021) 32904–32916.
[22] R. Li, L. Zhang, P. Wang, Rational design of nanomaterials for water treatment, Nanoscale 7 (41) (2015) 17167–17194.
[23] P. Wang, Rational Design of Next-Generation Nanomaterials and Nanodevices for Water Applications, IWA Publishing, 2016.
[24] Y. Zhou, E.M. Zahran, B.A. Quiroga, J. Perez, K.J. Mintz, Z. Peng, P.Y. Liyanage, R. R. Pandey, C.C. Chusuei, R.M. Leblanc, Size-dependent photocatalytic activity of carbon dots with surface-state determined photoluminescence, Appl. Catal. B Environ. 248 (2019) 157–166.
[25] B. Vercelli, The role of carbon quantum dots in organic photovoltaics: a short overview, Coatings 11 (2) (2021) 232.
[26] A. Vesel, R. Zaplotnik, G. Primc, M. Mozetič, A review of strategies for the synthesis of N-doped graphene-like materials, Nanomaterials 10 (11) (2020) 2286.
[27] J. Manioudakis, F. Victoria, C.A. Thompson, L. Brown, M. Movsum, R. Lucifero, R. Naccache, Effects of nitrogen-doping on the photophysical properties of carbon dots, J. Mater. Chem. C 7 (4) (2019) 853–862.
[28] Y. Xu, Y. Mo, J. Tian, P. Wang, H. Yu, J. Yu, The synergistic effect of graphitic N and pyrrolic N for the enhanced photocatalytic performance of nitrogen-doped graphene/TiO2 nanocomposites, Appl. Catal. B Environ. 181 (2016) 810–817.
[29] B. Li, T. Suo, S. Xie, A. Xia, Y.-j. Ma, H. Huang, X. Zhang, Q. Hu, Rational design, synthesis, and applications of carbon dots@metal–organic frameworks (CD@MOF) based sensors, TrAC, Trends Anal. Chem. 135 (2021), 116163.
[30] B. Wang, J. Yu, L. Sui, S. Zhu, Z. Tang, B. Yang, S. Lu, Rational design of multi-color-emissive carbon dots in a single reaction system by hydrothermal, Adv. Sci. 8 (1) (2021), 2001453.
[31] N. Abid, A.M. Khan, S. Shujait, K. Chaudhary, M. Ikram, M. Imran, J. Haider, M. Khan, Q. Khan, M. Maqbool, Synthesis of nanomaterials using various top-down and bottom-up approaches, influencing factors, advantages, and disadvantages: a review, Adv. Colloid Interface Sci. 300 (2022), 102597.
[32] A. Nair, J.T. Haponiuk, S. Thomas, S. Gopi, Natural carbon-based quantum dots and their applications in drug delivery: a review, Biomed. Pharmacother. 132 (2020), 110834.
[33] F. Gao, S. Ma, J. Li, K. Dai, X. Xiao, D. Zhao, W. Gong, Rational design of high quality citric acid-derived carbon dots by selecting efficient chemical structure motifs, Carbon 112 (2017) 131–141.
[34] Q.H. Pho, D. Losic, K. Ostrikov, N.N. Tran, V. Hessel, Perspectives on plasma-assisted synthesis of N-doped nanoparticles as nanopesticides for pest control in crops, Reaction Chem. Eng. 5 (8) (2020) 1374–1396.

[35] S. Mayakaduwage, M. Alamgir, L. Mosley, P. Marschner, Phosphorus pools in sulfuric acid sulfate soils: influence of water content, pH increase and P addition, J. Soils Sediments 20 (3) (2020) 1446–1453.
[36] K. Akbar, E. Moretti, A. Vomiero, Carbon dots for photocatalytic degradation of aqueous pollutants: recent advancements, Adv. Opt. Mater. 9 (17) (2021), 2100532.
[37] R. Wang, K.-Q. Lu, Z.-R. Tang, Y.-J. Xu, Recent progress in carbon quantum dots: synthesis, properties and applications in photocatalysis, J. Mater. Chem. 5 (8) (2017) 3717–3734.
[38] S.-H. Li, M.-Y. Qi, Y.-Y. Fan, Y. Yang, M. Anpo, Y.M. Yamada, Z.-R. Tang, Y.-J. Xu, Modulating photon harvesting through dynamic non-covalent interactions for enhanced photochemical CO2 reduction, Appl. Catal. B Environ. 292 (2021), 120157.
[39] S.-H. Li, R. Wang, Z.-R. Tang, Y.-J. Xu, Efficient visible-light-driven water remediation by 3D graphene aerogel-supported nitrogen-doped carbon quantum dots, Catal. Today 335 (2019) 160–165.
[40] R. Wang, K.-Q. Lu, F. Zhang, Z.-R. Tang, Y.-J. Xu, 3D carbon quantum dots/graphene aerogel as a metal-free catalyst for enhanced photosensitisation efficiency, Appl. Catal. B Environ. 233 (2018) 11–18.
[41] S. Bayda, E. Amadio, S. Cailotto, Y. Frión-Herrera, A. Perosa, F. Rizzolio, Carbon dots for cancer nanomedicine: a bright future, Nanoscale Adv. 3 (18) (2021) 5183–5221.
[42] Y. Sun, S. Zheng, L. Liu, Y. Kong, A. Zhang, K. Xu, C. Han, The cost-effective preparation of green fluorescent carbon dots for bioimaging and enhanced intracellular drug delivery, Nanoscale Res. Lett. 15 (1) (2020) 55, 55.
[43] S. Shishodia, V. Rimal, P.K. Srivastava, Synthesis of tunable high-thermal stability carbon dots via functionalisation for applications in high-temperature environment, Appl. Nanosci. 11 (5) (2021) 1691–1706.
[44] D. Xu, F. Lei, H. Chen, L. Yin, Y. Shi, J. Xie, One-step hydrothermal synthesis and optical properties of self-quenching-resistant carbon dots towards fluorescent ink and as nanosensors for Fe3+ detection, RSC Adv. 9 (15) (2019) 8290–8299.
[45] W. Den, V.K. Sharma, M. Lee, G. Nadadur, R.S. Varma, Lignocellulosic biomass transformations via greener oxidative pretreatment processes: access to energy and value-added chemicals, Front. Chem. 6 (2018).
[46] X. Ma, S. Li, V. Hessel, L. Lin, S. Meskers, F. Gallucci, Synthesis of N-doped carbon dots via a microplasma process, Chem. Eng. Sci. 220 (2020), 115648.
[47] Q.H. Pho, M. Escriba-Gelonch, D. Losic, E.V. Rebrov, N.N. Tran, V. Hessel, Survey of synthesis processes for N-doped carbon dots assessed by green chemistry and circular and EcoScale metrics, ACS Sustain. Chem. Eng. 9 (13) (2021) 4755–4770.
[48] Q. Wang, Q. Zhang, Y. Chen, J. He, K. Jiang, Z. Hu, X. Zhong, Blue luminescent amorphous carbon nanoparticles synthesised by microplasma processing of folic acid, Plasma Process. Polym. 15 (1) (2018), 1700088.
[49] S. Reuter, T. von Woedtke, K.-D. Weltmann, The kINPen—a review on physics and chemistry of the atmospheric pressure plasma jet and its applications, J. Phys. Appl. Phys. 51 (23) (2018), 233001.
[50] R. Wen, Q.H. Li, Y.S. Li, Y.X. Luo, X. Zhao, X.F. Gao, Synthesis optimisation of rich-urea carbon-dots and application in the determination of H(2)S in rich- and barren-liquids of desulphurising solutions, Analyst 146 (24) (2021) 7635–7644.
[51] L. Wang, W.M. Choi, J.S. Chung, S.H. Hur, Multicolor emitting N-doped carbon dots derived from ascorbic acid and phenylenediamine precursors, Nanoscale Res. Lett. 15 (1) (2020) 1–10.
[52] M. Perikala, A. Bhardwaj, Highly stable white-light-emitting carbon dot synthesis using a non-coordinating solvent, ACS Omega 4 (25) (2019) 21223–21229.
[53] A.M. Raj, G.T. Chirayil, Tunable direct band gap photoluminescent organic semiconducting nanoparticles from lignite, Sci. Rep. 7 (1) (2017) 1–9.
[54] S.D. Dsouza, M. Buerkle, P. Brunet, C. Maddi, D.B. Padmanaban, A. Morelli, A. F. Payam, P. Maguire, D. Mariotti, V. Svrcek, The importance of surface states in N-doped carbon quantum dots, Carbon 183 (2021) 1–11.
[55] T. Clark Brelje, M.W. Wessendorf, R.L. Sorenson, Chapter 5 - multicolor laser scanning confocal immunofluorescence microscopy: practical application and limitations, in: B. Matsumoto (Ed.), Methods in Cell Biology, Academic Press, 2002, pp. 165–249e.
[56] O. Koniev, A. Wagner, Developments and recent advancements in the field of endogenous amino acid selective bond forming reactions for bioconjugation, Chem. Soc. Rev. 44 (15) (2015) 5495–5551.
[57] B. Sharma, K. Luhach, G.T. Kulkarni, 4 - in vitro and in vivo models of BBB to evaluate brain targeting drug delivery, in: H. Gao, X. Gao (Eds.), Brain Targeted Drug Delivery System, Academic Press, 2019, pp. 53–101.
[58] M.K. Off, A.E. Steindal, A.C. Porojnicu, A. Juzeniene, A. Vorobey, A. Johnsson, J. Moan, Ultraviolet photodegradation of folic acid, J. Photochem. Photobiol. B Biol. 80 (1) (2005) 47–55.
[59] K. Chang, Q. Zhu, L. Qi, M. Guo, W. Gao, Q. Gao, Synthesis and properties of nitrogen-doped carbon quantum dots using lactic acid as carbon source, Materials 15 (2) (2022).
[60] M. Sudolská, M. Dubecký, S. Sarkar, C.J. Reckmeier, R. Zbořil, A.L. Rogach, M. Otyepka, Nature of absorption bands in oxygen-functionalised graphitic carbon dots, J. Phys. Chem. C 119 (23) (2015) 13369–13373.
[61] S. Sadjadi, Chapter 4 - the utility of carbon dots for photocatalysis, in: S. Sadjadi (Ed.), Emerging Carbon Materials for Catalysis, Elsevier, 2021, pp. 123–160.
[62] D. Kurniawan, W.-H. Chiang, Microplasma-enabled colloidal nitrogen-doped graphene quantum dots for broad-range fluorescent pH sensors, Carbon 167 (2020) 675–684.
[63] X. Ma, S. Li, V. Hessel, L. Lin, S. Meskers, F. Gallucci, Synthesis of luminescent carbon quantum dots by microplasma process, Chem. Eng. Process. Process Intensification 140 (2019) 29–35.
[64] Z. Wang, Y. Lu, H. Yuan, Z. Ren, C. Xu, J. Chen, Microplasma-assisted rapid synthesis of luminescent nitrogen-doped carbon dots and their application in pH sensing and uranium detection, Nanoscale 7 (48) (2015) 20743–20748.
[65] J.-S. Yang, D.Z. Pai, W.-H. Chiang, Microplasma-enhanced synthesis of colloidal graphene quantum dots at ambient conditions, Carbon 153 (2019) 315–319.
[66] X. Huang, Y. Li, X. Zhong, A.E. Rider, K. Ostrikov, Fast microplasma synthesis of blue luminescent carbon quantum dots at ambient conditions, Plasma Process. Polym. 12 (1) (2015) 59–65.
[67] C. Liu, F. Zhang, J. Hu, W. Gao, M. Zhang, A mini review on pH-sensitive photoluminescence in carbon nanodots, Front. Chem. 8 (2021).
[68] J.R. Lakowicz, Principles of Fluorescence Spectroscopy, Springer, 2006.
[69] X. Huo, H. Shen, R. Liu, J. Shao, Solvent effects on fluorescence properties of carbon dots: implications for multicolor imaging, ACS Omega 6 (40) (2021) 26499–26508.
[70] E.M. Hotze, T. Phenrat, G.V. Lowry, Nanoparticle aggregation: challenges to understanding transport and reactivity in the environment, J. Environ. Qual. 39 (6) (2010) 1909–1924.
[71] M. Bayati, J. Dai, A. Zambrana, C. Rees, M. Fidalgo de Cortalezzi, Effect of water chemistry on the aggregation and photoluminescence behavior of carbon dots, J. Environ. Sci. 65 (2018) 223–235.
[72] P.T. Snee, The role of colloidal stability and charge in functionalisation of aqueous quantum dots, Accounts Chem. Res. 51 (11) (2018) 2949–2956.

BLANK PAGE

Chapter 6

Insight into plasma-catalysis in triphasic microplasma synthesis for NCQDs

In chapter 6, the aim of this study is to understand the plasma-catalytic effect under the microplasma multiphase design and vice versa, to understand the multiphase design better. As an analytical method, optical emission spectroscopy (OES) investigations are appropriate to investigate the mechanism of how a plasma(-heterogeneous) catalyst in a multiphase reaction may affect the fabrication of NCQD from Vitamin B9. The key of this research is to determine and advance multiphase hydrodynamics and reaction by shaping a characteristic surface profile via deep penetration of the plasma jet into the liquid volume.

This chapter has been prepared as a research paper manuscript and supposed to be submitted to "Chemical Engineering Journal" as follows:

Pho, Q.H., Tran, H.Q., Zhuang C.P., Nguyen, V.L., Tran, N.N., Tran, T. T., Rebrov, E.V., Losic, D., and Hessel, V., 2023. Deciphering Plasma-Catalysis in Triphasic Microplasma for N-doped Carbon Quantum Dots from Vitamin B9 via Optical Emission Spectroscopy. (Ready manuscript)

Statement of Authorship

Title of Paper	Deciphering Plasma-Catalysis in Triphasic Microplasma for N-doped Carbon Quantum Dots from Vitamin B9 via Optical Emission Spectroscopy
Publication Status	☐ Published ☐ Accepted for Publication ☐ Submitted for Publication ☑ Unpublished and Unsubmitted w ork w ritten in manuscript style
Publication Details	Pho, Q.H., Tran, H.Q., Zhuang, C.P., Nguyen, V.L., Tran, N.N., Tran, T. T., Rebrov, E.V., Losic, D., Malacha, D., and Hessel, V., 2023. Deciphering Plasma-Catalysis in Triphasic Microplasma for N-doped Carbon Quantum Dots from Vitamin B9 via Optical Emission Spectroscopy. (Ready manuscript)

Principal Author

Name of Principal Author (Candidate)	Quoc Hue Pho		
Contribution to the Paper	Conceptualization, Methodology, Formal analysis, Investigation, Data curation, Writing – original draft		
Overall percentage (%)	65%		
Certification:	This paper reports on original research I conducted during the period of my Higher Degree by Research candidature and is not subject to any obligations or contractual agreements with a third party that would constrain its inclusion in this thesis. I am the primary author of this paper.		
Signature		Date	28.01.2023

Co-Author Contributions

By signing the Statement of Authorship, each author certifies that:

i. the candidate's stated contribution to the publication is accurate (as detailed above);
ii. permission is granted for the candidate in include the publication in the thesis; and
iii. the sum of all co-author contributions is equal to 100% less the candidate's stated contribution.

Name of Co-Author	Quan Hoang Tran		
Contribution to the Paper	Investigation and data curation		
Signature		Date	28.01.2023

Name of Co-Author	Changping Zhuang		
Contribution to the Paper	Investigation and data curation		
Signature		Date	28.01.2023

Please cut and paste additional co-author panels here as required.

Name of Co-Author	Nguyen Van Duc Long		
Contribution to the Paper	Investigation and data curation		
Signature		Date	31.01.2023

Name of Co-Author	Nam Nghiep Tran		
Contribution to the Paper	Conceptualization, Writing- Review and Editing.		
Signature		Date	28.01.2023

Name of Co-Author	Thanh Tung Tran		
Contribution to the Paper	Conceptualization, Writing- Review and Editing		
Signature		Date	1.2.2023

Name of Co-Author	Evgeny V. Rebrov		
Contribution to the Paper	Writing – review & editing		
Signature		Date	

Name of Co-Author	Dusan Losic		
Contribution to the Paper	Co-supervised and Writing- Review and Editing		
Signature		Date	2 feb 2023

Name of Co-Author	Zdenko Machala		
Contribution to the Paper	Investigation and data curation. Writing- Review.		
Signature		Date	06.02.2023

Name of Co-Author	Volker Hessel		
Contribution to the Paper	Supervised (scientific ideas, concepts, objectives, assessment of achievement degree, societal impact), Conceptualised, Writing – review & editing, and is the corresponding author.		
Signature		Date	28.01.2023

Deciphering Plasma-Catalysis in Triphasic Microplasma for N-doped Carbon Quantum Dots from Vitamin B9 via Optical Emission Spectroscopy

Quoc Hue Pho [a,c], Quan Hoang Tran [a], Changping Zhuang [a], Nguyen Van Duc Longs [a], Nam Nghiep Tran [a], Thanh Tung Tran [a,b], Evgeny V. Rebrov [c], Dusan Losic [a,b], Zdenko Machala [d], Volker Hessel [a,c]

[a] *School of Chemical Engineering, The University of Adelaide, Adelaide, SA 5005, Australia*

[b] *The ARC Graphene Research Hub, School of Chemical Engineering and Advanced Materials, The University of Adelaide, SA 5005, Australia*

[c] *School of Engineering, University of Warwick, Library Rd, Coventry CV4 7AL, England, UK*

[d] *Department of Astronomy, Earth Physics and Meteorology, Comenius University, Bratislava, Slovakia*

E-mail: volker.hessel@adelaide.edu.au

Abstract

Multiphase plasma catalysis is applied to fabricate N-doped carbon quantum dots by exposing a submerged plasma jet deep into a small liquid volume with the precursor and catalytic alloy flakes. Optical emission spectroscopy at the plasma-liquid-catalyst interface was used to investigate and understand the reaction mechanism, particularly the role of the plasma catalysis effect. Depending on the penetration depth of the jet, defining its contact with the liquid medium and the catalyst just underneath in a generic hydrodynamic regime, the deepest penetration, the 'deflection mode', generated more positively charged species from the metal catalyst. The bimetallic catalyst $Ni_{80}Cr_{20}$ demonstrated the strongest effect, which is correlated to the highest electric potential among the three alloy catalysts investigated. Seven steps are proposed for the reaction mechanism to yield the N-doped quantum dots. The temperature at the plasma-liquid-catalyst interface was lower than 25 ^{0}C, as determined by IR imaging. Nonetheless, notable water evaporation happens at the surface surrounded by highly convective phases.

Keywords: nonthermal microplasma, N-doped quantum carbon dots, optical emission spectroscopy, plasma catalysis, multiphase reaction

Highlights

- Optical emission spectroscopy at the plasma-liquid-catalyst interface was used to investigate and understand the reaction mechanism, particularly the role of the plasma catalysis effect.
- The deepest penetration, the 'deflection mode', generated more positively charged species from the metal catalyst.
- The bimetallic catalyst $Ni_{80}Cr_{20}$ demonstrated the strongest effect, which is correlated to the highest electric potential among the three alloy catalysts investigated.
- The temperature at the plasma-liquid-catalyst interface was lower than 25 ^{0}C, as determined by IR imaging.
- Seven steps are proposed for the reaction mechanism to yield the N-doped quantum dots.

1. Introduction

Since their initial discovery in 2004, carbon dots (CD) have attracted attention in research for various potential applications due to their unique properties, such as low toxicity, biocompatibility, water solubility, and excellent optical properties [1-3]. N-doped carbon quantum dots (NCQD) have the potential as multifunctional nanopesticides (pesticide nanocarriers [4], pesticides [5], pathogen targeting [6], and phytopathogen detecting [7]), are considered as a tool of the "agri-tech revolution" [8], which aims to enhance crop efficiency and meet the growing global demands for food [8, 9].

Extensive research studies on N-doped carbon quantum dots have been conducted, reporting a large number of diverse structures of this nanomaterial class with distinct properties, made *via* various synthetic techniques [10], including laser ablation [11], arc discharge [12], hydrothermal [13], pyrolysis [14], solvothermal [15] and ultrasonic [16] processing. Those manufacturing technologies differ in sustainability. In our previous research, green chemistry, circular and ecoScale metrics were used to assess those methods, which are common to judge sustainability for industrial-scale production of chemical processes [17], in particular in the pharmaceutical industry with similarly high-quality needs for functional nanomaterials. Among the six NCQD manufacturing routes, plasma synthesis had the best energy efficiency while lacking in mass efficiency [17]; meaning it does not have the productivity as the other processes, typically run in macroscopic reactors, whereas the plasma considered was a tiny jet.

Alike for microchannels, small reaction volumes do not inhibit productivity. Striving for process intensification to overcome the problem of low productivity of jet microplasmas, we designed a genuine process around enhancing mass transport in intensified gas (plasma)–liquid regimes and the facilitation of catalysis on metal particles in the liquid microvolume, achieving gram-scale synthesis, which is significant for a tailored nanomaterial [18]. This study will provide a closer look at the fundamentals to better understand plasma catalysis in a multiphase processing mode, including deciphering plasma-excited species and their reaction mechanism. This is motivated by our recent finding that the photoluminescence of the as-prepared NCQD increases by 18.4% in the presence of metal flakes as catalysts [18]. This evidence indicates a research gap in how these metal catalysts interact with plasma to enhance the production efficiency of NCQD.

The impact of this study is underlined by recent reports about the progress of plasma catalytic processes, for example, on the conversion of light hydrocarbons [19], CO_2 [20], and volatile

organic compounds (VOCs) [21]. Meng et al. developed a process combining nonthermal plasma with a photocatalyst to improve product yield and limit coke formation in a simulated natural gas conversion to C6–C9 branched-chain paraffins [22]. Ahmad et al. used a Ni/Al_2O_3 catalyst for the methanation of CO_2. The plasma-catalytic process achieved similar conversions and selectivities at lower temperatures than the thermal process [23]. Erik et al. also mentioned that plasma catalytic processes are already a highly successful approach for the small-scale fabrication of expensive materials such as CNTs [24-26] or inorganic nanowires [27, 28]. This evidences that the plasma-catalysis effect is also key in fabricating NCQD from folic acid (vitamin B9). However, the underlying plasma-catalyst effect and mechanism in the formation of NCDQ are unclear, which is tackled in this study.

For this reason, this study aims to understand the plasma-catalytic effect under that microplasma multiphase design and vice versa, to understand the multiphase design better. As an analytical method, optical emission spectroscopy (OES) investigations are appropriate to investigate the mechanism of how a plasma-(heterogeneous) catalyst in a multiphase reaction may affect the fabrication of NCQD from Vitamin B9. The key of our experiment is to determine and advance multiphase hydrodynamics and reaction by shaping a characteristic surface profile *via* deep penetration of the plasma jet into the liquid volume ('crater'). The jet can reach down to the bed of heterogeneous catalysts, metallic flakes, which are static, while exposed to a plasma flow field of very high velocity and drag force. The jet may likely contact both the thin liquid layer and the catalyst, meaning a genuine tri-phase process design possibly is generated, which is new to the literature and magnified by miniature dimensions, coined as 'micro-plasma'. Subtle details need a better understanding, e.g., how the fine droplet spray that has been detected under such conditions [29, 30], can add to reaction advancement.

2. Materials and methodology

2.1. Reactor configuration and experimental setup

Our experimental design is inspired by the concept of high-intensity gas-liquid reactors with powerful gas jets, which are known to improve phase mixing [31]. A high-velocity impinging flow reactor was developed to enter a small reactor volume and travel in counter current. Guided by a small nozzle, the gas and liquid streams meet in a small reactor volume, leading to a highly turbulent distribution of the gas phase in the liquid. The formation and collapse of gas bubbles enhance substance exchange. Another high-intensity gas-liquid reactor design

consists of a pump, an orifice, a vertical tube coaxial with the orifice, and a baffle plate [31]. The pump creates a downward vertical jet of liquid through the orifice, creating a gas-liquid dispersion in the tube. The two-phase jet is directed onto a baffle near the bottom of the tank and distributed throughout the liquid. The liquid is drawn under the baffle plate and recycled.

Our experimental design follows these high-intensity gas-liquid reactor concepts but should be simplified. It means that the plasma gas phase exists over long distances, which is difficult to achieve. Instead, we use a micro-plasma jet aimed at the liquid (Figure 1). We also withhold flow feedback for repeated gas-liquid interactions, as single contact is better shown to be fundamental for the process intensification [32].

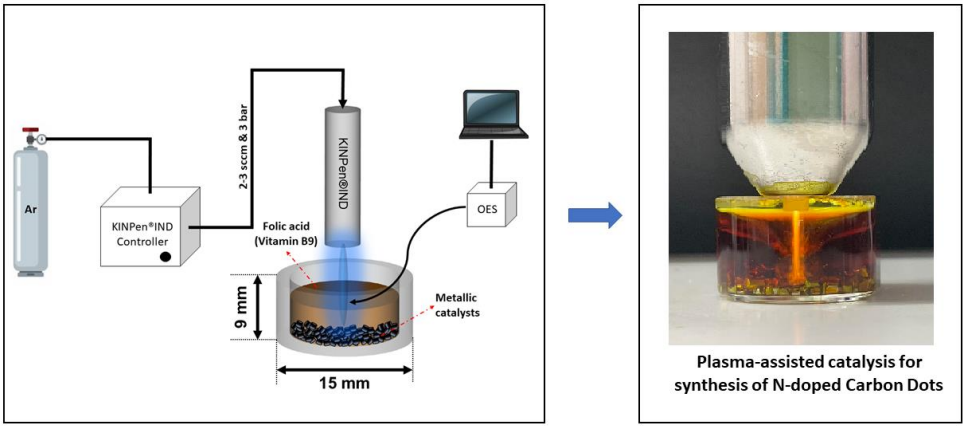

Figure 1. Reactor configurations and experimental setup of the synthesis process of NCQD.

The reactor configuration and experimental synthesis process were adopted from previous studies [31]. Simply put, the synthesis reactor consists of two parts: (1) A kINPen®IND microplasma jet with dimensions 105 × 180 × 330 mm (H × W × D) was purchased from Neoplas GmbH, Germany, and (2) a 9 mm open glass reactor was used in our study with designed and manufactured in-house 15mm (W x H) dimensions. A 110 VAC (50 Hz) power supply is connected to the kINPen®IND microplasma jet. A continuous gas stream of Ar (99.9%) was connected to the microplasma nozzle. A stable microplasma stream with a length of 1 cm was formed under Ar gas flow and a control pressure of 3 bar. To understand the reaction mechanism, we installed an optical fibre in the plasma-liquid-catalyst interface and detected the reactive species generated from the microplasma. The general synthetic procedure is also described in Figure 1. Briefly, a folic acid (FA) solution (0.1 g/mL) as a starting carbon source was obtained by dissolving 2 g of folic acid (98%) in 20 mL of

$NaHCO_3$ (0.5 M) as a solvent, resulting in an orange colour and prepared by stirring until the solution was evenly mixed. Then 1 ml of FA solution (0.1 mg/ml) was transferred to the open reactor and treated under microplasma with 0.5 g of various metal flakes (Sn coated Cu, $Ni_{90}Ni_{10}$, and $Ni_{80}Cr_{20}$) as catalysts.

2.2. Optical emission spectroscopy analysis

Optical emission spectroscopy (OES) is an essential technique for the multi-element analysis of various materials. This technology monitors the levels of various chemicals and trace elements in the environment and determines the composition of solids, liquids and gases. In optical emission spectroscopy, electrical energy is applied as a spark, created between an electrode and a metal sample, driving vaporised atoms into a high-energy state in a so-called 'discharge plasma'.

Plasma emissions with different flow velocities generated by the atmospheric pressure of the plasma jet system were recorded. The resulting spectral distribution was plotted as amplitude versus wavelength. The emission spectra of the synthesis reaction of NCQDs under microplasma were recorded using the OES technique. The spectrum consists of several characteristic spectral lines of specific atoms and ions of Ar. In this study, to observe the signals of nickel ions, the emission spectra were measured using an HR2000 + E.S. spectrometer (Ocean Optics, Inc.) during the reaction process (Figure 1).

2.2.1. Reaction setup

To carry out the OES measurements in the synthesis reaction of NCQDs, a 400-µm-in-diameter glass optical fibre with a length of 1 meter was connected to an HR2000 + E.S. spectrometer (Ocean Optics, Inc.). This optical fibre functions as a detection probe. The HR2000 + E.S. spectrometer was then connected to a computer where Oceanview 2.0.8 software was installed for data recording and control. Briefly, in each OES measurement, the optical fibre was positioned and fixed by a holder at a distance of 1 mm above the plasma-liquid-catalyst interface. The OES signal was recorded in a dark room to avoid systematic errors due to the noise from the visible light background. All spectra were recorded in the wavelength range 200 nm to 1000 nm, with an integration time of 100 ms and averaged over 20 measurements per spectrum. The experimental measurements were triplicated to avoid systematic errors.

2.2.2. Validating various bimetallistic catalysts on fabrication reaction of NCQDs

In this study, different types of multi-element metal catalysts (Sn-coated Cu, $Cu_{90}Ni_{10}$, and $Ni_{80}Cr_{20}$) were used to understand better the effect of plasma catalysis on the NCQDs synthesis. The experimental design for NCQDs plasma-assisted microplasma synthesis is shown in Table 1.

Table 1. *Experimental configuration of plasma-assisted microplasma synthesis of NCQD*

Configuration	Distant	Contact	Deflection
Plasma length	10 mm	10 mm	4 mm
Catalyst size	500 μm	500 μm	500 μm
Catalyst layer thickness	2 mm	2 mm	2 mm
Mass	0.5 g	0.5 g	0.5 g

2.3. Electric potential analysis of bimetallistic catalysts

Electric potential is created between two dissimilar metals in an electrochemical reaction. This potential measures the energy per unit charge available from the oxidation/reduction reactions to drive the reaction. It is customary to visualise the cell reaction in terms of two half-reactions, an oxidation half-reaction and a reduction half-reaction. The electrochemical potentials of the catalysts can be calculated as follows (1):

$$E^0_{Catalyst} = E^0_{Oxidation} - E^0_{Reduction} \quad (1)$$

2.4. Thermal Imaging using FLIR camera and surface profile

Regarding thermal imaging, a FLIR camera was set up to capture the thermal graphs of pure plasma, plasma-$Ni_{80}Cr_{20}$, and plasma-liquid-$Ni_{80}Cr_{20}$ interaction, by infrared imaging. The camera captured images of the reactor to reproduce the liquid surface profile. The plasma-liquid-catalyst interface was re-drawn by Adode Photoshop 2020 software. These surface curves are digitalised for further surface profile investigation.

3. Results and discussion

3.1. Setting of thin liquid layer and plasma–liquid–catalyst interfaces

As the main motivation, we aimed to advance multiphase plasma design to promote phase-physical properties and fluid/interfacial transport for chemical reactions. The chemical engineering literature often overlooks the plasma pre-determination of process design. Microfluidic operation and flow chemistry [33-37], have proven to be particularly beneficial

in the defined process setting and to intensify reactions. Our process design is driven by the microfluidic microplasma [35]. Micro-scale phenomena have been reported in plasma processing, including their impact on Brownian motion gas-liquid, 'multiphase') [38] and thermophoresis, selective particle movement along a temperature gradient [39].

As second motivation, our experiments are inspired by OES's reported monitoring effectiveness to steer multiphase plasma reactions [40] Aadim et al. reported that changing the gas flow can change the emission intensity, which means that the number of excited species can be tuned [40].

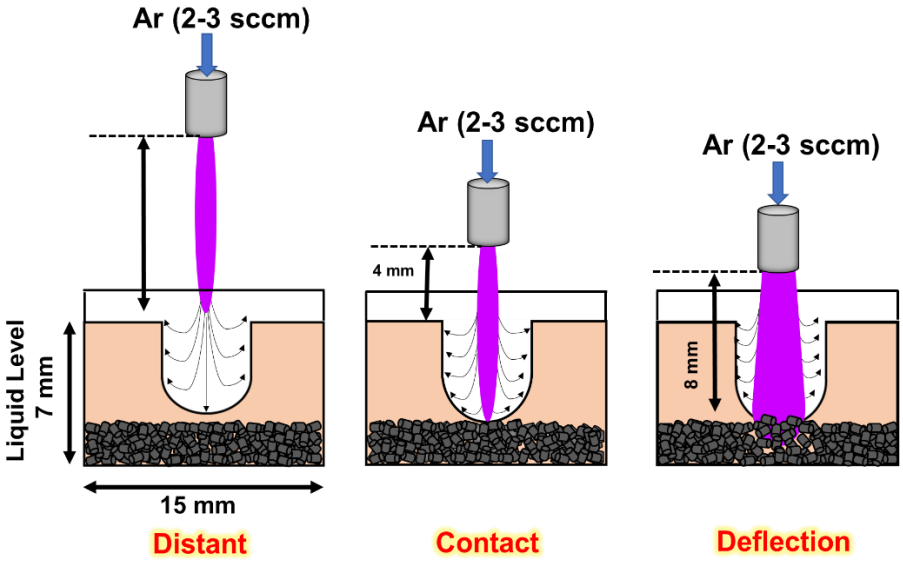

Figure 2. Generic configurations of the microplasma jet-liquid system at different operational modes with various metal catalysts.

We choose three generic configurations for positioning the plasma jet relative to the liquid surface (Figure 2). In the 'distant' position, the most protruding part, the tip of the microplasma jet, does not contact the liquid surface but rather generates only a small crater. The reaction is assumed to be essentially gas-liquid. It is believed to have little effect on liquid-phase hydrodynamics and mass transfer. In the 'contact' position, we emulate the high-intensity gas-liquid reactor, as reported on a macroscopic scale by Wild et al. [31]. The plasma jet penetrates deeper, forming a liquid film above the catalyst surface. In the "deflection" position, it emulates a "fast impinging jet reactor", a plasma reactor configuration proposed by Botes [32]. The liquid film is further thinned, the diameter of the plasma jet hitting the liquid is larger, and the plasma might penetrate the catalyst. The plasma jet is maximally harshly re-directed, creating a turbulence plasma-gas phase and potentially inducing recirculation of the bulk liquid to support the transport of folic acid

reactant to the film reaction zone and transport of carbon quantum dots out of it in the bulk liquid volume. What is expected is a multiphase system with the continuous renewal of the interface, possibly assisted by the generation and breakup of small droplets from the water surface, following the literature report [41].

3.1.1. Shaping surface profile by metallic flake catalysts

The plasma jet in the deflection mode is stopped at the metal ($Ni_{80}Cr_{20}$) flakes interface surrounded by a liquid, giving rise to a different surface profile than water alone, Figure 3. Thus, the flakes drain a liquid microvolume with a large specific interface to the plasma. This phenomenon is not given for the pure water phase. The metal flakes are needed for their catalytic function and to entrain the reaction solvent in a stationary bed by wetting and shaping the multiphase reaction design. Both 'deflection impingement' with and without flakes demonstrates the formation of a deep crater, which is only possible in a microvolume and would not occur with a conventional laboratory beaker size, e.g. 50 or 100 ml, and/or a larger plasma jet.

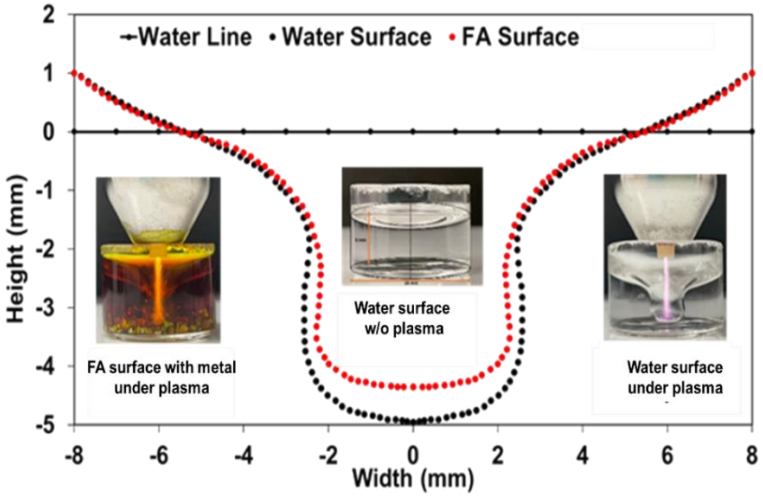

Figure 3. Surface profile of reaction liquid (folic acid) in the presence of $Ni_{80}Cr_{20}$ as compared with water surface with or without plasma at the deflection mode

3.2. Optimising argon ion and water-related excited species concentration at the plasma-liquid interface

The key is generating the right reactive species in great amounts and with high solubility, as the reaction is supposed to be mediated by the liquid phase.

Microfluidic operation is known to complete reactions in seconds which may otherwise take others. Thus, the first reaction experiment is motivated by maximising the number of reactive species per time. We assumed that the argon flow rate correlates with that, meaning the higher, the more reactive species. Our plasma system allows 2 and 3 sccm argon flow rate settings.

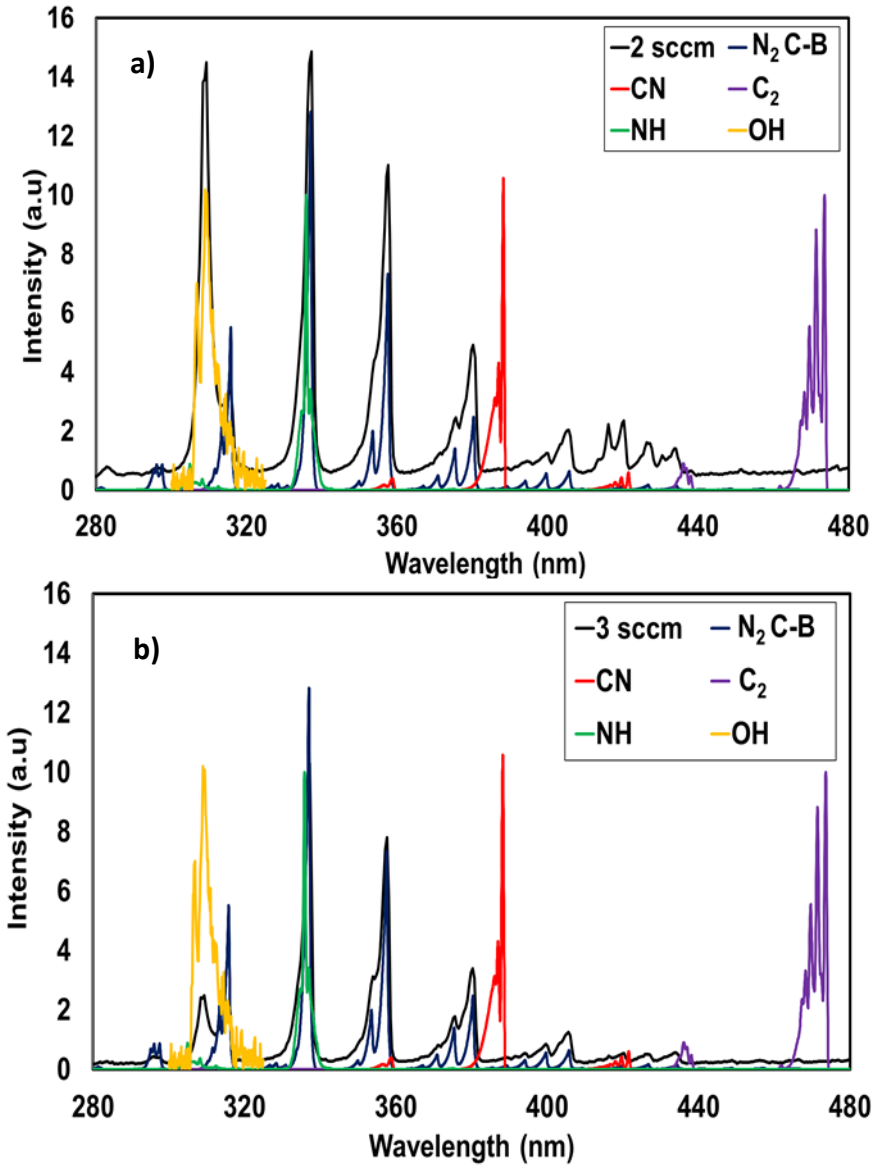

Figure 4. OES analysis of the flow-rate influence at (a) 2 sccm and (b) 3 sccm on the intensity of positively charged species in reaction at the plasma-liquid interface of the synthesis reaction of NCQD with the presence of $Ni_{80}Cr_{20}$ catalysts, as compared with modelled positively charged species (using Specair software)

OES analysis was used for a semi-quantitative determination of the ionised species, as proposed by Bruggeman et al. [42]. Their intensity close to the plasma-liquid interface is

higher at an argon flow rate of 2 sccm than that at a flow rate of 3 sccm, Figure 4 and Figure S1. The impact of longer residence time is more relevant than providing more reactive species. The OES spectrum at 2 sccm (Figure 4a) and 3 sccm (Figure 4b) detects a major share of N_2 C-B. The simulated N_2 0-0 band (337 nm) is narrower than measured, and the left wing of N_2 0-0 band is broader. This is explained by the measured gas temperature T_{gas} at the 2 sccm and 3 sccm being higher than as simulated at 700 K, which would raise the left wing.

The presence of N_2 C-B is because a protective shield was not used to avoid air entrapment to our reaction. Intentionally, we wanted to use N_2 from the air as an abundant source (78% in air) to be ionised by Ar^+ species to form primary N_2^+ species and other secondary ionised nitrogen species.

Besides Ar^+ as the primary reaction species of the plasma, oxygen-containing species such as OH• (309 nm) have to be considered as secondary reactive species from the reaction medium, water. Their concentration is higher at the 2 sccm argon flow rate, consistent with a higher Ar^+ concentration.

Bruggeman et al. reported that a stream of positively charged ions is generated in a plasma jet and bombarded into the plasma-liquid-catalyst interface, causing various reactions [43], given in the equations (2), (3), (4), and (5).

$$Ar + hv \rightarrow Ar^+ + e^- \quad (2)$$

$$N_2 + e^- \rightarrow N_2^* + e^- \quad (3)$$

$$N_2^* + O_2 \rightarrow N_2 + 2O^* \quad (4)$$

$$H_2O + hv \rightarrow OH\bullet + H^+ \quad (5)$$

These generated reactive species (Ar^+, N_2^+, O^+, OH•) can easily penetrate through the liquid surface because their potential energy is large compared to any activation energy barrier (such as surface tension) required to enter the liquid. So cations are mostly immediately solvated when striking the liquid [44]. In addition, these ionised reactive species carry high energy, which can cause reactions at the interface by breaking down the chemical bonding of folic acid in the liquid phase [44].

3.3. Excited species formation in different plasma-liquid-solid process designs

Our previous studies reported the impact of operational modes of the microplasma jet towards the production of NCQD throughout the photoluminescence performance [18]. In this study, we introduced the OES analysis approach to understand better how the

operational modes influence the intensity of ionised Ar gases at the surface interface of plasma-liquid. The position of the jet was adjusted towards the bottom of the reactors at a flow rate of 2 sccm, as described in Figure 2. The intensity of ionised Ar gases at the plasma-liquid-catalyst interface of the synthesis reaction of NCQD (from NIST atomic spectra database lines data) was recorded at distant, contact, and deflection mode (Figure 5).

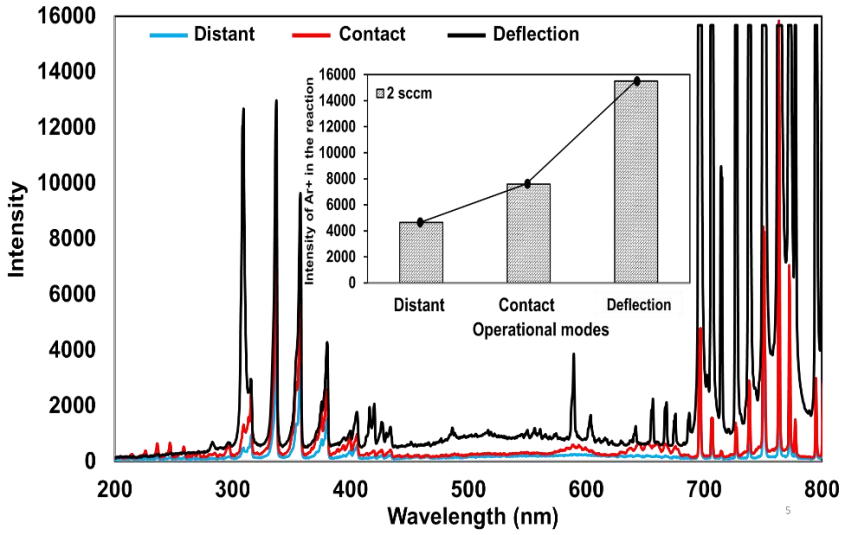

Figure 5. OES spectra of NCQD synthesis at various operational modes with the intensity of ionised Ar gases recorded from OES spectra at the plasma-liquid-catalyst interface (kINPen®IND microplasma jet, 25 °C, 0.1 g/mL folic acid solution, 0.5 g $Ni_{80}Cr_{20}$, 99.99 % Ar gas at 2 sccm).

Figure 5 shows that when shifting the 'distant mode' to 'deflection mode', the intensity of Ar^+ species increases significantly. In particular, the highest intensity of ionised Ar gases produced at the plasma-liquid-catalyst interface was recorded at "deflection" mode, which was nearly 4-fold higher than that at "distant mode". This can be explained by the fact that once the distance of the jet is adjusted closer to the metal layer at the reactor bottom (Figure 2), the morphology of the plasma and plasma-liquid interface becomes unstable or oscillated due to enhanced mixing, convection, and the dissipation of energy into the liquid [45]. Bruggeman et al. reported that external forces associated with plasma production could significantly perturb the surface of the liquid and metal surface at the plasma–liquid-solid interface [43, 46, 47]. Energetic particles at the interface, both charged and uncharged, bombard the surface stronger [48, 49]. Electric fields resulting from the applied voltage and space charge can physically distort the surface [50, 51]. The interaction of streamers at the interface can also be a source of acoustic energy or even shock waves. These acoustic

processes can drive radical production at the plasma-liquid interface or even within the bulk liquid [43]. As a result, the highest intensity of Ar^+ species can be detected in the 'deflection mode'. These instabilities may explain enhanced diffusion leading to in-volume mixing.
After penetrating through the liquid surface, Ar^+ and positively charged ions will cause the decomposition of folic acid into reactive fragments. It can be explained that at "deflection" mode, there is a bulk gas convection associated with plasma, leading to the convection in the liquid with speeds of several $cm.s^{-1}$, sufficient to dominate over diffusion. The moving gas's shear stress caused this induced liquid flow at the interface. Therefore, it can be concluded that the "deflection" mode is the most effective for reactive species transfer from the plasma into the liquid in this reaction.

3.4. Catalyst investigations

3.4.1. Optimising electric potential of bimetallic catalysts

We use metallic flakes of rod shape with mm length and diameter. Knowing from the literature that pure metals (copper) were not optimal for producing carbon quantum dots, we decided to investigate metal alloys. It is known that the electric potential determines the charge transfer capacity [52], and we hypothesised that it might impact the catalytic activity. Alloys provide a smart way to adjust this. This strategy may not only define the electric environment of the heterogeneous catalyst surface but also advance the capacity of the flakes to transfer charged ions from and to the microplasma source, adding homogeneous catalysts. Metallic flakes have been used in heterogeneous catalyses, such as Pd-Cu alloy as acetylene hydrogenation catalysts [53] and Cu–Ni alloy heterogeneous catalysis water dissociation [54]. To our best knowledge, flakes have not been used in plasma catalysis.
The electric potentials of Sn-coated Cu, $Cu_{90}Ni_{10}$, and $Ni_{80}Cr_{20}$ were computed as follows, using the equations (8), (9), and (10).

$$E^o_{Sn/Cu} = E^0_{Cu^{2+}/Cu} - E^0_{Sn^{2+}/Sn} = (+0.34).(0.99) - (-0.14).(0.01) = +0.338\ (V) \quad (8)$$

$$E^o_{Ni/Cu} = E^0_{Cu^{2+}/Cu} - E^0_{Ni^{2+}/Ni} = (+0.34).(0.9) - (-0.25).(0.1) = +0.331\ (V) \quad (9)$$

$$E^o_{Cr/Ni} = E^0_{Ni^{2+}/Ni} - E_{Cr^{3+}/Cr} = (-0.25).(0.8) - (-0.75)(0.2) = +0.350\ (V) \quad (10)$$

$Ni_{80}Cr_{20}$ has the highest electric potential with +0.350 (V), as compared to $Cu_{90}Ni_{10}$ with 0.331 (V) and Sn-coated Cu with 0.338 (V). Electrochemistry in $Ni_{80}Cr_{20}$ is supposed to be facilitated as compared to $Cu_{90}Ni_{10}$ and Sn-coated Cu. This also agrees with the results in

Figure 6 that the microplasma changed the surface structure of $Ni_{80}Cr_{20}$, leading to enhanced catalytic activity.

The structure and components of these catalysts in Figure 6c also explain that Ni is more reactive in electrochemical series than Sn, Cr, and Cu. Therefore, Ni can be easily ionised by charged ions from the plasma to form Ni (I) and Ni (II) ions. On the other, Cu is considered less active than its element counterparts, meaning that its ionisation capacity is much less than Ni, Sn, and Cr. In addition, Cu accounts for a major part of Sn-coated Cu (99.99%) and $Cu_{90}Ni_{10}$ (90%) (Figure 6a and Figure 6b). Therefore, the catalytic surface of these two materials is less activated in terms of electrochemistry.

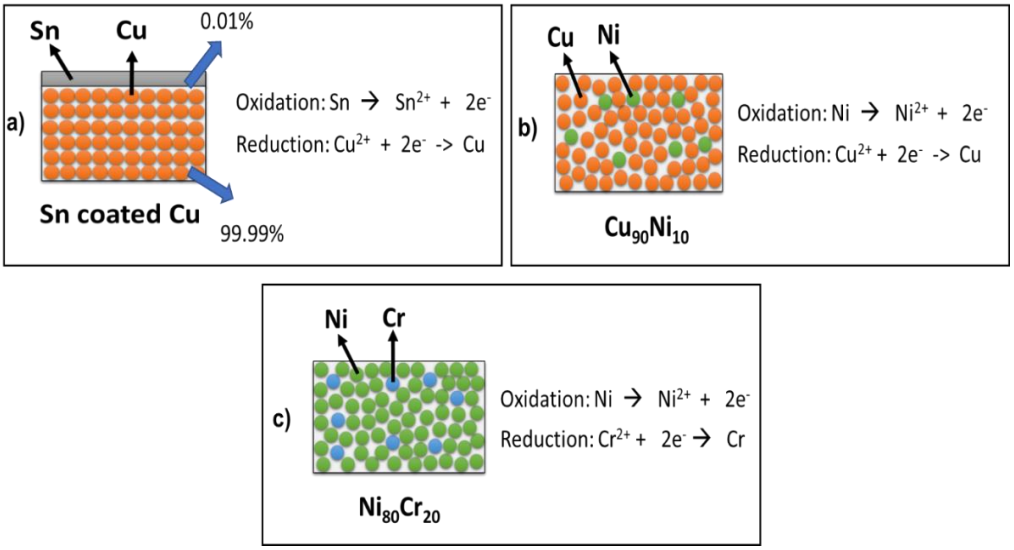

Figure 6. Structure, component, and electrochemistry reaction in (a) Sn-coated Cu, (b) $Cu_{90}Ni_{10}$, (c) $Ni_{80}Cr_{20}$

3.4.2. Copper-based bimetallic catalyst

It has been demonstrated that Cu nanoparticles may act as a catalyst for carbon nanotube growth. Still, growing carbon nanomaterials directly on bulk Cu is only possible with an additional catalyst [55, 56]. Copper is a poor catalyst for carbon nanomaterials growth like CNTs, with smaller activity catalysing the decomposition of carbon stocks and lower carbon solubility [57]. In this study, Sn and Ni were used to add assumed advantageous electric properties to copper, see 3.1., in the form of coated Cu and $Cu_{90}Ni_{10}$ catalysts, respectively [58, 59].

The bimetallic catalyst, Sn-coated Cu catalysis, has been reported to control the surface electronic state and binding energy in the electrocatalysis [60]. The introduction of Sn species in Cu changes the surface selectivity of the catalysts. As a result, the Cu–Sn bimetallic surface exhibited a highly selective and stable catalytic performance [61]. As Sn does not

possess d-vacancies in their electron configuration, the Cu-Sn bimetallic catalysts have negligible affinity for carbon [62].

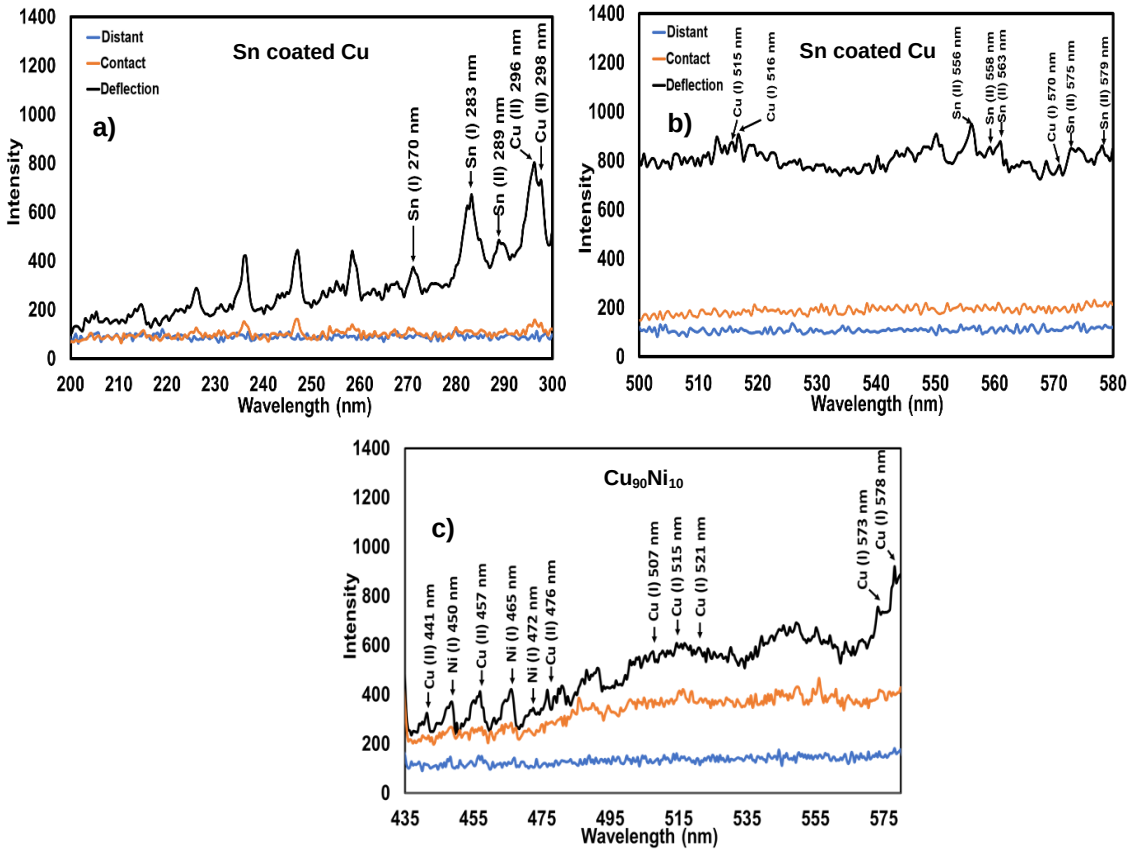

Figure 7. Detailed OES analysis of NCQD synthesis reaction using Sn coated Cu (a,b) and $Cu_{90}Ni_{10}$ (c) under kINPen®IND microplasma jet at various operational modes with Ar flow rate of 2 sccm.

In the excited state, elemental lines of Cu and Sn were detected after exposure to plasma, Figure 7a and Figure 7b. The electron transition at the excited state is described in Table 2, using NIST atomic spectra database [15]. In particular, various typical peaks of Cu (I) at the excited state can be observed, which generates d-vacancies in their electron configuration, such as 507 nm, 516 nm, 456 nm, 521nm, and 573 nm [$d^9(^2D)4s4p(3P^\circ) \rightarrow 3d^94s(^3D)5s$]. In comparison, peaks at 296 nm [$3d^9(^2D)4s4p(^3P^\circ) \rightarrow 3d^94s(^3D)5d$] and 298 nm [$3d^94s^2 \rightarrow 3d^9(^2D)4s4p(^3P^\circ)$] are attributed to Cu (II). The typical peaks of Sn (II) at the excited state after exposure to plasma can also be observed at 556 nm [$5s^26p\ 2P^\circ \rightarrow 5s^26d^2D$] and 289 nm [$5s^25p^2 \rightarrow 5s^25p6d$]. Sn does not play an important role as a catalyst. However, Sn is introduced into Sn-coated Cu to receive electrons from the d-orbital of Cu, leading to the generation of d-vacancies under microplasma treatment.

Previous studies demonstrated that Ni metals are a good catalyst candidate as they possess d-vacancies in their electron configuration [62-64]. Therefore, introducing Ni into Cu to form $Cu_{90}Ni_{10}$ can also enhance the catalytic activity of pure Cu metals. The results in Figure 6c expressed Cu and Sn elemental lines at the excited state after exposure to plasma. The electron transition at the excited state is described in Table 2, using NIST atomic spectra database [15]. Figure 6c showed typical peaks of Ni (I) at 450 nm, 465 nm, and 472 nm [$3d^9(^2D)4p \rightarrow 3d^8 4s(^4F)5s$], while typical peaks of Cu (II) can be observed at 441 nm [$3d^9(^2D^{5/2})4d \rightarrow 3d^9(^2D^{5/2})6p$], 457 nm [$3d^9(2D)4s4p(3P^\circ) \rightarrow 3d^9 4s(3D)5s$], 476 nm [3d8(3F)4s4p(3P°) → 3d9(2D3/2)5d]. In addition, typical peaks of Cu (I) can be observed at 507 nm, 516 nm, 456 nm, 521nm, and 573 nm [$d^9(2D)4s4p(3P^\circ) \rightarrow 3d^9 4s(3D)5s$], 578 nm [$3d^9 4s^2 \rightarrow 3d^{10}4p$].

Table 2. Summary of emission lines of Sn-coated Cu and $Cu_{90}Ni_{10}$ from OES spectra

Ions	Transition	Wavelength
Cu (I)	$3d^{10}4p \rightarrow 3d^{10}4d$	515 nm
	$3d^9(^2D)4s4p(^3P^\circ) \rightarrow 3d^9 4s(^3D)5s$	516 nm
	$3d94s^2 \rightarrow 3d^{10}4p$	570 nm
	$3d^9(^2D)4s4p(^3P^\circ) \rightarrow 3d^9 4s(^3D)5s$	507 nm
	$3d^9(^2D)4s4p(^3P^\circ) \rightarrow 3d^9 4s(^3D)5s$	521 nm
	$3d^9(^2D)4s4p(^3P^\circ) \rightarrow 3d^9 4s(^3D)5s$	573 nm
	$3d^9 4s^2 \rightarrow 3d^{10}4p$	578 nm
Cu (II)	$3d^9(^2D^{5/2})4d \rightarrow 3d^9(^2D^{5/2})6p$	441 nm
	$3d^9(^2D)4s4p(^3P^\circ) \rightarrow 3d^9 4s(^3D)5s$	457 nm
	$3d^8(^3F)4s4p(^3P^\circ) \rightarrow 3d^9(^2D^{3/2})5d$	476 nm
	$3d^9 4s^2 \rightarrow 3d^9(^2D)4s4p(^3P^\circ)$	298 nm
	$3d^9(^2D)4s4p(3P^\circ) \rightarrow 3d^9 4s(^3D)5d$	296 nm
Sn (II)	$5s^2 6p\ 2P^\circ \rightarrow 5s^2 6d^2D$	556 nm
	$5s^2 5d\ ^2D \rightarrow 5s^2 4f$	558 nm
	$5s^2 5p^2 \rightarrow 5s^2 5p6s$	563 nm
	$5s^2 5p6s \rightarrow 5s^2 5p4f$	575 nm
	$5s^2 5d\ ^2D \rightarrow 5s^2 4f$	579 nm
	$5s^2 5p^2 \rightarrow 5s^2 5p6s$	270 nm
	$5s^2 5p^2 \rightarrow 5s^2 5p6s$	283 nm
	$5s^2 5p^2 \rightarrow 5s^2 5p6d$	289 nm
Ni (I)	$3d^9(^2D)4p \rightarrow 3d^8 4s(^4F)5s$	450 nm
	$3d^8(^3F)4s4p(^3P^\circ) \rightarrow 3d^8 4s(^4F)5s$	465 nm
	$3d^8(^3F)4s4p(^3P^\circ) \rightarrow 3d^8 4s(^4F)5s$	472 nm

It can be concluded that the introduction of Sn and Ni metals can enhance the catalytic activity of Cu under plasma treatment. In addition, it can be seen in Figure 7 that increasing the distance of the jet to the "deflection" mode leads to a significant increase in the intensity of typical peaks with an election transition to the excited state, which then increases a negligible affinity for carbon species. At this position, the surface of Sn-coated Cu and $Cu_{90}Ni_{10}$ bimetallic catalysts is more catalytically activated by the stream of charged particles in plasma.

3.4.3. Ni-based bimetallic catalyst

$Ni_{80}Cr_{20}$ is a Ni-based bimetallic catalyst and alternative to Cu-based catalysts for the fabrication of NCQD. Unlike its copper counterpart, Ni is considered a transition metal with many d-vacancies in its electron configuration [62]. They have a high negligible affinity to attract reactive carbon species into their surface to form intermediate binding between metal-carbon [65]. In this study, Cr is introduced into Ni to form $Ni_{80}Cr_{20,}$ where Ni accounts for 80% of the mass.

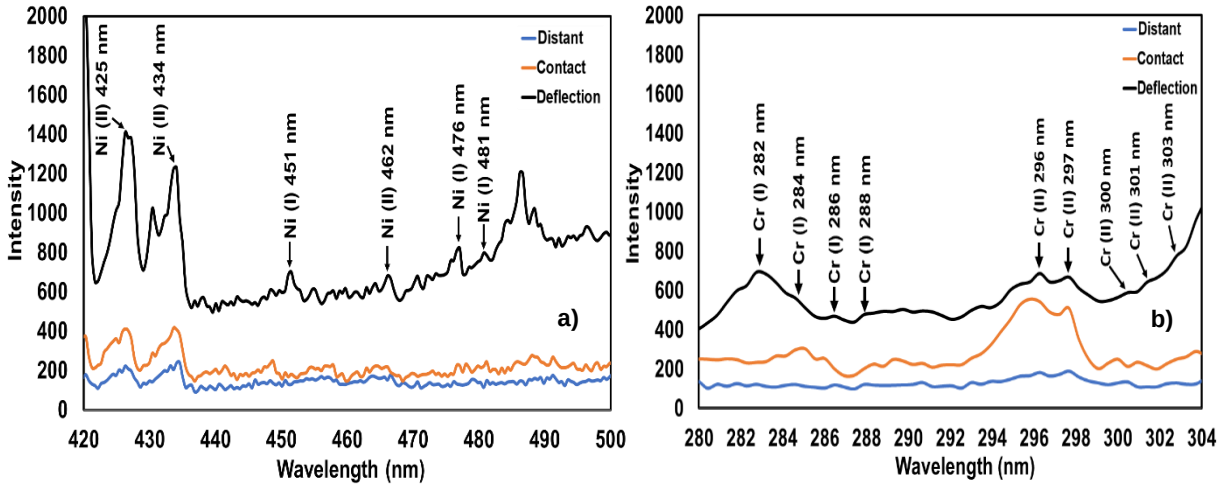

Figure 8. Detailed OES analysis NCQD synthesis reaction using nichrome catalyst under kINPen®IND microplasma jet at various operational modes with Ar flow rate of 2 sccm.

Elemental lines of Ni and Cr in the excited state are detected after exposure to plasma, Figure 8. The electron transition at the excited state is described in Table 3, using NIST atomic spectra database [15]. The results indicated that various strong peaks of Ni (II) at an excited state could be observed at 425 nm [$3p^6 3d^7 2F \rightarrow 3p^6 3d^7\ ^2D_1$], 434 nm [$3d^8(^1D)4s^2 \rightarrow 3d^8(^3F)4s4p(^3P^\circ)$], 462 nm [$3p^6 3d^9\ ^2D \rightarrow 3p^6 3d^8(3P)4s\ ^4P$]. Typical peaks of Ni (I) appeared at 451 nm, 476 nm [$3d^9(^2D)4p \rightarrow 3d^8 4s(^4F)5s$], and 481 nm [$3d^9(^2D)4p \rightarrow 3d^9(^2D_{3/2})4d$].

Typical peaks observed at 282 nm and 284 nm [$3d^4 4s^2 \rightarrow 3d^5(^4F)4p$], 286 nm [$3d^4 4s^2 \rightarrow 3d^4 4s4p$], and 288 nm [$3d^5(^4P)4s \rightarrow 3d^5(^4F)4p$] represent for Cr (I) at the excited state, while peaks at 296 nm [$3d^4(^3G)4s \rightarrow 3d^4(a^3F)4p$], 297 nm $3d^4(^3H)4s \rightarrow 3d^4(^3H)4p$], 300 nm [$3d^5 \rightarrow 3d^4(^3H)4p$], 301 nm [$3d^4(^5D)4p \rightarrow 3d^4(^5D)5s$], and 303 nm [$3d^5 \rightarrow 3d^4(^5D)4p$] are attributed at the excited state. In addition, as can be seen in Figure 8, the intensity of Ni (I) and Ni(II) is much higher than that of Cr (I) and Cr (II), meaning that Ni plays the main role in the catalytic activity of $Ni_{80}Cr_{20}$, while Cr (I) and Cr (II) is considered as a catalytic enhancer.

Table 3. Summary of elemental emission lines of $Ni_{80}Cr_{20}$ from OES spectra

Species	Transition	Wavelength
Ni (I)	$3d^9(^2D)4p \rightarrow 3d^8 4s(^4F)5s$	451 nm
	$3d^9(^2D)4p \rightarrow 3d^8 4s(^4F)5s$	476 nm
	$3d^9(^2D)4p \rightarrow 3d^9(^2D_{3/2})4d$	481 nm
Ni (II)	$3p^6 3d^7\ ^2F \rightarrow 3p^6 3d^7\ ^2D_1$	425 nm
	$3d^8(^1D)4s^2 \rightarrow 3d^8(^3F)4s4p(^3P^o)$	434 nm
	$3d^9(^2D)4p \rightarrow 3d^8 4s(^4F)5s$	462 nm
Cr (I)	$3d^4 4s^2 \rightarrow 3d^5(^4F)4p$	282 nm
	$3d^4 4s^2 \rightarrow 3d^5(^4P)4p$	284 nm
	$3d^4 4s^2 \rightarrow 3d^4 4s4p$	286 nm
	$3d^5(^4P)4s \rightarrow 3d^5(^4F)4p$	288 nm
Cr (II)	$3d^4(^3G)4s \rightarrow 3d^4(a^3F)4p$	296 nm
	$3d^4(^3H)4s \rightarrow 3d^4(^3H)4p$	297 nm
	$3d^5 \rightarrow 3d^4(^3H)4p$	300 nm
	$3d^4(^5D)4p \rightarrow 3d^4(^5D)5s$	301 nm
	$3d^5 \rightarrow 3d^4(^5D)4p$	303 nm

The elemental lines of Ni and Cr in the excited state indicate proficiency in d-vacancies in their electron configuration. This means that the microplasma changed the surface structure of $Ni_{80}Cr_{20}$, leading to enhanced catalytic activity.

The results in Figure 8 also indicated that the intensity of Ni and Cr increased significantly when shifting the operational modes from “distant” to “deflection”. This demonstrated that

plasma enhanced catalytic activity to $Ni_{80}Cr_{20}$ at "deflection" mode by bombarding an influx of electrically charged particles (electrons and ions) on this bimetallic catalyst's surface. The electrons in the surface of $Ni_{80}Cr_{20}$ are excited from the ground state to form an activated surface for catalysis.

3.4.4. *Selection of catalysts for carbon quantum dot synthesis*

It has been known that bimetallic catalysts can exhibit improvements over monometallic catalysts in various catalytic performance metrics for applications, including petrochemical processing, ammonia synthesis, and three-phase catalysis, among many others. Introducing a secondary metal atom to construct dual metallic, active sites is significantly effective in optimising the catalytic centres' adsorption–desorption behaviours. Copper-based and Ni-based bimetallic catalysts were investigated using OES analysis to select the best potential catalysts for plasma fabrication of NCQD.

In comparison with Sn-coated Cu and $Cu_{90}Ni_{10}$ counterparts (Figure 7), $Ni_{80}Cr_{20}$ catalysts (Figure 8) has a much higher intensity of Ni (I) and Cr (I) and Cr (II) at the excited state after exposure to microplasma with many typical sharp peaks. In particular, the intensity of Ni (I) can reach 1400 (a.u) in $Ni_{80}Cr_{20}$, while the intensity of Cu (I) can only reach roughly 800 (a.u), meaning that the surface of $Ni_{80}Cr_{20}$ is more catalytically activated than that of Sn coated Cu and $Cu_{90}Ni_{10}$. The results in Figure 8 also reflect the catalytic performance of $Ni_{80}Cr_{20}$ compared to that of Sn-coated Cu and $Cu_{90}Ni_{10}$. This result is also in agreement with electric potential calculations in section 3.4.1 that is more active in terms of electrochemistry.

3.5. Thermal analysis of the plasma-catalysis system

Thermal imaging of the fabrication reactors was conducted to understand better how plasma influences heat transfer. Figure 9 shows thermal imaging of the plasma jet, plasma-$Ni_{80}Cr_{20}$ interaction and plasma-liquid-$Ni_{80}Cr_{20}$ interaction. Reuter et al. reported that the nonthermal kINPen®IND is pen-sized and can be held like a scalpel or pencil [66]. Its low gas temperature of less than 40 °C and highly reactive non-equilibrium chemistry [66].

The results in Figure 9a indicate that the plasma temperature in the kINPen®IND jet is about 28 ^{0}C, meaning the plasma is nonthermal. The temperature changes when interacting with liquid and metal catalysts were also investigated. Figure 9b shows that the temperature in the reactor increases up to about 37 ^{0}C. This means that the plasma-$Ni_{80}Cr_{20}$ interaction induces a thermal effect in the system. The plasma stream of particles (ionised gas, electron,

etc.) with high-energy photons continuously bombards the surface of $Ni_{80}Cr_{20}$ [43]. The electrons at the plasma-$Ni_{80}Cr_{20}$ interface absorb the energy from the plasma to a higher level (excited state) [67]. These excited electrons return to the ground state and emit the emission light [67], which is recorded by the OES spectroscopy, Figure 8 in section 3.3.2. Along with the emission being emitted, the extra energy was released as a heat [43].

However, the temperature of the plasma-$Ni_{80}Cr_{20}$ interaction drops significantly to about 23 ^{0}C when the folic acid solution (as liquid) is added to the system (Figure 9c). Heat and mass transfer occur at the plasma-liquid-$Ni_{80}Cr_{20}$ interface, causing the water evaporation process. Evaporation is an endothermic process decreasing the temperature [68].

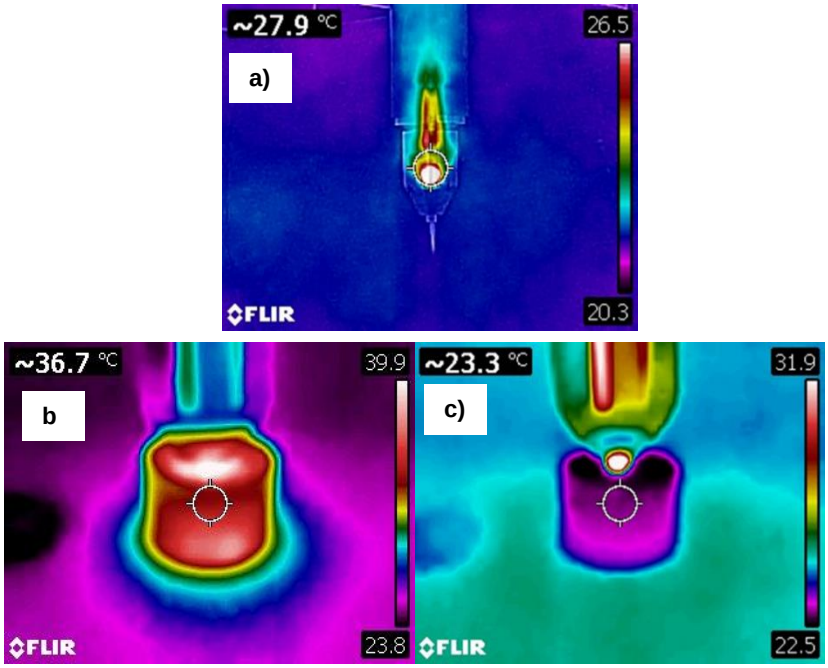

Figure 9. Thermal imaging of (a) pure plasma, (b) plasma-$Ni_{80}Cr_{20}$ interaction, (c) plasma-liquid-$Ni_{80}Cr_{20}$ interaction

3.6. Mechanism of plasma-liquid-catalysts synthesis of N-doped quantum dots

This study proposes a mechanism of the synthesis reaction of N-doped quantum dots in the plasma-liquid-catalyst system (Figure 10) based on the OES analysis and surface profile study provided in this manuscript. In the plasma catalysis [69], plasma affects the energy barrier of the reaction in synergy with the catalyst, thus changing the catalytic activity [27].

3.6.1. Our results summary

The following results led us to propose the reaction mechanism.

(1) A previous study demonstrated the presence of plasma catalysis, i.e. a higher conversion in the presence of a catalyst next to the plasma (reaction intensification) [69].

(2) This study identified the flow rate for delivery of maximal argon ion, Ar^+ concentration, which are formed in the gas phase. We found that Ar^+ generates secondary reactive species at the plasma-water interface, and O^+ and O.H.* were detected.

(3) The formation is maximal in the 'deflection case' with the liquid layer thinned much, facilitating the transport of the Vitamin B9 precursor to the plasma-liquid surface as well as to the catalyst and the contact of the plasma with the catalyst.

(4) The best catalyst was identified, meaning the right metals and their right dual composition to set the best electric potential.

(5) Metal reactive species were also detected in the gas phase near the liquid surface; it is unclear if they play a role in the catalysis of the reaction or signal that the plasma-catalysis is intense (as a signal effect, yet of no relevance to the reaction). If these catalyse the reaction, a homogeneous pathway is opened beside the known heterogeneous one.

3.6.2. Literature results summary

We add to our findings relevant knowledge from plasma-multiphase literature.

(1) It has been reported that charged ions and particles can penetrate through a plasma-liquid interface [43], as the potential energy of positive and negatively charged particles is larger than the surface tension energy [43]. Charged particles (Ar^+, N_2^+, O^+, e^-, etc.) are immediately hydrated when striking the liquid [70].

(2) Plasma is known for causing atomic abrasion of the surface of metal catalysts [71]. Photon, electron and ion deposition induces surface charging ($Ni^{2+}$and Ni^+) to attract more water molecules to form a hydrate complex.

(3) Water molecules absorb the UV energy photons to release more OH• reactive species, leading to intensification of reactive species in the liquid.

3.6.3. Deduction of reaction mechanism from own results and literature

Based on these experimental demonstrations and literature reports, seven steps are hypothesis for the mechanism of the plasma-catalytic Vitamin-B9 reaction.

(1) Creation of excited species from plasma gas and water solvent.

(2) Atomic abrasion of the metal surface of $Ni_{80}Cr_{20}$ catalysts.

(3) Mass transport of excited species (Ar^+, N_2^+, O^+, etc.) through the plasma-liquid interface and into the liquid film.

(4) Ionisation on the surface of catalyst to form charged surface.

(5) Nickel ions attracts water molecules to form a hydrate complex

(6) Water molecules absorb the UV energy photons to release OH• reactive species, leading to intensification of reactive species in the liquid.

(7) Ar^+, N_2^+, O^+ along with OH• reactive species decompose folic acid to form N-doped carbon quantum dots.

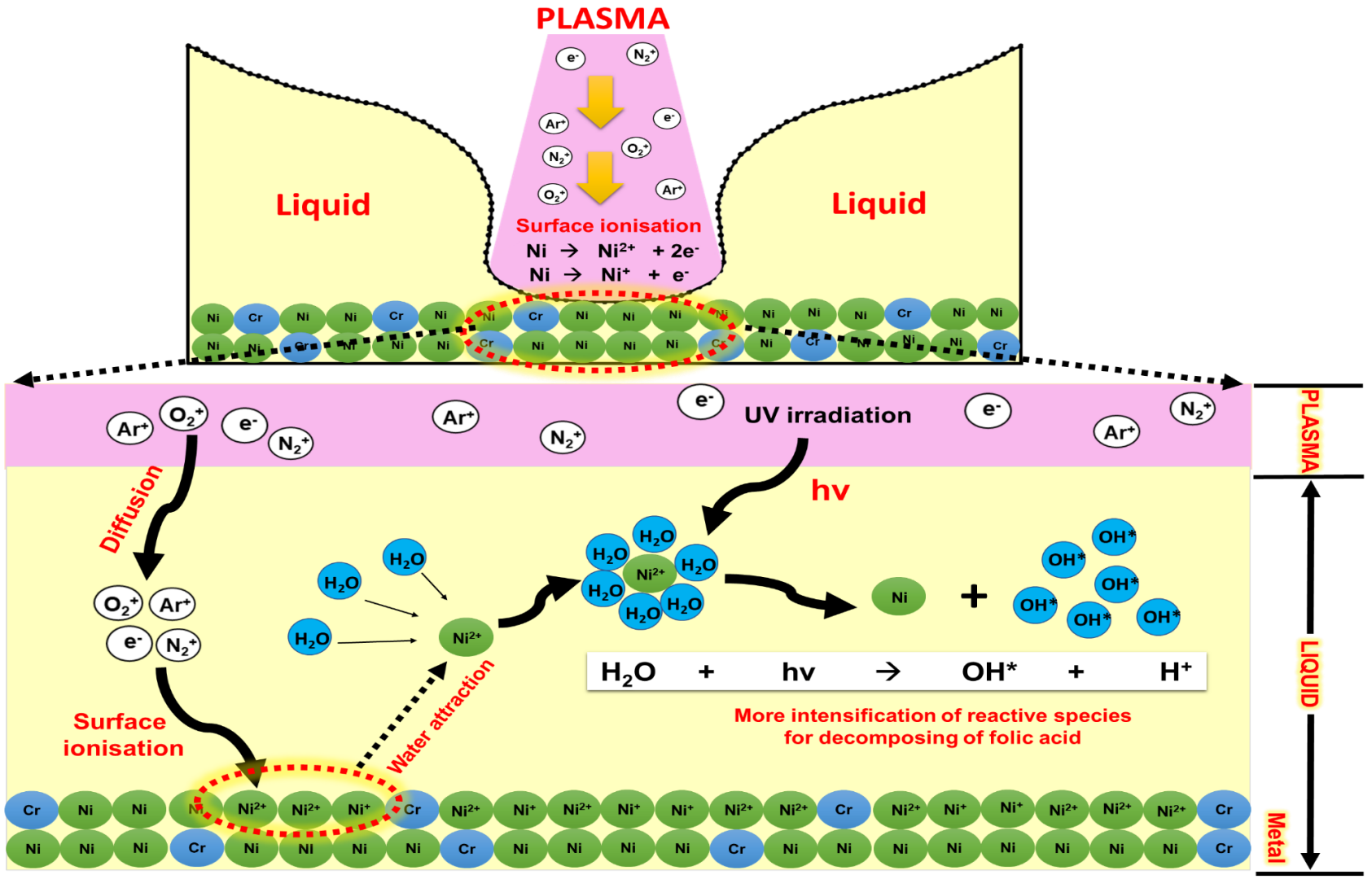

Figure 12. Proposed mechanism of plasma-liquid-catalyst synthesis of N-doped carbon quantum dots

4. Conclusions

The process of multiphase plasma catalysis, in this study, is utilized to synthesise N-doped carbon quantum dots. This is achieved by directing a submerged plasma jet into a small amount of liquid that contains the precursor and catalytic alloy flakes. Optical emission spectroscopy was used to observe and analyse the reaction mechanism, focusing on the role of plasma catalysis. The depth of the plasma jet's penetration affects the interaction with the liquid and catalyst in a typical hydrodynamic manner. The deepest penetration, referred to as the "deflection mode," produced more positively charged species from the metal catalyst. Among the three alloy catalysts examined, $Ni_{80}Cr_{20}$ showed the strongest effect, which correlated with the highest electric potential. There are seven main steps in the proposed reaction mechanism leading to the production of N-doped Quantum Dots. IR imaging indicated that the temperature at the plasma-liquid-catalyst interface was below 25 ^{0}C, although significant water evaporation occurred at the surface due to high convective phases.

5. Outlook

Therefore, we could conduct a comprehensive chemical engineering study, focusing on plasma catalysis reaction, electro-plasma chemistry, thermal properties of reaction, heat mass transfer, and fluid mechanics in the way of traditional reactor engineering and process design. We added the point of view of using catalysts for the plasma synthesis of NCQD, followed by the concept of using OES analysis for a simple and quick characterisation of the reaction. We proposed a mechanism of plasma-liquid-catalysts synthesis of N-doped quantum dots for the first time, which will open a new window in the synthesis of NCQD at the plasma-liquid-catalyst (solid) interface.

Credit authorship contribution statement

Quoc Hue Pho: Conceptualization, Methodology, Formal analysis, Investigation, Data curation, Writing – original draft. **Quan Hoang Tran, Changping Zhuang, Van Long Nguyen**: Investigation, Data curation. **Nam Nghiep Tran, Evgeny V. Rebrov**: Writing – review & editing. **Thanh Tung Tran**: Conceptualization, Writing- Review and Editing. Dusan Losic: Writing – review & editing, Supervision. **Zdenko Machala:** Formal analysis, Data curation. **Volker Hessel:** Conceptualization, Writing – review & editing, Supervision.

Conflict of Interest

The authors declare that they have no conflict of interest.

Acknowledgements

Mr. Hue Quoc Pho received the divisional ECMS and full-fee scholarships from the University of Adelaide, Australia. The authors acknowledge support from the ERC Grant Surface-Confined fast-modulated Plasma for process and Energy intensification (SCOPE) from the European Commission with grant number 810182.

References

1. Döring, A., E. Ushakova, and A.L. Rogach, *Chiral carbon dots: synthesis, optical properties, and emerging applications.* Light: Science & Applications, 2022. **11**(1): p. 1-23.
2. Li, S., et al., *The development of carbon dots: From the perspective of materials chemistry.* Materials Today, 2021. **51**: p. 188-207.
3. Wang, B. and S. Lu, *The light of carbon dots: From mechanism to applications.* Matter, 2022. **5**(1): p. 110-149.
4. Beckers, S., S. Peil, and F.R. Wurm, *Pesticide-Loaded Nanocarriers from Lignin Sulfonates—A Promising Tool for Sustainable Plant Protection.* ACS Sustainable Chemistry & Engineering, 2020. **8**(50): p. 18468-18475.
5. Tran, N.N., et al., *Nanofertilizers and Nanopesticides for Crop Growth*, in *Plant and Nanoparticles*, J.-T. Chen, Editor. 2022, Springer Nature Singapore: Singapore. p. 367-394.
6. Li, X., et al., *Review on Structures of Pesticide Targets.* Int J Mol Sci, 2020. **21**(19).
7. Shivashakarappa, K., et al., *Nanotechnology for the detection of plant pathogens.* Plant Nano Biology, 2022. **2**: p. 100018.
8. Lowry, G.V., A. Avellan, and L.M. Gilbertson, *Opportunities and challenges for nanotechnology in the agri-tech revolution.* Nature nanotechnology, 2019. **14**(6): p. 517-522.
9. Pho, Q.H., et al., *Perspectives on plasma-assisted synthesis of N-doped nanoparticles as nanopesticides for pest control in crops.* Reaction Chemistry & Engineering, 2020. **5**(8): p. 1374-1396.
10. Omar, N.A.S., et al., *A Review on Carbon Dots: Synthesis, Characterization and Its Application in Optical Sensor for Environmental Monitoring.* Nanomaterials (Basel), 2022. **12**(14).
11. Kaczmarek, A., et al., *Luminescent Carbon Dots Synthesized by the Laser Ablation of Graphite in Polyethylenimine and Ethylenediamine.* Materials (Basel), 2021. **14**(4).
12. Chao-Mujica, F., et al., *Carbon quantum dots by submerged arc discharge in water: Synthesis, characterization, and mechanism of formation.* Journal of Applied Physics, 2021. **129**(16): p. 163301.

13. Zhu, Z., et al., *One-pot hydrothermal synthesis of fluorescent carbon quantum dots with tunable emission color for application in electroluminescence detection of dopamine.* Biosensors and Bioelectronics: X, 2022. **10**: p. 100141.
14. Otten, M., et al., *Pyrolysis and Solvothermal Synthesis for Carbon Dots: Role of Purification and Molecular Fluorophores.* Langmuir, 2022. **38**(19): p. 6148-6157.
15. Zhang, D., et al., *One-Step Green Solvothermal Synthesis of Full-Color Carbon Quantum Dots Based on a Doping Strategy.* The Journal of Physical Chemistry Letters, 2021. **12**(37): p. 8939-8946.
16. Xu, J., et al., *Ultrasonic-Assisted Synthesis of N-Doped, Multicolor Carbon Dots toward Fluorescent Inks, Fluorescence Sensors, and Logic Gate Operations.* Nanomaterials (Basel), 2022. **12**(3).
17. Pho, Q.H., et al., *Survey of Synthesis Processes for N-Doped Carbon Dots Assessed by Green Chemistry and Circular and EcoScale Metrics.* ACS Sustainable Chemistry & Engineering, 2021. **9**(13): p. 4755-4770.
18. Pho, Q.H., et al., *Process intensification for gram-scale synthesis of N-doped carbon quantum dots immersing a microplasma jet in a gas-liquid reactor.* Chemical Engineering Journal, 2023. **452**: p. 139164.
19. Taheraslani, M. and H. Gardeniers, *Plasma Catalytic Conversion of CH4 to Alkanes, Olefins and H2 in a Packed Bed DBD Reactor.* Processes, 2020. **8**(7): p. 774.
20. Zhang, Y., et al., *Plasma-coupled catalysis in VOCs removal and CO2 conversion: Efficiency enhancement and synergistic mechanism.* Catalysis Communications, 2022. **172**: p. 106535.
21. Chang, T., et al., *A critical review on plasma-catalytic removal of VOCs: Catalyst development, process parameters and synergetic reaction mechanism.* Science of The Total Environment, 2022. **828**: p. 154290.
22. Meng, S., et al., *Nonthermal Plasma-Assisted Photocatalytic Conversion of Simulated Natural Gas for High-Quality Gasoline Production near Ambient Conditions.* The Journal of Physical Chemistry Letters, 2020. **11**(10): p. 3877-3881.
23. Ahmad, F., et al., *Low-Temperature CO2 Methanation: Synergistic Effects in Plasma-Ni Hybrid Catalytic System.* ACS Sustainable Chemistry & Engineering, 2020. **8**(4): p. 1888-1898.

24. Szymanski, L., et al., *Synthesis of Carbon Nanotubes in Thermal Plasma Reactor at Atmospheric Pressure.* Nanomaterials (Basel), 2017. **7**(2).

25. Yanase, T., et al., *Synthesis of Carbon Nanotubes by Plasma-Enhanced Chemical Vapor Deposition Using Fe1-xMnxO Nanoparticles as Catalysts: How Does the Catalytic Activity of Graphitization Affect the Yields and Morphology?* C, 2019. **5**(3): p. 46.

26. Li, D., L. Tong, and B. Gao, *Synthesis of Multiwalled Carbon Nanotubes on Stainless Steel by Atmospheric Pressure Microwave Plasma Chemical Vapor Deposition.* Applied Sciences, 2020. **10**(13): p. 4468.

27. Neyts, E.C., et al., *Plasma Catalysis: Synergistic Effects at the Nanoscale.* Chemical Reviews, 2015. **115**(24): p. 13408-13446.

28. Dey, A., et al., *Ultrafast epitaxial growth of CuO nanowires using atmospheric pressure plasma with enhanced electrocatalytic and photocatalytic activities.* Nano Select, 2022. **3**(3): p. 627-642.

29. Joshi, E., et al., *Formation of droplets in weightless complex plasmas.* Contributions to Plasma Physics, 2021. **61**(10): p. e202100081.

30. Xiong, H. and W. Sun, *Investigation of Droplet Atomization and Evaporation in Solution Precursor Plasma Spray Coating.* Coatings, 2017. **7**(11): p. 207.

31. Botton, R., et al. *A simple gas-liquid mass transfer jet system*. in *8th World Congress of Chemical Engineering*. 2009.

32. Botes, F., L. Lorenzen, and J. Van Deventer, *The development of high intensity gas-liquid jet reactors.* Chemical Engineering Communications, 1998. **170**(1): p. 217-244.

33. CambiØ, D., et al., *2 3 4 5 6 7 8 9 T. No l.* Chem. Rev, 2016. **116**: p. 10276-10341.

34. Billaud, E.M.F., et al., *Micro-flow photosynthesis of new dienophiles for inverse-electron-demand Diels–Alder reactions. Potential applications for pretargeted in vivo PET imaging.* Chemical Science, 2017. **8**(2): p. 1251-1258.

35. Lin, L., et al., *Microfluidic plasmas: Novel technique for chemistry and chemical engineering.* Chemical Engineering Journal, 2021. **417**: p. 129355.

36. Lin, L., et al., *Microfluidic fabrication of fluorescent nanomaterials: A review.* Chemical Engineering Journal, 2021. **425**: p. 131511.

37. Serra, C.A., et al., *Microfluidic Production of Micro- and Nanoparticles*, in *Encyclopedia of Polymer Science and Technology*.

38. Arkar, K., et al., *Dynamics of active Brownian particles in plasma.* Molecules, 2021. **26**(3): p. 561.

39. Lee, N. and S. Wiegand, *Thermophoretic micron-scale devices: practical approach and review.* Entropy, 2020. **22**(9): p. 950.

40. Aadim, K.A., et al. *Influence of Gas Flow Rate on Plasma Parameters Produced by a Plasma Jet and its Spectroscopic Diagnosis Using the OES Technique*. in *IOP Conference Series: Materials Science and Engineering*. 2020. IOP Publishing.

41. Shui, L., J.C.T. Eijkel, and A. van den Berg, *Multiphase flow in microfluidic systems – Control and applications of droplets and interfaces.* Advances in Colloid and Interface Science, 2007. **133**(1): p. 35-49.

42. Bruggeman, P.J., et al., *Plasma–liquid interactions: a review and roadmap.* Plasma Sources Science and Technology, 2016. **25**(5): p. 053002.

43. Bruggeman, P., et al., *Plasma–liquid interactions: a review and roadmap.* Plasma sources science and technology, 2016. **25**(5): p. 053002.

44. Nikiforov, A.Y., *Plasma sputtering of water molecules from the liquid phase by low-energy ions: Molecular dynamics simulation.* High Energy Chemistry, 2008. **42**(3): p. 235-239.

45. Thompson, L., *LK Doraiswamy,"Sonochemistry.* Science and engineering" Ind. Eng. Chem. Res, 1999. **38**(4): p. 1215-1249.

46. Zeleny, J., *Instability of electrified liquid surfaces.* Physical review, 1917. **10**(1): p. 1.

47. Melcher, J.R. and C.V. Smith, *Electrohydrodynamic charge relaxation and interfacial perpendicular-field instability.* The Physics of Fluids, 1969. **12**(4): p. 778-790.

48. Watson, P., *Electrostatic and hydrodynamic effects in the electrical breakdown of liquid dielectrics.* IEEE Transactions on Electrical Insulation, 1985(2): p. 395-399.

49. Sugimoto, T. and Y. Higashiyama, *Production of water drops and corona due to rupture of air bubbles at water surface under a positive dc electric field.* Journal of Electrostatics, 2001. **53**(3): p. 209-219.

50. Hase, M., S.N. Watanabe, and K. Yoshikawa, *Rhythmic motion of a droplet under a dc electric field.* Physical Review E, 2006. **74**(4): p. 046301.

51. Bruggeman, P., et al., *Water surface deformation in strong electrical fields and its influence on electrical breakdown in a metal pin–water electrode system.* Journal of Physics D: Applied Physics, 2007. **40**(16): p. 4779.

52. Guo, Z.-Y., H.-Y. Zhu, and X.-G. Liang, *Entransy—A physical quantity describing heat transfer ability.* International Journal of Heat and Mass Transfer, 2007. **50**(13-14): p. 2545-2556.

53. Qin, F. and W. Chen, *Copper-based single-atom alloys for heterogeneous catalysis.* Chemical Communications, 2021. **57**(22): p. 2710-2723.

54. Ray, D., S. Ghosh, and A.K. Tiwari, *Controlling Heterogeneous Catalysis of Water Dissociation Using Cu–Ni Bimetallic Alloy Surfaces: A Quantum Dynamics Study.* The Journal of Physical Chemistry A, 2018. **122**(26): p. 5698-5709.

55. Kruszka, B., et al., *Synthesis of carbon nanotubes and nanotube forests on copper catalyst.* Materials Research Express, 2014. **1**(3): p. 035040.

56. Atthipalli, G., et al., *Nickel catalyst-assisted vertical growth of dense carbon nanotube forests on bulk copper.* The Journal of Physical Chemistry C, 2011. **115**(9): p. 3534-3538.

57. Li, Y., et al., *How catalysts affect the growth of single-walled carbon nanotubes on substrates.* Advanced Materials, 2010. **22**(13): p. 1508-1515.

58. Ji, Y., A. Guan, and G. Zheng, *Copper-based catalysts for electrochemical carbon monoxide reduction.* Cell Reports Physical Science, 2022. **3**(10): p. 101072.

59. Aflak, N., et al., *Recent Advances in Copper-Based Solid Heterogeneous Catalysts for Azide–Alkyne Cycloaddition Reactions.* International Journal of Molecular Sciences, 2022. **23**(4): p. 2383.

60. Kramida, A., et al., *NIST Atomic Spectra Database (Version 5.8) 2020.* National Institute of Standards and Technology: Gaithersburg, MD, USA, 2020.

61. Sarfraz, S., et al., *Cu–Sn Bimetallic Catalyst for Selective Aqueous Electroreduction of CO2 to CO.* ACS Catalysis, 2016. **6**(5): p. 2842-2851.

62. Jourdain, V. and C. Bichara, *Current understanding of the growth of carbon nanotubes in catalytic chemical vapour deposition.* Carbon, 2013. **58**: p. 2-39.

63. Meloni, E., M. Martino, and V. Palma, *A Short Review on Ni Based Catalysts and Related Engineering Issues for Methane Steam Reforming.* Catalysts, 2020. **10**(3): p. 352.

64. Oshchepkov, A.G., et al., *Recent Advances in the Understanding of Nickel-Based Catalysts for the Oxidation of Hydrogen-Containing Fuels in Alkaline Media.* ACS Catalysis, 2020. **10**(13): p. 7043-7068.

65. Zhu, M., et al., *Vacancy engineering of the nickel-based catalysts for enhanced CO2 methanation.* Applied Catalysis B: Environmental, 2021. **282**: p. 119561.

66. Reuter, S., T. Von Woedtke, and K.-D. Weltmann, *The kINPen—A review on physics and chemistry of the atmospheric pressure plasma jet and its applications.* Journal of Physics D: Applied Physics, 2018. **51**(23): p. 233001.

67. Dorfs, D., et al., *Comprehensive Nanoscience and Technology (2011).* Ch. **1**: p. 219.

68. Kim, Y., et al., *Novel mechanical vapor recompression-assisted evaporation process for improving energy efficiency in pulp and paper industry.* International Journal of Energy Research, 2022. **46**(3): p. 3409-3427.

69. Yan, C., et al., *Recent Advances in Plasma Catalysis.* The Journal of Physical Chemistry C, 2022. **126**(23): p. 9611-9614.

70. Gaisin, A.F. and E.E.e. Son, *Vapor-air discharges between Jet electrolytic cathode and metal anode at low pressure.* Teplofizika vysokikh temperatur, 2010. **48**(3): p. 470-472.

71. Hartl, H., et al., *Multiscale Plasma-Catalytic On-Surface Assembly.* Small, 2020. **16**(12): p. 1903184.

BLANK PAGE

Chapter 7

Stagnant Liquid Layer as "Microreaction System" in Submerged Plasma Micro-Jet

This chapter aims to intensify reactivity via bespoke transient hydrodynamics in a plasma-activated three-phase catalyst system. In this hydrodynamic regime, plasma can penetrate the catalyst bed via the stagnant thin liquid film and polarise the plasma-liquid interface. Evidence for the effectivity of the new process regime is the determination of the enlargement of the reaction rate by increasing liquid component diffusivity towards the catalyst bed via reducing the solvent's viscosity.

This chapter has been prepared as a research paper manuscript and supposed to be submitted to "Chemical Engineering Journal" as follows:

Pho, Q.H., Hessel, V., Rebrov, E.V., Lamichhane, P., Tran, N.N., and Losic, D., 2023. Stagnant Liquid Layer as "Microreaction System" in Submerged Plasma Micro-Jet for Formation of Carbon Quantum Dots. Chemical Engineering Journal. **(Submitted).**

Statement of Authorship

Title of Paper	Stagnant Liquid Layer as "Microreaction System" in Submerged Plasma Micro-Jet for Formation of Carbon Quantum Dots
Publication Status	☐ Published ☐ Accepted for Publication ☑ Submitted for Publication ☐ Unpublished and Unsubmitted w ork w ritten in manuscript style
Publication Details	**Pho, Q.H.,** Hessel, V., Rebrov, E.V., Lamichhane, P., Tran, N.N., and Losic, D., 2023. Stagnant Liquid Layer as "Microreaction System" in Submerged Plasma Micro-Jet for Formation of Carbon Quantum Dots. Chemical Engineering Journal. **(Submitted).**

Principal Author

Name of Principal Author (Candidate)	Quoc Hue Pho		
Contribution to the Paper	Conceptualization, Methodology, Formal analysis, Investigation, Data curation, Writing – original draft		
Overall percentage (%)	65%		
Certification:	This paper reports on original research I conducted during the period of my Higher Degree by Research candidature and is not subject to any obligations or contractual agreements with a third party that would constrain its inclusion in this thesis. I am the primary author of this paper.		
Signature		Date	28.01.2023

Co-Author Contributions

By signing the Statement of Authorship, each author certifies that:

i. the candidate's stated contribution to the publication is accurate (as detailed above);
ii. permission is granted for the candidate in include the publication in the thesis; and
iii. the sum of all co-author contributions is equal to 100% less the candidate's stated contribution.

Name of Co-Author	Evgeny V. Rebrov		
Contribution to the Paper	Conceptualization, Data curation, Writing – review & editing, Supervision.		
Signature		Date	08.02.2023

Name of Co-Author	Nam Nghiep Tran		
Contribution to the Paper	Conceptualization, Writing- Review and Editing.		
Signature		Date	28.01.2023

Please cut and paste additional co-author panels here as required.

Name of Co-Author	Dusan Losic		
Contribution to the Paper	Co-supervised and Writing- Review and Editing		
Signature		Date	08.02.2023

Name of Co-Author	Pradeep Lamichhane		
Contribution to the Paper	Conceptualization, Writing- Review and Editing.		
Signature	on behalf of co-author	Date	08.02.2023

Name of Co-Author	Volker Hessel		
Contribution to the Paper	Supervised ((scientific ideas, concepts, objectives, assessment of achievement degree, societal impact), Conceptualised, Writing – review & editing, and is the corresponding author.		
Signature		Date	28.01.2023

Stagnant Liquid Layer as "Microreaction System" in Submerged Plasma Micro-Jet for Formation of Carbon Quantum Dots

Quoc Hue Pho[a, c*], Volker Hessel[a, c*,**], Evgeny V. Rebrov[c,d] , Pradeep Lamichhane[b], Nam Nghiep Tran[a], Dusan Losic [a, b]

[a] *School of Chemical Engineering, The University of Adelaide, Adelaide, SA 5005, Australia*

[b] *The A.R.C. Graphene Research Hub, School of Chemical Engineering and Advanced Materials, The University of Adelaide, SA 5005, Australia*

[c] *School of Engineering, University of Warwick, Library Rd, Coventry CV4 7AL, England, UK*

[d] *Department of Chemical Engineering and Chemistry, Eindhoven University of Technology, P.O. Box 513, 5600 MB, Eindhoven, the Netherlands*

* First author

** Corresponding author: E-mail: volker.hessel@adelaide.edu.au

Abstract

Reaction kinetics play a critical role in many chemical reactions and are essential for the cost and environmental profile of processes derived from the reactions. This study aims to intensify reactivity *via* bespoke transient hydrodynamics in a plasma-activated three-phase catalyst system. Likewise, three-phase plasma systems in literature are not well designed, understood and commercially available. The synthesised N-doped carbon quantum dots, with application as fertilisers and wastewater treatment was evaluated as a model reaction. We used a commercial plasma system generating a plasma microjet, creating an almost flat, large interface covering a thin stagnant liquid layer with a catalyst bed underneath. In this hydrodynamic regime, plasma can penetrate the catalyst bed *via* the stagnant thin liquid film and polarise the plasma-liquid interface. Evidence for the effectivity of the new process regime is the determination of the enlargement of the reaction rate by increasing liquid component diffusivity towards the catalyst bed via reducing the solvent's viscosity. The results show that the reaction rate is also determined by the interfacial area below the crater rather than the total gas-liquid interfacial area. The plasma process can compete energy-wise with the best dielectric barrier discharge (DBD) plasma processes and consumes lower energy than microfluidic processing in chemical microreactors. The high momentum

transfer from the plasma jet to the liquid causes partial evaporation of volatile additives, other than water, which has to be considered in process design and reduced.

Keywords: plasma three-phase system, N-doped carbon quantum dots, reaction rate, kinetics, diffusivity-limited.

1. Introduction

Alike for highly productive chemical microreactors, applying process intensification principles to small plasma-chemical reaction volumes is essential to amplify productivity. On that backdrop, this submerged plasma jet study reports deciphering the engineering fundamentals of how to enhance mass transport and facilitate catalysis via a metal particle bed of alloy particles to increase reaction rate; beyond the performance achieved in [1]. Leverage is provided *via* bespoke hydrodynamics when penetrating the jet deeper into the reactor volume, displacing the liquid and demonstrating a massive increase in productivity [1]. Depending on the jet penetration into the liquid medium depth, different crater configurations (distant, contact, deflection) form in the liquid, each with different hydrodynamics. Leverage is also provided *via* the achievement of a gas (plasma)–liquid-solid three-phase contact for facilitating catalysis, for which a mechanism was proposed based on excited state analytics using optical emission spectroscopy [2].

Reaction kinetics is critical in chemical and biochemical processes [3, 4]. Hydrodynamics must be tailored to enable the 'best' intrinsic kinetics rather than leading to effective kinetics of reduced effectiveness. Learning can be taken from the principles of high-intensity gas–liquid two-phase reactors [5]. Applications of plasma jet reactors exposed to liquid media have been reported for applications, including wastewater treatment [6] and nanoparticle synthesis [7]; yet their engineering and hydrodynamic principles have not been explored in detail. Previous studies demonstrated that evaporation plays a key role in plasma-liquid systems which motivated the evaporation investigation reported herein [8, 9].

This study varies physico-chemical parameters of the liquid phase to study the hydrodynamics and mass transport, in the absence or in the presence of a catalyst bed of alloy flakes. With the latter, it is determined whether charging effect of the bottom layer by charged plasma species could play an additional role to accelerate the reaction kinetics. A commercial plasma equipment enables facile experimentation, the KINPen®IND reactor, providing a cold atmospheric-pressure microplasma jet with noble gases such as argon [10,

11]. This microplasma jet reactor has attracted considerable literature studies and documentation [5, 12, 13].

As test reaction we selected the formation of carbon quantum dots (CQDs), a recently discovered "zero-dimensional" carbon nanomaterial [14-17], which have applications in various fields such as agriculture [18, 19], environment [20, 21], biology [22, 23], chemistry [24], food science [25, 26], and energy [27-30]. This is due to their favourable properties, such as low toxicity [31], intense luminescence [32], chemical stability [33], biocompatibility [34], and high specific surface area [35]. Extensive research studies on N-doped carbon quantum dots (NCQDs) have been conducted, reporting a large number of diverse structures of this nanomaterial class with distinct properties, made via various synthetic techniques such as pyrolysis [36], hydrothermal [37], solvothermal [38], microwave [39], chemical vapor deposition [40], electrochemical method [41], high-temperature combustion [42], etc.

A challenge still is the capacity for pilot or industrial production of these materials and how to fill this technology gap [43]; this paper explores fundamentals to transition. A techno-sustainability assessment compared six methods for producing NCQDs, with plasma synthesis having the highest energy efficiency but the lowest mass efficiency, resulting in lower productivity compared to the other processes; the latter being also due to the fact those processes are typically conducted in larger reactors. The approach of this study is to use a small reactor that can be numbered up, with high volume-specific productivity, both because of high mass and energy efficiency [44]. This submerged plasma microjet was previously shown to reach gram productivities in a few hours [1], compared to the best reactors in the field [43].

The goal of this study is to understand how the interface between the plasma and the liquid is deformed and how that might be utilised to increase mass transport. The latter effect is monitored via the NCQDs forming reaction rate (without presence of catalyst). In particular, the effect of diffusivity of the liquid reactant on the reaction rate is studied by changing the liquid viscosity. The effect of other physical parameters is also investigated, including density, polarity, and surface tension; in pure form and as combined effect. With that understanding, a fixed bed is placed on the floor of the reaction vessel, and operated in a mode that the bed is fully wetted and not dried out by the impinging plasma microjet. When using metal flakes as bed, the goal is to check for catalytic activity. In addition, the

extent of evaporation of the liquid component is investigated, as Bruggeman et al. reported that evaporation plays a key role in plasma-liquid two-phase systems. We add volatile components to change the physico-chemical parameters of the liquid phase [45].

2. Methodology

2.1. Experimental setup

Our experimental design is based on the idea of high-intensity gas-liquid reactors that are equipped with forceful gas jets, which are known to enhance phase mixing [46]. We used a 16m s^{-1} downward vertical plasma jet that enters a small reactor volume via a nozzle with a diameter of 1.6 mm and after reaching the bottom it turns and moves in the upward direction along the gas-liquid interface. The plasma stream forms a crater in the liquid, resulting in a highly turbulent movement of liquid inside the reactor volume due to gas to liquid momentum transfer. In addition, the creation and collapse of gas bubbles in the liquid enhances the mass transport between the two phases.

Another high-intensity gas-liquid reactor design includes a pump, an orifice, a vertical tube aligned with the orifice, and a baffle plate [46]. The pump produces a downward vertical jet of liquid through the orifice, generating a gas-liquid dispersion in the tube. The two-phase jet is directed onto a baffle near the bottom of the tank, distributing it throughout the liquid. The liquid is then collected and recycled under the baffle plate. Simplification of the high-intensity gas-liquid reactor concepts is required in our experimental design. The existence of the plasma phase over long distances is not achievable and poses a challenge. Instead, a micro-plasma jet aimed at the liquid is utilised, Figure 1. The flow feedback for repeated gas-liquid interactions is also withheld, as the fundamental nature of the process intensification is better demonstrated through single contact [46].

The experimental synthesis process and reactor configuration were taken, as reported in previous studies [1]. The synthesis reactor was comprised of two parts, a kINPen®IND microplasma jet (Neoplas GmbH, Germany), and a cylindrical glass reactor with a diameter of 15 mm, designed and manufactured in-house. An argon (99.9 vol.%) was fed via the nozzle with a mean velocity of 16 m s^{-1}. The jet length was 1 cm.

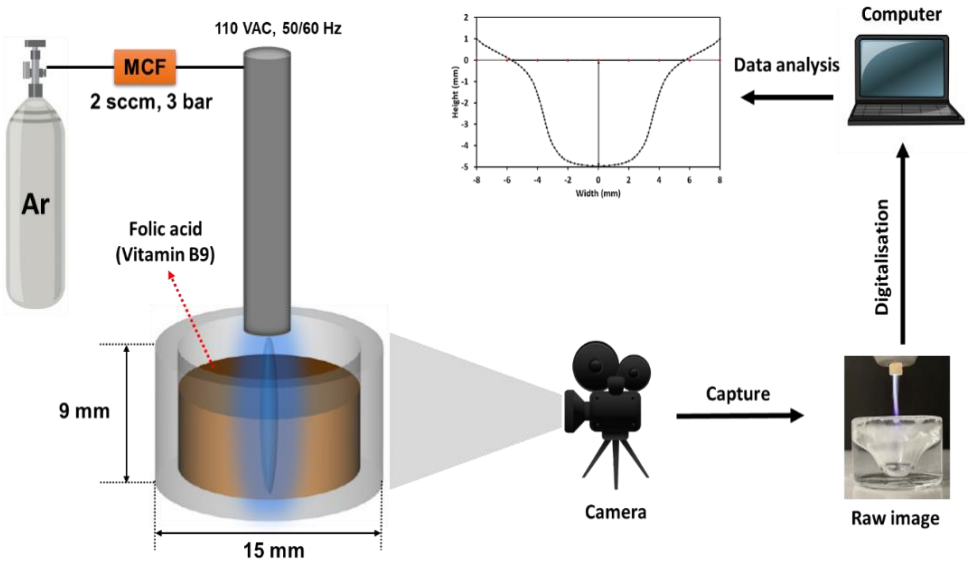

Fig. 1 *Experimental setup with plasma-liquid reactor and interfacial profile analytics.*

2.2. Physical parameter variation of the liquid reaction medium

In order to understand the influence of gas-liquid interfacial area and the diffusivity of the liquid reactant on the reaction rate, several solvents with different viscosity and surface tension were used as listed in Table 1.

Table 1. *Physical parameters of solvents used.*

Samples	Properties	
	Density (kg/m^3)	Viscosity (mPa.s)
Water	997	1.002
Glycerol	1258	1011
Water with sodium oleate, C.M.C. = 10^{-3} mol L^{-1}	997	1.01
Ethanol	785	1.1
Glycerol : Water = 1 : 3	1193	253
Water : Ethanol = 1 : 1	891	1.005
(Glycerol + Water) : Ethanol, indicated as Glycerol + Ethanol = 1 :1	766	127
Surfactant : Ethanol = 1 :1	891	1.055

2.3. Interfacial area of the crater and the liquid layer at the bottom

Calculation of specific surface area: When the plasma jet hits the liquid, a crater is formed. The total area of the crater was analysed by image analysis [47], Figure 1. It was assumed that the crater has an axisymmetric shape. The total interfacial area, as defined in

Figure 4, was calculated as the outer surface area of the cone obtained by rotation of a curve about the vertical axis. The curve describing the interface was fitted using a polynomial function of degree 4 to the experimental curve obtained from the image analysis. The gas-liquid interface area of the bottom liquid layer, as defined in Figure 4, was estimated by a simplified method. The shape of the bottom liquid layer below the crater, typically with a thickness in the 200-300-micron range, was approximated with straight lines to the polynomial curve describing the crater shape. Then the area was calculated from the obtained shape of the thin liquid layer below the crater.

Calculation of stagnant layer thickness: Water properties are assumed. Viscosity is μ = 0.001 Pa s, density is ρ = 1000 kg m^{-3}, and the diameter of the reaction vessel is x = 0.003 m. Then, the thickness δ of the stagnant layer (L) is given as follows, equation 1 (Eq 1).

$$\delta_L = \frac{2.74 \cdot 10^{-4}}{\sqrt{\upsilon_L}} \text{ [m]} \qquad \text{(Eq 1)}$$

The liquid velocity near the interface can be estimated based on the equal pressure drop over the interface. As then the ratio of the velocities in the gas and in the liquid can be approximated as reciprocal ratio of their viscosities. For the case of water, equation 2 can be derived.

$$\upsilon_L \simeq \frac{\mu_G}{\mu_L}\upsilon_G \approx \frac{1.8 \cdot 10^{-5}}{1 \cdot 10^{-3}}\upsilon_G \approx 0.018 \cdot \upsilon_G \text{ (m } s^{-1}\text{)} \qquad \text{(Eq 2)}$$

Then, the thickness of the stagnant layer δ_L is given as follows.

$$\delta_L = \frac{2.74 \cdot 10^{-4}}{\sqrt{0.018 \cdot \upsilon_G}} \text{ (m)} \qquad \text{(Eq 3)}$$

2.4. Evaporation rate and reaction rate

An aqueous solution containing 20 µL of folic acid (0.1 g/mL) 1 ml of a given liquid was transferred to the glass reactor. was added as a colour indicator and reactant to the liquid. The microplasma jet was vertically directed towards the reactor at three configurations (distant, contact, and deflection). After 10 minutes, the microplasma treatment of the liquid was stopped. The final volume of liquid was used to calculate the evaporation rate, Figure 2.

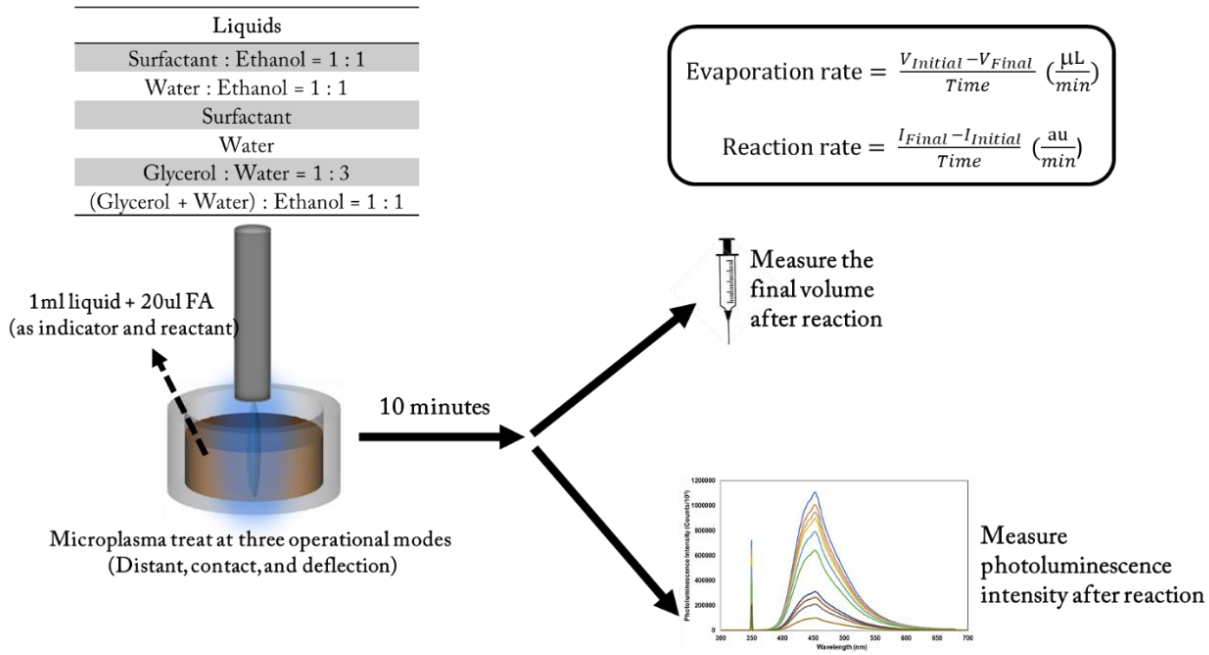

Fig. 2 *Schematic view of procedures applied for the calculation of evaporation and reaction rates in the synthesis of NCQDs.*

The fluorescence emission is one of the most unique features of NCQDs, utilised in many fields [48]. In this study, fluorescence emission is used for calculating the reaction rate, Figure 2. Folic acid (20 µL, 0.1 g/mL) was added to the liquid (1ml) in the reactor. The same three configurations of microplasma jet were used as those in our previous study [1]: (i) 'distant' (jet in contact with liquid with a weak momentum transfer), (ii) 'contact' (jet colliding deep into liquid, with a moderate impact on hydrodynamics), and (iii) 'deflection' (jet perforating liquid completely down to reactor floor; a strong momentum transfer) [2], Figure 2.

After 10 minutes, the jet was stopped, and the colour of the solution changed from orange to brownish. The solution was analyzed with a photoluminescence spectrometer (FLS 1000, UK). The excitation and emission wavelengths were set at 360 and 450 nm, respectively. The photoluminescence intensity of NCQDs was used to obtain the reaction rate. In several experiments, 0.5 g of $Ni_{80}Cr_{20}$ alloy flakes were placed at the bottom.

3. Results and Discussion

3.1. Hydrodynamics for process intensification created by microjet plasma

Different depth of penetration of the plasma microjet into the liquid microvolume creates genuine hydrodynamic regimes, characterised by a large interfacial area, and the

presence of a thin 'inner' liquid layer, at the floor of the reactor, with a moderate interfacial area. A catalyst can be added on the bottom as a fixed bed.

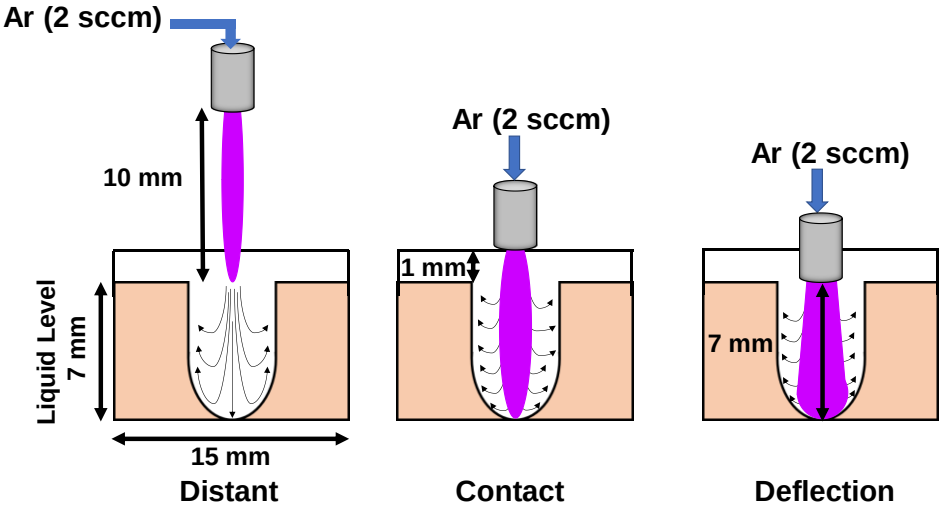

Fig. 3 *Hydrodynamic regimes by different depth of penetration of submerged microjet plasma into a liquid microvolume; termed distant (left), contact (middle), and deflection (right), [1].*

In the 'distant' position, the tip of the microplasma jet, which is the most protruding part, does not contact the liquid surface and only generates a small crater. In the 'contact' position, the plasma jet penetrates deeper, forming a liquid film above the catalyst surface. The 'deflection' position resembles the "fast impinging jet reactor," a plasma reactor configuration proposed by Botes [5]. In this configuration, the liquid film is further thinned, and the plasma gas stream is redirected harshly, creating turbulence in the plasma-gas phase and potentially recirculation in the bulk liquid; intensifying mass transport in both phases. As a result, a multiphase system with a continuous renewal of the interface is expected, possibly assisted by the generation and breakup of small droplets from the water surface, as reported in the literature [49].

We discovered that the highest intensity of charged (activated) species can be detected in the 'deflection' position [2]. The 'deflection' position is chosen as prime hydrodynamic setting for the study reported here, while the two other positions are co-investigated.

The new plasma microjet concept can compete energy-wise well with DBD plasma reactors and microreactors that are the standard in microfluidic processing. Only 1 W is consumed for the micro jet plasma in this study [10], although 56 W are needed for gas

pumping at very high gas flow rate of 2 L h^{-1} [50]. The latter may be optimised, as the deflection flow regime may be achieved by flower gas flow rates; yet manufacturer's restriction in flow rate setting prevents this study from testing this. For comparison, plasma generation of an energy-optimised laboratory DBD reactor takes 16 W (Pradeep et al., 2023), and pumping a gas flow rate of 0.2 L h^{-1} consumes about 6 W [50]; together 22 W. For comparison, pumping a microreactor with two HPLC pumps (each 100 W [51]), consumes 200 W.

3.2 Effect of physical parameters of the liquid on the crater shape

The plasma microjet displaces a major part of the liquid volume. It establishes a void gas volume that is characterized by a high-velocity gas downward that impinges on the liquid surface to be redirected upwards out of the void volume. Strong convection can be expected under those conditions ensuring good mass transport of the plasma to the gas-liquid interface. Relevant is that the use of the microjet secures that plasma contacts the liquid interface and potentially the catalyst beneath it. The high gas velocity transfers its momentum to the liquid phase to create a liquid recirculation loop, Figure 4. This liquid convection refreshes reactant in the stagnant layer from the 'feed' of the non-stagnant convective liquid zone; Figure 4a.

The stagnant liquid layer is controlled by diffusion, which is a slow process. Setting the stagnant layer to small dimensions, helps in fastening diffusion. Yet, a rough surface of a bed of $Ni_{80}Cr_{20}$ flakes underneath the stagnant liquid layer may introduce turbulence and therefore increase convection towards the catalyst; Figure 4b.

Another concept might be 'convectional pumping' of the plasma-activated species close to the catalyst; Figure 4c.

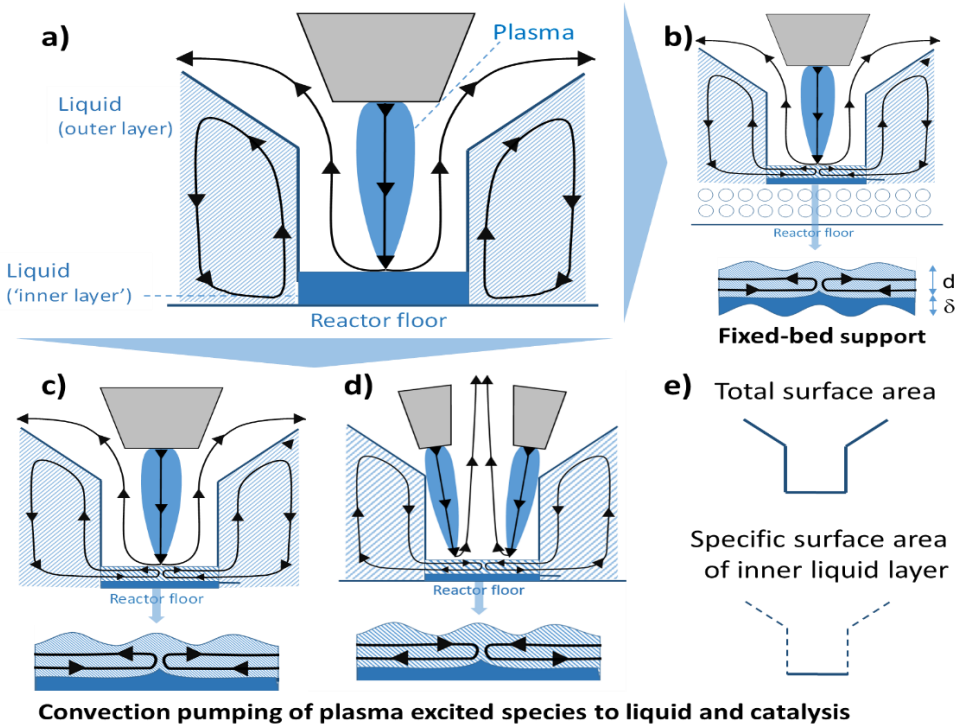

Fig. 4 *Schematic of the crater profile created by the submerged plasma microjet into a microvolume, showing hydrodynamic and reactor regions that determine the chemical engineering science. a) schematic profile as per experiments in this manuscript; b) same as a), yet with fixed bed support; c) same as a), yet with larger inner liquid layer to allow convection; d) same as a), yet with two jets placed at the outer part of the crater (instead of one jet in the crater centre); and e) schematics to define total surface area and specific surface area of inner liquid layer.*

A layer thicker than the velocity boundary layer thickness (⊠) allows a convective flow to enter into the 'inner liquid surface area', directly exposed to the plasma jet. As given in Figure 4c, this would actually pump the plasma-activated species away from the supposed reaction zone at the catalyst. This demands for a new positioning of the plasma jet from the centre position to an outside one; Figure 4d. A tilted arrangement of the jets is needed to achieve maximum transfer of gas momentum to the liquid. In this configuration, the convection flow would transfer plasma-excited species to the liquid stagnant ('reaction') zone and catalyst. Roughening of the stagnant liquid-solid interface would increase efficiency of this concept; extending use of concept in Figure 4b.

The surface profiles in the three positions were recorded (Figure 7), investigating phenomenonally the shape of the interface and its total surface area and its specific surface area below the crater. The optimum configuration for interface shape would be a rather flat

surface with a large surface area near the reactor floor (the potential position for a catalytic bed), Figure 4e.

To examine the magnitude of the effect, calculations of the gas velocity were done as a function of distance from the plasma-device outlet [10], Figure 5 Basic assumptions are (i) the velocity of air outside the plasma jet is considered as zero; (ii) temperature of gas is considered 300K; (iii) the diameter of nozzle is considered as 1.6 mm [10]; and the air flow rate is considered as 2 L.min^{-1}.

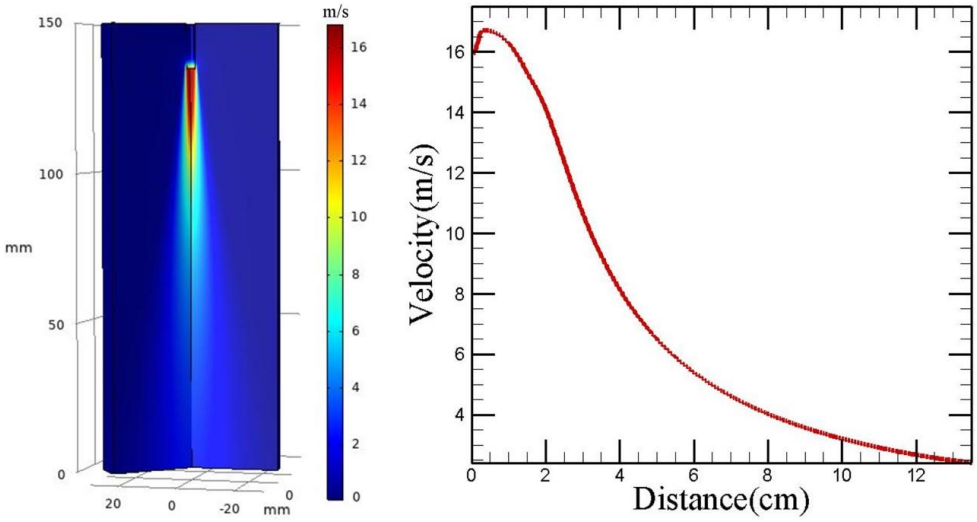

Fig. 5 *Gas velocity of the microjet plasma with distance; using the settings of the neoplas industrial plasma system [10].*

The pressure decreases when gas leaves the nozzle, and its velocity increases, in line with the Bernoulli's principle, Figure 5. Then, the gas velocity decreases downstream the nozzle due to frictional losses and volumetric expansion of the jet.

The thickness of the stagnant layer needs to be determined to check on which time scale diffusion might be effective. With reference to Figure 5 and a gas velocity around 15-16 m s^{-1}, the thickness of water velocity boundary layer around the solid surface (Eq. a1) is expected to be ca. 0.6 mm; meaning the plasma-activated species still need several minutes to reach the catalyst, Figure 6.

$$\delta_L = \frac{5x}{\mathrm{Re}^{0.5}} = 5\sqrt{\frac{\mu \cdot x}{\rho \cdot \upsilon_L}} \quad \text{(Eq.a1)}$$

where x is the length of the solid surface in the flow direction (3 mm), and Re is the Renoylds number of the liquid.

This shows the need to roughen the catalyst surface, Figure 4 upper left scheme.

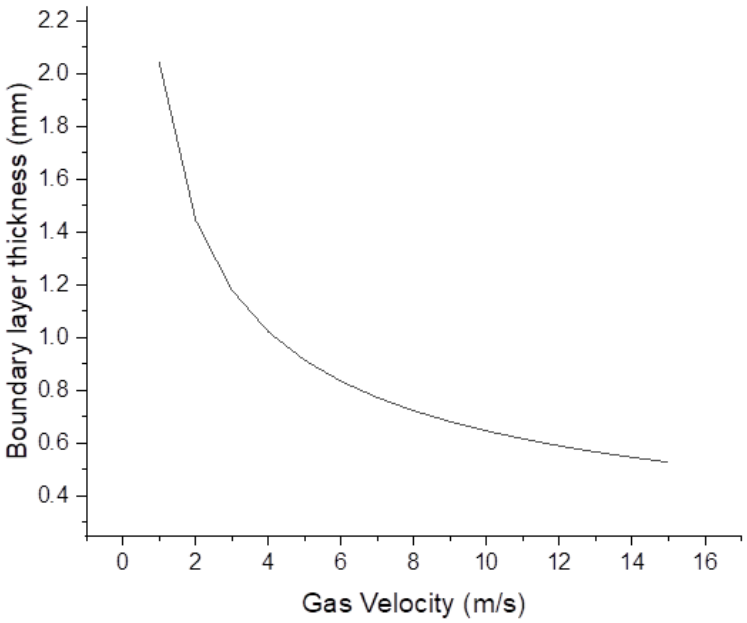

Fig. 6 *Stagnant layer thickness with gas velocity.*

To widen from using pure water only, glycerol, ethanol and sodium dodecyl sulphate (surfactant) were added to water to change viscosity, polarity, and surface tension of the liquid, respectively, and to study their impact on the crater surface area, liquid stagnant layer area and diffusivity of the reactant. The interface shape for different set of parameters was recorded and discussed below, Figure 7.

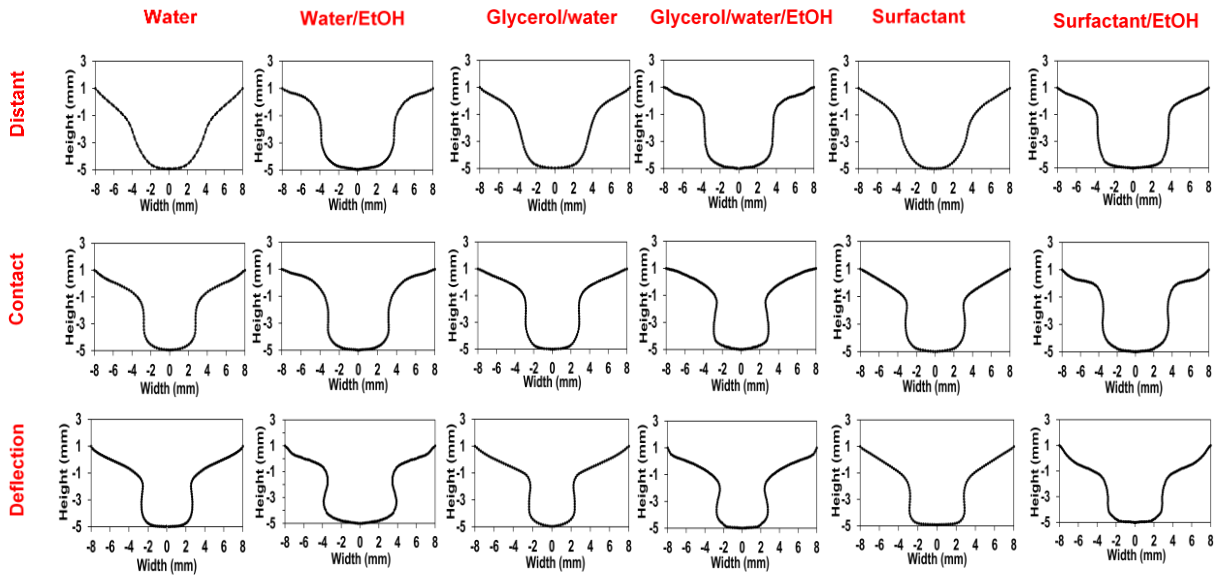

Fig. 7 *Plasma-liquid interface profile for pure water (viscosity: 1.002 mPa.s), water/ethanol 1:1 (viscosity: 1.005 mPa.s), glycerol/water 1:3 (middle, viscosity: 253.42 mPa.s), glycerol-water-ethanol (right, viscosity 127.27 mPa.s), water/surfactant 10^{-3} mol/l (viscosity: 1.01 mPa.s), and water/surfactant/ethanol (right, viscosity 1.055 mPa.s).*

For pure water, the above given criterion of a good surface profile is better met for the contact mode as compared to the distant mode, with slight further improvement in the deflection mode, Figure 7.

Adding glycerol to the aqueous solutions increases viscosity and slightly changes density. The impact on the desired process design is low, meaning the surface profiles are similar to those with pure water. The interfacial surface area increases from 238 to 249 mm^2, when moving to the deflection regime, Figure 7.

Adding ethanol alters polarity and adding surfactant surface tension. The profiles obtained are characterised by nearly vertical walls approaching a vertical well shape with a thin aqueous layer between the gas and the solid wall. This well shape is kept and the vertical alignment of the side walls improved when combining both or combining these with the glycerol (high viscosity) addition; for surfactant-ethanol (low surface tension – high polarity) it is found for all three positions (distant, contact, deflection).

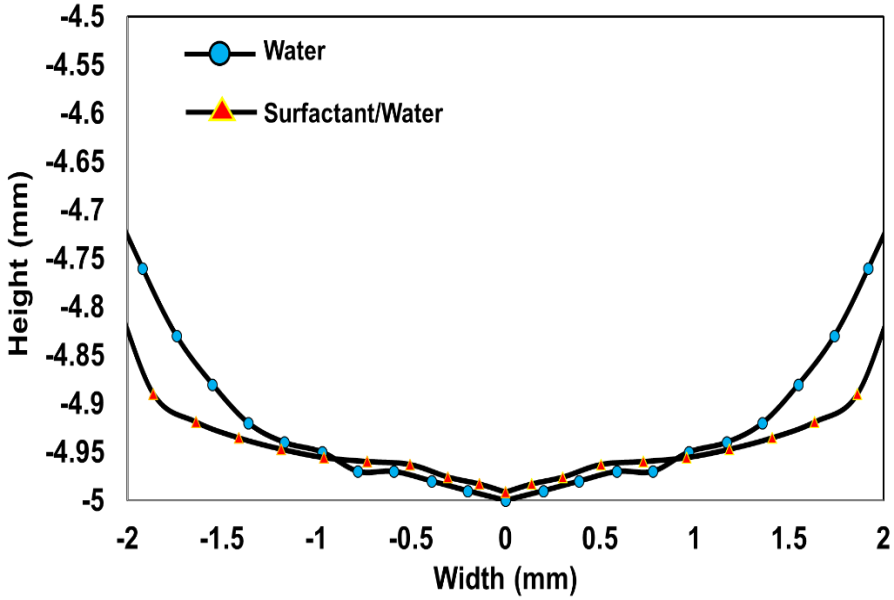

Fig. 8 *Water-surfactant vs water interface profiles above the inner liquid layer, at a magnification of the height (y-axis) about 0.5 mm.*

Adding ethanol and glycerol to the aqueous solutions increases both polarity and viscosity. The impact is more remarkable than changing viscosity alone. The gas-liquid interface gets more flattened, meaning the thin liquid layer has a rather constant thickness and a larger interfacial area. The large extent of flattening of the water-surfactant profile of the inner

aqueous layer is evident when comparing the respective water profile; using large magnification of this 'micro-zone', Figure 8.

3.3 Effect of physical parameters of the liquid on total surface area

While the jet penetrates the liquid microvolume deeper, the total surface area of the crater is decreased to a small or medium extent, Figure 9; counter-intuitive to the expectation about strong impingement effect. The total surface area is largest for the deflection mode, followed by the contact and distant mode; with the contact mode being closer to the deflection one. The total surface area of the crater is the largest for pure water, while the lowest for water-surfactant. The specific (volume-rated) surface area is for pure water *ca.* 250 m^{-1}, a value typical for advanced reactor equipment, yet lower than interfaces generated in microreactors (1,000 m^{-1} to 10,000 m^{-1}). The total surface is about 10 times larger than for a plain surface, non-perturbed by jet penetration.

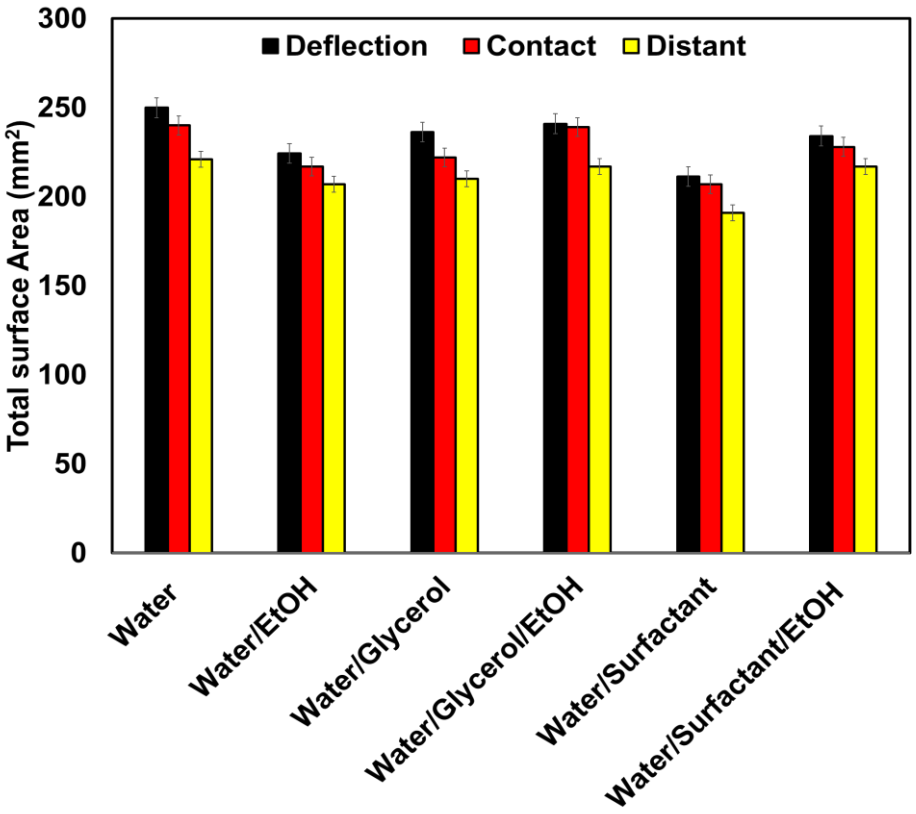

Fig. 9 *Total surface area at different liquid properties; taken for all three hydrodynamic regimes with distinct plasma crater profiles.*

3.4 Effect of physical parameters of the liquid on specific surface area of the inner liquid layer

We elucidated the specific interfacial area of the inner aqueous layer and the minimal water thickness of the inner water layer, the central point of the plasma cavity; revealing also the shape of the inner liquid layer surface. An ideal surface profile for chemical processing is flat (ultrathin) and thus constant in the water thickness, likely with diffusion being the governing mechanism of mass transport. This ultrathin liquid layer may also be ideal to employ reaction amplification by a catalyst.

The real inner surface profiles are curved, yet some are close to being ideal flat (water, water/surfactant, water/surfactant/ethanol, or water/glycerol/ethanol), Figure 9. While the surface areas differ, Figure 7, the average thickness of the inner water layer differs as well, Figure 6.

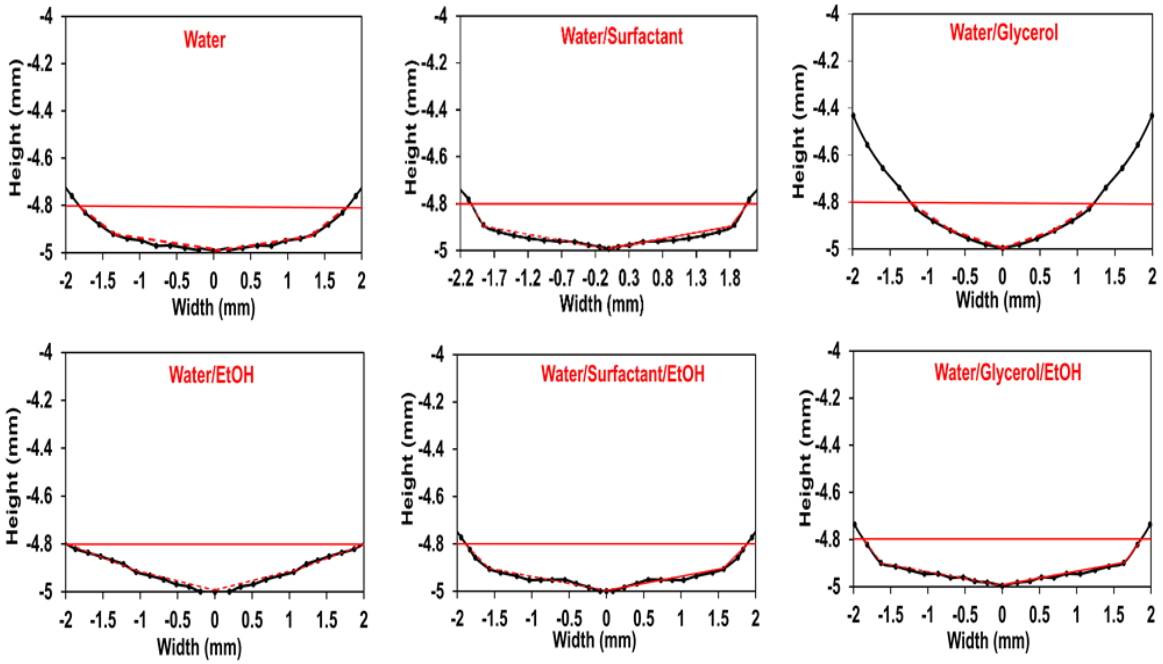

Fig. 9 *Schematic of the (experimentally determined) crater profile created by the submerged plasma microjet into a microvolume for systematic physcio-chemical variation, determining hydrodynamics and reactor regions.*

The scenarios considered have mostly mixed average hydrodynamic performance, e.g. having low average thickness of the inner water layer at low surface area, and vice versa. The scenarios water and water-surfactant have the best hydrodynamics. The profiles of aqueous systems with increased viscosity or reduced surface tension are close to an ideal flat surface, while having a larger depth of the inner layer throughout, and not only at the edges.

Therefore, the plasma jet-liquid system can be fine-tuned in terms of having either a thin inner liquid layer (averaged over the span) or a flat layer.

The surface of the inner aqueous layer at the bottom (Figure 10) is 20-25% of the total surface area of the crater (Figure 7), which fits to the observation of five zones in Figure 5 of almost equal length and curvature. The addition of ethanol allows to make it still larger than for pure water, including admixture of surfactant and glycerol, whereas the addition of (only) glycerol halve the specific surface area. Taking 28 mm^2 as highest value (assuming averaged 0.1 mm layer thickness at 2.8 mm^3 volume), the specific (volume-rated) surface area for pure water is *ca.* 10,000 m^{-1}, a value as high than the greatest interfaces reported for microreactors with capability for high capacity (1,000 m^{-1} to 10,000 m^{-1}); with up to 10,000 m^{-1} reported for analytical microchip devices [52]. The specific volume of the inner aqueous layer is just 0.28 % of the total volume (2.8 vs. 1000 mm^3), yet is supposed to make a major effort to the reaction outcome.

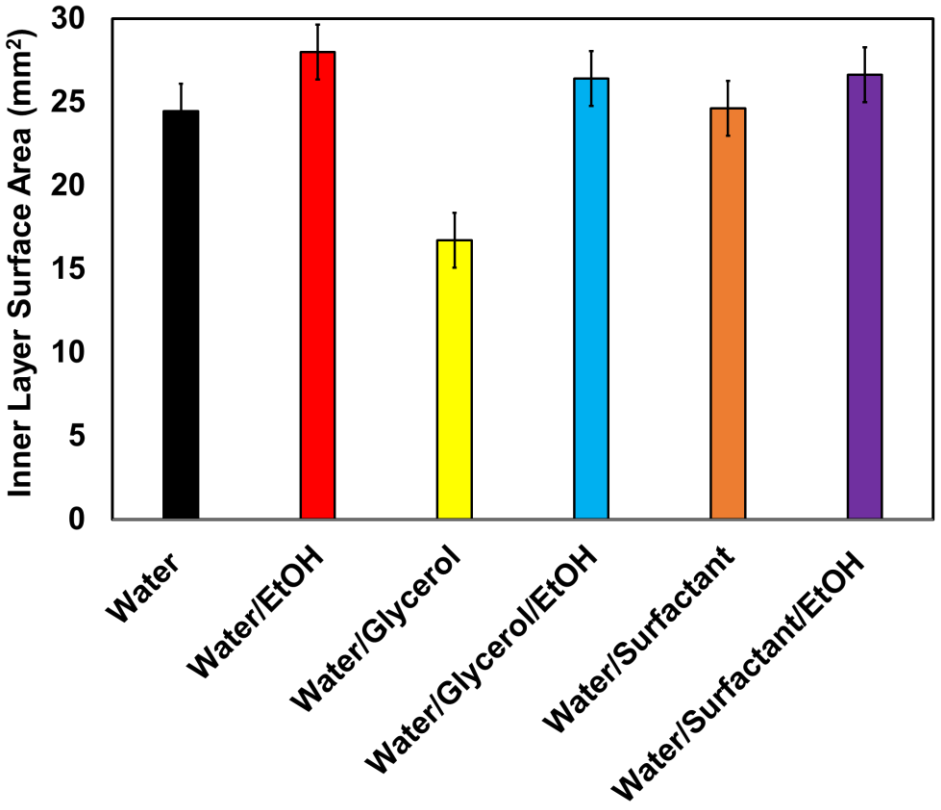

Fig. 10 *Surface of the inner aqueous layer, depending on additives given to modify the physico-chemical properties (density, viscosity, surface tension).*

3.5 Effect of physical parameters of the liquid on the inner liquid layer in the presence of a porous solid beneath

In order to achieve both a thin and flat inner liquid layer for one liquid system, the hydrodynamic profile is determined in the presence of a porous bed, composed of particles in the order of the size of the depth of the inner layer or somewhat larger; including glass spheres or metal flakes. The liquid will penetrate that bed and the surface of the liquid is not expected to be influenced by wetting of the glass reaction vessel; assumed to cause the larger depth of the inner layer for the viscous and surface tension-reduced liquids.

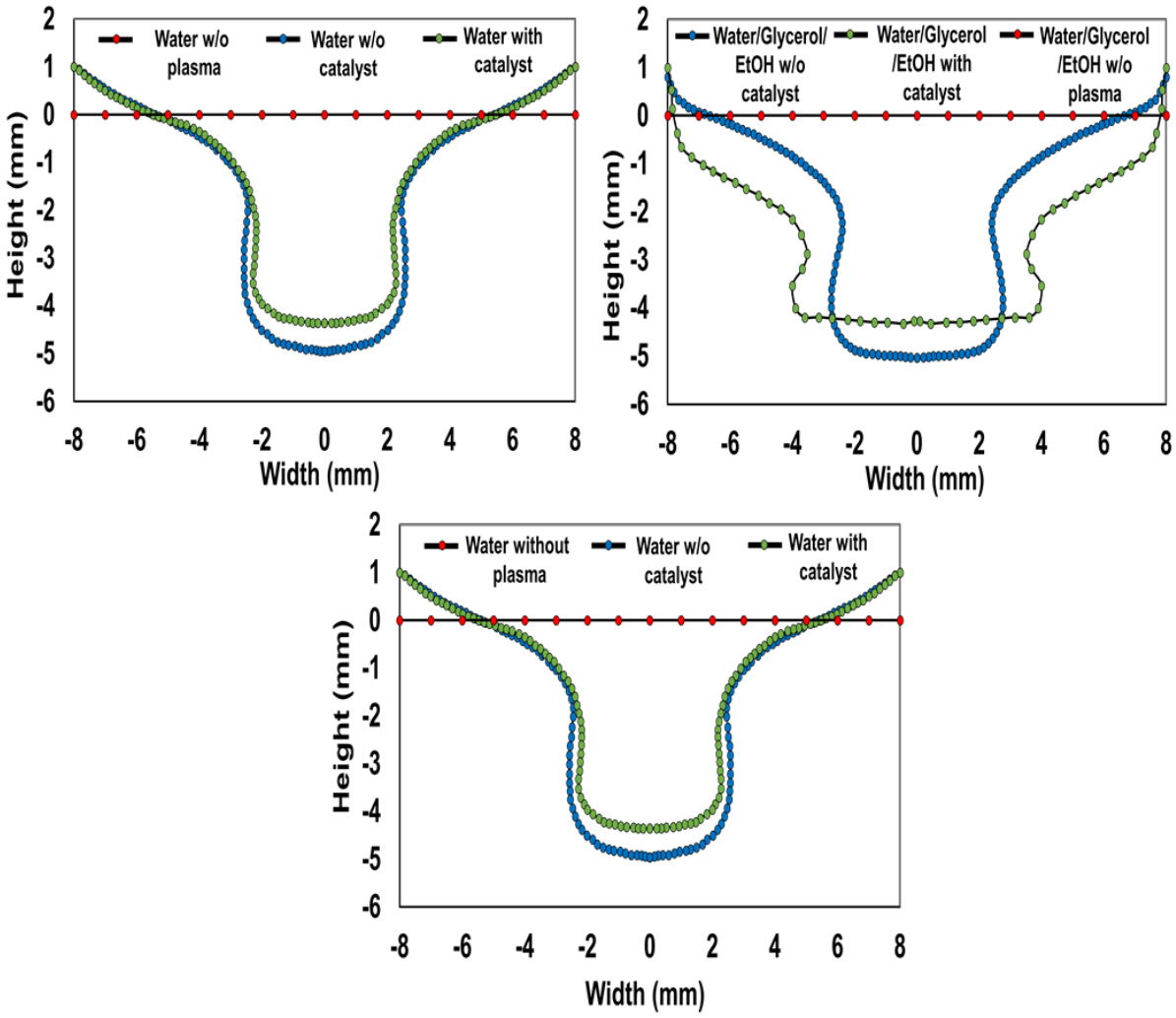

Fig. 11 *Surface profile of (a) pure water, (b) glycerol and (c) glycerol–ethanol mixture as compared with surface without plasma treatment at the deflection mode.*

The plasma jet in the deflection mode was exposed to a porous fixed bed of Ni-Cr alloy flakes draining a liquid, Figure 11. This changed the surface profile as compared to exposing the plasma microjet to water without fixed bed, Figure 10. An ideal flat profile is

obtained for the glycerol (high viscosity) and glycerol-ethanol (high polarity- high viscosity) mixtures. In the case of glycerol-ethanol (high viscosity-high polarity), the surface area of the liquid inner layer is larger than for the case without fixed bed. In the case of pure water, no effect is observed. The profile is just elevated to higher position. It is suspected that high surface tension of the gas/water interface prevents to form a flat profile as given for the other two cases.

3.6 NCQDs reaction effect by liquid viscosity to test diffusion

This study intends to deploy the above-mentioned variation of physical properties for intensifying the chemistry of the NCQDs formation. Surface tension alteration does not show reaction rate dependency, while having best hydrodynamic surface profile with most extended surface of the thin layer. Polarity variation has no effect on the reaction rate either.

However, the NCQDs reaction rate was a strong function of viscosity and therefore diffusivity of the liquid reactant. The experiments were directed to detail this effect. The reaction rate increases as viscosity decreases and it increases largely from the distant to contact position, Figure 12. It can be seen that the 'deflection' mode is best in overcoming viscosity limitation. The 'contact' mode is close to this performance. The 'distant' mode is behind the performances of the three modes.

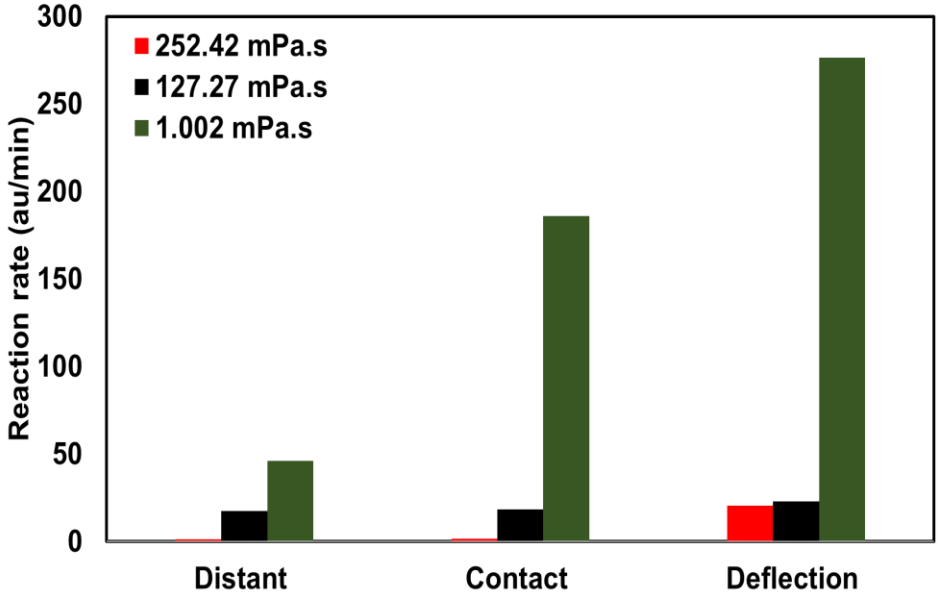

Fig. 12 *Reaction rate as a function of the distance from the nozzle in three configurations.*

Question is if that effect is related to unit operations (diffusivity) alone or transcribed by chemical effects (viscosity changing solvent polarity). The variation of viscosity, and the

other physical parameters, do not follow the common effect of square dependency of reaction rate with co-solvent/ingredient concentration (see Supplementary Material). A chemistry-induced change of reactivity can therefore be excluded, and conclusion is the reaction rate reflect intrinsic dependencies of hydrodynamics and mass transfer on the reaction rate, i.e. diffusivity.

To further corroborate that the reaction rate is diffusion limited, the rate was plotted vs reciprocal viscosity of the solvent, which is proportional to diffusivity, Einstein's equation, Figure 13 [53].

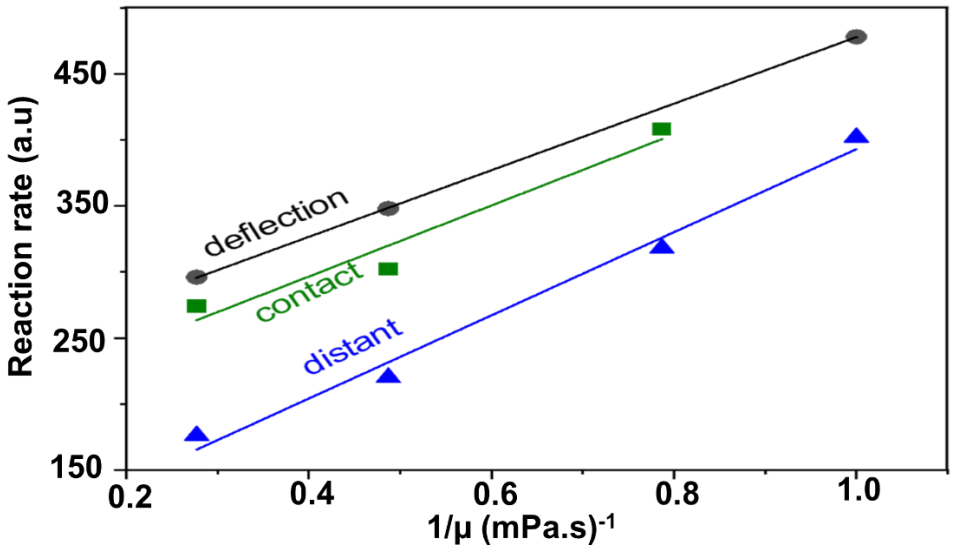

Fig. 13 *Reaction rate as a function of reciprocal viscosity for the three jet configurations.*

3.7 NCQDs reaction in presence of a metal flakes bed: test catalytic activity

A catalyst bed with the Ni-Cr alloy flakes was added. The effect of the Ni-Cr alloy catalyst to the plasma-liquid system to amplify the reaction rate was determined also for the combined viscosity-polarity effect, employing glycerol-ethanol-water mixtures. Hypothesis is that excited plasma species (Ar^+, N_2^+, O^+, OH^*) can diffuse faster to the catalyst beneath to induce the NCQDs formation [54, 55]. The deflection mode is best to utilise these plasma-excited species.

A rate enhancement of about 25% could be achieved for the catalyst-supported reaction experiment in the deflection position, Figure 14.

While this is not enough to justify proclaiming a catalytic effect in the classical meaning, it still marks a considerable process improvement. Of larger impact, in the order of five times intensification, the reaction rate increases from 76 to 387 (au/min) when

changing the position from distant to deflection. Yet this effect can only be leveraged in pure water, meaning at low viscosity (1.002 mPa.s); the Ni-Cr catalyst cannot overrule the diffusion limitation and the formation of a relatively thicker layer above the catalyst. Yet for constant (high) viscosity, the catalyst is effective to increase reaction rate as the determined rates show for glycerol + water (252.42 mPa.s) and glycerol +ethanol (127.27 mPa.s). The catalyst effect is strongest in the deflection mode, as given for the non-catalysed experiments, Figure 11.

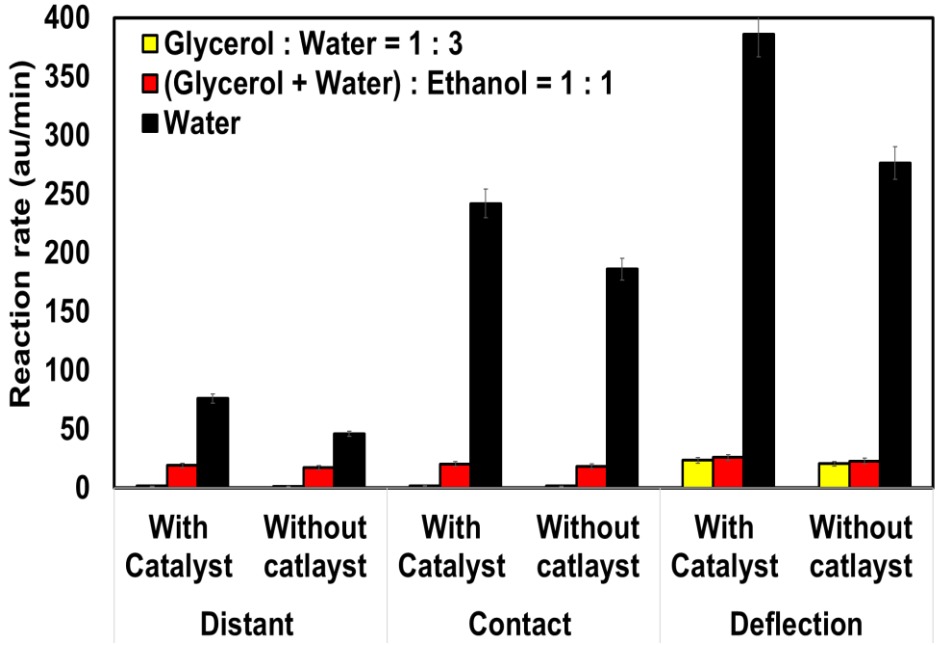

Fig. 14 *Reaction rate of the synthesis reaction of NCQDs with and without $Ni_{80}Cr_{20}$ catalysts various solvent liquids (pure water, glycerol + water, and glycerol + ethanol).*

3.8. Evaporation control to prevent liquid phase media change

Evaporation is likely to happen when a high-velocity jet impinges on a liquid surface of large specific area. Evaporation of solvent might change reaction rate and product quality of the NCQDs nanomaterial, making necessary metering and control of evaporation. This may be facilitated by the fact that plasma commonly transfers heat to the surface of the liquid [9].

The calculated evaporation and reaction rate were determined for the NCQDs synthesis in the deflection mode, when varying the physico-chemical parameters of the liquid reaction medium, Figure 15. The evaporation rate for pure water, surfactant, and glycerol : water (1:3) is relatively similar, in the vicinity of 30 (µL/min). This changes when ethanol is

added, a volatile solvent. The evaporation rate of water + ethanol, surfactant + ethanol, and glycerol +ethanol increased significantly, compared to reaction media without ethanol, Figure 15. The reaction rate decreased considerably, except for the case of glycerol + ethanol (20.49 au/min), which is almost invariant. The evaporated removal of ethanol might be one cause for the decline in reaction rate, adding to the other here reported causes, including the thickness of the inner liquid layer and the total and inner layer-related specific surface area.

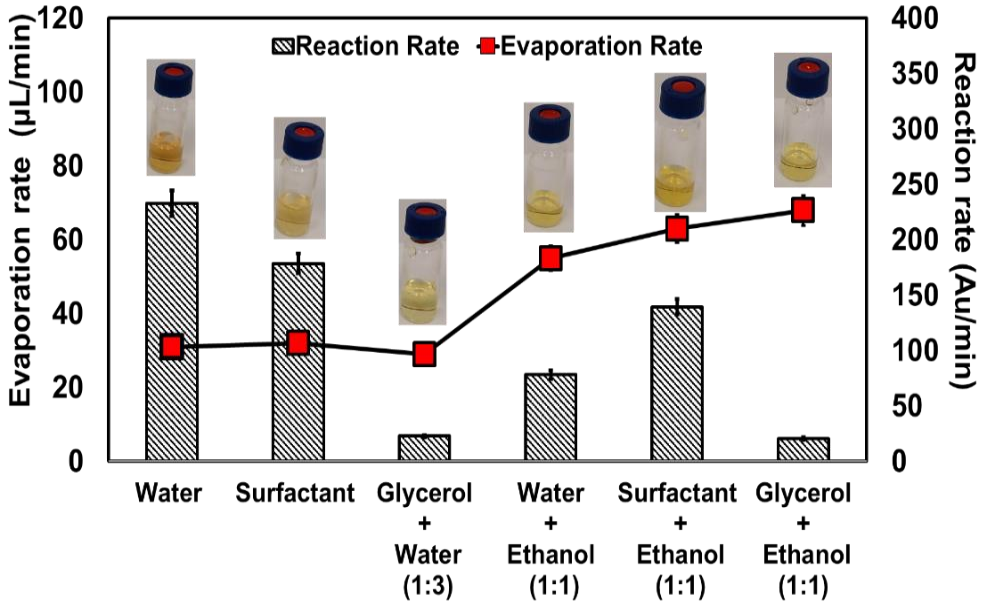

Fig. 15 *Influence of solvents on evaporation and reaction rate in the synthesis of NCQDs operated at deflection mode.*

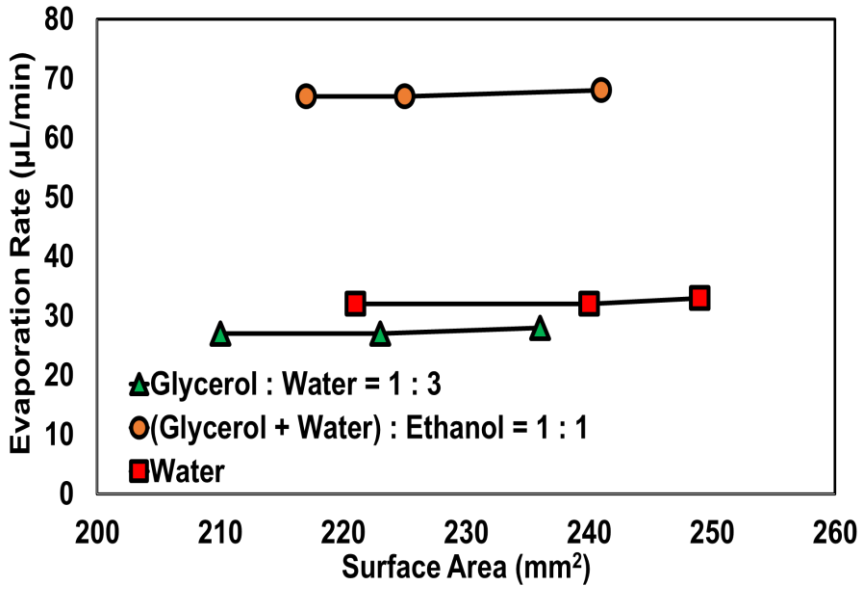

Fig. 16 *Evaporation rate as a function of the distance from the nozzle in the three hydrodynamic regimes of the plasma jet penetration in the liquid microvolume.*

Experiments demonstrate that the evaporation rate remains practically constant in all three hydrodynamic regimes within the investigated range, which is consistent with determination that the total surface area of the plasma crater only minorly varies for the regimes, Figure 16. The remaining difference might be due to that most evaporation takes place at the large specific surface of the inner aqueous layer, which is practically invariant to changes of the hydrodynamic regime and in the physico-chemical parameter; with one exception, Figure 9.

As expected, and seen in Figure 16, the addition of ethanol with a lower boiling point than water increases the evaporation rate. The addition of surfactant increases the total surface area. However, it does not change the evaporation rate; which is consistent with above stated independence of the rate from the total surface area.

4. Conclusions

This study explored a new reaction engineering concept to generate 'in-process' a thin, almost flat solvent layer out of a bulk liquid through impingement of a high-velocity gas jet (plasma). This layer is as thin, or thinner, as typical microfluidic flows, used for chemical processing. Specifically, the study demonstrates that a fixed bed at the floor of the reaction vessel can aid in improving the profile shape of the thin layer and deciphers how this is controlled by generic changes of physico-chemical parameters of the reaction solution. The fixed bed may add catalytic function, which cannot be leveraged in the liquid layer only, but contact to the gas phase is possible as well; enabling 'plasma catalysis' for the study here.

The variation of the physico-chemical parameters allowed to decipher which mechanisms rule the reaction investigated, the formation of NCQDs quantum dots from a dissolved precursor. This applies, in more general terms, also to a monomolecular reaction in a liquid phase that is non-thermally activated. It turned out that the plasma-liquid system is controlled by viscosity of the reaction solvent, which confirms diffusivity limitation as governing mass transfer mechanism. Polarity, density, or surface tension variation has no impact on the reaction rate; unless being combined with a viscosity change. Water, with lowest viscosity, as reaction medium proved to have the highest reaction rate for the NCQDs synthesis. Solvent admixtures, including ethanol, that keep high viscosity but change other physico-chemical parameters (polarity, surface tension), reduce the reaction rate in aqueous media.

The total surface area of the crater and the specific surface area of the thinned ('inner') solvent layer have no impact on the NCQDs reaction rate, at least within the possible range of variation in this study via the diversity of crater shapes created. This indicates that gaseous excited reaction species are in excess, and the gas-liquid interfacial transition is not a limiting factor but the diffusion of the precursors toward the interface. That also demonstrates that the reaction happens at the surface and does not penetrate the liquid; leaving diffusion in the liquid as a limiting factor.

Energy-wise, only 1 W is consumed for the plasma, although 56 W is needed for gas pumping at a very high gas flow rate of 2 L h^{-1}, totalling 57 W. Plasma generation of an energy-optimised laboratory DBD reactor takes 16 W and about 6 W for gas pumping; totalling in 22 W. Pumping energy of a microreactor consumes 200 W.

Evaporation is an unavoidable consequence of applying a high-velocity jet to a solvent or solvent mixture. It is undesired as it transiently changes the reaction medium and exposes volatile, potentially toxic organic matter to the environment. Evaporation does not depend on the surface area of the entire crater, which demonstrates that evaporation happens only in the narrow area near the jet, which is almost constant under any experimental variation. As expected, evaporation depends on the boiling point of the solvent. Low-boiling solvents should be avoided, even as admixtures to a main solvent.

Outlook

Understanding the fundamentals reported in this study opens paths for follow-up studies. The catalytic function needs to be corroborated and elucidated about the mechanism and how a catalyst needs to be designed to be optimal. For a broader and potentially larger impact of the new reactor engineering concept, tests with a very fast liquid reaction might exhibit a surface area dependence, impacting the interfacial transition of the excited species from the plasma phase. The surface area has been detailed in this study, and the way of changing and controlling it was deciphered. The new concept needs to be tested with reactions that do not impact polarity changes and might need to be stimulated in reaction rate by viscosity and density changes. Then the multitude of possible variations of surface profiles and hydrodynamics demonstrated in this study can be utilised for a broader application in synthetic chemistry, possibly even beyond plasma-chemical processing.

Acknowledgements

Mr. Hue Quoc Pho received the divisional E.C.M.S. and full-fee scholarships from the University of Adelaide, Australia. The authors acknowledge support from the ERC Grant Surface-Confined fast-modulated Plasma for process and Energy intensification (SCOPE) from the European Commission with grant number 810182.

References

[1] Q.H. Pho, L. Lin, E.V. Rebrov, M. Mohsen Sarafraz, T.T. Tran, N.N. Tran, D. Losic, V. Hessel, Process intensification for gram-scale synthesis of N-doped carbon quantum dots immersing a microplasma jet in a gas-liquid reactor, Chemical Engineering Journal 452 (2023) 139164.

[2] Q.H. Pho, H.Q. Tran, C.P. Zhuang, V.D.L. Nguyen, N.N. Tran, T.T. Tran, E.V. Rebrov, D. Losic, Z. Machala, V. Hessel, Deciphering Plasma-Catalysis in Triphasic Microplasma for N-doped Carbon Quantum Dots from Vitamin B9 via Optical Emission Spectroscopy Unpublished (2023).

[3] A. Bokhari, S. Yusup, S. Asif, L.F. Chuah, L.Z.Y. Michelle, Chapter 3 - Process intensification for the production of canola-based methyl ester via ultrasonic batch reactor: optimization and kinetic study, in: L. Singh, A. Yousuf, D.M. Mahapatra (Eds.) Bioreactors, Elsevier2020, pp. 27-42.

[4] E. Nagy, Basic equations of mass transport through a membrane layer, Elsevier2018.

[5] F. Botes, L. Lorenzen, J. Van Deventer, The development of high intensity gas-liquid jet reactors, Chemical Engineering Communications 170 (1998) 217-244.

[6] L. Chandana, P. Manoj Kumar Reddy, C. Subrahmanyam, Atmospheric pressure non-thermal plasma jet for the degradation of methylene blue in aqueous medium, Chemical Engineering Journal 282 (2015) 116-122.

[7] A. Ananth, S. Dharaneedharan, H.-J. Seo, M.-S. Heo, J.-H. Boo, Soft jet plasma-assisted synthesis of Zinc oxide nanomaterials: Morphology controls and antibacterial activity of ZnO, Chemical Engineering Journal 322 (2017) 742-751.

[8] F. Rezaei, P. Vanraes, A. Nikiforov, R. Morent, N. De Geyter, Applications of plasma-liquid systems: A review, Materials 12 (2019) 2751.

[9] P.J. Bruggeman, M.J. Kushner, B.R. Locke, J.G.E. Gardeniers, W.G. Graham, D.B. Graves, R.C.H.M. Hofman-Caris, D. Maric, J.P. Reid, E. Ceriani, D. Fernandez Rivas, J.E. Foster, S.C. Garrick, Y. Gorbanev, S. Hamaguchi, F. Iza, H. Jablonowski, E. Klimova, J. Kolb, F. Krcma, P. Lukes, Z. Machala, I. Marinov, D. Mariotti, S. Mededovic Thagard, D. Minakata, E.C. Neyts, J. Pawlat, Z.L. Petrovic, R. Pflieger, S. Reuter, D.C. Schram, S. Schröter, M. Shiraiwa, B. Tarabová, P.A. Tsai, J.R.R. Verlet, T. von Woedtke, K.R. Wilson, K. Yasui, G. Zvereva, Plasma–liquid interactions: a review and roadmap, Plasma Sources Science and Technology 25 (2016) 053002.

[10] S. Reuter, T. Von Woedtke, K.-D. Weltmann, The kINPen—A review on physics and chemistry of the atmospheric pressure plasma jet and its applications, Journal of Physics D: Applied Physics 51 (2018) 233001.

[11] S. Bekeschus, A. Schmidt, K.-D. Weltmann, T. von Woedtke, The plasma jet kINPen – A powerful tool for wound healing, Clinical Plasma Medicine 4 (2016) 19-28.

[12] A.L. Garner, T.A. Mehlhorn, A review of cold atmospheric pressure plasmas for trauma and acute care, Frontiers in Physics 9 (2021) 774.

[13] O. Assadian, K.J. Ousey, G. Daeschlein, A. Kramer, C. Parker, J. Tanner, D.J. Leaper, Effects and safety of atmospheric low-temperature plasma on bacterial reduction in chronic wounds and wound size reduction: A systematic review and meta-analysis, International Wound Journal 16 (2019) 103-111.

[14] Z. He, S. Liu, C. Zhang, L. Fan, J. Zhang, Q. Chen, Y. Sun, L. He, Z. Wang, K. Zhang, Coal based carbon dots: Recent advances in synthesis, properties, and applications, Nano Select 2 (2021) 1589-1604.

[15] M. Behi, L. Gholami, S. Naficy, S. Palomba, F. Dehghani, Carbon dots: a novel platform for biomedical applications, Nanoscale Advances 4 (2022) 353-376.

[16] W. Liang, C.E. Bunker, Y.-P. Sun, Carbon dots: zero-dimensional carbon allotrope with unique photoinduced redox characteristics, Acs Omega 5 (2020) 965-971.

[17] J. Liu, R. Li, B. Yang, Carbon Dots: A New Type of Carbon-Based Nanomaterial with Wide Applications, ACS Central Science 6 (2020) 2179-2195.

[18] Q.H. Pho, D. Losic, K. Ostrikov, N.N. Tran, V. Hessel, Perspectives on plasma-assisted synthesis of N-doped nanoparticles as nanopesticides for pest control in crops, Reaction Chemistry & Engineering 5 (2020) 1374-1396.

[19] Y. Li, X. Xu, Y. Wu, J. Zhuang, X. Zhang, H. Zhang, B. Lei, C. Hu, Y. Liu, A review on the effects of carbon dots in plant systems, Materials Chemistry Frontiers 4 (2020) 437-448.

[20] N.-A. Tran, N.T. Hien, N.M. Hoang, H.-L.T. Dang, D.Q. Huy, T. Van Quy, N.T. Hanh, N.H. Vu, V.-D. Dao, Carbon dots in environmental treatment and protection applications, Desalination 548 (2023) 116285.

[21] C. Long, Z. Jiang, J. Shangguan, T. Qing, P. Zhang, B. Feng, Applications of carbon dots in environmental pollution control: A review, Chemical Engineering Journal 406 (2021) 126848.

[22] P. Lesani, A.H. Mohamad Hadi, Z. Lu, S. Palomba, E.J. New, H. Zreiqat, Design principles and biological applications of red-emissive two-photon carbon dots, Communications Materials 2 (2021) 108.

[23] J. Wang, J. Qiu, A review of carbon dots in biological applications, Journal of materials science 51 (2016) 4728-4738.

[24] S.K. Kailasa, J.R. Koduru, Perspectives of magnetic nature carbon dots in analytical chemistry: From separation to detection and bioimaging, Trends in Environmental Analytical Chemistry 33 (2022) e00153.

[25] W. Zhang, H. Zhong, P. Zhao, A. Shen, H. Li, X. Liu, Carbon quantum dot fluorescent probes for food safety detection: Progress, opportunities and challenges, Food Control 133 (2022) 108591.

[26] L. Zhao, M. Zhang, A.S. Mujumdar, H. Wang, Application of carbon dots in food preservation: a critical review for packaging enhancers and food preservatives, Critical Reviews in Food Science and Nutrition (2022) 1-19.

[27] A.S. Rasal, S. Yadav, A. Yadav, A.A. Kashale, S.T. Manjunatha, A. Altaee, J.-Y. Chang, Carbon quantum dots for energy applications: a review, ACS Applied Nano Materials 4 (2021) 6515-6541.

[28] Z. Jiang, L. Guan, X. Xu, E. Wang, C. Wang, Applications of carbon dots in electrochemical energy storage, ACS Applied Electronic Materials 4 (2022) 5144-5164.

[29] Y. Liu, S. Roy, S. Sarkar, J. Xu, Y. Zhao, J. Zhang, A review of carbon dots and their composite materials for electrochemical energy technologies, Carbon Energy 3 (2021) 795-826.

[30] L. Đorđević, F. Arcudi, M. Cacioppo, M. Prato, A multifunctional chemical toolbox to engineer carbon dots for biomedical and energy applications, Nature Nanotechnology 17 (2022) 112-130.

[31] C.Y. Chung, Y.J. Chen, C.H. Kang, H.Y. Lin, C.C. Huang, P.H. Hsu, H.J. Lin, Toxic or Not Toxic, That Is the Carbon Quantum Dot's Question: A Comprehensive Evaluation with Zebrafish Embryo, Eleutheroembryo, and Adult Models, Polymers 13 (2021).

[32] Y. Zhai, Z. Zhu, C. Zhu, J. Ren, E. Wang, S. Dong, Multifunctional water-soluble luminescent carbon dots for imaging and Hg 2+ sensing, Journal of Materials Chemistry B 2 (2014) 6995-6999.

[33] Y. Sun, X. Wang, C. Wang, D. Tong, Q. Wu, K. Jiang, Y. Jiang, C. Wang, M. Yang, Red emitting and highly stable carbon dots with dual response to pH values and ferric ions, Microchimica Acta 185 (2018) 83.

[34] S. Pandiyan, L. Arumugam, S.P. Srirengan, R. Pitchan, P. Sevugan, K. Kannan, G. Pitchan, T.A. Hegde, V. Gandhirajan, Biocompatible Carbon Quantum Dots Derived from Sugarcane Industrial Wastes for Effective Nonlinear Optical Behavior and Antimicrobial Activity Applications, ACS Omega 5 (2020) 30363-30372.

[35] S. Lu, B. Yang, Carbon dots are shining in the world, SmartMat 3 (2022) 207-207.

[36] X. Qin, C. Fu, J. Zhang, W. Shao, X. Qin, Y. Gui, L. Wang, H. Guo, F. Chen, L. Jiang, Direct preparation of solid carbon dots by pyrolysis of collagen waste and their applications in fluorescent sensing and imaging, Frontiers in Chemistry 10 (2022).

[37] Y. Xian, K. Li, Hydrothermal Synthesis of High-Yield Red Fluorescent Carbon Dots with Ultra-Narrow Emission by Controlled O/N Elements, Advanced Materials 34 (2022) 2201031.

[38] D. Zhang, D. Chao, C. Yu, Q. Zhu, S. Zhou, L. Tian, L. Zhou, One-Step Green Solvothermal Synthesis of Full-Color Carbon Quantum Dots Based on a Doping Strategy, The Journal of Physical Chemistry Letters 12 (2021) 8939-8946.

[39] M.P. Romero, F. Alves, M.D. Stringasci, H.H. Buzzá, H. Ciol, N.M. Inada, V.S. Bagnato, One-pot microwave-assisted synthesis of carbon dots and in vivo and in vitro antimicrobial photodynamic applications, Frontiers in Microbiology 12 (2021) 662149.

[40] Y. Gang, E. Sarnello, J. Pellessier, S. Fang, M. Suarez, F. Pan, Z. Du, P. Zhang, L. Fang, Y. Liu, T. Li, H.-C. Zhou, Y.H. Hu, Y. Li, One-Step Chemical Vapor Deposition Synthesis of Hierarchical Ni and N Co-Doped Carbon Nanosheet/Nanotube Hybrids for Efficient Electrochemical CO2 Reduction at Commercially Viable Current Densities, ACS Catalysis 11 (2021) 10333-10344.

[41] Q. An, Q. Lin, X. Huang, R. Zhou, X. Guo, W. Xu, S. Wang, D. Xu, H.-T. Chang, Electrochemical synthesis of carbon dots with a Stokes shift of 309 nm for sensing of Fe3+ and ascorbic acid, Dyes and Pigments 185 (2021) 108878.

[42] C. Russo, B. Apicella, A. La Rocca, M. Sirignano, Fluorescent carbon dots synthesis in premixed flames: Influence of the equivalence ratio, Carbon 201 (2023) 659-666.

[43] J. Zhang, S.-H. Yu, Carbon dots: large-scale synthesis, sensing and bioimaging, Materials Today 19 (2016) 382-393.

[44] Q.H. Pho, M. Escriba-Gelonch, D. Losic, E.V. Rebrov, N.N. Tran, V. Hessel, Survey of Synthesis Processes for N-Doped Carbon Dots Assessed by Green Chemistry and Circular and EcoScale Metrics, ACS Sustainable Chemistry & Engineering 9 (2021) 4755-4770.

[45] P. Bruggeman, M.J. Kushner, B.R. Locke, J.G. Gardeniers, W. Graham, D.B. Graves, R. Hofman-Caris, D. Maric, J.P. Reid, E. Ceriani, Plasma–liquid interactions: a review and roadmap, Plasma sources science and technology 25 (2016) 053002.

[46] R. Botton, D. Cosserat, S. Poncin, G. Wild, A simple gas-liquid mass transfer jet system, 8th World Congress of Chemical Engineering, 2009, pp. CDrom du congrès.

[47] S.R. McNeill, M.A. Sutton, Z. Miao, J. Ma, Measurement of surface profile using digital image correlation, Experimental Mechanics 37 (1997) 13-20.

[48] F. Yan, Z. Sun, H. Zhang, X. Sun, Y. Jiang, Z. Bai, The fluorescence mechanism of carbon dots, and methods for tuning their emission color: a review, Microchimica Acta 186 (2019) 583.

[49] L. Shui, J.C. Eijkel, A. Van den Berg, Multiphase flow in microfluidic systems–Control and applications of droplets and interfaces, Advances in colloid and interface science 133 (2007) 35-49.

[50] A. Hendrawan, A. Cilacap, Calculation of power pumps on otec power plant ocean (ocean thermal energy conversion), ICoSASTE 201 9) Kupang, May 14-15, 201 9 The 1 International Conference on Science, Applied Science, Teaching and Education 2019, 2019, pp. 1-13.

[51] B. Liu, W. Li, Y. Chang, W. Dong, L. Ni, Extraction of berberine from rhizome of Coptis chinensis Franch using supercritical fluid extraction, Journal of Pharmaceutical and Biomedical Analysis 41 (2006) 1056-1060.

[52] K. Sato, A. Hibara, M. Tokeshi, H. Hisamoto, T. Kitamori, Microchip-based chemical and biochemical analysis systems, Advanced Drug Delivery Reviews 55 (2003) 379-391.

[53] I. Avramov, Relationship between diffusion, self-diffusion and viscosity, Journal of Non-Crystalline Solids 355 (2009) 745-747.

[54] H. Kyushiki, A. Ikai, The effect of solvent viscosity on the rate-determining step of fatty acid synthetase, Proteins 8 (1990) 287-293.

[55] A.F. Olea, J.K. Thomas, Rate constants for reactions in viscous media: correlation between the viscosity of the solvent and the rate constant of the diffusion-controlled reactions, Journal of the American Chemical Society 110 (1988) 4494-4502.

BLANK PAGE

Chapter 8

Conclusions & Perspectives

In this chapter, the main findings, challenges, and future direction of this thesis PhD are summarised. This chapter consists of the summary of the conducted experiments, contributions of each chapter, and research conclusion carried out throughout this project study. Finally, perspectives and recommendations for the future direction of this work are also described.

1. Conclusions

This thesis contributes to developing a new kind of microplasma to address the challenges associated with the large-scale production of multifunctional advanced nanomaterials for selected emerging applications (nanofertilisers/nanopesticides, environmental treatment, and theranostic medicine) in a sustainable manner (green, eco-friendly, energy-efficient production). This comprehensive study aims to address specific challenges associated with the large-scale synthesis of NCQDs, which will have an enormous impact on agriculture, the environment, and the healthcare system. In essence, this thesis is devoted to the discovery and development of a microplasma jet (kINPen®IND)-based reactor to produce high-quality N-doped carbon quantum dots with outstanding properties (water-soluble, intense fluorescence, ultrasmall size, crystallinity, etc.) from a green chemical (Vitamin B9). Then, an attempt to improve mass production efficiency by process design engineering and the support of catalysts, as well as to understand the synthesis reaction mechanism, has been made in this thesis. Four main concepts can be summarized based on the research outcomes in this thesis:

Chapter 3 focuses on a deep understanding of available six large-scale synthesis methodologies of N-doped carbon dots (NCQDs) in the up-to-date literature review. Then, based on collected information from the literature review, a comprehensive assessment to compare the key components (greenness, sustainability, energy-efficiency, and cost) of these fabrication methodologies using green chemistry, circular and ecoScale metrics. Following are the main findings and contributions of this chapter **(Aim 2)**:

- Thermal synthesis method (scenario 3) of NCDs using citric acid with monoethanolamine, show the most promise when all assessments are considered. Scenario 3 is circular, with the highest material circularity indicator (MCI) of 0.971 and the second-best EcoScale index of 56%.
- Thermal synthesis method (scenario 2), using oleic acid and sucrose for NCDs synthesis, scores best at 60%.
- The assessment of the six synthesis process methodologies for N-doped carbon dots nanoparticles determines that hydrothermal (scenario 1), thermal (scenario 3), and microwave (scenario 4) score best in terms of green metrics, while thermal (scenarios

2 & 3), and thermal plasma (scenario 5) do likewise with circular metrics. Finally, concerning good manufacturing criteria, thermal (scenarios 2 & 3) and microwave (scenario 4) shows the best performance. NCDs produced from hydrothermal (scenario 1), microwave (scenario 4), and thermal methods (scenario 2) need a purification process for good sustainability performance.

- Considering all metrics, scenario 3 (thermal method using citric acid with MEA) ranks best, followed by scenario 4 (microwave with glucose). Interesting to note that thermal plasma (scenario 5) shows good indices despite the high-energy consumption. The latter is overcompensated by the fact that scenario 5 (as well as scenario 3) does use neither water nor solvent, which reduces waste generation. Therefore, any improvement in energy consumption for the thermal plasma would let it jump up to even the best scenario. This also gives hope for future use of nonthermal plasma and its miniaturized version (scenario 6), also known as an energy-consuming technology, yet with considerable improvements over the years. It needs fewer operating processes than conventional methods and profits from process simplicity. Yet this is not paid off so far in terms of green chemistry and circularity.
- "Utility" is a strong point to enhance circularity in the Ellen MacArthur definition. The plasma-prepared nanomaterials are rich in functional groups such as $-NH_2$, -COOH, -CHO, etc., without requiring chemicals for surface modification. Those surface groups are key to the NCD functionality, *i.e.* their photoluminescent properties.
- Based on the information provided by the manufacturer, the power consumption of this device is 50 W. It was calculated that about 1 g of NCQDs per day (24 hours). To produce 1 gram of NCQDs, this device will consume 1200 watts of energy per day. Based on this calculation, non-thermal plasma is considered superior in terms of "gram-scale synthesis" in relation to plasma power consumption. The power consumption of a plasma system is an important factor to consider when evaluating its efficiency and cost-effectiveness for gram-scale synthesis. Generally, a plasma system that can produce a high yield of material with a low power consumption is considered more efficient than one that requires a higher power input for the same amount of material produced. Therefore, when evaluating the efficiency of a plasma

system for gram-scale synthesis, it's important to consider not only the productivity (in grams per second or gram/s) but also the power consumption (in watts or joules). A system that can produce a high yield of material while consuming relatively little energy (i.e., a high gram/s/Watt or gram/Joule ratio) is generally considered more efficient than one that consumes more energy for the same amount of material produced.

Chapter 4 focuses on the improvement of the mass efficiency of the microplasma jet-based synthesis process, which was revealed after the comprehensive assessment from Chapter 3. The aim of this chapter is to attempt to reach the gram-scale production of N-doped carbon dots by adjusting the distance of the tip of the microplasma jet to the water surface in three steps, named distant, contact, and deflection modes. As a further variation, the liquid volume is either stirred or unstirred and may contain glass beads or metal flakes. In this way, the mass transfer, hydrodynamics, and the electrical field are influenced and create the specific gas–liquid interface, possibly including plasma-catalytic effects. Following are the main findings and contributions of this chapter **(Aim 3)**:

- The closer it came, the more the plasma was deformed and spread out into the whole gaseous reaction volume. In the contact and deflection mode, the jet penetrated the liquid volume down to the reaction well floor.
- Stirred microwell operation delivers higher photoluminescence than unstirred one. The addition of glass beads results in higher photoluminescence, demonstrating the impulse transfer-based mass transfer improvement than the unstirred mode but cannot reach the quality of the stirred plasma operation.
- Adding metal flakes is superior to all modes of operation. This cannot be alone because of better mass transfer and hydrodynamics but may be due to changing the electrical field and possibly plasma-catalytic effects.
- A thermofluidic analysis confirms a uniform temperature profile and a positive temperature effect on mass transfer. In this way, the research demonstrated that we achieved process intensification.
- The photoluminescence intensity's intended performance for the foreseen applications of the nanomaterial was maximised. In addition, we could reach a

productivity of 1 g per day. This is much more than many reported plasma-based and other process-based nanomaterial syntheses in literature and is even quoted to be on the way to production (as nanomaterials most often are only needed in minute volumes).

Chapter 5 focuses on developing a new conceptual strategy to rationally design and synthesise the desirable for three main applications (nanopesticides, water purification, and theranostic treatment). One of the critical problems of CD in these applications is enhancing the high-quality intrinsic properties of CD, including water solubility, stability, and fluorescence intensity. Therefore, this conceptual design approach is proposed to address these problems and achieve these desired properties, targeting to create CD with the required modification of the CD's bulk/size, surface, and morphology. Following are the main findings and contributions of this chapter **(Aim 4)**:

- Three molecular targets guiding the rational designs have been achieved in a proof-of-principle fashion. The NCQD were monodispersed with a mean particle size of 3.13 nm. The core structure of NCQD was in the form of a crystalline. It consisted of multilayered graphitic- and pyrrolic-nitrogen-defected graphene sheets, while their surface was decorated by $–NH_2$, –OH, and –COOH functional groups. The resulting NCQD had an intensely blue fluorescence performance with a QY of 35%, the highest among other plasma synthesis approaches and the best of all methods applied.
- NCQD showed the most intense fluorescence in pH values of 6–8. By performing the strongest fluorescence in water, the NCQD was considered hydrophilic, in line with the presence of protic and polar surface groups. DLVO theory predicts that at a potential of ±40 mV, NCQD may have the most stable colloidal behaviour in water.

Chapter 6 investigates the relationship between the microplasma multiphase design and the plasma-catalytic effect. To do this, the study employs optical emission spectroscopy (OES) to examine how a plasma-heterogeneous catalyst in a multiphase reaction impacts the generation of NCQD from Vitamin B9. The focus is on understanding and improving multiphase hydrodynamics and reactions by using a plasma jet to create a specific surface

profile that penetrates deep into the liquid volume. Following are the main findings and contributions of this chapter **(Aim 5)**:

- The gas flow of Ar at 2 sccm at "deflection" mode enhanced the intensity of positively charged species.
- $Ni_{80}Cr_{20}$ exhibited a better catalytic activity based on OES analysis and electric potential comparison.
- The thermal imaging results also indicated that the reaction temperature at the plasma-liquid-catalyst interface is lower than 25 ^{0}C. Heat and mass transfer processes play a key role in controlling the temperature of the reaction via water evaporation.
- The plasma jet in the deflection mode is stopped at the metal ($Ni_{80}Cr_{20}$) flakes interface surrounded by a liquid, giving rise to a different surface profile than water alone.
- The mechanism of plasma-liquid-catalysts synthesis of N-doped quantum dots was proposed with seven main steps.

Chapter 7 aims to improve reactivity in a plasma-activated three-phase catalyst system using bespoke transient hydrodynamics. Existing three-phase plasma systems are poorly designed, understood, and not commercially available. The study evaluated N-doped carbon quantum dots as fertilizers and wastewater treatment using a commercial plasma system generating a plasma microjet. The plasma can penetrate the catalyst bed via the stagnant thin liquid film and polarize the plasma-liquid interface, resulting in an increased reaction rate by reducing the solvent's viscosity and increasing liquid component diffusivity towards the catalyst bed. Following are the main findings and contributions of this chapter **(Aim 6)**:

- N-doped carbon quantum dots were used as a model reaction for fertilizer and wastewater treatment applications.
- A commercial plasma system generating a plasma microjet was used to create a hydrodynamic regime where plasma can penetrate the catalyst bed.
- The reaction rate is enlarged by increasing liquid component diffusivity and interfacial area below the crater.
- The plasma process is energy-efficient and consumes lower energy than microfluidic processing but requires consideration of volatile additive evaporation.

- Reaction kinetics are critical for cost and environmental profile of processes derived from the reactions.

2. Perspectives

This research study marked an exciting journey with the novel discovery underpinning the mastery of nitrogen fixation microplasma synthesis technology for multifunctional nanoparticles towards selected applications that open many new frontiers requiring further exploration. For future direction, several key aspects highlighted as the following are recommended to fully unlock the potential of nitrogen fixation microplasma synthesis technology and N-doped carbon quantum dots:

1) Scaling up the nitrogen fixation microplasma synthesis process of N-doped carbon quantum dots.

Scaling up the microplasma synthesis process of N-doped carbon quantum dots (NCQDs) refers to increasing the production of these quantum dots using the microplasma synthesis method. This can be achieved by increasing the size of the reactor, increasing the flow rate of the precursor solution, or by running the process in parallel reactors. One of the main challenges in scaling up the microplasma synthesis process is maintaining the quality of the NCQDs produced. When scaling up the process, it is important to ensure that the reaction conditions, such as the plasma power, the precursor concentration, and the reaction time, are maintained at optimal levels. Another approach to scaling up the microplasma synthesis process is to develop new reactor designs that can handle larger quantities of precursor solution and generate a more uniform microplasma. This could include using continuous flow reactors (microfluidic microplasma), which can handle a larger volume of solution than batch reactors, and parallel reactors (an array of microplasma jets), which can produce a larger quantity of NCQDs in a shorter period.

The microfluidic microplasma synthesis of N-doped carbon quantum dots (NCQDs) is a method for producing NCQDs that utilizes a microfluidic device to generate a microplasma within a liquid solution containing the precursor materials for the NCQDs. The microfluidic device consists of two main components: a microchannel and an electrode. The microchannel is used to flow the precursor solution through, while the electrode is used to generate the microplasma. The electrode can be made of various materials such as stainless steel, gold, or carbon. The microplasma is generated by applying a high-voltage electric field

across the microchannel and the electrode, which causes the precursor solution to become ionized and form a plasma. The microfluidic microplasma synthesis method has several advantages over other methods for producing NCQDs. For example, the small scale of the microfluidic device allows for precise control of the reaction conditions, such as the flow rate of the precursor solution and the plasma power. This enables the production of NCQDs with high reproducibility and uniformity. The microfluidic microplasma synthesis method can produce NCQDs with a high nitrogen content, which is important for many applications, such as bio-imaging and catalysis. Another advantage of the microfluidic microplasma synthesis method is that it is a green and eco-friendly method, as it consumes less energy, and generates less waste and pollution than other methods. It is worth mentioning that, the microfluidic microplasma synthesis method is still an active area of research, and further optimization of the reaction conditions and the design of the microfluidic device are needed to improve the yield and quality of the NCQDs produced.

An array of microplasma jets allows for the simultaneous synthesis of multiple NCQDs, which can increase the overall yield and productivity of the synthesis process. Additionally, the small scale of the microplasma jets allows for precise control of the reaction conditions, such as the flow rate of the precursor solution and the plasma power, which can lead to the production of NCQDs with high reproducibility and uniformity. Another advantage of using an array of microplasma jets is that it allows for a low-power plasma source, which reduces energy consumption and the cost of the synthesis process. Microplasma jet methods have been widely used to synthesise various materials. However, it is still an active area of research in the field of N-doped carbon quantum dots, and further optimization of the reaction conditions and the design of the microplasma jets are needed to improve the yield and quality of the NCQDs produced. It is worth mentioning that the microplasma jet method is a greener and eco-friendly method, as it consumes less energy and generates less waste and pollution than other methods.

Additionally, using advanced process control techniques such as computer-controlled systems and implementing quality control methods such as statistical process control (SPC) can help maintain the quality of the NCQDs produced while scaling up the process. Overall, scaling up the microplasma synthesis process of NCQDs is an active area of research, with the goal of making this technology more accessible for various applications by producing NCQDs in large quantities at a lower cost.

2) Optimizing purifying process for N-doped carbon quantum dots.

In this thesis, the results indicated that purifying N-doped carbon quantum dots and recycling the unreacted reactants improve the sustainability of the overall production process. This study has paved the way for large-scale purification and recycling research to enhance the quality of NCQDs products. Several methods can be used to purify N-doped carbon quantum dots (NCQDs), depending on the desired purity level and the specific application of the NCQDs. One common method for purifying NCQDs is size-exclusion chromatography (SEC), which is based on the principle of separating particles based on their size. SEC can be used to separate NCQDs from impurities such as unreacted precursors, by-products, and other contaminants. Another method that can be used for purifying NCQDs is centrifugation. This method separates NCQDs from impurities based on their density. The NCQDs are centrifuged at high speed, and the impurities are separated from the NCQDs due to their different densities. Other methods that can be used to purify NCQDs include: Dialysis, which is a method that separates small molecules from large ones by passing the solution through a semi-permeable membrane. Ultracentrifugation is a method that separates particles based on their size, shape, and density by centrifuging the solution at very high speeds. Precipitation is a method that separates dissolved substances from a solution by adding a reagent that causes the substance to form a solid precipitate. Additionally, advanced purification techniques such as high-performance liquid chromatography (HPLC) and solid-phase extraction (SPE) can purify NCQDs to a very high purity level. It is important to note that the purification process of NCQDs may vary depending on the synthesis method and the impurities present in the initial sample. Therefore, optimising the purification methods for each specific synthesis method is important.

3) Using the rationally designed NCQDs from microplasma jet-based synthesis in crop control, environmental treatment, and theranostic medicine

The outcome of this study finishing to demonstrate the concept of using a microplasma jet-based reactor for generating high-quality NCQDs. At the early stage, these as-prepared NCDs are rationally designed with purposes for agriculture, environmental treatment, and

theranostic medicine, which opens new doors for generating desired and on-purpose NCQDs for specific applications.

Using rationally designed N-doped carbon quantum dots (NCQDs) from microplasma jet-based synthesis in crop control, environmental treatment, and theranostic medicine is an emerging area of research. In crop control, NCQDs have been shown to have the potential as a photosensitizer for photodynamic therapy (PDT) in controlling plant pathogens. In addition, NCQDs have also been used to improve the efficiency of fertilizers in crop growth by acting as a catalyst for nitrogen fixation. In environmental treatment, NCQDs have been shown to have potential for use in the removal of heavy metals and pollutants from water bodies and in the treatment of wastewater. Additionally, NCQDs have also been used as catalysts for the degradation of pollutants in the air. In theranostic medicine, NCQDs has been used as a contrast agent for imaging in cancer diagnosis and as a drug delivery system for cancer therapy. They have also been used as a therapeutic agent for the treatment of various diseases, such as inflammation and infections. Overall, rationally designed NCQDs from microplasma jet-based synthesis have shown great potential in various fields such as crop control, environmental treatment, and theranostic medicine. However, more research is needed to fully understand their potential applications and to develop appropriate methods for their use in these fields.

4) Investigating the safety and environmental risk of developed N-doped carbon quantum dots

After demonstrating the potential of these NCQDs in crop control, environmental treatment, and theranostic medicine. A study on a comprehensive assessment of the safety and environmental risk of NCQDs also should be accomplished in the future. The safety and environmental risks of developed N-doped carbon quantum dots (NCQDs) are currently an active area of research, as there is limited information available on these materials' potential hazards and effects. Regarding safety, NCQDs are considered low-toxicity materials, as they are made from carbon and nitrogen atoms, which are abundant in nature. However, some studies have shown that NCQDs may cause some toxicity to cells and organisms, especially when they form nanoparticles. Therefore, it is important to use appropriate protective measures when handling NCQDs, such as wearing gloves and masks and avoiding inhalation and ingestion of the materials. Regarding environmental risks,

NCQDs are considered relatively benign materials, as they are not persistent in the environment and do not bioaccumulate. However, some studies have shown that NCQDs can impact aquatic organisms when released into water bodies. Therefore, it is important to implement appropriate measures to prevent the release of NCQDs into the environment.